Magnetism and Resistivity due to 3d impurities in Zinc and Gallium

by

Paul L. Camwell, B.Sc.

A thesis submitted for the degree of
Doctor of Philosophy
of the University of Warwick.

School of Physics,
University of Warwick.

October, 1974.

Memorandum

This dissertation is submitted to the University of Warwick in support of my application for admission to the degree of Doctor of Philosophy. It contains an account of my work carried out at the School of Physics of the University of Warwick in the period October 1970 to December 1973 under the supervision of Dr. R. Dupree. No part of it has been used previously in a degree thesis submitted to this or any other University. The work described is the result of my own independent research except where specifically acknowledged. The susceptibility results for the gallium-3d metal alloy systems have been published in J. Phys. F : Metal Physics, 3, 1015, 1973. It is anticipated that the results for the zinc-chromium alloys and the resistivity results for the gallium-3d metal alloys will be published shortly.

Paul L. Camwell

P. L. Camwell
October 1974.

Acknowledgements

It is a pleasure to record my gratitude to my supervisor Dr. Ray Dupree for his patience and guidance during the period of the work contained in this thesis. Thanks are due to Professor E. F.W. Seymour, Dr. G.A. Styles, Dr. C. J. Ford and Mr. T. B. Sheffield of the N.M.R. group for their continual interest and help during my stay at the University of Warwick. Appreciation is due also to Dr. J. M. Dixon for attempting to explain crystal field effects to me and Mr. J. Huckfield for his continual repair of broken glassware. Dr. W. Gardner of A.E.R.E. Harwell very kindly allowed me the use of his low temperature susceptibility apparatus to conclude the ZnCr results in October, 1973. I wish also to thank Professor J. A. Forty for allowing me to use the facilities of the School of Physics and the Science Research Council for a maintenance grant.

Finally, I would like to thank my wife for her transcription of the draft and Mrs. Annette Evans for her rapid and careful typing of this manuscript.

To my parents and my wife

whose encouragement and support were invaluable.

Abstract

The resistivity and susceptibility due to 3d transition metal impurities in dilute alloys of gallium were measured in the liquid state and are compared with other systems. A localised magnetic moment is shown to exist in a Curie-Weiss sense for GaMn and GaCr throughout the measuring temperature range.

Phase-shift analysis gives good agreement for both the resistivity results and the impurity spin value obtained from the susceptibility results.

The susceptibility of single crystals of ZnCr were measured from 4.2 K to ~400 K for both crystallographic directions and the magnetic moment and θ-values determined. A method is presented whereby the results can be treated in such a manner as to "remove" the De Haas-Van Alphen oscillations from the parallel axis of zinc, enabling the field-free impurity effects to be compared for both axes. This method is shown to be consistent with results obtained from zinc single crystals and allows an estimation of the Dingle temperature to be made. A temperature-dependent anisotropy was observed, the ratio of the perpendicular and parallel incremental susceptibilities being greater than 1 in the low temperature region and the opposite in the high temperature region, assuming a Curie-Weiss law holds. Simple crystal field theory is presented and shown to be inadequate in explaining the anisotropy results.

Contents

CHAPTER 1

Introduction

Ideally the comparison of experiment and theory should provide a useful study whereby theory can predict and explain the experimental results, which in turn may be able to point out the shortcomings and lead to improvements of a particular theory. The situation is usually not ideal in physics, and this is certainly so in the present investigation of the problem of the behaviour of localised magnetic moments. In essence the problem can be stated thus: why does an alloy comprising a particular impurity in a certain host metal become magnetic under various circumstances and why should the same impurities that are magnetic in a particular host become nonmagnetic in a similar metallic host? Sundry phenomena caused by the occurrence of magnetic moments initiated a large number of theoretical papers after 1964 when Kondo published his explanation of the most characteristic local moment phenomena - the minimum in the resistivity vs. temperature curve. This breakthrough renewed interest in the problem which had begun in 1930 when Meissner and Voigt found a minimum in the resistivity of supposedly pure gold. In many cases from 1964 to about 1968, experimental results led the theory and possibly caused some misconceptions, two in particular being unfortunate. As we now know, many dilute alloys were not dilute enough to make ordering effects unimportant at low temperatures and could often mask the effects of real interest (Rizzuto, 1974); the central question then discussed was to do with the formation of magnetic moments, not as would appear more fruitful now, to inquire into the conditions for moment retention (Wohlleben and Coles, 1973). A proper understanding of the problem requires a subtle approach because the effect comes about due to two differently-treated properties (Blandin, 1973). For a moment to exist on an impurity site,

one may start by describing the electrons on one atom, retaining the intra-atomic Coulomb interaction, but because the impurity magnetic energy levels fall within the host conduction band and thus delocalise the valence electrons, an alternative approach is to use a one-electron theory of electrons moving in an average field of all the atoms. It would seem therefore that the most realistic picture would be local magnetic properties formed from itinerant electron states. The difficulty lies in theory being able to cope satisfactorily with only one of these approaches at a time, the end result usually being a simplified and restricted solution. It is therefore to be expected that until a properly unified approach is achieved, the theories can only be expected to explain various aspects of the local moment phenomena. It is appropriate to mention the major theories and the limits of their success here before going into more detail in Chapter 2.

Friedel (1956) showed that using a Hartree-Foch approach an impurity in a free electron-like metal creates a potential such that the change in electron density $\Delta d(r)$ is given by:

$$\int_o \Delta d(r) d^3r = (2/\pi) \sum_l (2l + 1) \cdot \eta_l (E_F) \qquad 1.1$$

where r = distance from the impurity
l = orbital quantum number
$\eta_l(E_F)$ = phase shift at Fermi surface

Equation 1.1 can be equated to the charge difference (Z) between host and impurity and is known then as the Friedel sum rule. A virtual bound state results if the perturbing potential is not quite strong enough to permanently capture a host electron. The corresponding density of localised states/spin ($d_l(E)$) is given by:

$$d_l(E) = ((2l + 1)/\pi) \cdot d\eta_l(E)/dE \qquad 1.2$$

and gives a peaked state centering around E_d (where l = 2 for 3d transition metals) with width Δ as shown schematically as in figure 1.1.

Figure 1.1 Localisation of electron density for a virtual bound state

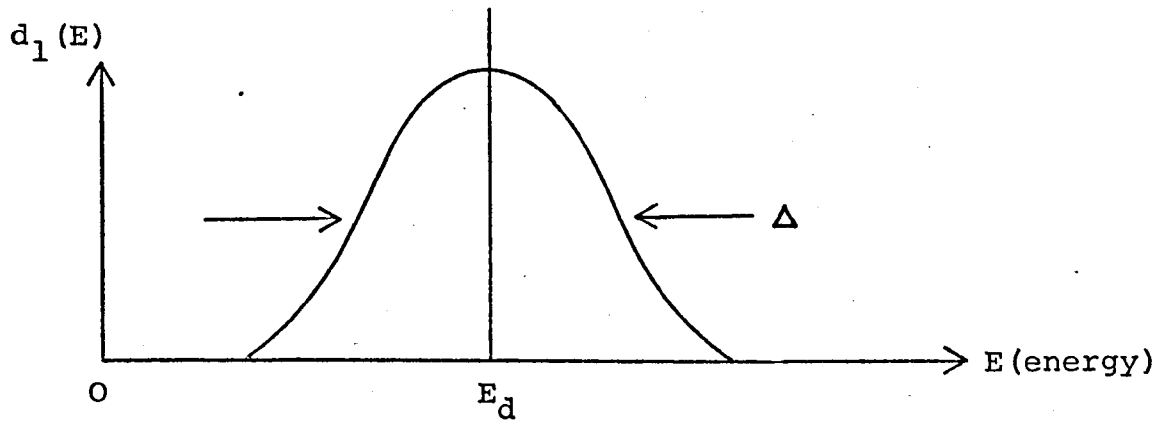

To determine if a 3d impurity in a metal is magnetic or not, a criterion was devised (Blandin and Friedel, 1959) which can conveniently be summarised by reference to figure 1.2 below.

Figure 1.2 Magnetic/Nonmagnetic transition for 3d metals

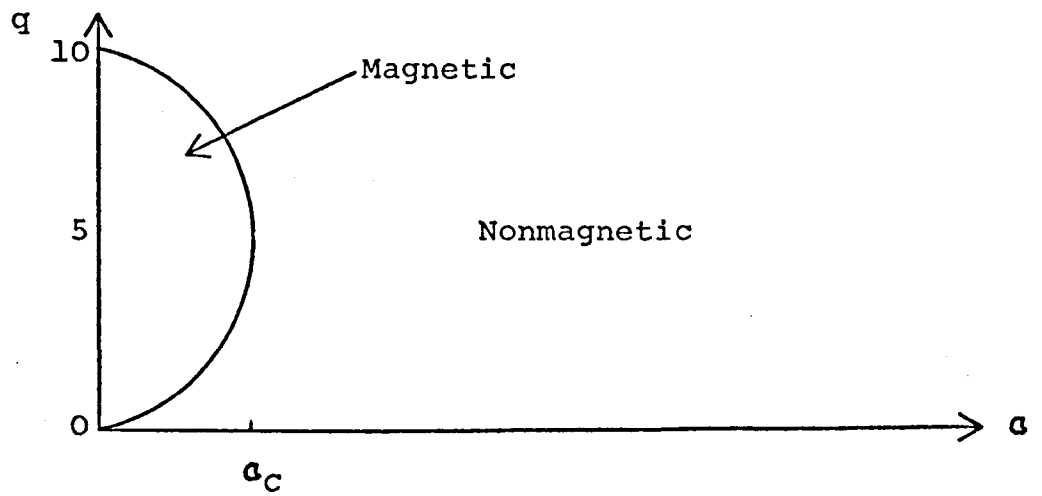

The quantities q and α refer respectively to the number of d-electrons and the ratio of width Δ to the average exchange parameter E_{ex}. Aluminium as a host has a large Fermi level ($\sim$13 eV) which results in a large Δ, thus allowing α to exceed the critical transition value α_c. Thus one expects the incremental resistivities of the 3d metals in aluminium to exhibit a single-peaked structure with a maximum at manganese (q = 5) and a twin-peaked structure for a metal such as copper (where $E_F \simeq 5$ eV) due to the virtual bound states for up and down spins crossing E_F. This is indeed what is seen to happen experimentally (Blandin, 1973).

A model Hamiltonian, widely used for theoretical investigations into the localised properties of impurities in metals, has been devised by Anderson (1961). For d-orbitals it takes the form:

$$H = H_s + H_d + H_{sd} \qquad 1.3$$

where $H_s = \sum_{s\sigma} E_s n_{s\sigma}$

$H_d = \sum_{d\sigma} E_d n_{d\sigma} + U\, n_{d\uparrow} n_{d\downarrow}$

$H_{sd} = \sum_{sd} V_{sd} n_{s\sigma} + V_{ds}\, n_{d\sigma}$

and $n_{s\sigma} = c^*_{s\sigma}\, c_{s\sigma}$ etc.

" = occupation number operator

s = conduction electron state

d, d' = d electron orbitals

σ = spin orientation $\downarrow, \uparrow$

$E_{s,d}$ = conduction, d, electron energy

V_{sd} = admixture matrix element between d states and conduction electrons

U = Coulomb exchange integrals between two electrons localised on an impurity atom

H_{sd} is the Hamiltonian describing the covalent admixture of s and d states which are separately defined by H_s and H_d.

Equation 1.3 must be treated by a many-body theory, the simplest of which is the HF approximation. Anderson, by using Green's functions, has derived parameters similar to those given by Friedel but in this case finds:

$$d_{d\sigma}(E) = (\Delta/\pi)((E - E_d)^2 + \Delta^2)^{-1} \qquad 1.4$$

$$\Delta = \pi \langle |V_{ds}|^2 \rangle_{av.} d(E) \qquad 1.5$$

The magnetic/nonmagnetic transition is given by:

$$U.d_d(E_F) = 1 \qquad 1.6$$

where $d_d(E_F)$ is the nonmagnetic density of states, with the system being nonmagnetic if $U\, d_d(E_F) < 1$ (Blandin, 1973).

The correspondence between Friedel and Anderson's theories is given by:

$$2E_{ex} = U, \quad d_1(E) = d_d(E) \qquad 1.7$$

To extend Anderson's model to orbitally degenerate cases, an exchange integral J is included which modifies equation 1.6 (Blandin, 1973) to :

$$\begin{aligned}(U + 21J).d_1(E_F) &> 1 \text{ for spin magnetism} \\ (U - J).d_1(E_F) &> 1 \text{ for orbital magnetism}\end{aligned} \qquad 1.8$$

A major difficulty for Friedel and Anderson's theories appears in the HF approach when the equations are extended to finite temperature T (all the above equations hold for T = 0). This difficulty is that the magnetic moment increases with decreasing temperature when experimentally the opposite happens. The latter is ascribed to a Kondo spin-condensation (see Chapter 2) where the impurity is screened more effectively at lower temperatures by the host conduction electrons. Further difficulties occur for T > 0, so these two theories must be regarded as giving useful predictions only for T = 0.

An alternative way of treating nearly magnetic dilute alloy

PAGE NUMBERING AS IN THE ORIGINAL THESIS

systems is by using localised spin fluctuation (l.s.f.) theory. The significance of this approach was first pointed out by Caplin and Rizzuto (1968) was found that the incremental resistivity followed a T^2 law for AlMn and AlCr. The conduction electrons are scattered by virtual bound states undergoing spin fluctuations centred around each impurity ion, these fluctuations being characterised by a scaling temperature T_s. An extended resistivity behaviour ranging from T^2 through T and lnT to a T^{-1} law is predicted (Rivier and Zlatic, 1972). Various dilute alloy systems can be described by T^2, T and lnT behaviour (Rizzuto, 1974) but observation of T^{-1} behaviour so far seems to be absent because of the very high measuring temperature necessary in this particular regime. Magnetic systems such as ZnMn are not described by l.s.f. theory.

Crystal field effects may be seen when there is an orbital contribution to the spin, though for transition metals this has usually been considered to be quenched (Moriya, 1967). A crystal field model for rare earth systems (Dixon and Dupree, 1971) has shown that for MgEr and ZrEr orbital contributions are present and are enhanced over those predicted by a simple point charge model. Heavy rare-earth metals are also treated but lack of experimental data precludes quantitative agreement with their model, though qualitative agreement is obtained for these systems. Crystal field effects are investigated in the present work using relatively simple theories in an attempt to explain the susceptibility of dilute single crystals of ZnCr. As very little work at present has been published on the 3d transition metals in various crystalline environments and it is therefore interesting to note the success or otherwise of simple crystal field theory as given here.

Hirst (1970) has produced a theory which treats the local moment problem from another point of view - he assumes

impurities retain their valence electrons in a similar fashion to a free atom or an atom in an insulator. The zero-order solution gives the impurity many - electron eigenstates due to a hierarchy of energy splittings, then the first order solution considers the interaction with host conduction electrons. In fact in this ionic-based approach the problem resolves into a calculation of how far this mixing interaction affects the magnetic behaviour of the impurity ion. Hirst finds that when the energy splitting between the ground state and the first excited state is greater than Δ, the impurity retains an ionic-type structure though it may be masked at very low temperatures where the Kondo effect of spin-condensation could occur. This theory appears to hold the greatest promise in explaining in general terms the magnetic/nonmagnetic transition though the detailed temperature behaviour in both regions requires development.

Experimentally the most straightforward ways of characterising a localised magnetic moment system is by its suceptibility and resistivity behaviour. The systems ZnCr and Ga-3d metals were chosen for the reasons given below and the results from these techniques are presented in Chapters 4 and 6. When alloyed with metallic hosts the 3d transition metals are likely candidates to form a local moment due to their unfilled d shells, and so this thesis deals with aspects of dilute alloys containing them as impurities. Zinc was chosen as a host because of the possibility of obtaining crystal field information from its anisotropy when in single crystal form. Also the relative lack of dislocations and grain boundaries compared with a polycrystal may allow a sample with a greater than normal impurity concentration ($\sim$ 1 at.% at room temperature) to be obtained. It would be reasonable to assume that the Ga-3d metal systems are nonmagnetic because of the close electronic similarity of gallium to aluminium where the Al-3d metal systems were

shown to have no local moment formation (Boato et al., 1966). Such a view is incorrect however, as work on concentrated GaMn (Wachtel and Nier, 1965) indicated the existence (in a Curie-Weiss sense) of a local moment. Therefore gallium was chosen as a host to investigate a more dilute ($\leq$ 2 at.%) series of 3d metal alloys.

An attempt to explain the zinc results using simple crystal fields theory is given in Chapter 5.

References

Anderson, P.W.,	Phys. Rev	124,	41.1961
Blandin,A., Friedel,J.,	J. Phys. Radium	20,	160,1959
Blandin, A.,	(ed.Rado & Suhl) Acad.Press	5,	3,1973
Boato,G., Bugo.,M., Rizzuot,C.,	Nuovo Cimento,	45,	226,1966
Caplin,A.D., Rizzuto,C.,	Phys. Rev. Lett.,	21,	746,1968
Dixon,J.M., Dupree,R.,	J. Phys. F:Metal Phys.,	4,	1,1971
Friedel, J.,	Can. J. Phys.	34,	1190,1956
Hirst, L.L.,	Phys. Kondens. Materie,	11,	225,1970
Kondo, J.,	Progr.Theoret.Phys. (Kyoto)	32,	37,1964
Meissner,W., Voigt,G.,	Ann. Physik.,	7,	761,1930
Moriya, T.,	Proc.Varenna School,(ed.W.Marshall)Acad.Press		1967
Rivier,N., Zlatic,V.,	J. Phys. F:Metal Phys.,	2,	87,1972
Rizzuto, C.,	Rep. Prog. Phys. (G.B.)	37,	147,1974
Wachtel,E., Nier,K.J.,	Zeit Metallkde.,	56,	779,1965
Wohlleben, D.K., Coles,B.R.,	Magnetism (ed. Rado and Suhl) Acad.Press,		1973

CHAPTER 2

REVIEW OF LOCALISED MAGNETIC MOMENTS

2.1. Introduction

The problems of explaining the properties of a metal containing a small amount of impurity, which may or may not then be magnetic, can usually be reduced to the problem of solving the scattering probability of the conduction electrons from a single impurity atom. The historical method of treating this problem of dilute alloys is usually setting up the potential due to the added impurity and solving the one-electron Schodinger equation (e.g. Mott and Jones, 1936; Friedel, 1954; Blatt, 1957). In this manner specific heat, susceptibility, resistivity, etc. have been determined for nonmagnetic dilute alloys. The problem becomes more complicated if the impurity on alloying remains magnetic and anomalous (usually spin-dependent) properties result. For example the experimental values for resistivity and giant thermopower are not explained by the above method. Resistivity and susceptibility will form the main subject of this review as the thesis as a whole is concerned with them, and they form the most easily identifiable characteristics of a local moment system.

Up to the present time, many theoretical aspects remain unsatisfactory and experimental problems abound. For instance, in most local moment systems, a very low ($\ll$ 1 atomic %) concentration of impurity must be used to reduce coupling and ordering effects (Rizzuto, 1974). When T<0.01K in the CuMn system for instance, a concentration as low as $\sim$1mppm is too great (Hirschkoff et al., 1971). The first indication that c must be carefully controlled was in 1930 when Meissner and Voigt observed the resistance minimum in the resistance vs. temperature curve when the temperature was 10K with supposedly "pure" gold. This result created a certain amount of interest though no real explanation was forthcoming until 1964 when Kondo showed the

origin of the minimum. To review the experimental facts up to that time one may refer to van den Berg (1964), and for the theoretical aspects up to 1965 to Bailyn (1966). Since 1964 a plethora of information has been published though many aspects still remain unresolved, so only the most successful theories corroborated by experiment will be discussed in this chapter.

We will be concerned with the effect of alloying transition elements in various metallic hosts so it is convenient to consider how the d electrons of the impurity interact with the host conduction electrons. In 1951 Zener showed that a partially successful model of ferro-magnetic transition metals could be constructed by assuming localisation of d electrons at atomic sites and an exchange interaction between them and the conduction electrons (s-d model). This model is of questionable validity when taken to first order for the 3d metals but is an adequate approximation for the 4f metals (Yosida, 1964) because one may be more certain of the orbitals being localised near the nucleus in the latter case. The s-d model has been used to describe dilute magnetic alloy systems where the impurity atoms retain their net spin. To first order a ferromagnetic coupling between local spins via conduction electrons is achieved, though there is no dependence on the separation of the spins in this model, - a result in contradiction to a requirement of Freidel's work utilising partial wave analysis (Hart, 1957). Ruderman and Kittel (1954), independently of Kasuya (1956) and Yosida (1957), carried through the calculation to second order and found decreasing oscillatory polarisation of the conduction electron spins with distance from the impurity, in accordance with results on dilute magnetic alloys and rare-earth metals (Yosida, 1957). This theory became known as the RKKY interaction and plays an important part in explaining the width of NMR lines in some metals (e.g. see Bloembergen and Rowland, 1955), and can cause interaction effects that may drastically modify the local impurity characteristic temperature of a system, e.g. AuV (Van Dam and Gubbens, 1971).

2.2. Theory

Friedel in 1956 gave a phenomenological explanation of the formation of localised magnetic moments in terms of a virtual bound state (v.b.s.). He showed that the 3d orbitals of the first row transition metals dissolved in a metallic host would retain some of their localised character despite being embedded in or very close to the conduction band of the host. To understand this in a very simple manner we may consider a one-dimensional potential model as shown below, following Kondo (1969).

Figure 2.1
One Dimensional Potential Well

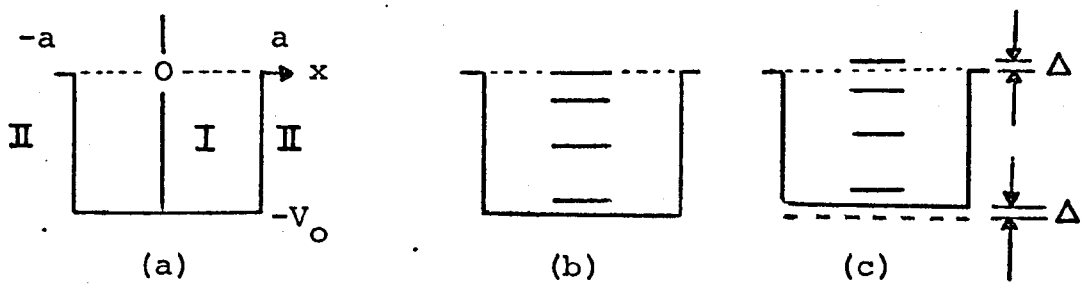

In this we imagine the 3d states to be contained in the square well potential using the Fermi energy level of the host conduction band as zero as shown in figure 3(a). Neglecting Coulomb interactions, the wavefunction solution ψ in region I is :

$$\psi = \cos k x \qquad 2.1$$

where $E + V_o = \hbar^2 k^2 / 2m_o$

and E = energy of the wavefunction

V_o = potential well depth

m_o = effective electron mass

k = wavenumber

Region II has a solution of :

$$\psi = A \cos kx + B \sin kx \qquad 2.2$$

where A and B are coefficients and :

$$A^2 + B^2 = (1 + V_o/E) \sin^2 ka \qquad 2.3$$

Discrete energy levels as shown in figure 3(b) exist for large V_o ($V_o > E$), and the condition that the n'th level V_n occurs at E = O is that :

$$V_n = (n-1)^2 \pi^2 \hbar^2 / 2m_o a^2 \qquad 2.4$$

If $V_n - V_o = \Delta$ as shown in figure 3(c), then the level at V_n cannot be a true eigenstate of ψ, i.e. this level is not a truly bound state. Normally the wavefunction is large in region II, as shown by equation 2.3 where $A^2+B^2 \gg 1$ for $V_o \gg E$, but there is a possibility of reducing this and forming a v.b.s. at $E = \Delta$ where:

$$A^2 + B^2 \simeq (1+V_o/E)((n-1)^2 \pi^2 (E-\Delta)^2/4V_n^2)) \qquad 2.5$$

Thus $A^2 + B^2$ has its smallest value when one allows E to be equal to Δ (equation 2.5) and the wavefunction is now localised in region I

The three dimensional case was discussed by Friedel who used phase-shift methods in solving the equivalent scattering problem (de Faget de Castlejau and Friedel, 1956, Daniel and Friedel, 1965) where one assumes that alloying the 3d impurity causes it to give up all its s and d electrons to the host, thereby creating a Coulombic potential well. This well has the effect of enhancing the d-wave portion of the scattered conduction electrons such that the excess positive charge localised around the impurity is screened - this effect is described by the Friedel sum rule:

$$Z = (2/\pi) \cdot \sum_l (2l+1).\eta_l (E_F) \qquad 2.6$$

where η_l = phase shift of the scattered outgoing spherical wave of order l

Z = perturbing charge difference.

Introducing the Coulomb interaction now allows the presence of a net spin on the impurity to be retained. This can be seen simply as follows: if a v.b.s. exists and a 3d electron of spin q is introduced into it, the gain in Coulombic energy is $-q^2/\Delta E/2$, where $\Delta E \sim$ atomic energy (Kondo, 1969). The loss in orbital energy becomes now $q^2/4d$, where $d = (5/\pi)d\eta/dE$ is the density of the states/spin of the v.b.s. and η is the phase shift of the scattered conduction electron at energy E (l = 2 in this example).

Differentiating the spin with respect to energy gives the condition that if $2\Delta E.d>1$, then the existence of a net spin will be energetically favourable. To illustrate this visually for various systems, Friedel (1956) devised a table that predicted the probable existence of localised moments on the basis of the above equation, and this is reproduced in table 2.1 below (after Daybell and Steyert, 1968).

TABLE 2.1 Prediction of moments in dilute alloys

Host	Au	Ag	Cu	Mg	Zn	Al
Impurity						
Ti	-					-
V	+					-
Cr	+	+	+		+	-
Mn	+	+	+	+	+	-
Fe	+		+	+	-	-
Co	+		?			-
Ni	-		-		-	-

+ = moment

- = no moment

It follows from the equation given above that two general conditions will result. If the Fermi energy E_F of the host is large, the resonance energy (i.e. perturbation of the Fermi sea) width is also large. A sharp resonance is generally needed to maintain a net spin, thus no permanent moments exist for the 3d transition elements in aluminium.

In going across the 3d row with aluminum as host, the excess charge of titanium is not great enough to broaden its 3d level as far as E_F, in fact this does not happen until one alloys chromium in aluminium, and further alloying across the row takes the level below E_F. As the maximum electronic current is carried at E_F, whenever the conduction band of the host and the impurity d-levels coincide at E_F then the impurity contribution to the resistivity is a maximum. Thus the incremental resistivity has a maximum at chromium and decreases approximately symmetrically on either side. Alternatively in copper as a host where these elements have local moments existing, going across the row shows two peaks in the residual resistivity. This is because the resonance is spin-split and the first peak at vanadium occurs when the up-spin passes through E_F and the second peak at iron when the down-spin passes through it (Vassel, 1958).

The modification of equation 2.6 that is necessary for a magnetic system is :

$$Z = Z\uparrow + Z\downarrow = (1/\pi)\sum_l (2l+1)(\eta_{l\uparrow} + \eta_{l\downarrow}) \qquad 2.7$$

Where the arrows indicate the spin state of the local moment. The charge difference due to the impurity atom allows a net spin S to be defined thus:

$$S = Z\uparrow - Z\downarrow = (2l + 1)(\eta_{l\uparrow} - \eta_{l\downarrow})/\pi \qquad 2.8$$

Equation 2.8 is useful because phase shifts for an alloy as determined by a resistivity experiment can be compared with the spin value predicted by a susceptibility experiment. The resistivity derived by partial wave analysis is given by:

$$\Delta\rho/c = (h \times 10^{-9}/50\, Z_h e^2 k_F) \sum_{l\geq 0} l\sin^2(\eta_l - \eta_{l-1}) \quad \text{cm/at.\%} \qquad 2.9:$$

where Z_h = host valency

k_F = host wave vector at E_f

The next development was Anderson's more quantitative analysis (1961) using the Hartree-Fock approximation. He assumed that if an electron occupied a d-orbital of energy E_d below the Fermi level, then another d-electron of opposite spin could occupy a state at energy $-E_d + U$, which could be above or below E_F, where U is the repulsive Coulomb interaction. If $-E_d + U < E_F$, then there will be no net spin. Alternatively, it may be that $-E_d + U > E_F$, which must necessarily be empty. The s-d interaction will cause the localised levels to be broadened and shifted such that the E_d level will have a portion of its energy distribution above E_F and similarly a portion of the $-E_d + U$ level will be brought below E_F. U reduces in strength as the occupation number of the E_d state may be less than 1, and that of $-E_d + U$ greater than 0. Should the interaction be too great (i.e. compared with the interaction between the d-electrons), then this situation becomes unstable and two degenerate levels and no net spin will result (Daybell and Steyert, 1968). This happens for hosts with a large density of states at E_F, such as aluminium, and also for impurity levels far from E_F with the d-levels of both spin directions either nearly empty or nearly full (Fischer, 1971). The validity of this model is confined to the nonmagnetic region $U/\Delta < 1$ (where Δ is the width of the v.b.s.) because of the constraints of the Hartree-Fock approximation. Δ is given by:

$$\Delta = \pi V_{sd}^2 d_l \qquad 2.10$$

where V_{sd} = mixing interaction

d_l = unsplit v.b.s. density of states:

$d_l = (2l+1)(\sin^2 \eta_l)/\pi$

In terms of the phase shifts the width may be written:

$$\Delta = (E_{d\uparrow,\downarrow} - E_F) \tan \eta_{l\uparrow,\downarrow} \qquad 2.11$$

A convenient criterion for the case where $\eta_1\uparrow \neq \eta_1\downarrow$ is given by :

$$U.d_1 > \Gamma \qquad 2.12$$

Thus equation 2.12 can be used to predict the transition from nonmagnetic behaviour (where the HF approximation is valid) by noting the trend of the d_1 for a series of impurities (e.g. 3d metals) in a particular host where U is known. A more realistic theory has been developed by Anderson, still in the HF approximation (Anderson and Clogston, 1961) and others (e.g. Schrieffer , 1967; Yosida et al., 1965) to include the case where many degenerate d-levels are present, though for simplicity only the spin-degeneracy is usually considered, as found necessary to explain experimental results with alloys containing the iron-group transition elements (Heeger, 1969).

The theories so far had in effect merely explained the conditions necessary for the formation of a localised magnetic moment but did not show the details of the effect, e.g. the changing temperature dependence (except at high temperature where a Curie law was expected to hold) and the magnetic/nonmagnetic transition, or in fact the fundamental cause of the resistance minimum. The s-d model or modifications of it is unsatisfactory for two basic reasons: weakly magnetic systems (e.g. AlFe) were not described, even at high temperatures as a Curie law does not hold in these systems, and below the characteristic temperature T_K where $\Delta\rho$ increases as T decreases the model is not valid as a many-body theory is necessary for a true description (Fischer, 1971). Basically the fault is that the s - d model starts by assuming the existence of an impurity spin with a fixed magnitude (i.e. a well-defined spin is expected only in the infinite Coulomb limit). To overcome this the Anderson (1961) and Wolff (1961) models had no limitation on spin magnitude. The Wolff model is similar to that of Anderson's as described above, except that where Anderson neglects the Coulombic

interaction of the host electrons retaining only the weak conduction-electron/d-orbital interaction at the extra localised d level (v.b.s.), thus restricting his model to nonmagnetic hosts (e.g. Au) where there are little spin-enhancement effects, Wolff assumes a strongly localised potential created by an unfilled impurity d-shell such that resonance scattering of host conduction electrons is only possible for sufficiently strong interaction with the impurity. That is to say that Wolff model is expected to work best with an impurity in an exchange-enhanced host, e.g. a 3d metal in a 4d host.

The s-d model does not describe experiment for the reasons given above and the Anderson model as it only applies to nonmagnetic materials (a consequence of the Hartree-Fock approximation). The major objection to the Wolff model is that it does not show a resistance minimum.

In 1964, Kondo showed that the exchange scattering cross section diverges at low temperatures when one assumes an impurity spin S interacts with conduction electrons at the impurity via an isotropic s-d Hamiltonian $\mathcal{H}_{ex}$, viz:

$$\mathcal{H}_{ex} = -J\Omega\, \underline{S}\cdot\underline{s} \ , \quad J<0 \qquad 2.13$$

where J is the s-d exchange coupling constant,
Ω is an atomic volume.

In deriving this result Kondo partially explained the phenomena of the resistance minimum, and also a resistance maximum occurring at lower temperatures on the basis of this s-d type model (Kondo, 1969). For experimental details of the various dilute alloy systems one may refer to van den Berg (1964), Heeger (1969) and Rizzuto (1974). To indicate how Kondo arrived at a reasonably accurate (for the time) description of the experimental situation, we will consider the following.

The resistivity of dilute alloy systems may be characterised by one of the curves in figure 2.2.

Figure 2.2 Typical Resistivity/Temperature Curves

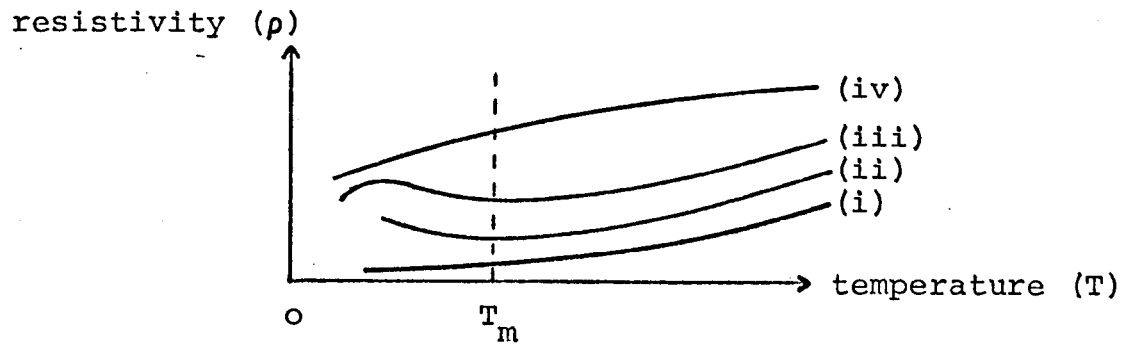

Curve (i) is that of a nonmagnetic alloy with its temperature variation due to lattice scattering and the residual resistivity at T = 0 K due to impurity scattering. An impurity which remains magnetic on alloying gives curve (ii) with T_m usually $\simeq$ 10 - 20K. If one increases the concentration of the impurity over that which gave curve (ii), then curve (iii) results with the onset of magnetic ordering. Further increase in concentration moves the minimum to high T_m, until it disappears as in curve (iv). The experimental evidence is that the maximum only occurs in relatively high concentration alloys. The resistance minimum always seems to occur with the formation of a localised moment, and an example of this was shown by Sarachik et al. (1964). She used various proportions of niobium to molybdenum as host alloys, and introducing $\sim$ 1 at. % iron as impurity found a concentration-dependent transition (via susceptibility measurements) from moment formation to no-moment formation at 60% Mo, 40% Nb. The latter showed no resistance minimum whilst it was evident in the former. Knook (1962) has also shown this correspondence by alloying the second row transition elements with gold as host whence only for Mo is there a minimum and only in this system is there a negative magnetoresistance. Kondo, following Kasuya (1956) and Yosida (1957) took the perturbation due to the impurity to be the sum of exchange and spin-independent

scattering, and also including the Zeeman energy of the impurity spins derived the incremental resistivity to be (Wilson, 1953) :

$$\Delta\rho = (2m_o/zNe^2)\left(\int(-df/dE)\left(\tau\uparrow(E) + \tau\downarrow(E)\right)dE\right)^{-1} \qquad 2.14$$

where z = valence difference
N = total number of impurities/unit volume
df/dE = Fermi function
$\tau\uparrow,\downarrow$ = relaxation time for spin up, down
E = energy relative to Fermi energy E_F.

The resistance minimum is not implicitly contained in equation 2.14 because the calculation is inadequate at low temperatures where the Zeeman splitting remains less than kT, and the value of τ^{-1} is taken to be a constant to first order. Going therefore to higher order in τ, an expansion about the Fermi surface gives :

$$\tau(E) = \tau(E_F)\left(1 + \alpha(E-E_F)/E_F + \beta((E-E_F)/E_F)^2 + \text{- - - -}\right) \qquad 2.15$$

where α, β, - - - are coefficients. The third term makes a contribution to the resistivity but as it is of the order $(kT/E_F)^2$, it is too small to explain the phenomenon in the large number of systems in which it has been observed. Returning to equation 2.13, it can be shown (Kondo, 1964) that to second order the matrix elements of scattering events are:

$$(J/N)^2(S_Z^2 + \tfrac{1}{2}(S_+S_- + S_-S_+))\sum_{k''} 1/(E_k - E_{k''}) + (J/N)^2(S_-S_+ - S_+S_-)\sum_{k''}(f_{k''} - \tfrac{1}{2})/(E_{k''} - E_k) \qquad 2.16$$

For potential scattering, the S+, S- terms are replaced by V^2 and the term involving the Fermi function vanishes.

The other term in equation 2.16 is about J/E_F times smaller than a first order calculation (which gives $-(J/N)S_z$), thus showing that the second order processes are very small. This does not hold for exchange scattering where $S_+S_- \neq S_-S_+$. It can be shown that for this case where the spins do not commute, $\tau(E)$ may be written as :

$$\tau_s(E)^{-1} = (2\pi d_s\, c/h)S(S+1)J^2(1+4Jg(E)) \qquad 2.17$$

where $g(E) = N^{-1}\sum_{k''} (f_{k''}-\frac{1}{2})/(E_{k''} - E)$

To proceed with the calculation a simplifying assumption that the density of states/spin/impurity atom (d_s) is in the form of a square well potential is made :

i.e. $d_s(E) = d_s$ when $-D \leq E \leq D$

$= 0$ otherwise

and $2D \simeq$ width of the conduction band.

Thus $g(E) \simeq d_s \ln \left| E/D \right|$ 2.18

Substituting equation 2.17 into equation 2.14 and expanding in $Jg(E)$ results in :

$$\Delta\rho = C\, J^2 S(S+1)(1+4Jd_s.\ln\,(kT/D)) \qquad 2.19$$

where $C = 2\pi\, d_s c/\hbar$

This last well know equation shows that in the second Born approximation the resistivity diverges logarithmically for negative J as the temperature is reduced. This divergence arises from the dynamical nature of the spin system and the singularity at T = 0 K is due to the sharpness of the Fermi surface. The sign of J is determined by the relative proportions of the admixture interaction between s and d electrons (negative J) and the direct exchange interaction

(positive J). An expression for the antiferromagnetic exchange coupling constant J is :-

$$J = V_{sd}^2((E_d - E_k,)^{-1} + (E_k - E_d - U)^{-1}) \qquad 2.20$$

where E_k ,E_k, = s-wave resonance energies

The total resistivity of a dilute magnetic alloy may be considered to be made up of terms due to lattice scattering, the impurity potential difference and the spin scattering, i.e :

$$\rho = aT^5 + c\rho_A + c\rho_M(1+4Jd_s\ln(kT/D)) \qquad 2.21$$

where a = lattice constant (phonon term)

ρ_A = temperature-independent constant proportional to valence difference

$\rho_M = C\ J^2S(S+1)$

Differentiating equation 2.21 with respect to T and equating with zero gives a value for the resistance minimum temperature (T_{min}) :

$$T_{min} = (4|J|d_s\rho_M/5a)^{1/5}c^{1/5} \qquad 2.22$$

Equation 2.21 has been shown to explain the logarithmic behaviour of a number of systems (e.g. AuFe, MacDonald, 1962), and the resistance minimum occurring in the CuFe system follows equation 2.22 (Franck et al., 1961) very well. Equation 2.21 is expected to be valid in the region where the impurity spin splitting is small compared with the kT. The value of J is usually about -0.2eV (Jaccarino, 1967).

In a similar fashion to the above various other physical parameters may be deduced, for instance the magnetic susceptibility has been found by Yosida and Okiji (1965) to be :

$$\chi = \chi^{o}(1+4J^{2}d_{s}^{2}\ \ln(kT/D))(1-2Jd_{s}\ln(kT/D))^{-1}) \qquad 2.23$$

where $\chi^{o} = (2\mu)^{2}S(S+1)/3kT$

The other experimentally-determined quantities may be referred to in various review articles, notably Kondo (1969), Heeger (1969), Fischer (1971) and Rizzuto (1974).

Important a step forward as it was, Kondo's extension of the s-d model to second order in the Born approximation must be regarded only as indicative of the actual physical processes going on, not a true description of the processes themselves because the perturbation method breaks down as T tends to zero below a characteristic temperature $T_K = (D/k)\ \exp\ (-2|J|d_s)$. Various methods have been presented to overcome this, but as it is beyond the scope of this review to discuss them due to the complicated nature of the mathematics involved, the main results of these authors may be referred to in the review by Heeger (1969) and Fischer (1971) and a summary of the end results of the many theories is given in table 2.2. In many cases it is difficult to distinguish experimentally between the different theories because many of the expressions contain lnT terms, thus making extended temperature measurements desirable, but which may not be attainable for several reasons (see for example Chapter 4). One interesting aspect that may be worth pointing out here is that below T_K a quasi-bound state is expected to form (Daybell and Steyert, 1968). Below T_K no logarithmic divergence occurs because it appears that a polarised cloud of impurity-spin compensating conduction electrons from the host will screen the spin of the localised moment, thus causing the net spin/impurity as seen by, for example, a static susceptibility experiment, to tend to zero as T tends to zero. This leads to the conjecture that many systems that exhibit no localised moment below some temperature may in fact be high temperature 'Kondo' systems. This is quite likely considering that the characteristic temperature has an exponential dependence on J and d_s and can therefore

Table 2.2 Summary of theoretical formulae derived by various authors (e.g. see Heeger, 1969).

a) Resistivity ($T \ll T_K$)

$$\Delta\rho \simeq 1 - A/\ln^2(T/T_K)$$
$$" \quad 1 - B((T/T_K)\ n\ T/T_K)^2$$
$$" \quad 1 - C(T/T_K)^2$$

b) Specific heat ($T \ll T_K$)

$$\Delta C \simeq (T/T_K)^{0.57}$$
$$" \quad T^{\frac{1}{2}}$$
$$" \quad T\ln(T/T_K)$$
$$" \quad T/T_K$$

c) Magnetic susceptibility

$$\Delta\chi \simeq \mu_{eff}^2/T_K \quad (T \simeq 0K)$$
$$" \quad S(S+1)-(S+\tfrac{1}{2})+(S+1)(1+a/\ln T/T_K)/\ln T/T_K$$
$$T<T_K \quad " \quad T^{\frac{1}{2}}$$
$$" \quad 1 - (T/T_K)^2$$
$$T \simeq T_K \quad " \quad \mu_{eff}^2/(T+\theta),\ \theta \simeq -5T_K$$
$$" \quad \mu_{eff}^2(T)/3kT$$
$$T \gg T_K \quad " \quad \mu_{eff}^2/3k(T+\theta),\ \theta \simeq 0\ K$$

allow T_K to vary over say a 10^6 range (Schrieffer, 1967). Thus the possibility exists of changing T_K by the introduction of another metal in the base (e.g. see Star, 1968) and causing moment/no-moment formation to take place, presumably as may explain the experiments of Sarachik et al., 1964, and may be explored (with reference to the present work) in the system GaAlMn.

The expression for T_K given above has been shown to be fairly well obeyed (Daybell and Steyert, 1968) for 3d impurities in hosts such as copper and gold when J is replaced by SJ_d with d_s and J_d being constants (for each host). Thus the change in $\ln T_F$ in going across the series from Ti to Ni is due to the variation in S, and confirmation by experiment of the V-shape in $\ln T_F$ vs. impurity having its minimum at Mn shows Hund's first rule is an important factor here (Wohleben and Coles, 1973).

A "rival" set of theories dealing with localised magnetic moments has recently come to prominence with the appearance of papers by Caplin and Rizzuto (1968), Rivier and Zuckerman (1968), Zuckerman (1972) amongst many others. This deals with the problem in another way and is usually considered to be appropriate to systems that are not strongly magnetic in the Curie-Weiss sense (e.g. AlMn). Experiments on palladium (Clogston et al., 1962) originally led to the ideas of spin fluctuation utilising the Wolff model (Lederer and Mills, 1967) because the static spin susceptibility is about ten times the value expected from the Pauli paramagnetic susceptibility as deduced from the free-electron model (Budworth et al., 1960). The Coulomb interactions of the d electrons within an atom are exchange-enhanced in the Hartree-Fock theory by an amount $(1-U_o d_d)^{-1}$ where U_o is the intra-atomic Coulomb interaction and d_d is the density of states of the d electrons at E_F. The Stoner (1938) enhancement factor from specific heat measurements is found

to be ~10 (Doniach and Engelsberg, 1966), and as $(1-U_o d_d)$ is very close to zero, one may expect to find low-frequency fluctuations in the d-electron spin density. Alloying iron and cobalt in palladium has given anomalously large impurity moments, of the order of 10 or 12 μ_B (Shaltiel et al., 1964), thus one expects these giant moments to be caused by long range polarisation of the conduction electrons of the host centred round the impurity (RKKY interaction). This has been found to be the case (Low and Holden, 1966) as NMR (Ehara, 1962) and Mossbauer experiments (Craig et al., 1965) show the impurity moments have lower ($\sim 3\ \mu_B$) moments in the impurity cell. Thus a host which is strongly exchange-enhanced may be sufficiently perturbed about an impurity site for long-lived moments to exist in a ferromagnetic sense. This presumably is caused by the coupling due to Hund's rule. Schindler and Rice (1967) investigated the typical spin fluctuation system PdNi and found that the alloy became magnetic when the concentration of nickel exceeded about 2 at.%. Their data was examined by Lederer and Mills (1967) who conclude that the region around the impurity is likely to be closest of all to the magnetic instability limit (i.e. where $U_o d_d = 1$), thus the amplitude of the spin density fluctuations in the d band is likely to be a maximum here. The electrical resistivity is due mainly to s-electron scattering from these fluctuations (the effective mass of the d electrons is much larger than the s electrons because of the fluctuations (Doniach and Engelsberg, 1966) and as the flucutation amplitude is temperature-dependent, the impurity resistivity is also. Lederer and Mills find a T^2 dependence dominating the resistivity (i.e. dominating the T^5 term) below 9 K. This is because the scattering mechanism is an electron-electron collision (Baber, 1937) with s electrons inelastically scattering from the local d-electron spin fluctuations, leading to a linear concentration-dependent resistivity. These results agree with experiment when $c \leq 1$ at.%.

The localised spin fluctuation model (l.s.f.) should be appropriate for nearly magnetic 3d impurities in 4d and 5d hosts from the same or similar columns of the periodic table. Thus IrFe has been shown to be adequately described by the l.s.f. model (Kaiser and Doniach, 1970) where host and impurity have a somewhat similar electronic structure. Similarly RhFe fits the l.s.f. model, but going to either side of rhodium gives RuFe a nonmagnetic system and PdFe, which is ferromagnetic.

Kaiser and Doniach have extended the approximate calculations of Lederer and Mills (1967) to greater temperature ranges and have derived a universal curve for resistivity showing that the T^2 law as discussed previously gradually changes to a linear T dependence. This change sets in at about $0.25T_s$ where T_s is a scaling temperature characteristic of a l.s.f. system and is given by $kT_s \simeq E_F(\alpha(T))^{-1}$ where $\alpha(T)$ is the exchange enhancement factor at the impurity sites. Fitting to the systems PtFe (Loram et al., 1972) RhFe, IrFe, PdNi, the values of T_s that are found are: $\sim 0.2K$, $<1.5K$, $\sim 30K$, $\sim 80K$ respectively. If one were to assume that RhFe and IrFe were Kondo systems and fit a Curie-Weiss law the characteristic temperatures T_K here would be $\sim 10K$ and $\sim 100K$ respectively. Kaiser (1971) has proposed a means whereby the applicability of the l.s.f. model for these systems can be tested. He suggested that measuring the thermal resistivity and the Lorentz number temperature dependence gives a direct means of showing which of the characteristic temperatures is relevant though very few results of this have been reported, and these appear to indicate that no new information is gained beyond that given already by thermopower and resistivity measurements (Star et al., 1971).

Rivier and Zlatic (1972) have considered alloys exhibiting a resistance minimum and applying their theory notably to AlMn have shown that in these cases the Anderson (1961) model is needed for a description rather than the Wolff (1961) model. In essence the conduction electrons are scattered from an extra localised d orbital (v.b.s.) of spin up or down caused by the perturbing presence of an impurity. The

v.b.s. which is undergoing spin fluctuations has its spin structure for a lifetime τ_{sf}, thus implying that at high temperatures where $T > T_{sf}$, ($\tau_{sf}^{-1} = kT_{sf}$) such that thermal fluctuations are less long-lived than the spin fluctuations, the resistivity becomes logarithmically temperature dependent (Rivier and Zuckermann, 1968). Using a Green function formalism, Rivier and Zlatic find that the resistivity due to the unrenormalised l.s.f.'s is given by :

$$\rho = (1 - 2\ln 2 - (2x)^{-1} + 2\psi(2x) - 2\psi(x))^{-1} \qquad 2.24$$

where $x^{-1} = 2\pi kT/M$

and $M^{-1} = Ud_d \tau sf$

$\psi(x)$ = digamma function

This is shown in figure 2.3 below plotting ρ against the reduced temperature x^{-1}. Three main temperature regimes are distinguished :

(i) $\underline{x^{-1} < 0.4}$

This is a low temperature region for AlMn as can be seen from substituting for the parameters of this system :

i.e. $Ud_d \simeq 0.9$

$T_{sf} \simeq 900K$

so as $T = x^{-1} T_{sf} (2\pi Ud_d)^{-1}$

then $T \leq 64K$

Equation 2.24 in this case gives:

$$\rho = 1 - (T/\theta_1)^2 \qquad 2.25$$

where $\theta_1 = 2^{\frac{1}{2}} T_{sf} (Ud_d \pi)^{-1} \simeq 450K$

θ_1 is in agreement with the experimental result of $530 \pm 30K$ (Caplin and Rizzuto, 1968).

(ii) $\underline{0.9 < x^{-1} < 2.1}$

This is an intermediate region where the temperature, calculated similarly to (i) above, is $140K < T < 330K$.

Equation 2.24 now becomes :

$$\rho = \alpha'(1 - T/\theta_2) \qquad 2.26$$

where $\alpha' = 1.074$

$\theta_2 = 2.83\ \theta_1 \simeq 127$OK

Thus the resistivity is linear here, in good agreement with Csetenyi et al., (1972) and only fair agreement with Babic et al., (1971) who found $\theta_2 = 160$OK.

(iii) $6.5 < x^{-1} < 9$

In this region where 100OK < T < 140OK, a logarithmic law holds :

$$\rho = 3.622 - 0.565 \ln T \qquad 2.27$$

T is above the possible Kondo temperature of ~53OK for AlMn , and equation 2.27 is characteristic of magnetic impurity systems.

Above 140OK, $\rho \longrightarrow 0$ as T^{-1}.

Figure 2.3 Resistivity vs. reduced temperature x^{-1}
(after Rivier and Zlatic)

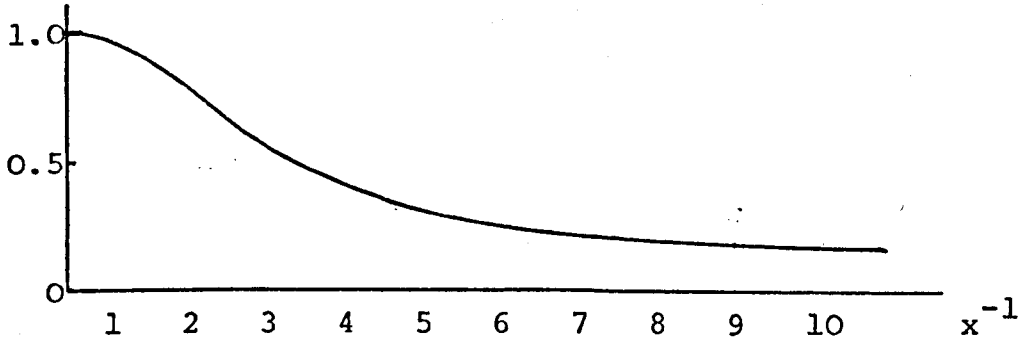

Region (ii) is only brought about by a coupling of regions (i) and (iii) at their common point of inflexion, though it may be derived via an interpolation formula originally suggested by Hamann (1969).

A model which takes into account the fact that some dilute alloys exhibit free-spin behaviour in magnetic fields, negative magnetoresistance and magnetisation which can be expressed as a function of H (field)/T (e.g. PdFe), in contrast to others that do not (e.g. RhFe) has been proposed by Loram et al. (1972). The positive temperature coefficient of the resistivity for Pd and Pt containing Ni and Co for instance is also predicted as is the more usual negative coefficient for Pd and Pt with Cr as an impurity. This has been achieved in a phenomenological manner by using partial wave analysis and assuming a probability of thermally excited spin fluctuations which gives the mean-square spin/impurity $\langle m^2 \rangle$ to be of order $\Delta\chi T^2/T_{sf}$ for low temperatures (where $\Delta\chi$ is the impurity susceptibility), and of order $\Delta\chi kT$ for high temperatures when $T \gg T_{sf}$. Loram et al. show the impurity resistivity is given by :

$$\Delta\rho = \Delta\rho_o + (\pi^2/5)c.\rho'.\cos(\pi Z/5\langle m^2\rangle)) \qquad 2.28$$

when $T \ll T_{sf}$

and

$$\Delta\rho = \Delta\rho_o + 5c.\rho'.\cos(\pi Z/5).\sin^2(\pi S/5) \qquad 2.29$$

when $T \gg T_{sf}$

where $\Delta\rho_o = 5c.\rho'.\sin^2(\pi Z/10)$ i.e. T = 0 resistivity

ρ' = unitarity limit

Z = valency difference

S = value of the order of impurity spin from $\Delta\chi$

In going from one regime to the other, a monotonic variation from equation 2.28 to 2.29 is expected to occur. The sign of the temperature coefficient of the resistivity is determined by the value of Z, which is given by the phase shifts η_l (see chapter 6). Introducing reasonable values for these with l = 0, 1, 2 gives fair results for the experimental resistivity data of Pt and Pd alloyed with the first-row transition elements.

It may seem at first sight that a dilute alloy would usually fall into a basically well-defined category ie Kondo system, l.s.f. system but various authors have concluded that it is difficult to make such a rigid decision. Indeed reinterpretations of experiments (e.g. that of AuV of Kume (1967) by Rizzuto et al., 1973) have been made that show it is possible to make more accurate fits to later theories than with those available at the time. It seems fair to say that the present theoretical situation is such that one cannot compare the two basic systems and find a tangible difference that would imply a clear-cut description (for the range both above and below the characteristic temperature) of belonging to either theory (see for instance Narath and Weaver, 1969; Caroli et al., 1969; Dworin, 1971). It is possible that an improper subtraction of the host properties at low temperatures has caused some of the confusion though for the resistivity experiments, recent work by Caplin and Rizzuto (1971) which has determined more accurately than before the phonon resistivity (for temperatures below the Debye temperature) for a variety of metals allows a comparison of systems where a T^2 law initially holds (Rizzuto et al., 1973).

Under a Kondo-type description (where the lifetime of the impurity spin is taken to be infinite) a symmetry of the lnT behaviour about T_K in $\Delta\rho$ experiments is expected. In fact it is found that the range of lnT behaviour for $T < T_K$ is less than when $T > T_K$. To account for the well verified T^2 law one needs to go over to the l.s.f. theory. Evidence seems to suggest that detailed predictions of dilute alloy systems are in general given more accurately by a l.s.f. description (Rizzuto, 1974).

A trend away from the itinerant aspects of the local moment problem towards a more ionic-based approach appears to be taking place at present (Wohlleben and Coles, 1973). Previous models in effect took all the valence electrons from

the impurity shells without retaining intraionic correlations due to the then localised electrons. These effects (which are the basis for Hund's rule) should be retained for an accurate generalised description of the magnetic behaviour of an impurity. The justification for not doing so in previous models based on the s-d exchange Hamiltonian was that they correctly predicted such experimental facts as the resistance minimum and a peak in the specific heat vs. temperature curves for dilute magnetic alloys. The conduction electrons were then treated as if they were non-interacting quasi-particles. An alternative model has been proposed by Hirst (1970) who treats the localised electrons accurately and takes the correlations between the conduction electrons into account by using a mean-field approximation. He assumes that to zero-order the localised orbitals are approximately equal to the free atom orbitals and so the occupation numbers of the magnetic shells are integers in accordance with Hund's rule. The various unsplit energy levels E(n) corresponding to each integer value fall roughly on an interpolated parabola given by :

$$E(n) = \tfrac{1}{2}(n - n_m)^2 F_o + \text{constant} \qquad 2.30$$

where $n_m = \tfrac{1}{2} - V_o/F_o$

n = integer value

F_o = lowest-order Slater Coulomb integral

V_o = nuclear potential energy

Each E(n) in fact represents a group of levels formed from the many-electron ionic states which may be split by various interactions, e.g. spin-orbit coupling. The ground state is taken to be at n_o so excitation to a higher state is achieved by adding or subtracting a conduction electron, and the minimum energy required to reach this higher level is given by E_{exc}. The position of the minimum of the parabola (n_m) is determined by the relative strengths of the Coulomb repulsion and the attractive potential well. A parameter such as pressure could change n_m though Hirst leaves it as

a parameter to be determined experimentally. It is expected that n_m should be similar to n_o because the model assumes the screened impurity to be similar to a neutral atom. Figure 2.4 indicates this general scheme:

Figure 2.4 Energy levels in the ionic model

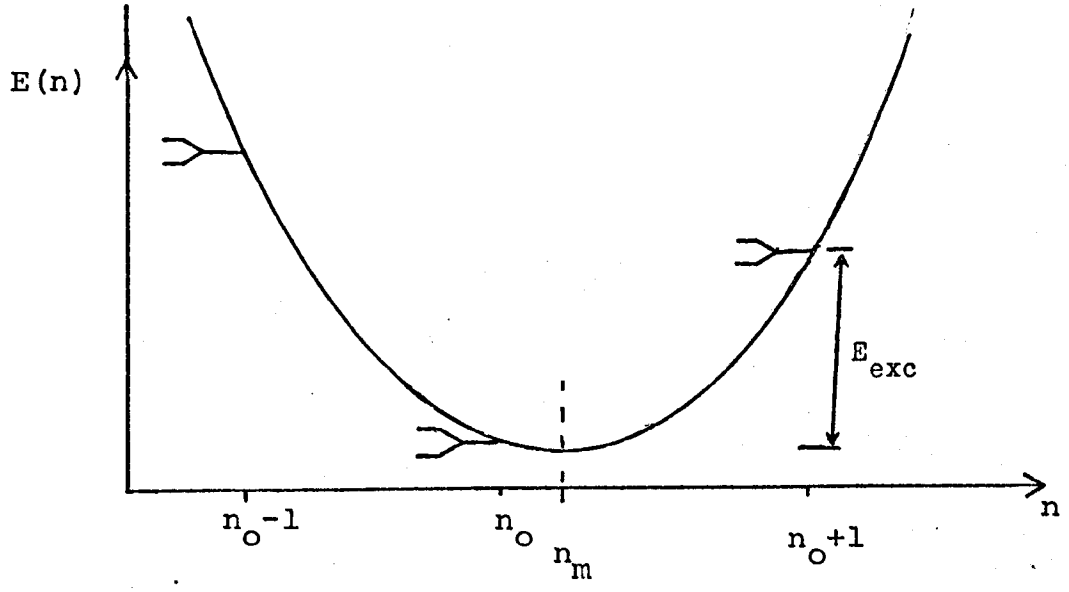

However, n_m can be treated as a continuous variable which has a periodic effect on E_{exc} as shown in figure 2.5. The energy E_{exc} is a mixing interaction caused by electron transfer from the v.b.s. formed at the localised shell to the conduction band and back. In effect a forbidden band gap of width E_{exc} is formed with the alloy being termed magnetic if E_{exc} is greater than the v.b.s. width i.e. :

$$E_{exc} > \Delta \qquad 2.31$$

Figure 2.5 Periodic variation of E_{exc} with n_m

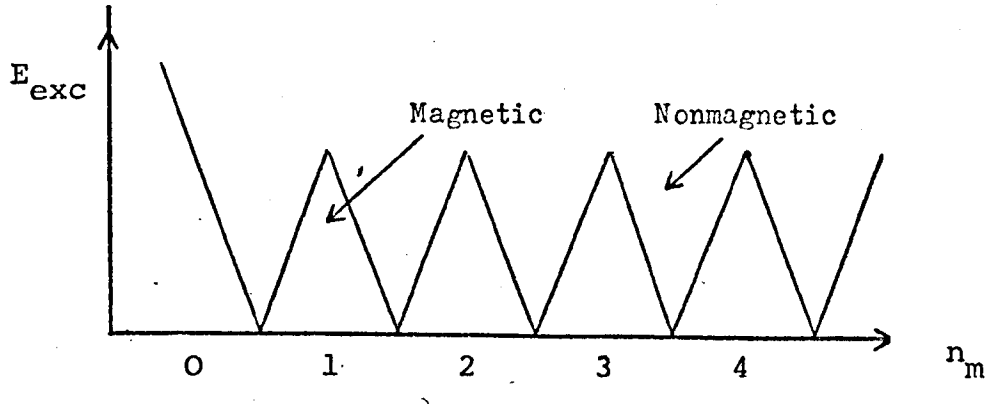

Values of Δ for 3d impurities are expected to be $\sim$1eV and $\sim$ 0.01eV for 4f impurities, so from figure 2.4 it can be seen that for n_m close to an integer value the condition for magnetic behaviour as given by equation 2.31 can be satisfied as E_{exc} can range from 0 to $\sim$10 eV. The Cu 3d impurity series of alloys evidently have n_m near to integer values. For half-integer values of n_m the inequality is $E_{exc} < \Delta$, giving rise to nonmagnetic behaviour (e.g. Al 3d impurities). In this case the well-defined configuration states become blurred with the eigenstates involving mixtures of different spin states, the magnetic behaviour being wiped out by the relatively large coupling to the conduction electrons.

A further consequence of Hirst's model is that when $E_{exc} \simeq \Delta$ then the mixing interaction cannot be used as a perturbation in his finite-order treatment and the method breaks down, leading to nonmagnetic behaviour. This result follows from the generalisation of the original Kondo model, where nonmagnetic behaviour is due to spin-condensation. The equivalence is shown by replacing Kondo's simple exchange coupling J with Hirst's more general interaction H_{eff}, resulting in a different characteristic temperature T_K i.e.

$$T_K \simeq T_F \exp(-H_{eff} d_s)^{-1} \simeq T_F \exp(-E_{exc}/\Delta) \qquad 2.32$$

where $H_{eff} \simeq -|V_{sd}|^2/E_{exc}$

Thus from this point of view the Kondo-type condensation does not fully break up the ionic configuration except at half-integer values when $T_K \simeq T_F$ ($\sim 5 \times 10^4$K). The magnetic moment is centred about an integer value, the region where the moment remains well-defined depends on the value of E_{exc} relative to Δ i.e. minimum T_K and so for 3d impurities the intervening nonmagnetic region is fairly wide, much more so than for 4f impurities where Δ is smaller. This explains why the Al3d series are close to being magnetic despite n_m in this case probably being half-integer.

It has been pointed out (Hirst, 1971) that due to the scarcity of data little is known about the possible spin state of 3d impurities in non-cubic host environments. In h.c.p. metals for instance an unquenched L would produce a large anisotropy which should be apparent in a static susceptibility experiment. In fact for an orbital doublet being the lowest energy level the anisotropy would be 100% (see Chapter 5) and it is expected that an anisotropic Curie-like law would hold, even about $\sim$ 100 K. A non-S state ion is likely to be found for 3d impurities in an h.c.p. host so searching for an anisotropy in such a system would be useful method for determining the spectroscopic state of such impurities.

2.3 Experiment

In view of the excellent reviews by Heeger (1969) and Rizzuto (1974) on the present experimental situation, no attempt at a similar comprehensive review need be undertaken here. Instead, systems that appear typical of a particular group, or those to amplify a theoretical point will be presented. Because of the state of flux of the theories (see above) it would be unwise to tie a particular experiment firmly to a particular theory, so following Rizzuto (1974) trends will be pointed out and a general classification according to whether an approximately temperature-independent, strongly temperature-dependent or Curie-like susceptibility is followed will usually be made. Confirmation of the information gained will be made where possible with the resistivity information on the same or similar systems.

Those systems where small or no temperature dependence is seen, i.e. that may be described by a Pauli-type susceptibility law are exemplified by for instance AlV (Aoki and Ohtsuka, 1969), BeNi (Klein and Heeger, 1966) and CuCo (Tournier and Blandin, 1970). Resistivity experiments on

these same systems usually reinforce belief in this behaviour which, with reference to the above remarks, may indicate the temperature range over which the experiments were done was below the characteristic temperature where spin-compensation sets in. One may remark at this point that the complementarity of these two parameters (ρ and χ) would allow the supposition that the two experiments are really just measuring different aspects of some fundamental phenomenon. This will appear clearer in the next class of systems.

YCe (Nagasawa et al., 1968), MoCo (Narath et al., 1970) and AuFe (Loram et al., 1970) are examples of systems where a Curie-Weiss law holds, though with an increasingly smaller θ , which ranges from $\sim$ -40K in the first case to $\sim$ -0.4K in the last. In fact it is possible to find θ varying by five orders of magnitude with the inclusion of AuV where $\theta \simeq$ -300K (Kume, 1967) and AuMn where $\theta <$ -0.01K (Hurd, 1969), Thus this classification is necessarily flexible with systems that are borderline magnetic or nonmagnetic. The temperature variation from resistivity measurements shows the range of T^2 to lnT behaviour as predicted by Rivier and Zlatic, 1972.

The third group whose behaviour is characterised by a Curie law (e.g. AgGd) or that more usually of a free ion subjected to a crystalline environment contains notably the rare earths in a gold or silver host (e.g. Murani, 1970; Williams and Hirst, 1969). From the high temperature data the effective impurity spin value is usually in good agreement with the free ion value. Whilst the difference between the first two groups may merely be due to the scaling parameter i.e. the characteristic temperature (in the present notation θ), the state of the ion in this last group appears different - presumably a cause of the energy levels resulting from the crystalline electric field (see Chapter 5).

With reference to the present work, it is of interest here to study in some more detail the reported (Rizzuto, 1973) values of the zero-temperature susceptibility ($\Delta\chi_o$) and

zero-temperature resistivity ($\Delta\rho_o$) for the 3d metals in aluminium and compare them with those of other hosts (figures 2.6 and 2.7).

Figure 2.6 Zero-temperature susceptibility of 3d metals in various hosts (after Rizzuto, 1974).

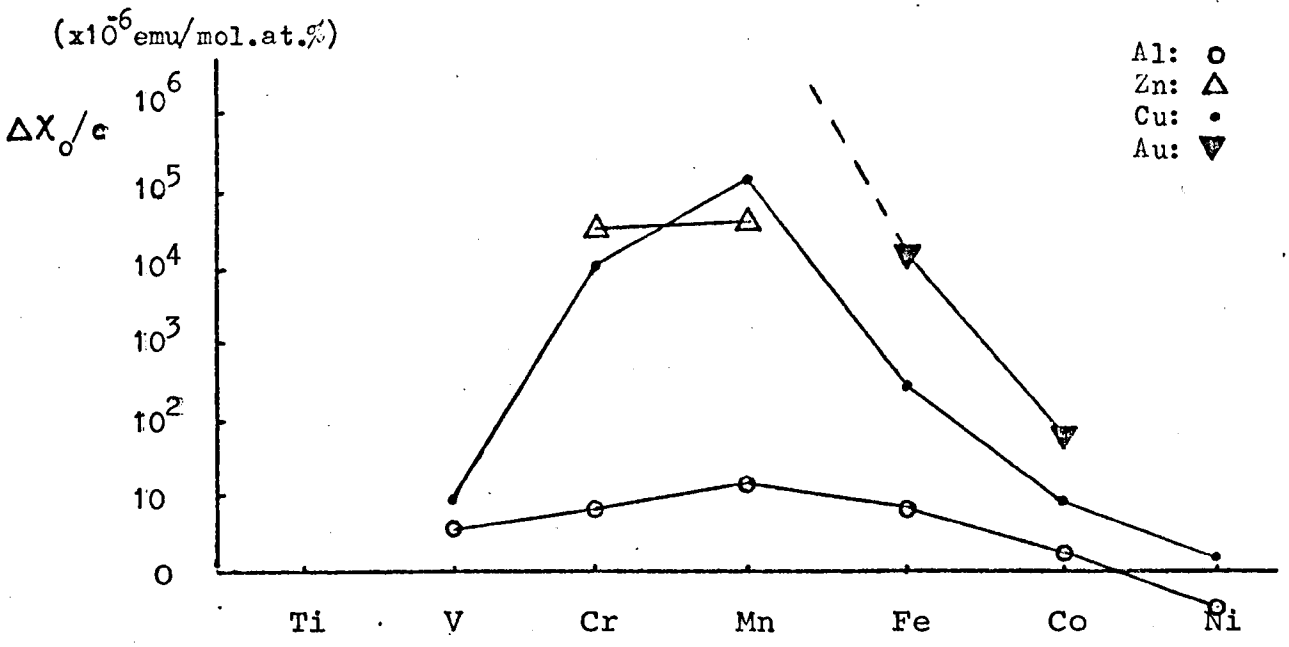

Figure 2.7 Zero-temperature resistivity of 3d metals in various hosts (after Rizzuto, 1974).

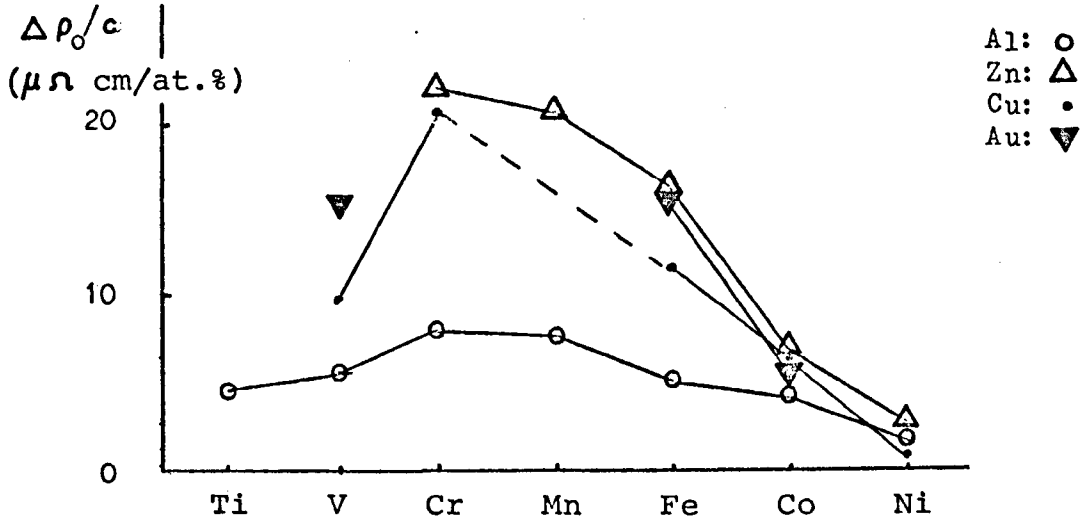

An important conclusion from figure 2.6 is that there is a very small variation of $\Delta\chi_o$ with 3d impurity for aluminium compared with zinc, copper and gold, and suggests that by using the aluminium data as the basic additional contribution caused by a Pauli-like effect, then the other data can be approximately scaled by an enhancement factor η (Rizzuto, 1974), where

$$\Delta\chi_o/c = \mu_B^2 . \eta . d_d + R \qquad 2.32$$

(where R is an orbital-type contribution).

It is tempting to try a similar imposed analysis on the resistivity data of figure 2.7 where the behaviour along the 3d series is similar for aluminium and zinc. This is what Rizzuto et al., (1973) did for a number of systems that show a low temperature T^2 dependence where they plotted a normalised resistivity of $\Delta\rho(T)/\Delta\rho_o$ against T/θ_R, where $\Delta\rho(T)$ is the impurity resistivity at finite T and θ_R is a characteristic temperature such that the equation 2.33 given below holds:

$$\Delta\rho(T) = \Delta\rho_o\ (1-(T/\theta_R)^2) \qquad 2.33$$

The AuMn, AuCr and CuMn systems do not follow the smooth curves as shown by the other alloys in figure 2.7 because magnetic moments have formed and a spin-splitting has occurred, thus causing a double peak (see Chapter 6).

The results of the analysis using equation 2.33 are shown below in figure 2.8.

Figure 2.8 Normalised resitivity/temperature in some dilute alloys (After Rizzuto et al., 1973)

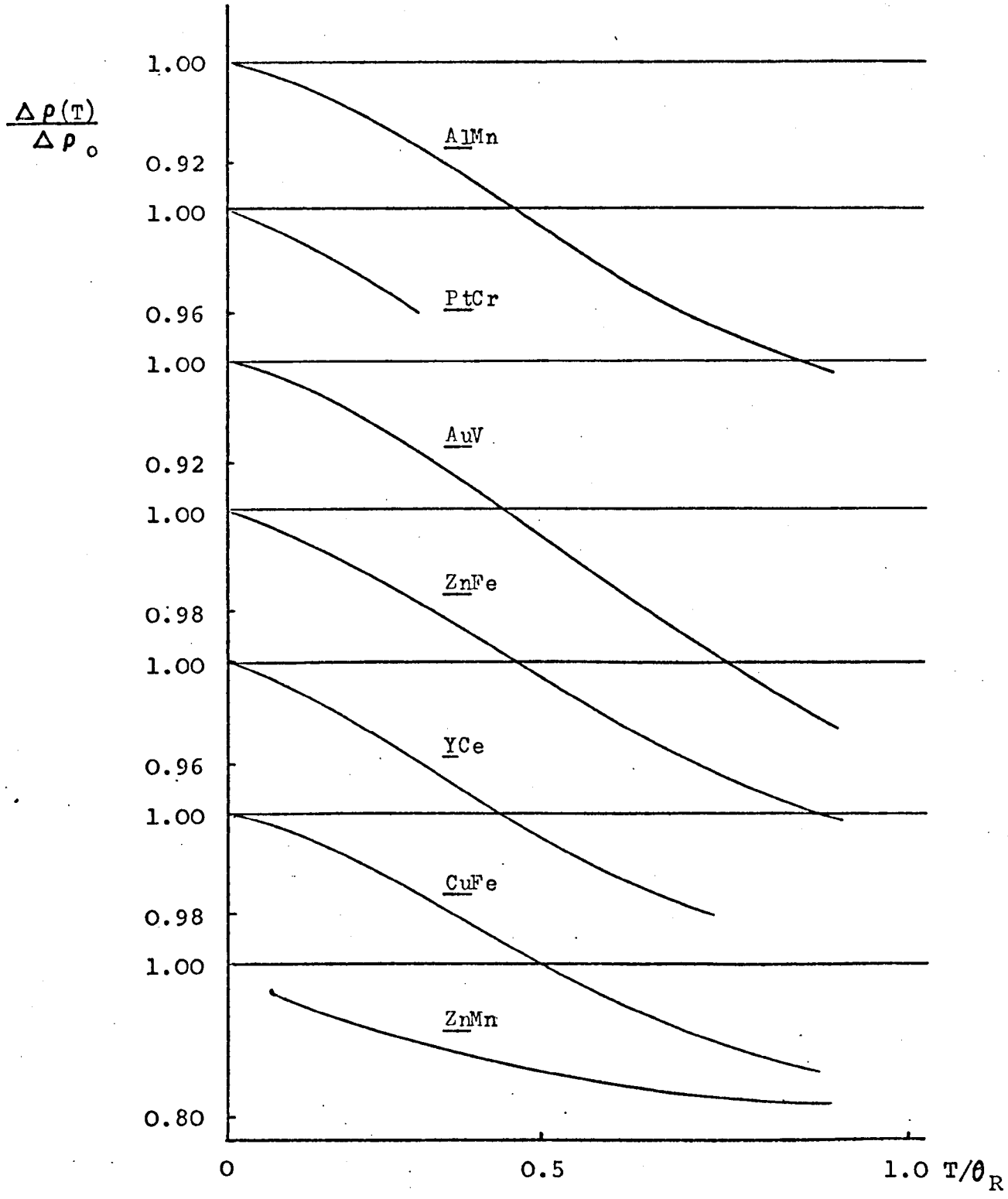

After subtraction of the host phonon contribution to the resistivity (Caplin and Rizzuto, 1971), the best fit in most cases was found to be a linear T law over a region from $\sim 0.1\,\theta_R$ to $\sim 0.5\,\theta_R$ though some systems e.g. AuV

and AlMn extend the fit to higher regions. The scaling temperature θ_R taken to fit each temperature was :

AlMn : θ_R = 530K

PtCr : " = 200K

AuV : " = 280K

ZnFe : " = 80K

YCe : " = 40K

CuFe : " = 21K

ZnMn : " = 0.9K

It can be seen that the extended linear T law fits best for high θ_R - value systems, in agreement with general conclusions given previously. A T^2 dependence is seen below $\sim 0.1\,\theta_R$ and at about $0.7\,\theta_R$ a lnT appears to set in which is probably where the thermal fluctuation lifetime is comparable with T_{sf} allowing a Heisenberg-type interaction (equation 2.13) to produce the Kondo logarithmic effect. This is certainly so for ZnMn where a lnT law is well documented (Ford et al., 1972) even above θ_R. Thus a previously unconnected series of alloys can be described reasonably well by a unifying theory based on the l.s.f. concept. The susceptibility results for aluminium as a host are not generally changed from those taken at 1363K (Flynn et al., 1967). It may turn out therefore that a suitable theoretical description of a dilute alloy system hinges on whether the impurity is magnetic or not in a Curie-Weiss sense and where, in relation to the characteristic temperature θ, (derived either by susceptibility or resistivity measurements - in most cases they appear to be the same) the experiment is performed.

It must be stressed that there are many spurious interaction effects that can complicate interpretation of an experiment.

The most common is the ordering effect (e.g. RKKY interaction) where below some temperature there is a deviation usually proportional to concentration. Thus the CuMn magnetisation experiments of Hirschoff et al., (1971) show a departure from a Curie law even down to 4.2 mppm at very low temperatures, so the only way to exclude this effect is to make sure the alloys are sufficiently dilute that no deviation is apparent. Clustering effects where two or more impurity atoms are in close proximity may result in the superposition of several Curie-Weiss laws and may therefore give the impression of a spin compensation effect. Deviations from Matthieson's rule are important in many cases of resistivity measurements and thus it may be better to subtract not merely the host characteristic but host plus "inert" impurity (e.g. Cu, see Chapter 4). As mentioned previously, the host phonon contribution in the aluminium-based alloys has been determined sufficiently accurately to have more confidence in the detailed temperature behaviour of several other alloys (Campbell et al., 1971).

An effect that has been put down basically to the relevant host and impurity energy widths being comparable is the positive temperature coefficient for the impurity resistivity in cases such as RhMn, RhFe, PtCo, etc. The resistance minimum resulting from a decrease in $\Delta\rho$ with increasing temperature (e.g. CuNi, PtCr) is thought to occur when the impurity v.b.s. energy is less than ~ 0.1 of the host conduction band.

References

Anderson, P.W.,	Phys. Rev.	124,	41, 1961
Anderson,P.W., Clogston,A.M.,	Bull. Am. Phys. Soc.	6,	124, 1961
Aoki,R., Ohtsuka,T.,	J. Phys. Soc. (Japan),	26,	651, 1969
Baber, W.G.,	Proc. Roy. Soc.	A158,	383, 1937
Babic, E., et. al.,	Phys. Rev. Lett.	27,	805- 1971
Bailyn, M.,	Advan. Phys. (Phil. Mag. Supp.)	15,	179, 1966
Blatt, F.J.	Sol.Stat. Phys.,	4,	199, 1957
Bloombergen,N., Rowland,T.J.,	Phys. Rev.,	97,	1679, 1955
Budworth,D.N., Hoare,F.E., Preston,J.,	Proc. Roy. Soc.	A257,	250, 1960
Campbell,I.A., Caplin,A.D., Rizzuot,C.,	Phys. Rev. Lett.,	26,	239, 1971
Caplin,A.D., Rizzuto,C.,	Phys. Rev. Lett.,	21,	746, 1968
Caplin,A.D., Rizzuto,C.,	Aust. J. Phys.,	24,	309, 1971
Caroli,B., Lederer,P., Saint James, D.,	Phys. Rev. Lett.,	23,	700, 1969
Chew, G.F., Low, F.E.,	Phys. Rev.,	101,	1570, 1956
Clogston, A.M., et. al.,	Phys. Rev.,	125,	541, 1962
Craig, P.P., et al.,	Phys. Rev.,	138,	A1460,1965
Csetenyi,E.K., Kedves,F.J., Gergely,L., Gruner,G.,	J. Phys. F.	2,	499, 1972
Daniel,E., Freidel,J.,	Proc. 9th Int. Conf. on Low Temp. Phys. (ed. Daunt, Edwards,...), Plenum Press, N.Y.		933, 1965
Daybell, M.D., Steyert,W.A.,	Rev. Mod. Phys.,	40,	380, 1968
De Faget de Casteljau, P., Freidel, J.;	J. Phys. Radium,	17,	27, 1956
Doniach,S., Engelsberg,S.,	Phys. Rev. Lett.,	17,	750, 1966
Dworin, L.,	Phys. Rev. Lett.,	26,	1372, 1971
Ehara, S.,	J. Phys. Soc. (Japan)	17,	726, 1962
Fischer, K.,	Phys. Stat, Sol.,	46,	11, 1971

Flynn,C.P., Rigney,D.A., Gardner,J.A., Phil. Mag., 15, 1255, 1967

Ford,P., Rizzuto,C., Salamoni,E., Phys. Rev., B6, 1851, 1972

Franck,J.P., Manchester,F.D., Martin,D.L., Proc. Roy. Soc., A263, 449, 1961

Friedel, J., Adv.Phys.(Phil.Mag.Supp), 3, 446, 1954

Friedel, J., Can. J. Phys., 34, 1190, 1956

Hamann, D.R., Phys. Rev. 186, 549, 1969

Hart, E.W., Phys. Rev. 106, 467, 1957

Heeger, A.J., Solid State Physics (ed. Seitz, Turnbull, Ehrenreich), Acad. Press, 23, 283, 1969

Hirschkoff,E.C., Symko,O.G., Wheatley, J.C., J. Low Temp. Phys., 5, 155, 1971

Hirst, L.L., Phys. Kondens, Materie, 11, 255, 1970

Hirst, L.L., Zeit. Physik., 241, 9, 1971

Hurd, C.M., J. Phys. Chem. Sol., 30, 539, 1969

Jaccarino, V., Int. Cong. Magn., Cam., Mass., 1967

Kaiser, A.B., Doniach,S., Int. J. Magn., 1, 11, 1970

Kaiser, A.B., Phys. Rev. B, 3, 3040, 1971

Kasuya, T., Prog.Theoret.Phys.(Kyoto) 16, 45, 1956

Klein,A.P., Heeger,A.J., Phys. Rev., 144, 458, 1966

Knook, B., Ph.D. Thesis, University of Leiden, 1962

Kondo, J., Prog.Theoret.Phys. (Kyoto), 32, 37, 1964

Kondo, J., Solid State Physics (ed. Seitz, Turnbull, Ehrenreich), Acad. Press, 23, 184, 1969

Kume, K., J. Phys. Soc. (Japan) 23, 1226, 1969

Lederer,P., Mills,D.L., Sol. Stat. Comm., 5, 131, 1967

Loram,J.W., Grassie,A.D.C., Swallow, G.A., Phys. Rev., B2, 2760, 1970

Loram,J.W., White,R.J., Grassie,A.D.C., Phys. Rev., B5, 3659, 1972

Low,G.G., Holden,T.M., Proc. Phys. Soc., 89, 119, 1966

MacDonald,D.K.C., Pearson,W.B., Templeton, I.M.,	Proc. Roy. Soc.	A266,	161,	1962
Meissner, W., Voigt, G.,	Ann. Physik.,	7,	761,	1930
Mott,N.F., Jones,H.,	"The Theory of the Properites of Metals and Alloys", O.U.P.,			1936
Murani, A.P.,	Journal of Phys. (Suppl)	C3,	153,	1970
Nagsawa,H., Yosida,S.,Sugawara,T.,	Phys. Lett.,	26A,	561,	1968
Narath, A., Weaver, H.T.,	Phys. Rev. Lett.,	23,	233,	1969
Narath,A., Brog,K.C., Jones,W.H.,	Phys. Rev.,	B2,	2618,	1970
Rivier,N., Zlatic,V.,	J. Phys. F_Metal Phys.,	2,	87,	1972
Rivier,N., Zuckermann,M.J.,	Phys. Rev. Lett.,	21,	904,	1968
Rizzuto,C., Babic,E., Stwart,A.M.,	J. Phys. F,	3,	825,	1973
Rizzuto, C.,	Rep. Prog. Phys. (G.B.),	37,	147,	1974
Rudderman,M.A., Kittel,C.,	Phys. Rev.,	96,	99,	1954
Sarachik,M.P.,Corenzwit,E., Longinotti,L.D.,	Phys. Rev.,	35,	A1041,	1964
Scalapino, D.J.,	Phys. Rev. Lett.,	16,	937,	1966
Schindler,A.I., Rice,M.J.,	Phys. Rev.,	164,	750,	1967
Schrieffer,J.R.,	J. Appl. Phys.,	38,	1143,	1967
Shaltiel, D.,	Phys. Rev.,	135,	A1346,	1964
Star, W.M.,	Phys. Lett.,	26A,	502,	1968
Star,W.M., Gubbens,P.C.M., DeJong, J.J.,	Phys. Lett.,	36A,	15,	1971
Stoner, E.C.,	Proc. Roy. Soc.,	A165,	372,	1938
Suhl, H.,	Phys. Rev.,	138,	A515,	1965
Tournier,R., Blandin,A.,	Phys. Rev. Lett.,	24,	397,	1970
van Dam,J., Gubbens,P.C.M.,	Phys. Lett.,	A34,	185,	1971
van den Berg, G.J.,	Progress in Low Temp. Physics (ed. C.J. Gorter), North Holland Publ.,	4,	194,	1964
van den Berg,G.J., van Dam,J.E.,	Phys. Stat. Sol.,	3,	853,	1970
Vassel, C.R.,	J. Phys. Chem. Sol.,	7,	90,	1958

Williams,G., Hirst,L., Phys. Rev., 185, 407, 1969

Wilson, A.H., "The Theory of Metals", Cambridge University Press, 1953

Wohlleben,D.K., Coles,B.R., Magnetism (ed. Rado & Suhl), Acad. Press, 5, 3, 1973

Wolff, P.A., Phys. Rev., 124, 1030, 1961

Yosida, K., Phys. Rev., 106, 893, 1957

Yosida, K., Progress in Low Temp. Physics (ed. C.J. Gorter) North Holland Publ., 4, 265, 1964

Yosida,K., Okiji,A., Chikazumi,S., Prog. Theoret. Phys. (Kyoto) 33, 559, 1965

Zener, C., Phys. Rev., 81, 440, 1951

Zuckermann, M.J., J. Phys. F., 2, L25, 1972

CHAPTER 3

EXPERIMENTAL METHODS

3.1 Magnetic Susceptibility

3.1.1. Magnet & Balance

Magnetic susceptibilities were measured using the Faraday technique (Bates, 1963). In this method, the mass susceptibility is proportional to the apparent change in weight of a small(<1 gm) sample in an inhomogeneous magentic field. The force in the vertical direction on the sample due to this field is :

$$Fz = m\, Hx\, dHx / dz\, \chi = mD\, \chi$$

where m is the mass of the sample

χ is the mass susceptibility

H is the magnetic field

x is the direction perpendicular to z and the pole faces of the magnet

$$D = Hx\, dHx/dz$$

The pole piece design (Ford, 1972) was such that D went through a positive and negative extremum as a function of z. The magnet was moved in the z direction (fig. 3.1) and Fz noted at each extremum.

Hence: $$(Fz)_1 - (Fz)_2 = m\,(D_1 - D_2)\,\chi$$

where '1' refers to the positive and '2' to the negative extremum. Sensitivity was maximised by making D large. The size of the sample was limited by the uniformity of D at each extremum. Tests showed that as long as the sample was placed midway between the pole pieces in the x direction, D was uniform over the volume of the sample bucket (5mm high, 4mm diameter).

Figure 3.1 Pole Pieces

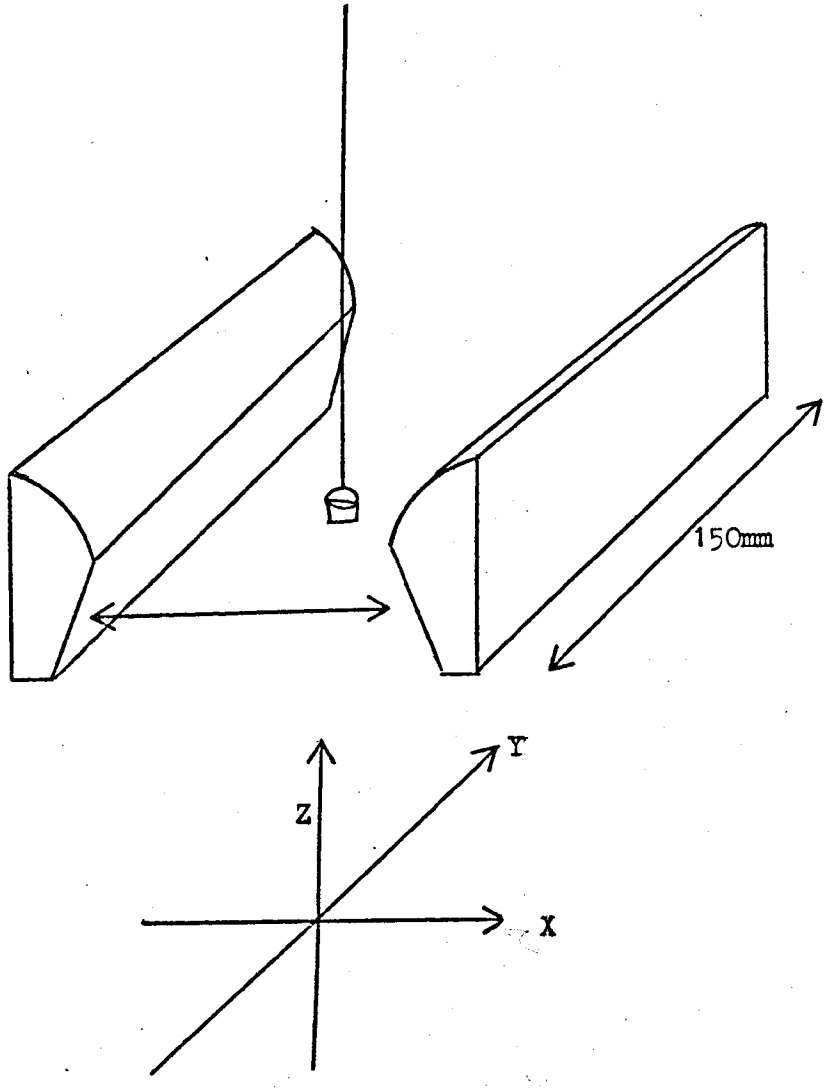

Figure 3.2 Furnace

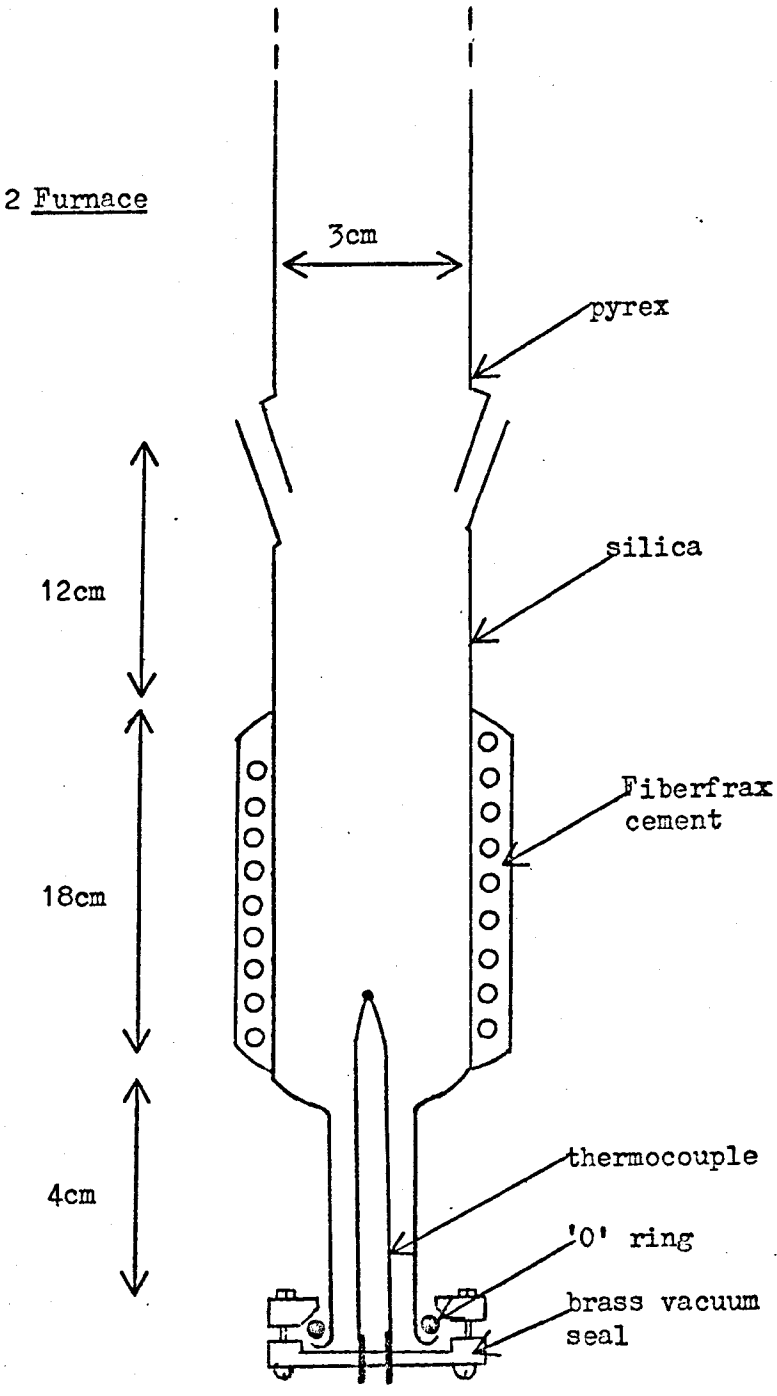

Position along the $\underline{Y}$ direction is not so critical, as the two pole pieces are parallel for 150 mm. The apparatus was calibrated with silver as this had a large and accurately measured susceptibility (taken to be -0.186 x 10^{-6} e.m.u./gm) and is resistant to chemical attack.

As $\underline{D}_1 - \underline{D}_2$ is a constant for a particular magnet current, the sample susceptibility is simply :-

$$m\chi_{sample} = m\chi_{silver} \times \frac{((F\underline{z})_1 - (F\underline{z})_2) \mid sample}{((F\underline{z})_1 - (F\underline{z})_2) \mid silver}$$

The current for the magnet is controlled to 1 in 10^5 by a Mullard precision current controller. The weight of the sample is measured by a Sartorius 4102 electronic microbalance. The sample is suspended from one end of a quartz beam, its weight being compensated by a counterweight at the other end and a torque generated by a coil at the fulcrum. In equilibrium the beam is held in a horizontal position. The force needed to hold this is proportional to the current in the coil which is calibrated in weight units. Thus the change in weight of the sample caused by the inhomogeneous magnetic field can be read out directly.

The balance was protected from vibration by mounting it on layers of neoprene, lead and slate, the whole supported by two brick pillars and connecting it to the vacuum system by a copper bellows and rubber pipe. These precautions were necessarily elaborate as the balance by itself could measure to 0.5μg and using a digital voltmeter (Solartron A212), weight changes as small as 0.05μg could be seen. Tapping the balance lightly produced apparent changes of tens of milligrams.

The magnet was mounted on a hydraulic jack to give relative motion ($\underline{z}$) between the pole pieces and the sample. In practice

the measurements were taken with the magnet descending as its rate of fall could be accurately controlled. The magnet was caused to fall slowly through extremum D positions and rapidly in between.

3.1.2. High Temperature System

To measure susceptibilities over a wide temperature range, an evacuable furnace was constructed. This furnace (fig. 3.2) was made out of silica to enable measurements to be taken from room temperature to 1300K. The heating element was 20 s.w.g. nichrome wire insulated with several layers of Fiberfrax paper and cement, and was powered by a Roband T112 d.c. unit. A chromel-alumel thermocouple was situated within 5 mm. of the sample and led out through the bottom of the furnace by a brass vacuum seal. A pyrex tube connected the furnace to the balance via cone joints, high melting point silicon grease being used as the sealing compound.

Fine silica suspension wires supported the silica sample bucket, the two being joined by a platinum hook. This gave high resistance to corrosion and very reproducible susceptibility results even after cleaning in acid. This was important as a dummy run had to be made to subtract the effect of the bucket from that of the sample.

Tests showed that the temperature gradient never caused more than 5K error even at the highest temperatures (Ford, 1972). As most metals oxidise readily at high temperatures, the whole balance and sample system was made evacuable (fig. 3.3). Helium or argon at pressures between 1 and 760 torr were used, the pressure being chosen to minimise sample movement due to convection currents whilst giving a reasonably efficient exchange gas.

The balance was connected to a pump and a gas reservoir. Helium was the most commonly used gas as it is inert and

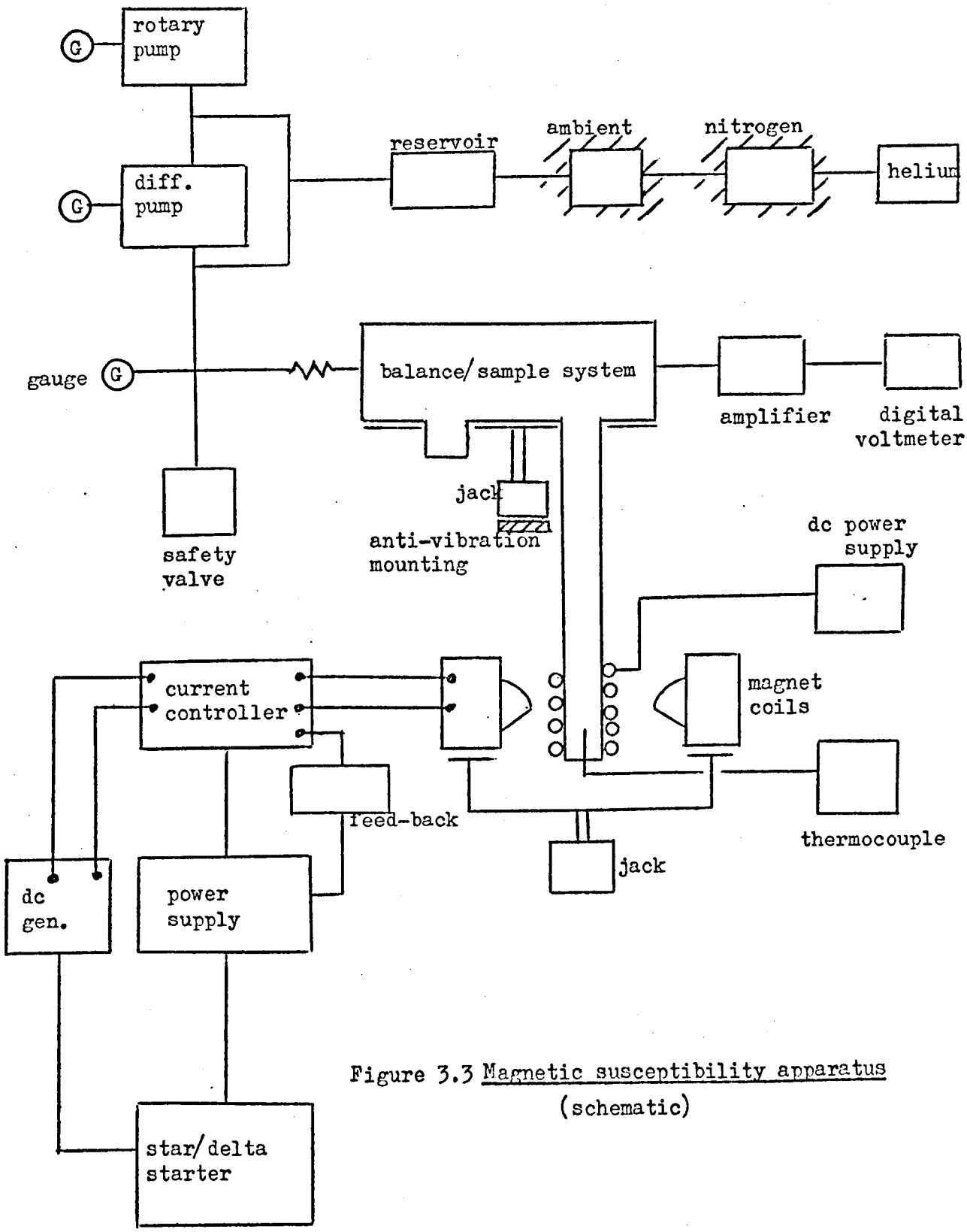

Figure 3.3 Magnetic susceptibility apparatus (schematic)

relatively free from oxygen impurities, though it did sometimes contain water vapour, so this was frozen out by passing it through a liquid nitrogen bath before bringing it back to ambient temperature via a large copper coil and thence to the reservoir. The usual operating pressure for high temperature work was 400 torr.

The sample was loaded by suspending it inside the silica furnace tube from a wire held at the top opening, positioning the furnace under the pyrex tube and connecting the quartz fibre to a similar one from the balance. This fibre protruded just below the pyrex tube so the two could be easily hooked together. With the sample freely suspended, the furnace was carefully raised until the two tubes were mated at the cone joints. The balance was positioned so the sample hung symmetrically between the pole pieces, then the furnace aligned by levelling the track on which the balance jack was held.

A safety valve was constructed and permanently left in the balance - pump line. This was to protect the delicate balance mechanism as the quartz beam with its fine wire suspension and diamond/sapphire stirrup bearings were very fragile. Too great a gas flow through the mechanism could throw it out of calibration and if an overpressure built up, this would eject the furnace or counterweight (tare) glass tubing from their cone-joint mounts. The explosive release of pressure could possibly wreck the balance and break the glassware. The valve was merely a small (¼" diameter) brass disc held by a spring against an 'O' ring which was set in an annulus. Varying the compression of the spring gave different venting pressures. It was usually set to vent to the atmosphere at 790 torr, so, as the vacuum system was used for the most part below 760 torr, the weakly held disc was aided by the pressure difference in forming a good seal.

3.1.3. Low Temperature System

To enable measurements to be taken from 4.2K to room temperature, a commercially available cryostat was modified to fit onto the balance system. The furnace and the cryostat are connected to the balance in a similar manner, though with a few modifications in the latter case (fig. 3.4). These were caused by gas purity and orientation problems.

As previously mentioned, commercial helium gas sometimes contains small quantities of water vapour which must be removed, especially for low temperature work. A liquid nitrogen bath does this. Alternatively the helium exhaust can be re-used. This facility permits economic use of the liquid helium because more than one sample can be measured without having to bring the cryostat up to room temperature. Water vapour would freeze on the sample and sample tube at each low temperature removal, so the cryostat, from Thor Cryogenics Ltd., was modified with a thin-walled stainless steel tube which just fitted inside the sample tube. It was secured at its top end by a ring of Bostik epoxy resin, and extended just below the top of the copper heat shield at the lower end of the sample tube. Pure helium gas was blown down the annulus via the sample port. By careful control the pressure was kept a few torr above atmospheric pressure whilst the balance and connecting tube were jacked up from the cryostat. The escaping helium gas prevented any water vapour condensing down inside the sample tube whilst the suspension was disengaged and the sample removed. Of course, the exchange gas space was pumped hard at this time to reduce the helium boil-off rate to a minimum.

The interest at low temperatures was in single metal crystals which had an anisotropic susceptibility. This resulted in an anistropic force which in some cases produced a torque (e.g. Bates, 1966). To determine χ along a particular crystallographic axis, a suspension had to be made which would not twist. Two quartz fibres were held side by side by strands of Durofix, the whole resembling a ladder. This proved sufficiently rigid not to twist under the torques

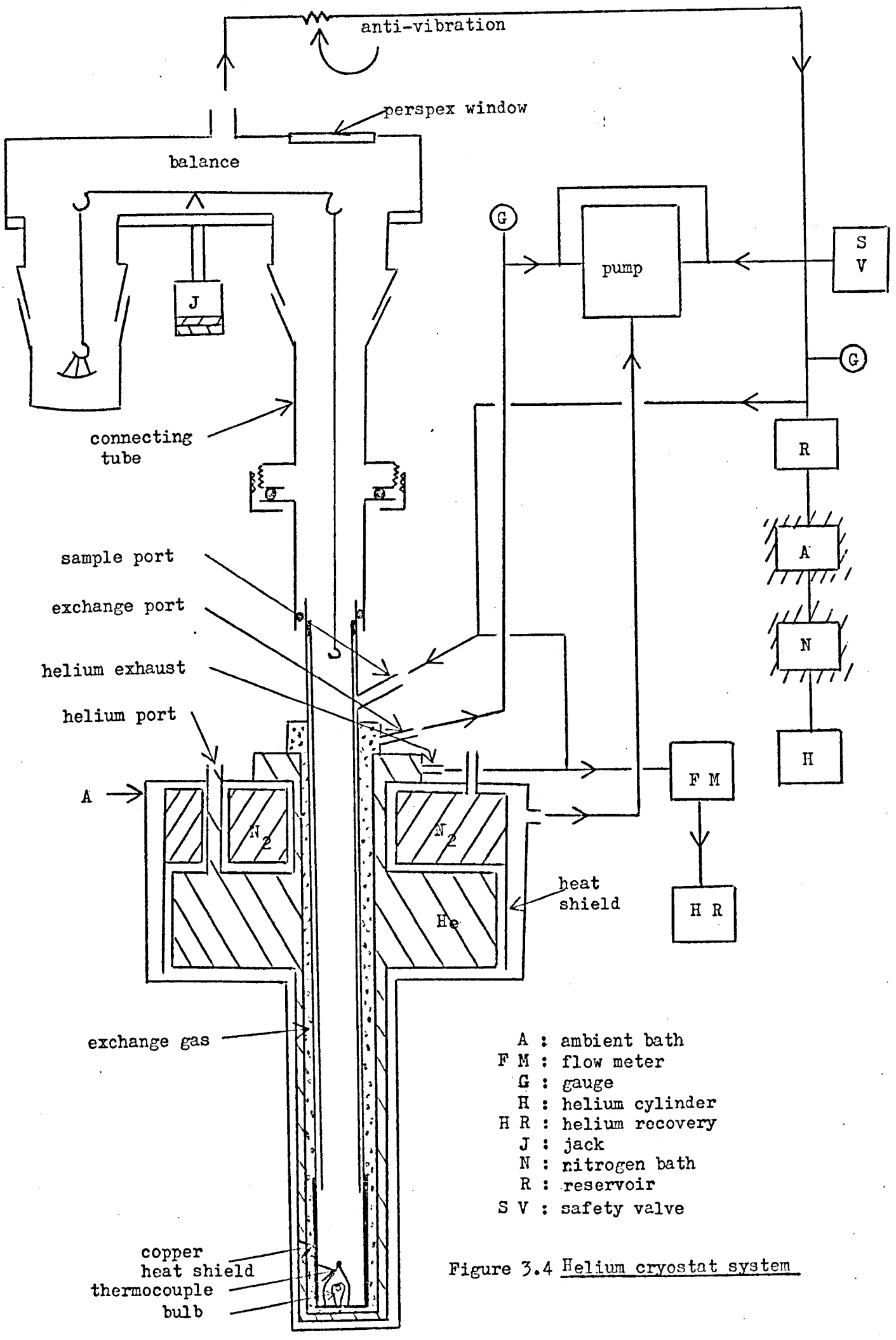

A : ambient bath
F M : flow meter
G : gauge
H : helium cylinder
H R : helium recovery
J : jack
N : nitrogen bath
R : reservoir
S V : safety valve

Figure 3.4 Helium cryostat system

experienced though had the disadvantage of departing slightly from a straight line along its length. The glue was difficult to apply equally to each fibre at each 'rung' and so dried exerting unequal stresses, giving rise to the distortion. This made orientation of the cryostat more difficult, as it could not be assumed that if the sample tube was vertical and the suspension was positioned at the centre of the entrance, it would hang down the middle of the tube under gravity.

The cryostat was slung under the balance by three screwed rods passing through a triangular plate fixed to it at point A as in fig. 3.4. Nuts screwed onto each rod allowed the cryostat to be aligned in any direction a few degrees about the vertical. This was often necessary as the ladder suspensions usually hung a little to one side. Errors in calibrating the magnet (section 3.1.1.) were minimised by orienting the suspension so the departure from the vertical axis was along the Y direction. The top of the sample tube came out of coincidence with the balance connecting piece during this alignment. Provision was therefore made for the cryostat to move a small distance horizontally on its supporting triangular plate. As the tail of the cryostat was constrained by a small gap between the pole pieces (fig. 3.1), further provision for ease of alignment was incorporated in the design. The connecting tube was made in two parts, each part meeting in a flange with an 'O' ring seal, with a flanged nut to pull them together. A sideways movement of 4 mm. between the two tubes was available whilst retaining a good vaccum seal. This facility was used in the final lining up procedure which was done by observation.

A small light bulb was mounted at the bottom of the copper heat shield and when switched on, the whole of the sample tube could be viewed from a perspex window built into the top of the balance. The hanging sample could clearly be seen, and the cryostat aligned so the suspension hung freely down the centre of the sample tube.

As the sample bucket was made of transparent silica and the cryostat sample space tube was mainly shiny stainless steel, some contrast was necessary in order to see clearly the relative positions. A simple dimmer consisting of a 100 Ω 1 watt variable resistor in series with the bulb was found adequate as it could turn the bulb from very dim to its full 1 watt brightness. The bulb, an L.E.S. 6 volt pilot bulb, stood up to vacuum and temperatures of 4.2K very well.

3.1.4. Balance Mounting

The balance was fixed above a base plate by four upright screwed rods which allowed the balance to be levelled. The base plate was mounted on a mechanical jack, which in turn was supported by a trolley. The jack consisted of a cylindrical nut free to move vertically in a tube. A locating peg stopped the nut from turning, and a bolt (made to rotate by two bevel gears) forced the nut up or down, thus raising or lowering the base plate which was fixed to it. The parts were machined to a high tolerance to give smooth movement and no rocking motion, to protect the balance and give accurate reproducible results. The trolley was of a semi-kinematic design so the balance position, with respect to the cryostat and magnet, remained the same after each removal of the sample. The main features of this design were the wheels which had high quality ball bearings and were located in a 'v'-shaped and a wide 'u'-shaped groove set in the trolley track.

Wear was reduced by making bearing surfaces of dissimilar metals. For instance, the brass wheels ran on dural tracks and the steel nut ran in a brass tube.

3.1.5. Sample Loading Procedure

The sample, usually a metal single crystal, was fixed to the bottom of the silica bucket by a very small amount of Durofix glue. This was so that a specific crystallographic axis could be aligned with the magnetic field and the sample could not be shaken or twisted out of alignment. Durofix was

chosen as it had a negligible effect on the net susceptibility even down at 4.2K. The bucket and ladder suspension were carefully lowered into the cryostat and suspended from a piece of wire shaped in an inverted 'U' and hung over the mouth of the sample tube. The balance suspension hung just below the connecting tube and ended in a small square metal frame. This suspension consisted of two wires which were hooked to the stirrup on the quartz beam and so could not rotate.

The balance was raised to its maximum height by the jack, then wheeled directly over the cryostat and locked into position. The sample suspension was then raised until a stiff wire, curved at one end, could be placed under a 'rung'. This was then used to hook the suspension to the square frame. After approximately orienting the cryostat so the sample swung free of the sides of the surrounding tube, the counterweight was tared up. This was always a non-magnetic substance similar in weight and buoyancy to the sample.

The flanged nut was slackened to give free lateral motion to the bottom half of the connecting tube and the balance lowered until the sample was at its normal position in the centre of the copper heat shield. After finally orienting the cryostat by use of the bulb and the window, the nut was tightened up and the system pumped out and flushed several times, ready for use.

When the cryostat was below 50K, it could be seen that the tubes in the tail of the cryostat had not all contracted symmetrically. This was shown up by a slight twisting off axis and sometimes resulted in the bucket just touching the sides. The cryostat then had to be realigned whilst under operating conditions so only a single 'O' ring formed the seal between the top of the sample tube and connecting tube.

Below the "O" ring, the brass tube was cut away so the two tubes could be slightly out of coincidence without producing any undue stress. It was found that the sample could always then be centralised. Sometimes the magnet could not be raised sufficiently high due to the bulk of the cryostat for the first D extremum to be clearly observed when the composite effect of sample and bucket changed from dia- to paramagnetic as a function of temperature. As the absolute vertical position of the extremum D depended on whether the sample was diamagnetic or paramagnetic, the balance jack provided a convenient means of changing the sample position to accommodate this.

3.2 Resistivity

There are many ways of measuring resistivity though the choice of technique is usually limited to only a few by the constraints of the material to be measured. Historically, the first method to be scientifically employed was the potentiometric method used by Weber in 1887. He attached two potential leads and two current leads to his samples, and merely measuring the ratio of the voltage and current values resulted in a value accurately proportional to the resistivity. In the cases where the resistance of a sample cannot be directly measured, a rotating magnetic field may be used to produce a torque by inducing eddy currents in the surface of a conducting material. The principles of this method were established by Braunbeck in 1932 and refined by Roll et al. in 1956 then further developed by Basu, Biswas, Fees and Ozelton among others, in the nineteen-sixties.

Another important method is that used by Haisty and Krebs in 1967 where they rapidly dropped their specimen through the coil of an r.f. oscillator. This caused resistive losses in the coil which were proportional to the specimen resistivity, though accuracies of only 10% to 20% are achieved. Despite this, samples with a large coefficient of resistivity, such as the GeSbSe system may be satisfactorily measured as the range of a typical instrument is from 10^{-6} to 10^{+8} $\mu\Omega$cm. Modifications of this design, such as that used by Newrock et al. 1971, where the sample causes an out of phase component in one half of a secondary coil of a transformer system, can give an accurate relative change in resistivity.

Edmonds and Smith (1972) have developed a spectrometer for use with solid samples which enables the real or imaginary component of permittivity (or resistivity) to be recorded over a frequency range of 1Hz to 1MHz. Previous instruments required extensive recalibration to attain this range and

did not have the sensitivity that these authors claim (a typical loss tangent of 10^{-3}).

The indirect methods suffer largely from calibration errors which in turn are caused mainly by variation in sample sizes. At best, results are usually presented to 2% to 5% accuracy. The direct potentiometric method is inherently far more accurate and it is not uncommon for 0.1% accuracy to be claimed. Sample dimensions of liquid metals can be accurately reproduced by using containers with very low coefficients of thermal expansion, so for these reasons it was decided to measure the resitivity of liquid gallium-3d transition metal alloys by a potentiometric technique outlined below.

3.2.1. High Temperature Cells

Various resistivity cells were constructed, all on the basic plan of using an overpressure of argon to force molten metal into the cell. Tungsten or molybdenum were used as the current and potential probes, as they are the least likely metals to contaminate the sample at high temperatures.

The first and simplest (fig. 3.5(i)) was useful only up to about 900K. This was because the tungsten probes had to pass through the side wall of the cell and remain leak-tight. As the coefficient of linear expansion of tungsten is $6 \times 10^{-6}\ K^{-1}$ and the silica is $45 \times 10^{-8}\ K^{-1}$, the difficult process of melting several concentric layers of graded glasses around the probe in the form of a bead had to be perfected (fig. 3.5(ii)). The strains of differential expansion were accommodated by making the final shape of the bead spherical. Imperfections in this shape caused the glass around the probe to crack, and strains imposed by handling and the pull of the connecting wires, also served to limit the cell lifetime to about one or two runs.

The next cell developed (fig. 3.6(i)) was more robust and allowed a longer lifetime (four to five runs) with temperatures up to 1000K. As molybdenum is 1.5 times (Samsonov, 1968)

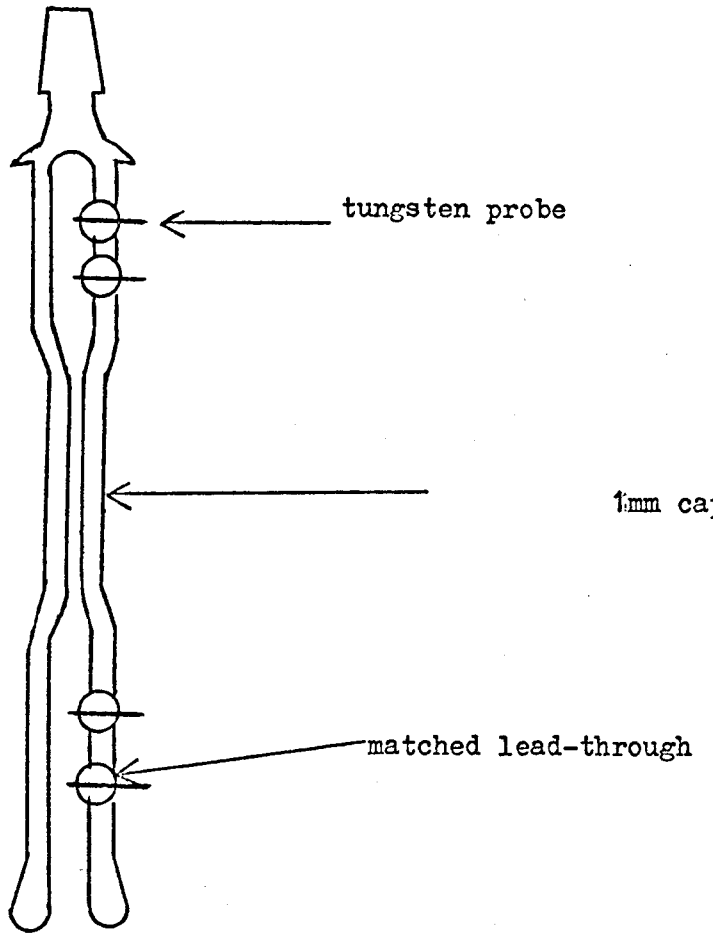

Figure 3.5(i) Resistivity Cell

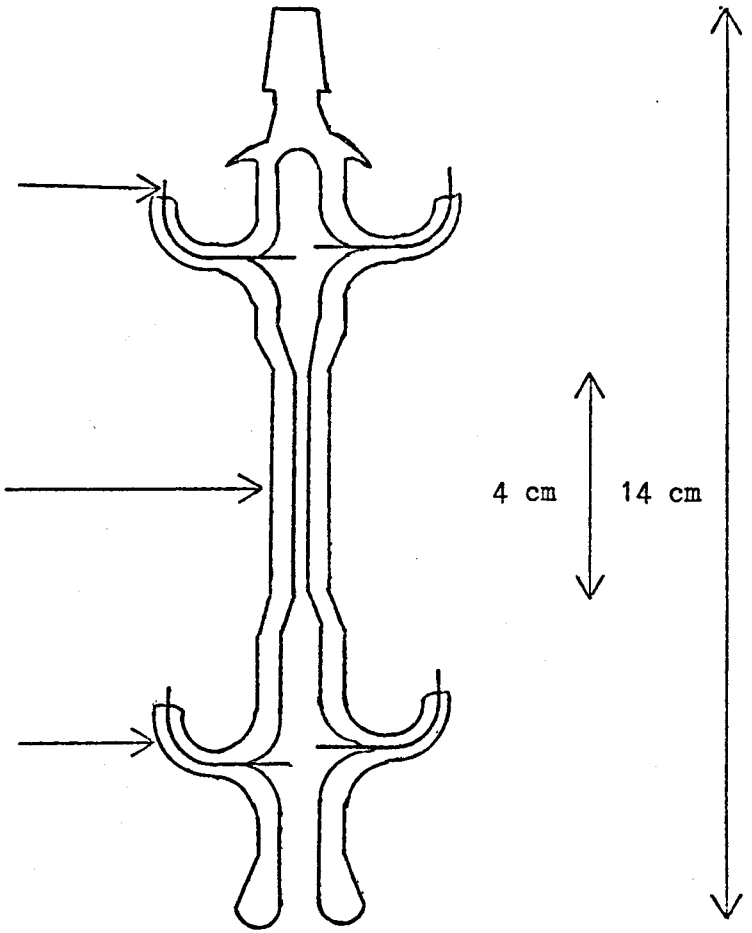

Figure 3.6(i) Resistivity Cell

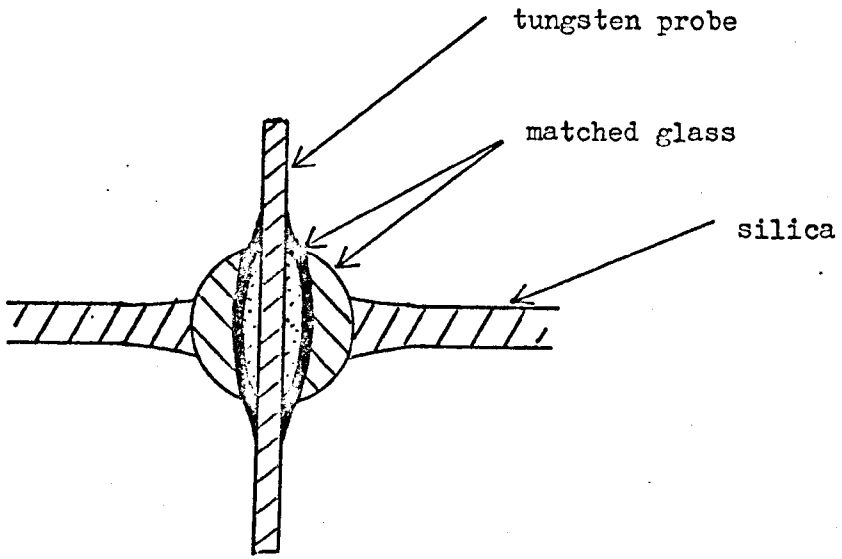

Figure 3.5(ii) Glass-to-metal seal

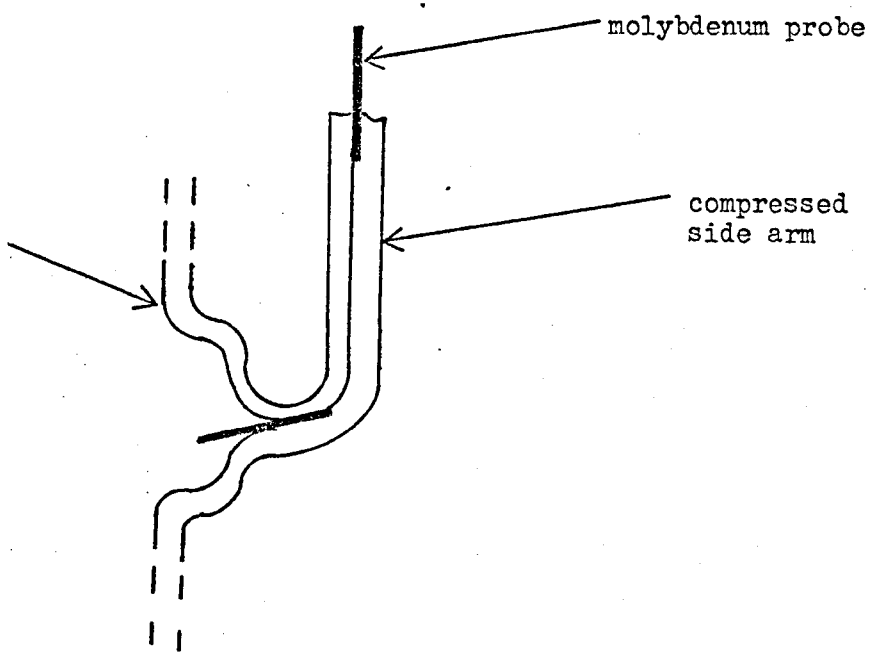

Figure 3.6(ii) Molybdenum strip seal

more malleable than tungsten, it was decided to use very thin foils of molybdenum as the probes. These were made in three pieces (fig. 3.6(ii))- the two end pieces 0.16 mm. thick for mechanical strength and the inner piece 0.07 mm. thick so as to give a leak-tight length along the side arms. The latter was done as follows. The composite probe was assembled by spot-welding and electrolytically etched in dilute caustic soda solution to clean and further thin the middle piece, then inserted in a side arm tube sufficient for one end to project about 1 mm. inside the cell body. The arm was then heated and compressed hard by pliers along the middle section and then just nipped in for a small length along the junction of the thin and thick pieces of molybdenum to give strength, though not so far as to cause the glass to crack in the subsequent high temperature experiments. The side arms running parallel to the body had the advantage of reducing breakages when removing and replacing the cell in the furnace. For added strength the arms were usually attached to the body at their top ends by a button of silica. Molybdenum had a substantially shorter lifetime than tungsten due to corrosion, so was abandoned as probe material.

The most successful cell removed the need for high temperature lead-throughs with its attendant difficulty of being leak-tight. Figure 3.7 shows how this was done.

As the top part of the cell was held a long way from the furnace in a water-cooled environment, it was made out of pyrex, less fragile than silica, though it softens at a lower temperature, 900K. The lead-throughs in the bulbous part of the cell were never hotter than 300K and so did not leak due to differential thermal expansion. The cone joints were held together by springs and sealed by high temperature silicon grease, a rather unnecessary precaution as the temperature there hardly ever exceeded 305K. Immediately below this a silica tube was joined on using graded glasses. A silica capillary tube was joined on at the bottom to make the standard resistivity cell. Two short lengths of capillary

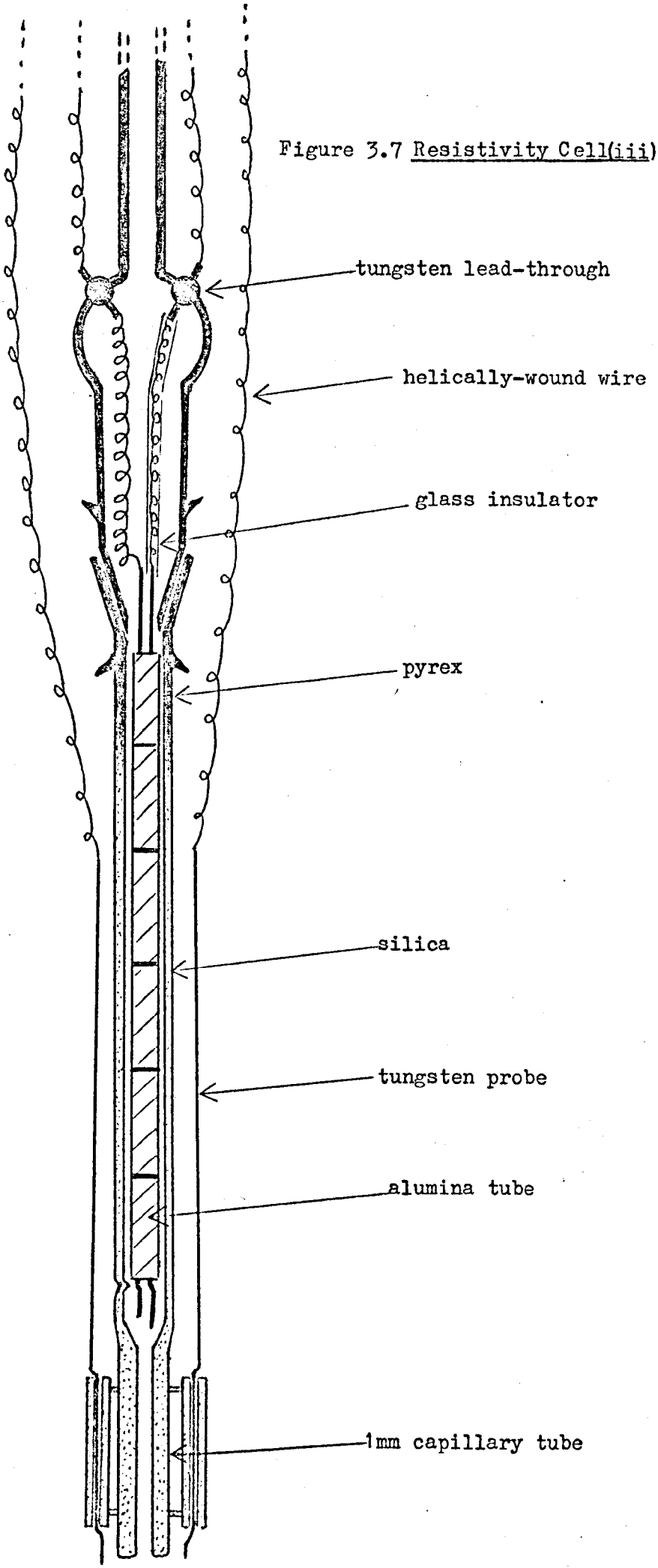

Figure 3.7 Resistivity Cell(iii)

tube were joined either side of this as holders for the two lower tungsten probes which were made out of 1 mm. diameter tungsten rod and shaped so they could not ride up, and a small rectangular sheet of tungsten spot-welded to them immediately at the top of the holders so they could not move down, thus ensuring they stayed in the same position for all experiments. 32 s.w.g. tungsten wire was wound in a helical form and one end spot-welded to the top of the rods and the other taken to a lead-through in the top cap.

The two inner probes were made in a similar manner, and held apart by being threaded through twin-bored alumina tubing. They were kept in position by being bent slightly as they left the lower end of the alumina, which in turn was held by a small indentation in the silica tube. Thin helically wound wire, welded to the top of these probes, allowed the two halves of the cell to be taken apart for cleaning without the glass-to-metal seals at the top being over-stressed as the alumina was often held firmly in the lower portion of the silica tube by solidified metal droplets. One of these two wires was protected by a glass tube to prevent them touching. These probes were continued by two more lengths of helically-wound wire taken from the seals to the top cap.

This connecting method enabled the cell to be moved relative to the cap without exerting any undue force. Two chromel-alumel thermocouples were wound in the same way and attached near to the end of the sample capillary. All unprotected wires were covered by Refrasil sleeving.

3.2.2. Reproducibility of Results

Each cell was calibrated with triply distilled mercury at room temperature, obtaining a numerical constant for each individual cell. This value was still essentially correct

at high temperature (1300K) as the coefficient of expansion of silica is very low (45×10^{-8} K^{-1}) and at the highest temperature would make the cell constant different by only 0.05%. This change is therefore negligible. The overall accuracy was found to be limited by temperature stability and, to a greater extent, by impurity concentration. Over the length of the sample cell, the temperature could be controlled to $\pm$2K, with a gradient of less than 1K. The temperature coefficient of resistance (α) of Ga over the measured range was $0.02 \mu\Omega cmK^{-1}$ (fig. 6.5), the temperature variation over the sample would give a change in α of 0.1%, this value also holding for the alloys measured.

As α is linear in the range investigated (fig. 6.5) a temperature difference of 1K between top and bottom of the cell would result in a mean resistivity being measured, this being at most 0.03% inaccurate. This temperature gradient would only be serious near the liquidus of an alloy due to probable composition change through the interface, or a eutectic point caused by electrotransport (Verhoeven 1963).

Thermal e.m.f.s. were large, especially at high temperatures where they could be of the same order as the sample e.m.f.s. Rapidly reversing the current and averaging the resultant e.m.f. enabled the true sample e.m.f. to be determined and this was confirmed by measurements, using different currents (20, 40, 80mA.) giving results within 0.5% of each other.

In an attempt to reduce thermals to a minimum for reliability measurement the probes, necessarily comprising several pieces, were made into a continuous length of the same metal as far as the lead-outs at the low temperature end of the cell and the top cap. Tungsten was found to be the best material but is brittle and will not easily spot-weld. A capacitor-discharge method of spot-welding was found necessary

as only this gave sufficiently high temperatures for a short enough time for the join to have reasonable mechanical strength. Otherwise, a stainless steel 'sandwich' was needed, but this had a 'one-run' lifetime due to the corrosive effects of the alloys at high temperatures.

It was found that the corrosive effects of gallium-transition alloys increased with temperature and impurity concentration. Inspection of the cells showed the silica and the tungsten were usually etched after each run, the tungsten especially being covered by a non-conducting oxide. This was characterised by large fluctuations in the current, eventually making measurements impossible.

The maximum temperature at which resistivities were measured was 1300K, with an upper limit of impurity concentration of 2 at.%, these conditions giving rise to experimental difficulties. Above 1 atomic % impurity and 1000K no current would pass until forming gas (15% hydrogen, 85% nitrogen) was used instead of argon. The system had to be flushed out several times after each sample change and pumped hard to remove all oxygen traces. Even so, GaCr still remained difficult to measure at elevated temperatures due to poor electrical contact at the probes. Pure hydrogen, though no doubt dangerous, would help alleviate this problem.

Bubbles occluded in the sample were a problem until steps were taken to remove them. They could readily be identified by the large temperature coefficient and the large change in resistance with pressure in the sample. Alloys were usually degassed by being held at 900K and 5×10^{-5} torr for about thirty minutes before the cell was filled. There was a negligible loss of sample due to this process.

All errors except those due to fluctuations caused by corrosion would be expected to give inaccuracies of at most 0.7%. The scatter of points in the worst case of GaCr gives an error of approximately 11%, thus pinpointing that the biggest disadvantage of the potentiometric method in the Ga - transition metal alloy systems is caused by non-conducting corrosion products being formed on the probes.

3.2.3. Furnace

This consists (fig. 3.8) of a silica tube, 31 mm. inside diameter, 56 cm. long, the lower 35 cm. being non-inductively wound with about 10 m. of 20 s.w.g. nichrome wire. This was covered with two successive layers of Fiberfrax cement and paper, then a layer of aluminium foil to reduce temperature gradients, more cement, another layer of foil and a final coating of cement. The noninductive winding was to prevent any magneto-resistance in the sample from the a.c. heater current. The foil was to reduce temperature gradients.

To prevent heat being lost by convection, the furnace was surrounded by a pyrex tube. Around this a bright layer of foil was wrapped to reduce radiation losses.

Two windows were cut through the cement and foil, enabling the cell and sample to be seen, though experience later showed this was unnecessary. In fact, the samples evaporated very slightly and over a few weeks obscured the windows which then became difficult to clean.

Due to its relatively small thermal capacity, the furnace had a rapid response. In practice, 10 amps through the he heater windings raised the temperature from 300K to 1350K in fifteen minutes. Removing the outer shield allowed it to cool back to room temperature in about one hour.

3.2.4. Gas Handling System

The furnace and resistivity cell were supported by a water-cooled brass top cap (fig. 3.9). It was originally built to a design by Dr. G.A. Styles (Lambert, 1970), then modified to enable temperatures in excess of 1300K at the furnace to be achieved without damaging the support 'O' rings, and to keep cool the glass-to-metal seals in the bulb of the cell.

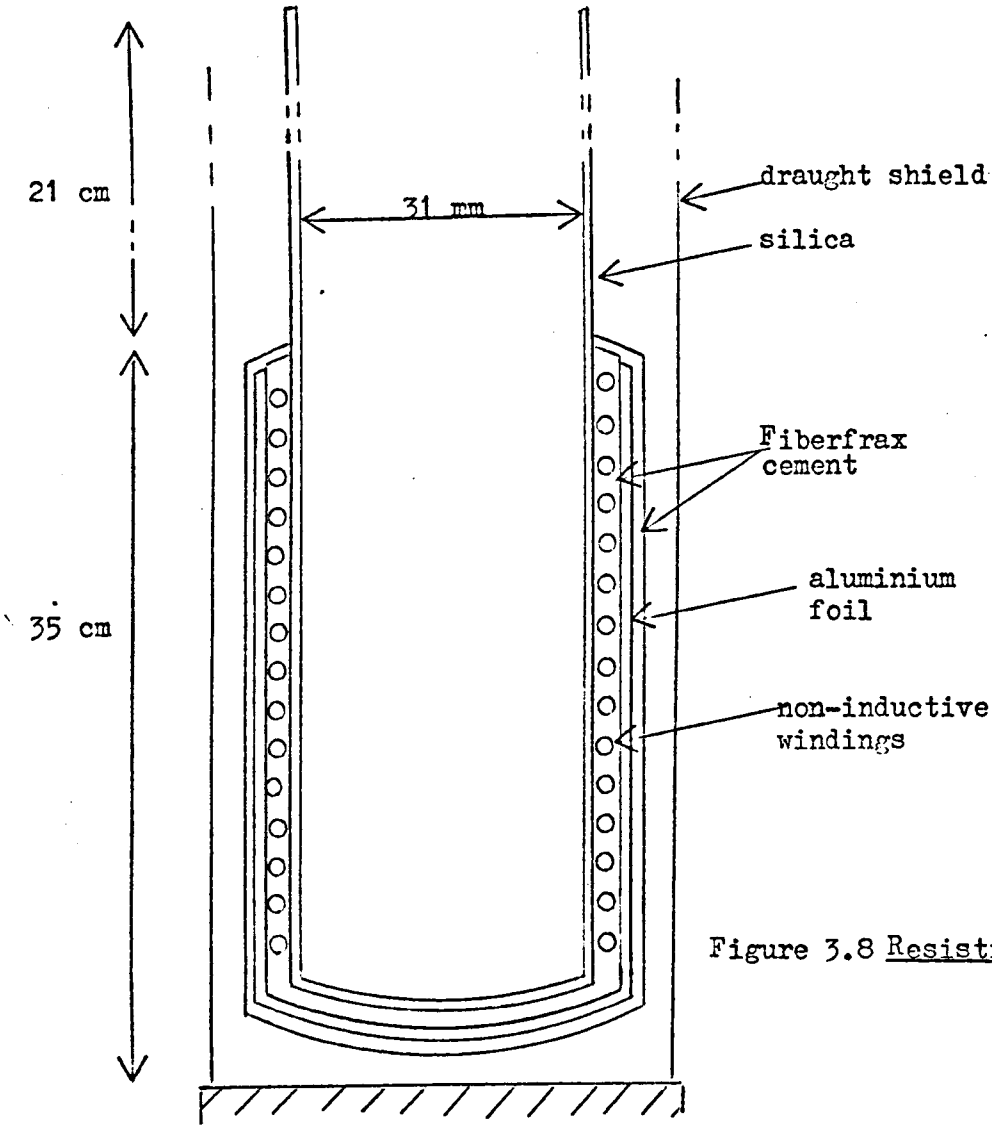

Figure 3.8 Resistivity Furnace

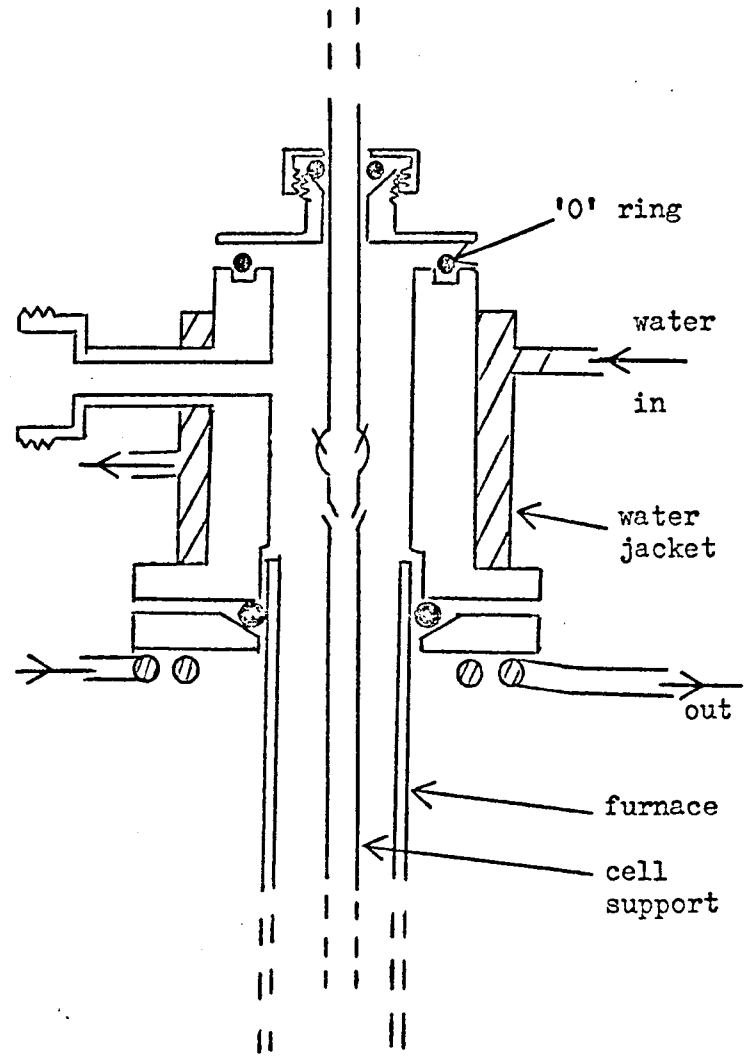

Figure 3.9 Top cap assembley

The furnace could be removed by slackening the bolts at the base, and the cell removed by taking off the top plate. Slackening the screw cap enabled the cell to be moved up and down relative to the furnace without opening it to the atmosphere.

The whole cap was held by four legs above a steel frame containing the furnace, and could be pumped or connected to a gas supply. The liquid sample was forced into the cell by a pressure difference, the cell connected at its top to the gas supply and the pressure monitored by two 0 -760 torr Bourdon gauges and the difference by a mercury manometer. After degassing, 5×10^{-5} torr were readily obtained in the furnace. The manometer was connected to the system via two Dreschel bottles to prevent mercury getting into the system if the wrong valve was accidentally opened. As further protection, a few cm. of water were put in each arm of the manometer, so that if one arm was pumped hard, the water would noticeably boil before the mercury began to evaporate and possibly contaminate the laboratory.

3.2.5. Electrical Circuit

Current for the resistance cell was supplied by a stabilised power source in series with a fixed and variable resistor and a 100 mA. f.s.d. milliammeter. It was then passed via a reversing switch (Radio Spares 2p 2w) to the series connected cell and a 0.01Ω Tinsley standard resistance. The circuit (fig. 3.10) was complete only when the cell was full.

The potentials from the remaining two probes and the standard resistance were taken via a Tinsley reversing switch (type 5500, Minimum Universal) to a Pye potentiometer (type 7600). This potentiometer could measure to $0.1 \frac{\mu\Omega}{cm}$ which, when used with the Tinsley galvanometer (type MR4) proved extremely accurate. The Tinsley switch had a thermal e.m.f. of 0.15 $\mu\Omega$cm across the brass contacts, but as this was highly reproducible it was accounted for in the analysis procedure.

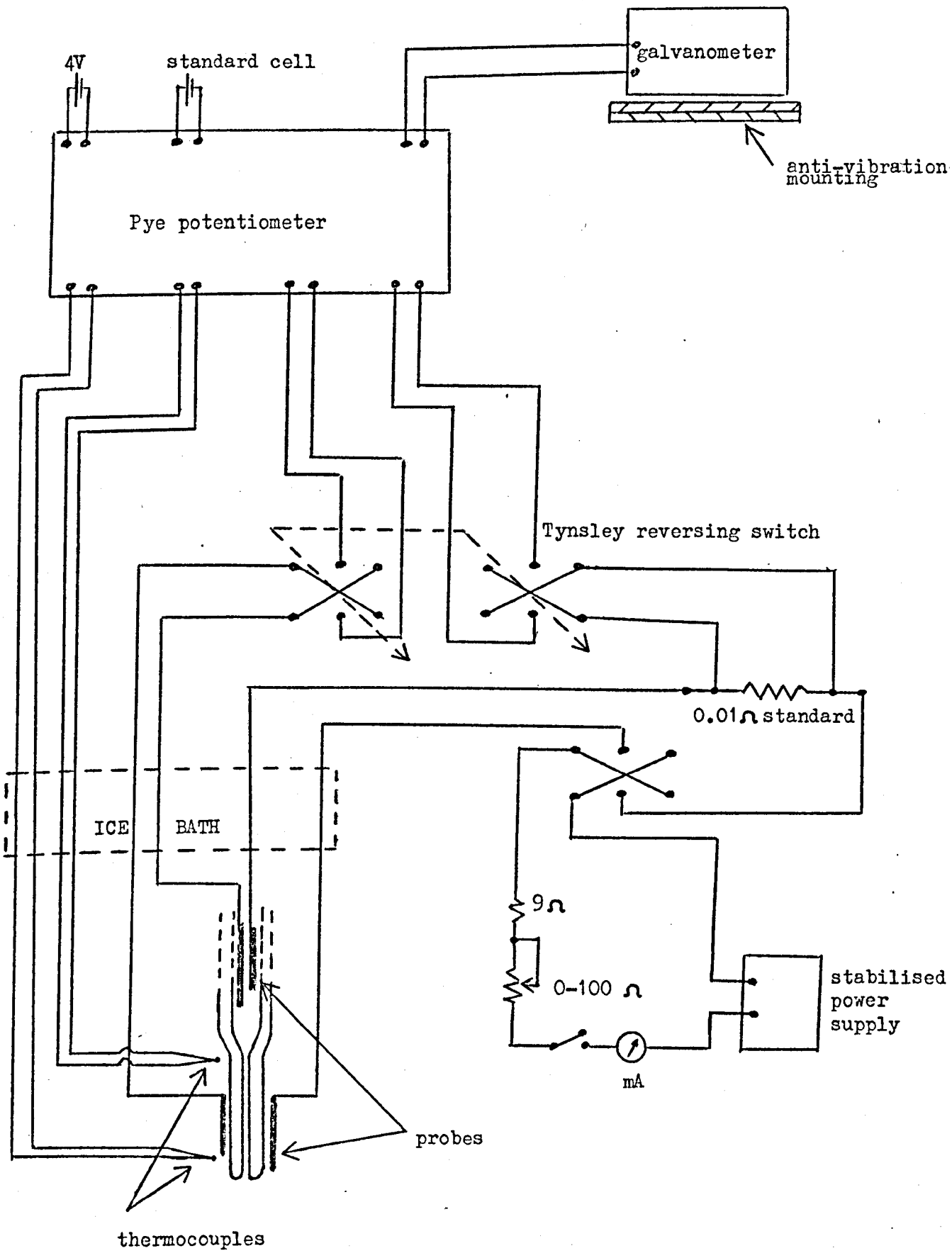

Figure 3.10 Potential measuring circuit

The potentials from the two chromel-alumel thermocouples at each end of the capillary tubing were also measured by the potentiometer. To minimise thermal e.m.f.s., all current and potential leads from the cell were taken through an ice bath and the switches, resistors and milliammeter were mounted inside a lagged wooden box.

The furnace temperature could be rapidly and accurately controlled, using an Ether temperature controller type 18-98 with a thyristor unit. The required temperature was dialled up and the error signal corresponding to the difference between this and the chromel-alumel thermocouple potential determined the portion of the a.c. waveform fed to the furnace via two back-to-back thyristors. A 15 amp Variac was used for the furnace supply merely to limit the maximum current through the windings. This system was able to give temperatures far in excess of the upper limit of 1350K where silica softens.

3.3. Procedure

The solubility of 3d metals in gallium is very low, in fact hardly any metal will remain in solution in solid gallium, so only high temperature work in the liquid phase is possible using the potentiometric method adopted here. Mixing of the constituents occurs only after agitation at high temperatures, otherwise what appears to be surface tension effects keep the two metals separate.

3.3.1. Sample Preparation

The metals used were all 99.999% pure or better from Johnson Matthey or Koch-Light. They were weighed out accurate to 0.1 mg. and placed in the sample bucket. A Nikrothel wire susceptor was wrapped around this and the whole lowered into a flat-bottomed silica tube which was then flushed with argon

several times and pumped out to 10^{-3} torr and sealed (fig. 3.11). A radio frequency furnace was used to heat the sample to a red colour, 950K (Walden, 1939), when all the constituents had thoroughly mixed after slightly shaking the tube. The alloy was allowed to cool before being lowered into the resistivity furnace.

This pre-mixing procedure was found preferable to melting the metals in the resistivity furnace as both visual observation and analysis usually showed a significant fraction of the transition metals did not become absorbed into the alloy. The life of the furnace was also increased by lessening the time spent at elevated temperatures.

The Nikrothel susceptor was found necessary as the usual 30 gm. sample of the gallium was insufficient by itself to couple into the r.f. furnace field. Contamination by the wire was negligible as weighings before and after melting showed.

3.3.2. Calibration

Triply distilled mercury was put in the sample bucket and the apparatus pumped down to about 400 torr. The cell was then lowered into the mercury and sufficient gas let into the furnace to force the mercury through the capillary as far as the top two probes, when the milliammeter registered current. The standard resistance and the sample potentials were measured several times, reversing the current each time. The cell constant was calculated as the ratio of the measured resistance to the theoretical resistivity of mercury given (Kaye & Laby, 1966) by :-

$$\rho(\mathrm{Hg}) = 94.1\ (1 + T \times 10^{-3}) \quad \text{where} \quad \rho = \text{resistivity in } \mu\Omega\text{cm.}, \quad T = \text{temperature in } {}^{\circ}\mathrm{C}.$$

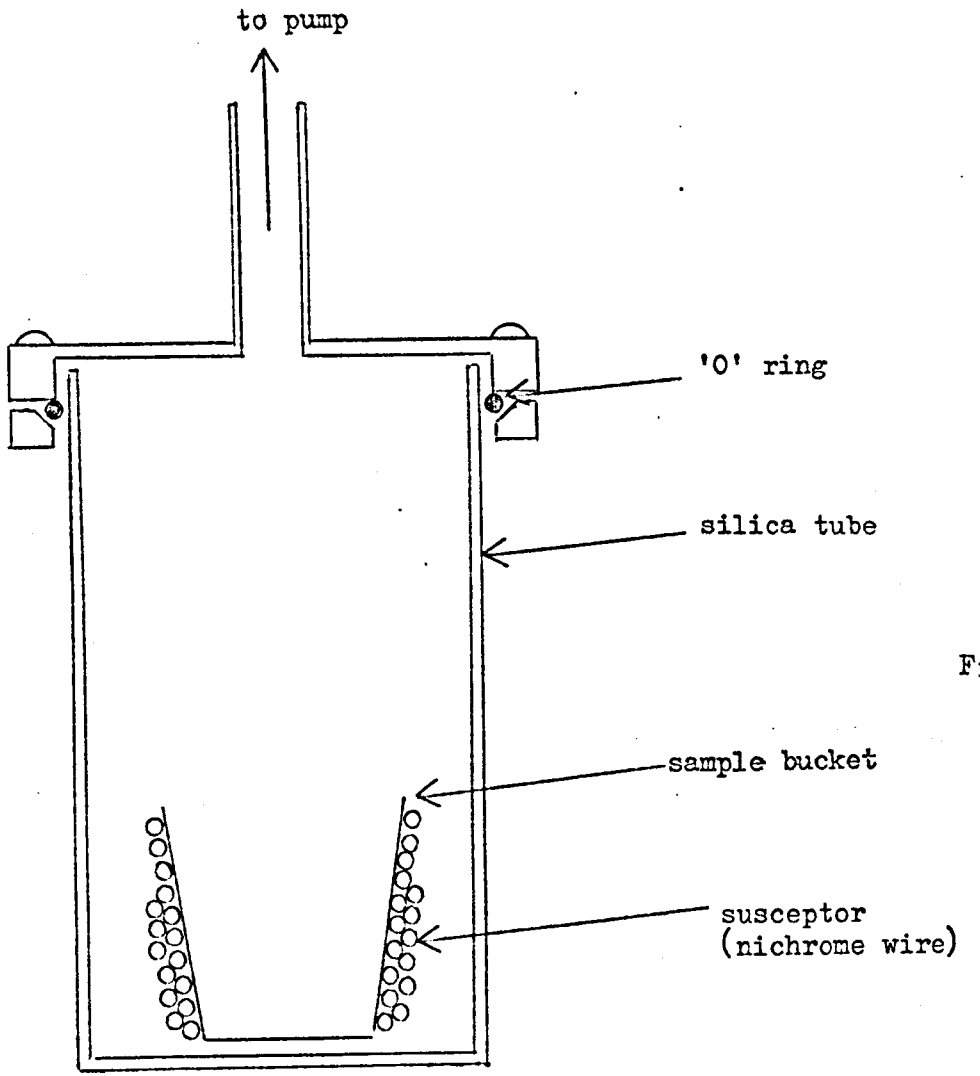

Figure 3.11 Mixing furnace

3.3.3. Measurement

The sample was heated in the furnace to about 900K at a pressure of $\sim 5 \times 10^{-5}$ torr for thirty minutes to allow all the transition metal to be reabsorbed and to get rid of any occluded gas. The cell was then lowered into the molten metal after raising the pressure to about 200 torr. This figure was found to be the mean between having an efficient exchange gas and minimising heat loss by convection to the top cap. A little more gas was then let into the furnace causing the metal to rise up the cell and so make electrical contact. This action could be repeated several times if a stirring action became necessary, though increasing the risk of bubbles in the capillary.

Monitoring the mercury manometer gave an indication of the height of gallium in the cell, after taking into account the fact that gallium is 0.47 times as dense as mercury (Kaye & Laby, 1966). Knowledge of the height was useful for subsequent cleaning purposes, if, for some reason, the current failed to register when the cell was full. Leaks in the cell /furnace system were also clearly shown by the fall in the mercury column.

The temperature was allowed to stabilise at each measurement for about ten minutes, after which the gradient along the cell became less than 1K. It was usually sufficient to take a set of three readings per potential per temperature, reversing the current at each reading. As mentioned previously, each potential when averaged gave a final reading free from thermal e.m.f. effects.

To minimise further any possible electrotransport effects, the current (40mA) was switched on only when taking a measurement. Pure gallium never corroded the tungsten probes. It was only when first row transition metals were added that forming gas was needed to reduce the oxide, and stable readings were possible.

3.4 Crystal Growing

Single crystals of zinc may readily be grown but adding even a few tenths of a percent of a 3d impurity makes growing them much more difficult. Phase diagrams (e.g. Hanson 1958) of the zinc - 3d series shows that elevated temperatures (1000K) are necessary to dissolve these impurities in quantities greater than 1 - 2 at. %, and at room temperature crystals of typically 10^{-2} at. % may be expected to be thermodynamically stable. The situation in single crystals may be better than in polycrystals as there are less dislocations and grain boundaries for the impurity to precipitate out to.

3.4.1. Apparatus

Zinc and zinc-3d transition metal single crystals were grown by an adaptation of the Bridgman technique (fig. 3.12). The sample was contained in a sharp-ended silica crucible and lowered slowly through a furnace. The crucible was in the form of a cylinder 6 cm. long and 1 cm. in diameter, with one end formed in a hook and the other pulled to a point. This was so the sample would seed from there and a single crystal grow from this as the crucible was lowered through the sharp temperature gradient of the furnace (fig. 3.13). This temperature gradient was achieved by winding the centre portion of the alumina furnace tube with twice the turn density of (20 s.w.g. nichrome) wire at the two ends. The tube was 37 cm. long and 3.5 cm. in diameter. About 15 m. of wire was used. The top was closed by an asbestos plug except for a small hole for the suspension wire to pass through, and the bottom was left open.

Crucible lowering rates of 4cm/hour to 0.2cm/hour were achieved by a system of gears and pulleys. A Citenco motor type KQR/155 was used as the drive - this gave a torque of 20 oz.-ins. and a variable speed range of 50 to 300 revolutions/minute. It was mounted on rubber to reduce vibration and

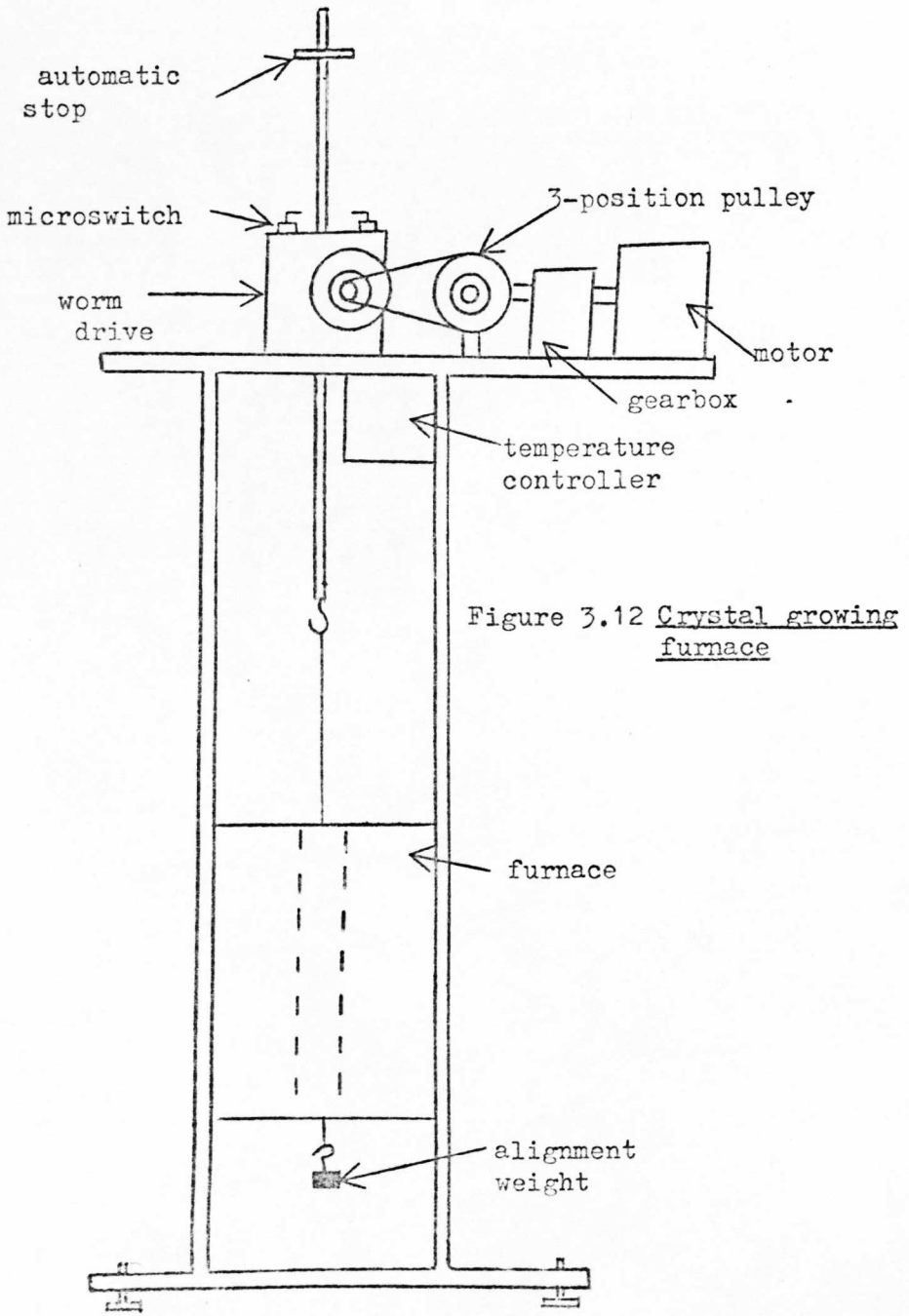

Figure 3.12 Crystal growing furnace

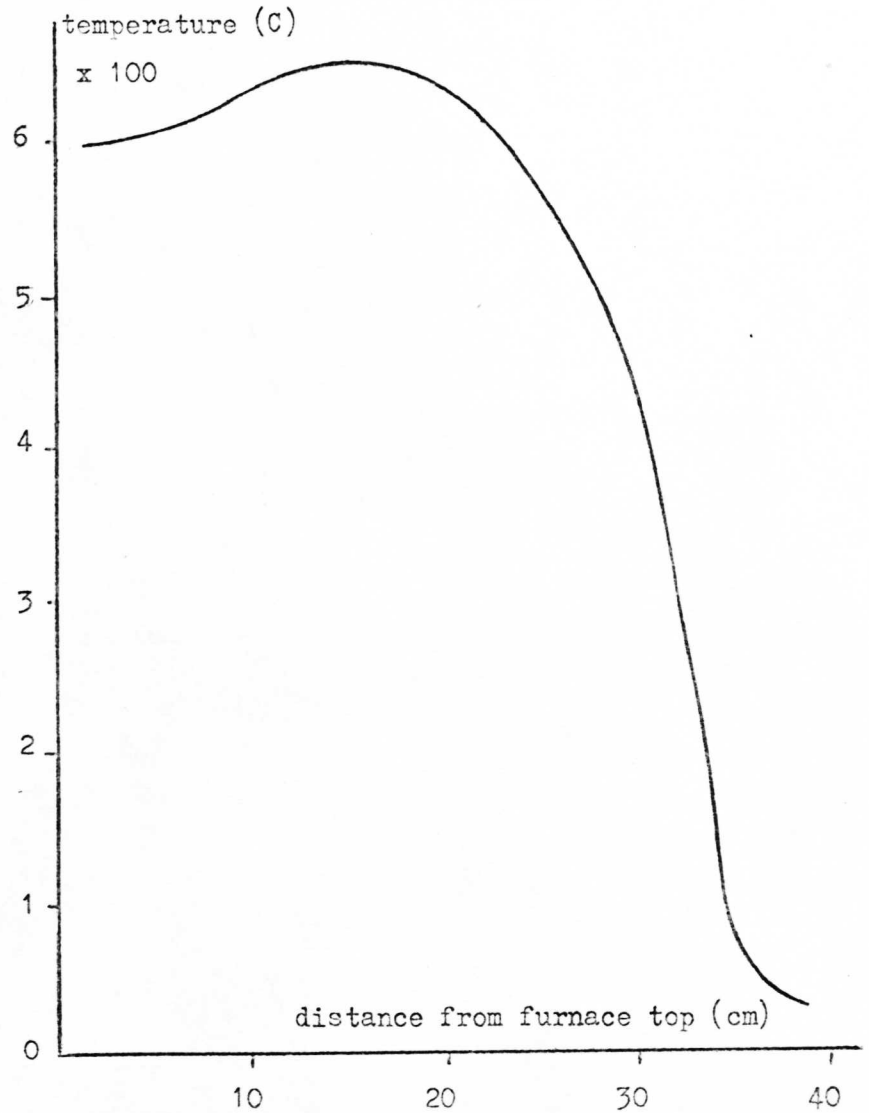

Figure 3.13 Crystal furnace temperature profile

and drove a 10:1 reduction gearbox via a universal drive. The gearbox drove two pulleys, each of which had belt grooves at 2 cm., 5 cm., and 8 cm. diameter to give a 3:1, 1:1 and 1:3 change in speed. The final pulley turned a rod on which a 20 t.p.i. Whitworth thread was cut. This meshed with a 2" diameter horizontally mounted gear on which a similar thread was cut. A screwed rod, again 20 t.p.i. Whitworth, ran vertically through the middle of this gear. A groove was cut along the length of the rod in which fitted a locating peg to stop it turning. This arrangement constrained the rod to move solely in the vertical direction, thus providing a hoist from which the crucible could be suspended. To pass a sample through the furnace took typically 36 hours so an automatic stop was incorporated. This consisted of two microswitches mounted on top ofthe worm drive box and a disc attached near the top of the vertical rod. When the rod travelled about 40 cm. down from its raised position, the disc connected with the microswitches and turned off first the furnace and then the drive motor.

The furnace temperature controller was a Skil Type S9C/S122, and a chromel-alumel thermocouple sampled the temperature at the centre winding of the furnace. Zinc melts at 420°C, so the hottest zone was usually set to 650°C.

Two or three crucibles were usually passed through the furnace each time, the bulk usually being asymmetrical which caused them to touch the alumina tube. Lowering them set up vibrations so a heavy alignment weight was hung below on the 36 s.w.g. Nikrothal suspension wire. Single crystals could usually then be grown.

3.4.2. Sample Preparation

The zinc and the 3d transition metals were bought from Koch-Light and were 99.999% or better purity. They were weighed out to 0.1 mg. A silica tube, about 1 cm. in diameter

was prepared by pulling one end to a sharp point, and cleaned in acid, distilled water and ether.

The metals, which had also been cleaned in dilute acid before weighing, were transferred to the tube using stainless steel tweezers. The tube was connected to a vacuum pump and flushed several times with argon before pumping out to about 0.01 torr. It was then carefully sealed off and a hook formed at the end.

The metals were then heated and thoroughly mixed. This was done by rolling the tube on a piece of asbestos while playing an oxygen-gas flame on it. The tube was shaken until the 3d metal had completely disappeared into the host. The sample was cooled in water, making sure the billet was tapped away from the glass as sometimes the two stuck together, and the rapidly contracting metal cracked the glass.

Two or three crucibles were tied together and suspended in the furnace, pointed ends down. The alignment weight not only kept them straight but also reduced convection currents. Single crystals of zinc were produced at nearly every attempt, though increasing the impurity concentration above 0.1 atomic % reduced the successes to about 1 in 3. The failures were sometimes useable as the polycrystals were of a sufficient size to cut out and measure in the susceptibility apparatus.

The crystals could be easily cleaved at liquid nitrogen temperatures and cut to a final shape with a spark cutter in a paraffin bath. They were cleaned in a similar manner to the silica crucibles.

To test for iron impurities, the standard Honda-Owen plot of force against reciprocal field was carried out for all crystals and those which showed a slope of greater than 1% were discarded.

3.5. Chemical Analysis of ZnCr

3.5.1. Introduction

The crystals were analysed by an atomic absorption technique. An E.E.L. spectrophotometer model 140 was used, as this was inherently capable of measuring the chromium in the zinc to an accuracy of better than 1 part in 10^6. The instrument consists basically of a source of light emitting chromium lines at 357.8, 359.3, 360.5 and 425 nm., an atomiser, a stable flame, a monochromator, a photomultiplier and a readout meter.

The sample to be analysed is made into a solution and an aspirator draws this into a flame through which passes the light- beam. The flame (NO_2/acetylene) (Willis, 1965) is merely to convert the solution into atomic form. Despite temperatures of ~ 5000K, the majority of chromium atoms are in their ground state and so absorb the chromium lines. The abundance of the chromium species determines the total amount of absorption. The instrument was calibrated using standard chromium solutions.

3.5.2. Procedure

The standard solutions were prepared from 0.0984 gm. of potassium chromate (K_2CrO_4) dissolved in 500 ml. of water. This gave a 50 p.p.m. solution and a portion of this was further diluted to give 25 p.p.m. These standards were chosen as the response of the spectrophotometer was linear in this range using the NO_2/acetylene flame (fig. 3.14). The zinc chromium crystals were dissolved in concentrated hydrochloric acid (using the least amount of acid possible to dissolve the metal in a reasonable time) and made up to 2 ml. with water.

The instrument was left to warm up for about thirty minutes, after which drift in the lamp and photomultiplier were negligible. The slit width on the monochromator was set to

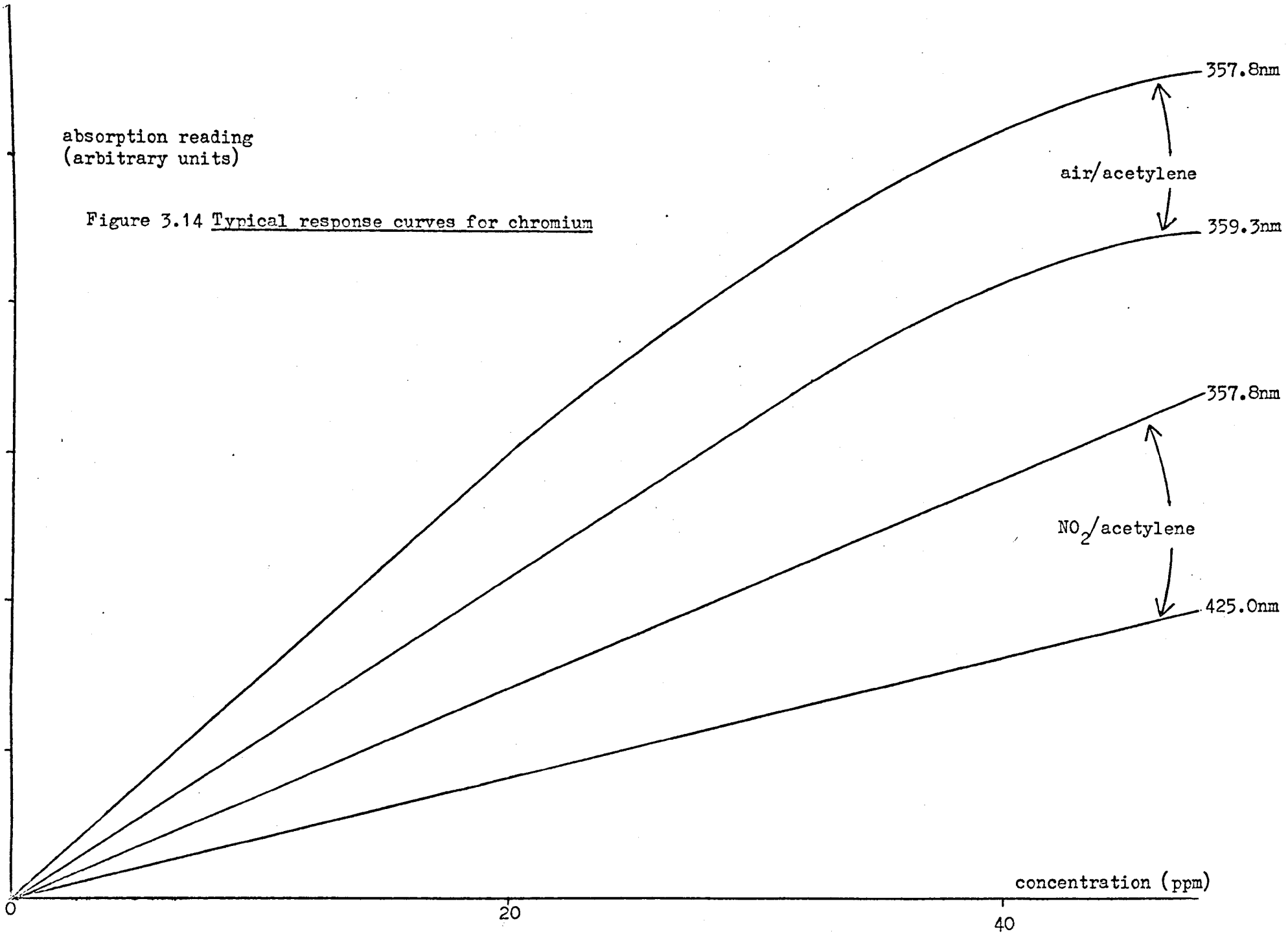

Figure 3.14 Typical response curves for chromium

0.08 mm. to ensure good separation of the 357.8, 359.3 and 360.5 nm. lines and the wavelength control set to 357.8 nm. This value was chosen as it gives the greatest absorption for the NO_2/acetylene flame, whilst remaining linear (fig. 3.15).

The flame was then lit, a flow rate of 10 p.s.i. for NO_2 and 8 p.s.i. for acetylene being found best for the standard burner supplied by E.E.L. Fine adjustments of the acetylene were made to give the flame an inner rose-red cone between 6 and 13 mm. high. A galvanometer was used to amplify the scale reading for greatest accuracy and set to read 100 when water was passed through the flame, and 0 with the 50 p.p.m. chromium solution. The 25 p.p.m. solution was used to check the linearity of the scale, and a calibration curve in mppm was plotted.

Both standard solutions were made acidic by adding hydrochloric acid in the same proportion as the metal solutions to ensure 1:1 correspondence between calibration and sample solutions. The presence of the following metals have no influence on the absorption of chromium :-

Na, Al, Ca, Co, Cu, Mn, Ni, V, Mo, Zn.

Excess hydrochloric acid does not affect the absorption, whereas sulphuric acid and nitric acid do (Feldman & Pardy, 1965; Kinson et al, 1963; Rann & Hambly, 1965).

Basu, P., Roll, A.,	Z. Metallkde	54,511,	1963
Bates, C.,	Modern Magnetism, (C.U.P.)		1963
Biswas, T.K., Roll, A.,	Z. Metallkde	55,794,	1964
Braunbeck, W.,	Z. Phys.	73,312,	1932
Edmunds,I.R., Smith,M.J.A.,	J. Phys. E.	5,1067,	1972
Fees,G., Roll,A.,	Z. Metallkde.	51, 540,	1960
Feldman, F.J., Pardy, W.C.,	Anal. Chim. Acta.	33, 273,	1965
Ford, C.J.,	Ph.D. Thesis, University of Warwick		1972
Haisty,R.W., Krebs,H.,	J. Non-Crystalline Solids	1, 399,	1969
Hanson,M.,	Constitution of Binary Alloys (McGraw Hill)		1958
Kaye,G.W.C., Laby,T.H.,	Tables of Physical & Chemical Constants. (Longman.)	p.118,	1966
Kinson, K., Hodges,R.J.,	Anal. Chim. Acta,	33, 273,	1965
Lambert, K.M.,	M.Sc. Thesis, University of Warwick		1970
Newrock,R.S., Serin,B., Vig, J., Boato, G.,	J. Low Temperature Phys.	5, 701,	1971
Ozelton,M.W., Wilson,J.R.,	J. Sci. Instrum.	43, 359,	1966
Rann,C.S., Hambly,A.N.,	Anal. Chem.	37, 879,	1965
Roll,A., Felger,H., & Motz,H.,	Z. Metallkde.	47, 707,	1956
Samsonov, G.V.,	Handbook of Physicochemical Properties of the Elements		1968
Verhoeven,J.D., Hucke,E.E.,	A.I.M.E. Trans.	227,1156,	1963
Walden, L.,	J. Sci. Instrum.	16, 1,	1939
Weber, C.L.,	Ann. Phys.	31, 243,	1887
Willis, J.B.,	Nature	207, 715,	1965

CHAPTER 4

ZINC ALLOY RESULTS

4.1. Low Temperature

4.1.1. Introduction

Dilute samples of polycrystalline ZnCr and ZnMn have been shown to follow a Curie-Weiss law up to 15K (Bell 1972) when a concentration-dependent host susceptibility is subtracted from the measured susceptibility. Experiments have been performed on single crystals of ZnCr to gain information about anisotropy parameters and hence the crystal field. To reduce possible impurity - impurity effects low concentrations of chromium must be used, and low temperatures attained to make the paramagnetic effect of chromium the dominant contribution to the measured susceptibility. Unfortunately these conditions are ideal for De Haas - Van Alphen (DHVA) oscillations to appear parallel to the crystallographic 'c' axis in zinc so a procedure has been devised to eliminate the field dependence from this cause. The lowest concentration alloy measured was Zn46Cr (where the concentration is in mppm), and since this is the least likely to have impurity - impurity effects and also less likely to have metallurgical problems than the more concentrated alloys, the major effort has been to deduce its anisotropic susceptibility and then compare the others with it. An outline of the method is given below.

In view of Bell's experiments, it is assumed that both axes of the zinc alloys obey a Curie-Weiss law, and that the host susceptibility of a polycrystal becomes approximately concentration (c) - independent when $c \gtrsim 150$ mppm. The perpendicular axis of zinc is not affected by DHVA oscillations, so a least squares analysis of the inverse incremental susceptibility change with temperature on these unambiguous results gives a value for the perpendicular host

susceptibility ($\chi_{\perp}^{o}$) needed to give the best straight line fit to a Curie-Weiss law. This value can then be combined with the appropriate polycrystalline host susceptibility to furnish information on the parallel axis host susceptibility ($\chi_{\parallel}^{o}$) at various temperatures. This information is used in conjunction with the $\chi_{\parallel}$ results of a more concentrated crystal (Zn135Cr) where the increase in c has greatly reduced the DHVA effect thus enabling a correlation to be made where the only unknown is the incremental susceptibility ($\Delta\chi_{\parallel}$) of the Zn46Cr crystal. Subtracting $\chi_{\parallel}^{o}$ from this gives a derived value of $\chi_{\parallel}$ for Zn46Cr which can be compared with the actual results to see if the two are in reasonable agreement. Then the anisotropy of several ZnCr crystals can be determined with values for the effective spin moment n and Curie-Weiss intercept θ . Further analysis with work on pure zinc can give a quantitative measure of the success of the above procedure and indicate a value for the Dingle temperature.

4.1.2. Results

The susceptibilities of several ZnCr single crystals were measured (section 3.1.3) between 4.2 and 50K, and these are shown in figures 4.1 to 4.7. The results for Zn46Cr and Zn135Cr were taken on a susceptibility system at A.E.R.E. Harwell, made available by Dr. W. Gardner. They show that the measured susceptibilities are independent of field for the case when the applied magnetic field is perpendicular to the crystallographic c-axis ($\chi_{\perp}$). This is not the case for the parallel axis ($\chi_{\parallel}$) where the DHVA effect is markedly show up for low concentrations of Cr at low temperatures. A polycrystalline metal does not have DHVA oscillations as the Fermi surface of each crystallite must be aligned similarly throughout the bulk of the crystal with respect to the magnetic field. Recently Bell has done some work on polycrystalline ZnCr and ZnMn and knowledge of this coupled with the present data allow the temperature dependence of the susceptibility of the principal axes to be derived. Hence knowledge of the anisotropy, Curie-Weiss θ and effective spin value n

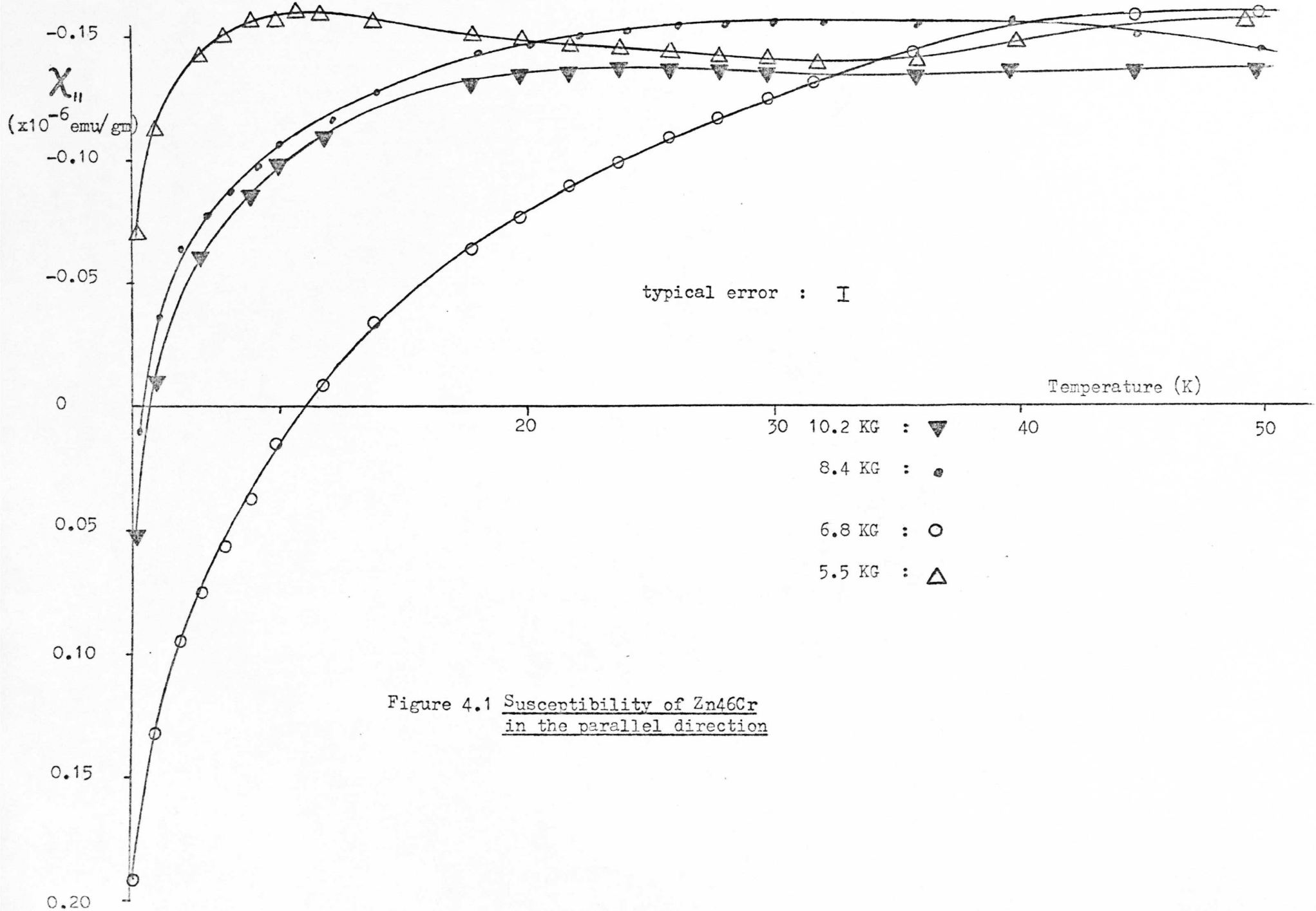

Figure 4.1 Susceptibility of Zn46Cr in the parallel direction

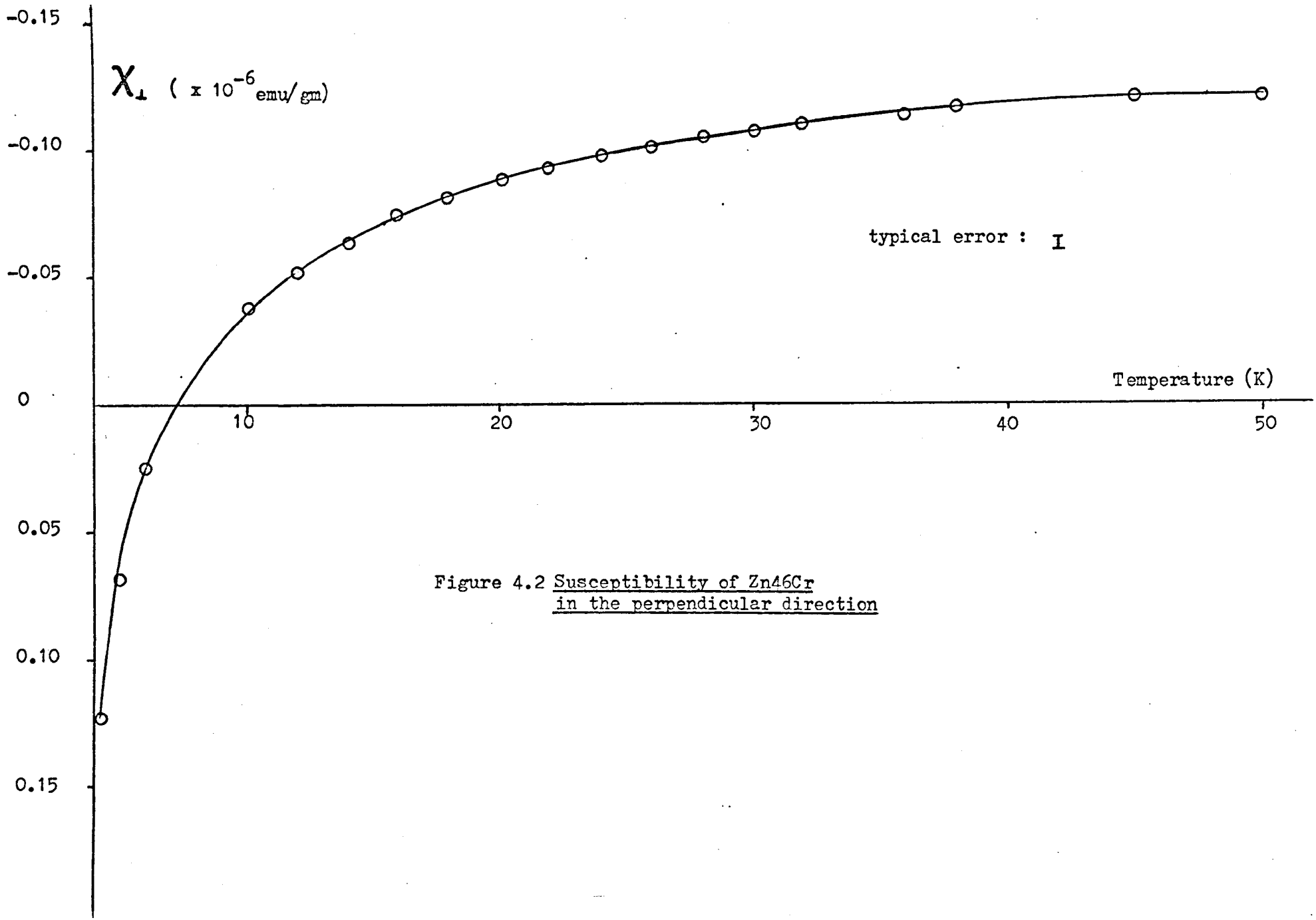

Figure 4.2 Susceptibility of Zn46Cr
in the perpendicular direction

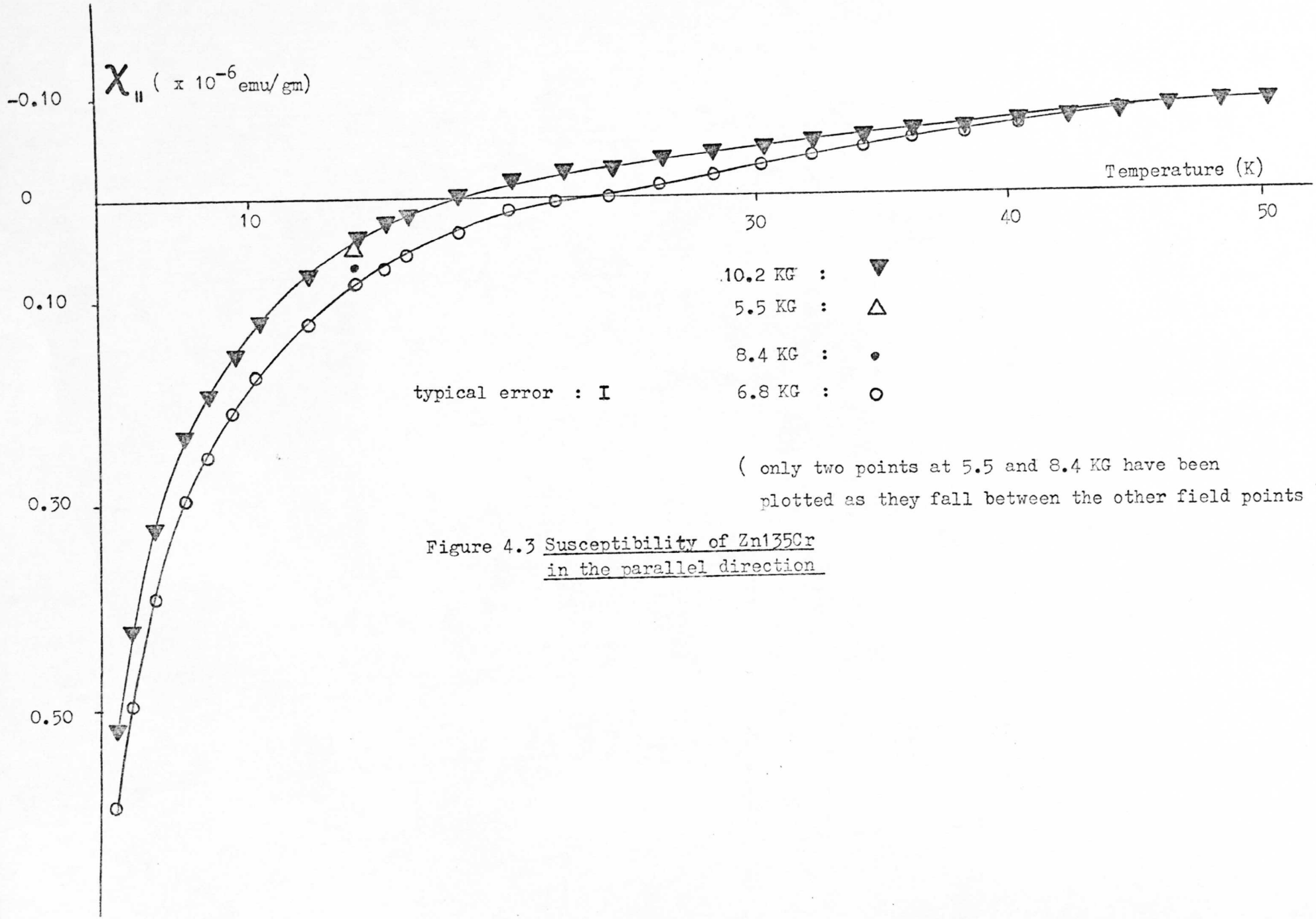

Figure 4.3 Susceptibility of Zn135Cr in the parallel direction

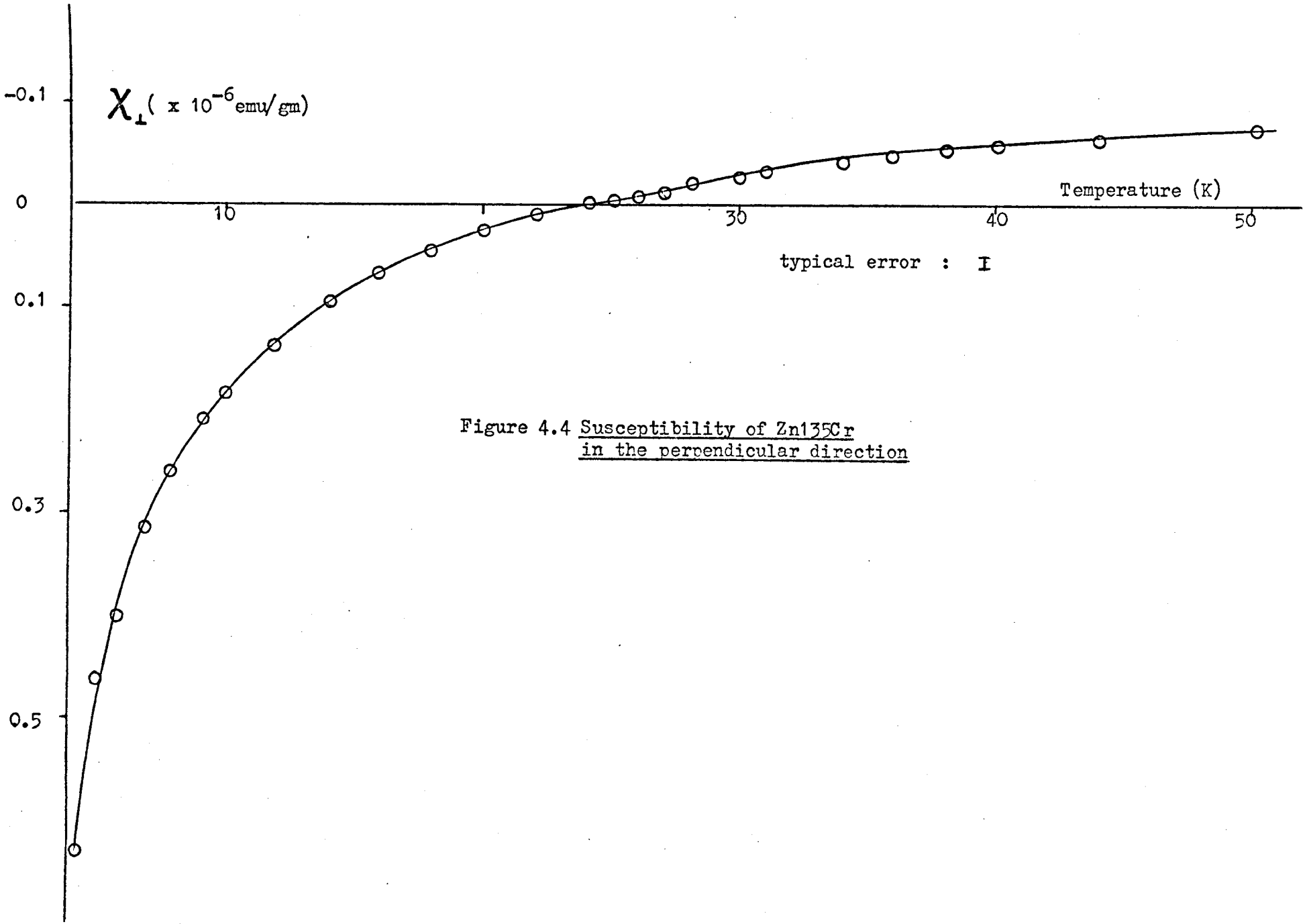

Figure 4.4 Susceptibility of Zn135Cr in the perpendicular direction

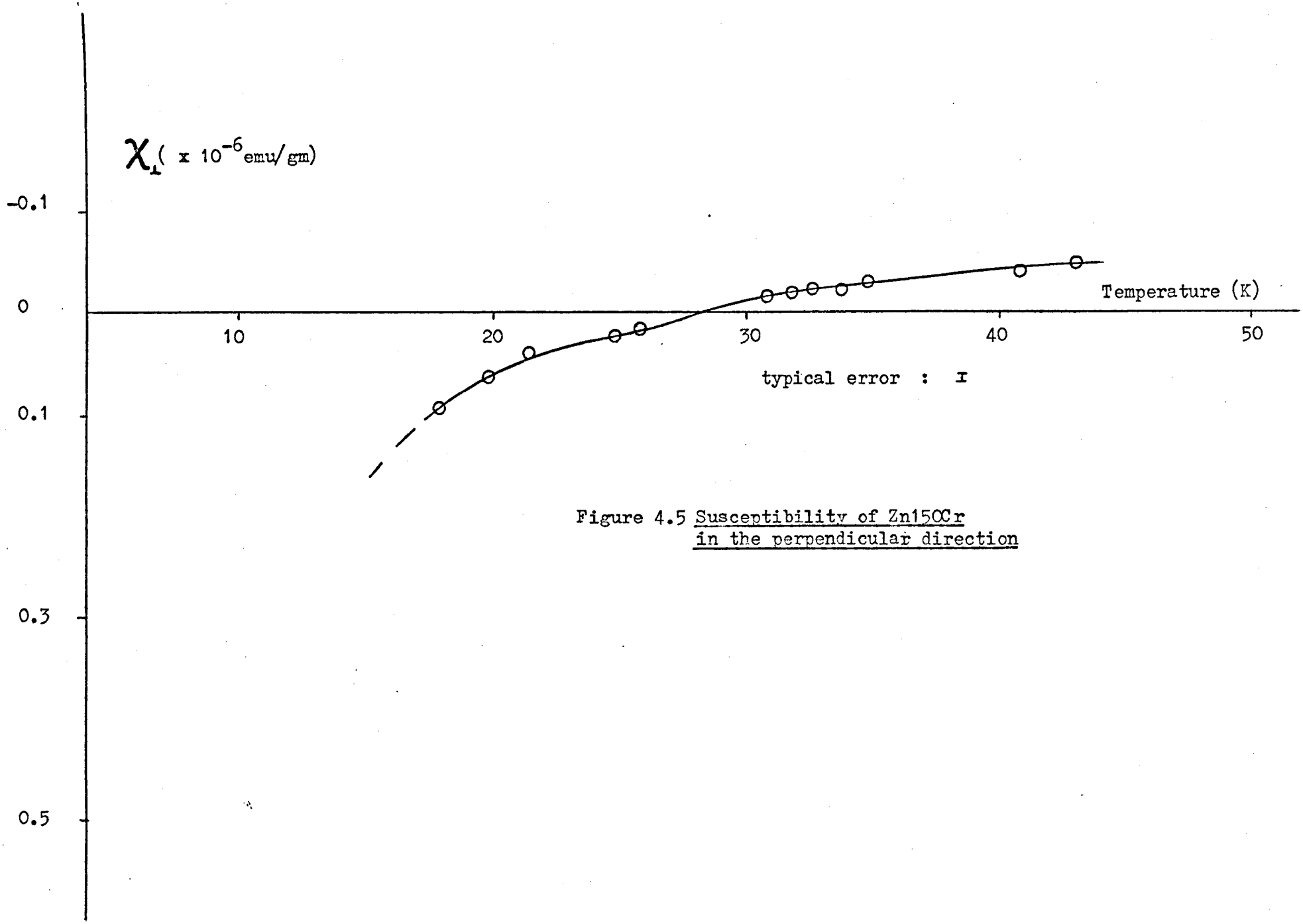

Figure 4.5 Susceptibility of Zn15OCr in the perpendicular direction

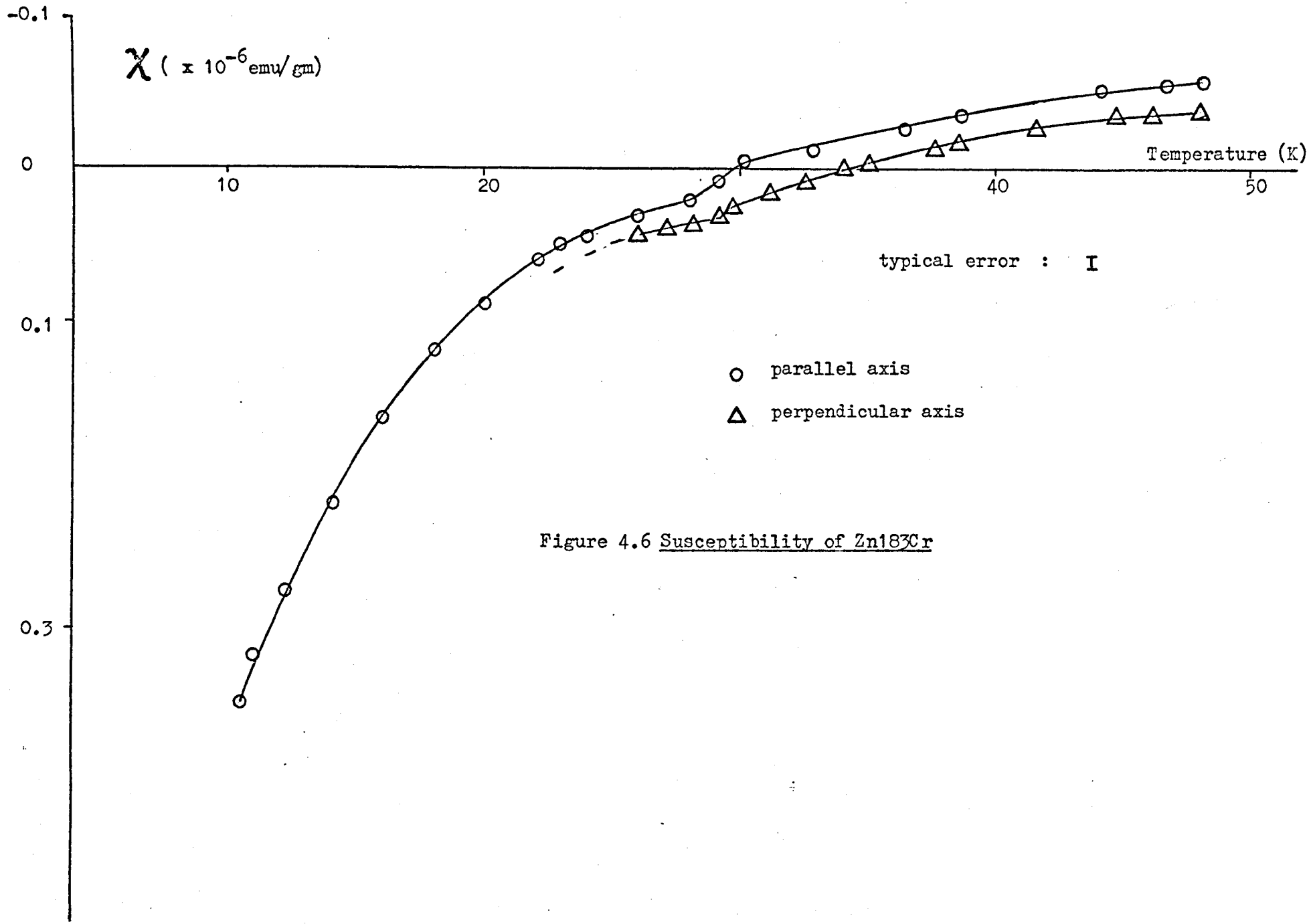

Figure 4.6 Susceptibility of Zn183Cr

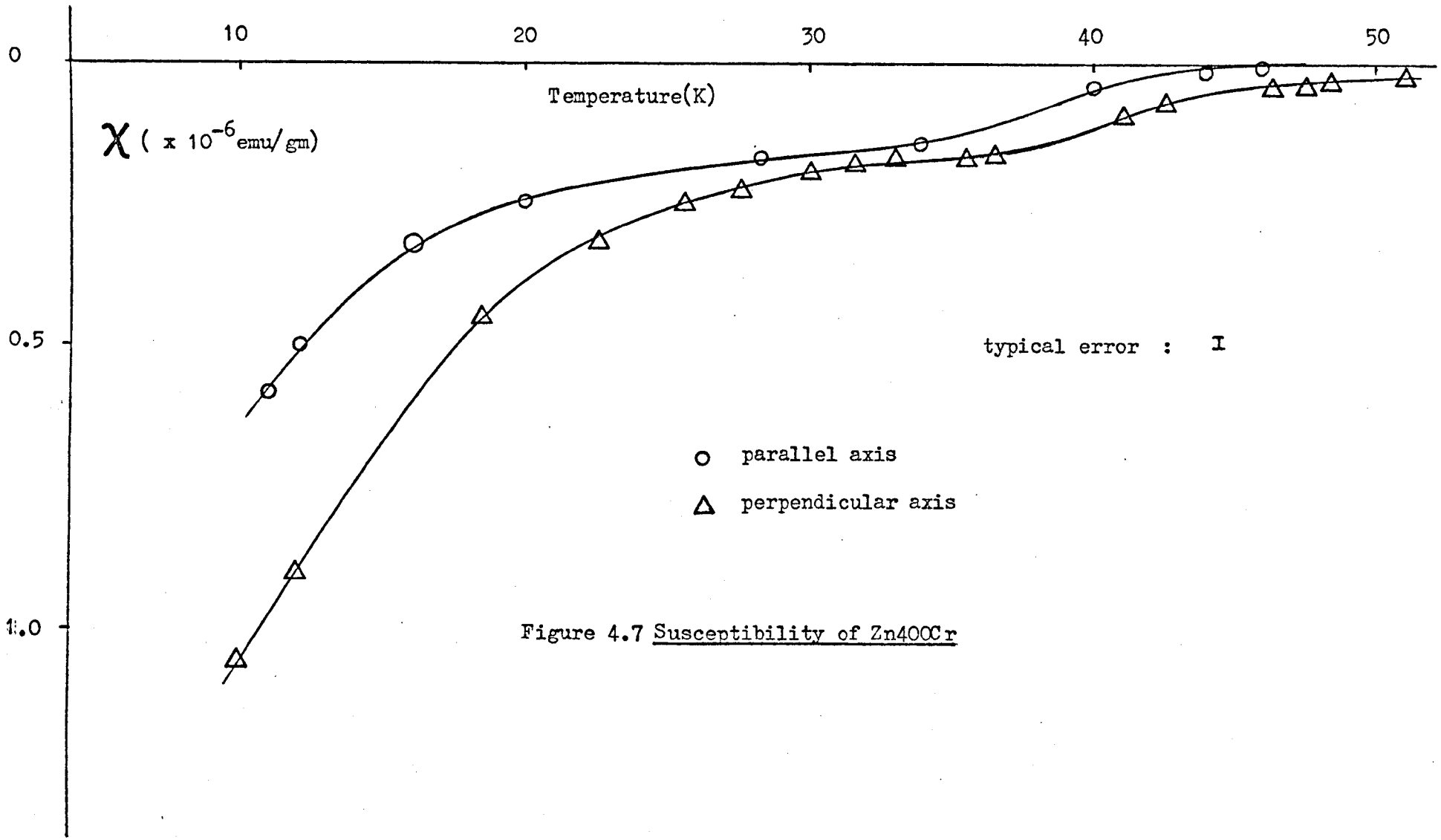

Figure 4.7 Susceptibility of Zn400Cr

can be obtained.

4.1.3. Analysis

For an isotropic magnetic material one can write :

$$\chi_m = \chi_h + \chi_{mag} \qquad 4.1$$

where χ_m = measured susceptibility

χ_h = host susceptibility

χ_{mag} = 'magnetic' susceptibility

The units for susceptibility will in nearly all cases be 10^{-6} emu/gm. For ZnCr, χ_{mag} is the magnetic contribution (in a Curie-Weiss (C-W) sense) due to the chromium atoms in the zinc environment. χ_h is determined by the host containing non-magnetic impurities. One can further divide χ_h via :

$$\chi_h = \chi_{i.c.} + \chi_{el} \qquad 4.2$$

where $\chi_{i.c.}$ = ion core contribution

χ_{el} = electronic contribution

and: $$\chi_{el} = \chi_{DHVA} + \chi_e \qquad 4.3$$

where χ_{DHVA} = De Haas-Van Alphen effect on susceptibility

χ_e = oscillatory terms made up of Pauli, Landau and orbital effects.

So: $$\chi_m = \chi_{i.c.} + \chi_e + \chi_{DHVA} + \chi_{mag} \qquad 4.4$$

The ion core term variation is small (Dupree et al. 1971) compared with the other terms in equation 4.4 so will be ignored. Subsequent analysis will remove the DHVA effect leaving a field-independent term χ_e and the magnetic term χ_{mag} for single crystals of ZnCr.

For an hexagonal crystal, the isotropic susceptibility can be written in terms of susceptibility parallel and perpendicular to the principal crystallographic axis (c-axis in zinc) :

$$\chi = 1/3(\chi_{\parallel} + 2\chi_{\perp}) \qquad 4.5$$

Equation 4.5 will be used for a ZnCr alloy, but for a single crystal of zinc or zinc-nonmagnetic impurity, a superscript 'o' will be added:

$$\chi^{o} = 1/3(\chi^{o}_{\parallel} + 2\chi^{o}_{\perp}) \qquad 4.6$$

To determine if a Curie-Weiss law is followed, it will be convenient to define an incremental susceptibility $\Delta\chi_{a}$:

$$\Delta\chi_{a} = \chi_{a} - \chi^{o}_{a} \qquad 4.7$$

where a = principal axis ($\parallel$ or $\perp$)
χ_{a} = measured susceptibility along one axis
χ^{o}_{a} = host susceptibility along the same axis

With equation 4.7 thus defined, $\Delta\chi_{a}$ can be equated with χ mag and χ^{o}_{a} with χ e (where χ^{o}_{a} here means a host of zinc plus nonmagnetic impurity).

Firstly it is necessary to determine a value for χ^{o}_{a}. From the concentration dependence of chromium in zinc Bell (1972) found χ^{o} was -0.153 $\pm$ 0.005 when c $\simeq$ 50mppm (figure 4.8). Extrapolating to higher concentration gives $\chi^{o} \simeq$ -0.134 $\pm$ 0.01 when c $\gtrsim$ 150mppm, though it may be shown that even a 10% error in this value for the host susceptibility is not important at low temperatures. The susceptibility of pure zinc as host need not necessarily be the value to subtract from ZnCr as the lattice may distort due to the added impurity and change the Fermi surface. Therefore copper, cadmium and iron were added to zinc to gauge the effect this had, with the results shown in figures 4.9, 4.10 and 4.11. Figures 4.9 and 4.10 show that $\chi^{o}_{\perp}$

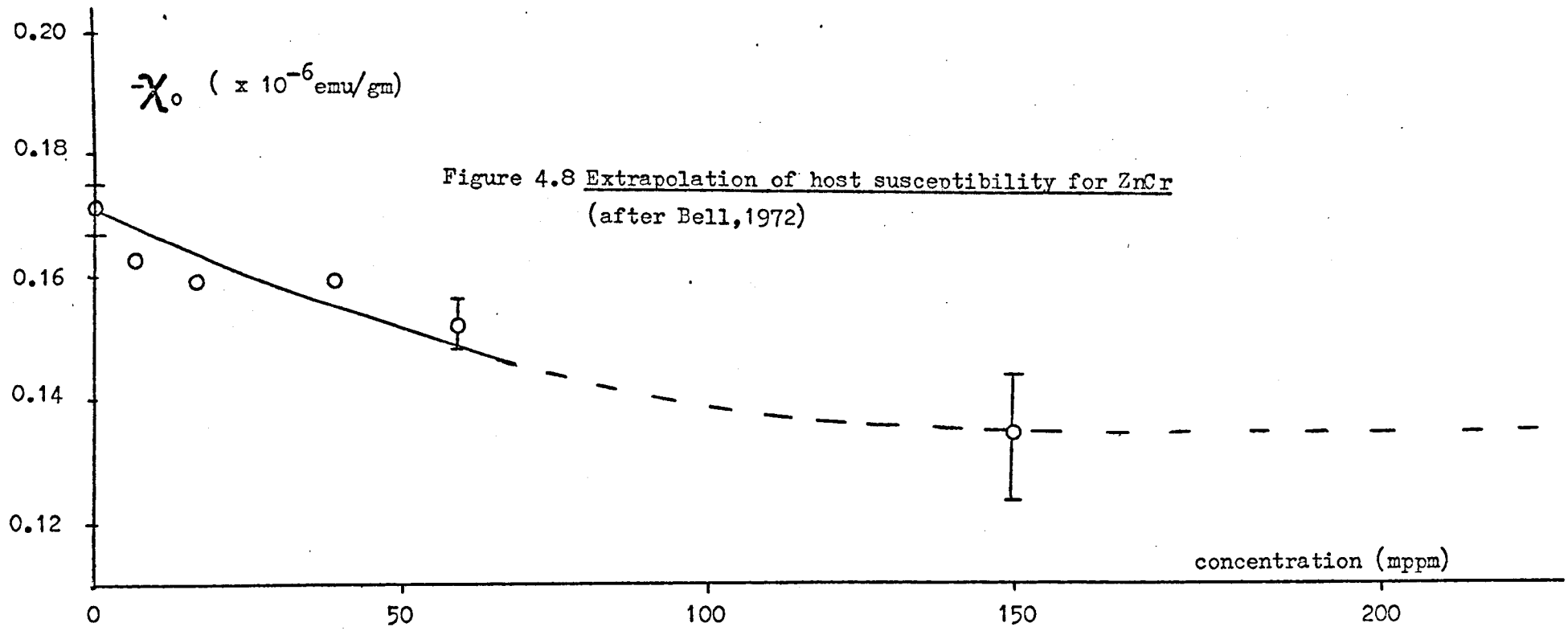

Figure 4.8 Extrapolation of host susceptibility for ZnCr
(after Bell,1972)

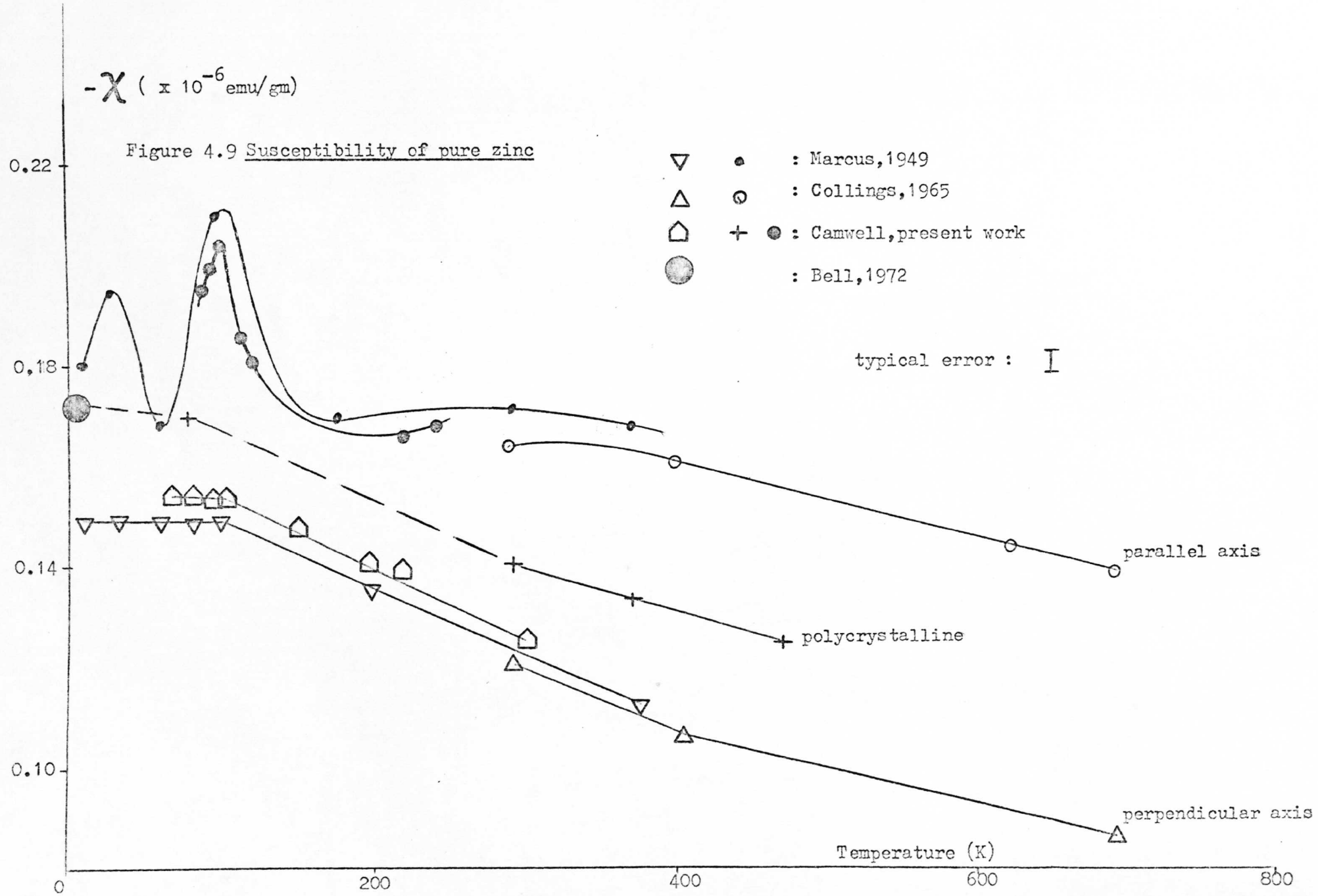

Figure 4.9 Susceptibility of pure zinc

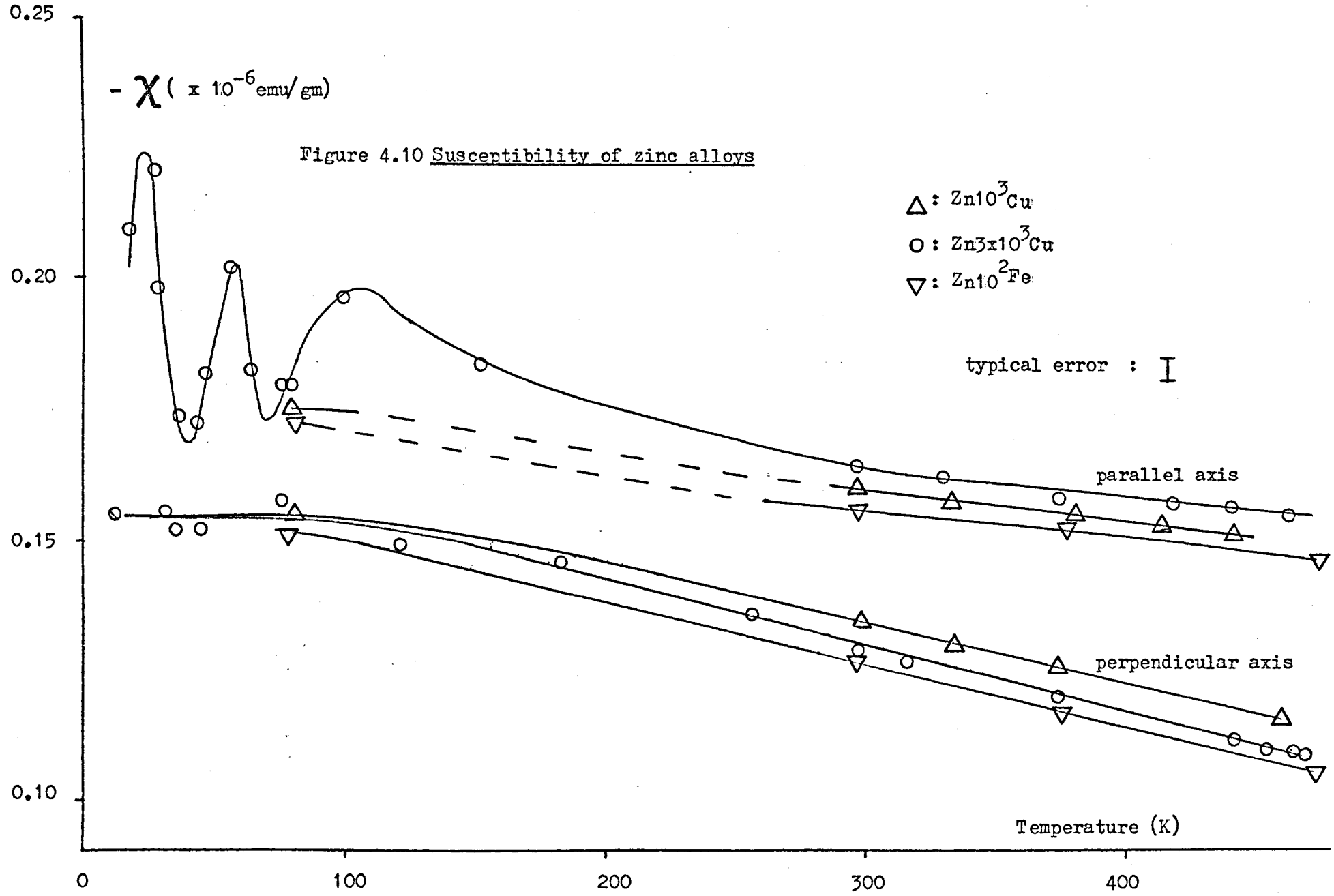

Figure 4.10 Susceptibility of zinc alloys

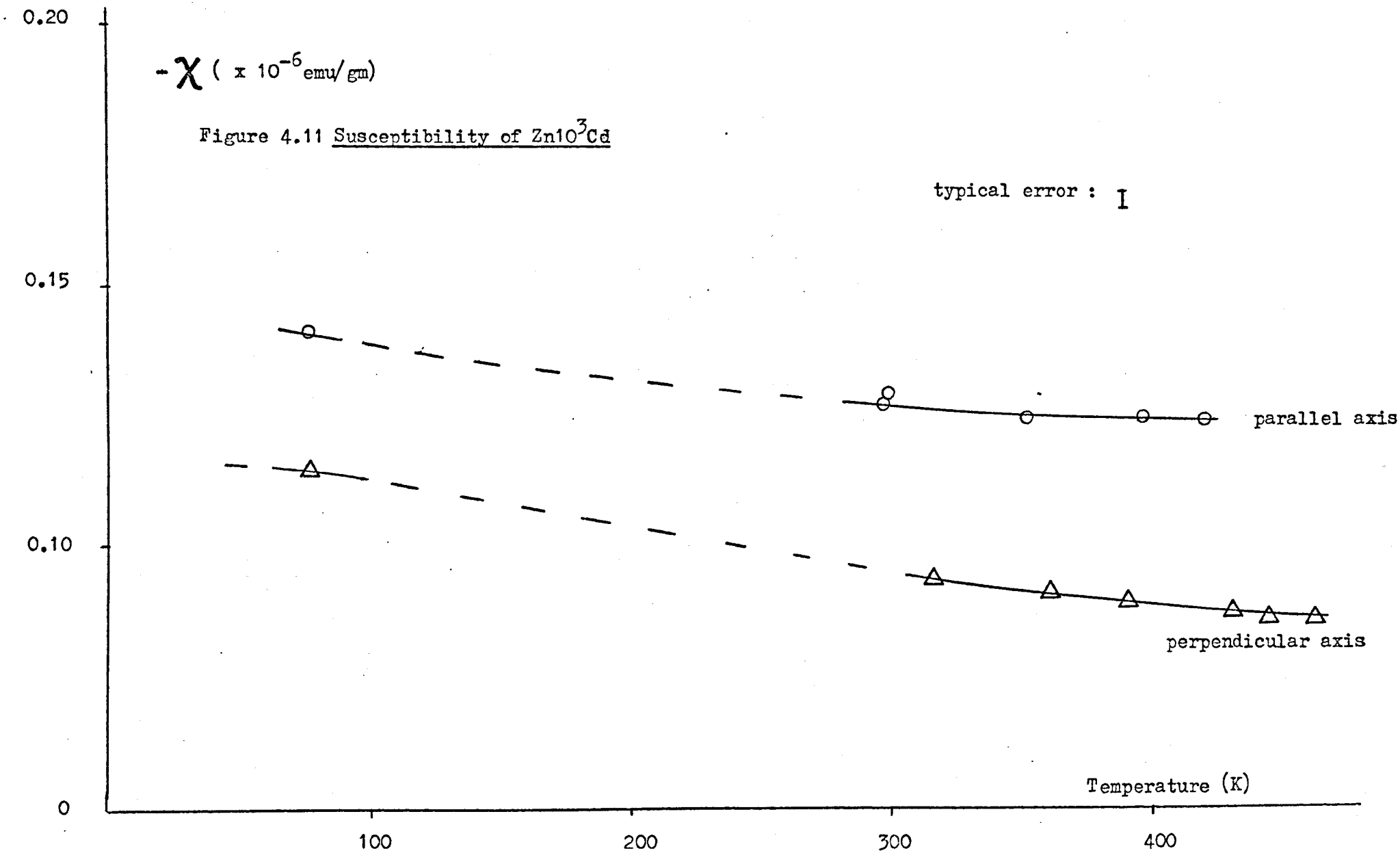

Figure 4.11 Susceptibility of $Zn10^{3}Cd$

remains essentially constant at -0.155 ± 0.005 when the temperature T $\lesssim$ 77K for Zn, Zn10^3Cu, Zn3×10^3Cu and Zn10^2Fe. As Bell has shown a C-W law holds for polycrystalline ZnMn and ZnCr at low temperatures (T $\lesssim$ 15K), a least squares analysis was carried out on $1/\Delta\chi_a$ vs. T for single crystals of Zn46Cr and Zn400Cr to see that the C-W law is followed. The relevant equation is :

$$\Delta\chi_a = \frac{D\ c}{(T+\theta)} \qquad 4.8$$

where $D = \frac{n^2\beta^2 Na}{3kA}$

n = effective spin value
β = Bohr magneton
Na = Avogadro's number
A = atomic weight of zinc
k = Boltzmann's constant

The analysis treats $1/\Delta\chi_a$ as linear in T so a C-W law is obeyed when the errors are minimised (see figures 4.12 to 4.17). The value of χ^o where the error in the intercept θ (and equivalently the error in the slope S) is a minimum is chosen. For all crystals it was found that the 'best' value of $\chi^o_\perp$ was -0.1475 ± 0.005. A typical result of the least squares analysis is shown in table 4.1.

Table 4.1 Zn 135 Cr

$-\chi^o_a$	0.140	0.145	0.150	0.155	0.160
S	0.298	0.287	0.276	0.266	0.257
δS	0.00270	0.00257	0.00250	0.00252	0.00257
$-\theta$(K)	0.233	0.440	0.643	0.846	1.032
$\delta\theta$(K)	0.121	0.116	0.117	0.123	0.130

Temperature range from 4.2K to 22K — δS = error in S
Number of measurements = 13 — $\delta\theta$ = error in θ

The curve resulting from plotting $\delta\theta$ and δS against χ_a^o is always shallow because the paramagnetism of chromium at low temperatures can be as much as an order of magnitude greater than the diamagnetism of the zinc host. Changing χ_a^o by the amount shown in table 4.1 has therefore only a small effect on the net susceptibility .

Having determined the perpendicular host value, equation 4.7 gives a value for $\Delta\chi_\perp$. The two lowest concentration crystals, namely Zn46Cr and Zn135Cr, can be correlated to eliminate the DHVA effect at each temperature thus :

T = 4.2K

$$\Delta\chi_\perp(46) = 0.1215 - (-0.1475) = 0.2690 \pm 0.005$$
$$\Delta\chi_\perp(135) = 0.63 - (-0.1475) = 0.7775 \pm 0.005$$

So:

$$\frac{\Delta\chi_\perp(135)}{\Delta\chi_\perp(46)} = \frac{0.7775}{0.2690} = 2.890 \pm 0.006 = \frac{\Delta\chi_{II}(135)}{\Delta\chi_{II}(46)} \qquad 4.9$$

$$\therefore \Delta\chi_{II}(46) = \frac{\Delta\chi_{II}(135)}{2.890} \qquad 4.10$$

Equation 4.10 will be used to determine the DHVA - free susceptibility for Zn46Cr because inspection of figures 4.1 to 4.7 show this crystal has no discernible anomalies due to possible impurity clustering or intermetallic compounds forming. The value of $\Delta\chi_{II}(135)$ can be found by using equation 4.6 with $\chi^o = -0.134$ and $\chi_\perp^o = -0.1475$ to give $\chi_{II}^o(135) = -0.107 \pm 0.030$, then taking the mean of $\chi_{II}(135)$ to be 0.555 ± 0.040 from figure 4.3 at this temperature (4·2K) where the DHVA oscillations are greatly reduced in this sample (compared with Zn46Cr) due to the greater concentration of chromium, results in $\Delta\chi_{II}(135) = 0.662 \pm 0.040$. Equation 4.6 similarly furnishes a value of -0.161 ± 0.005 for $\chi_{II}^o(46)$ with $\chi^o = -0.152$ so equation 4.10 can be re-written :

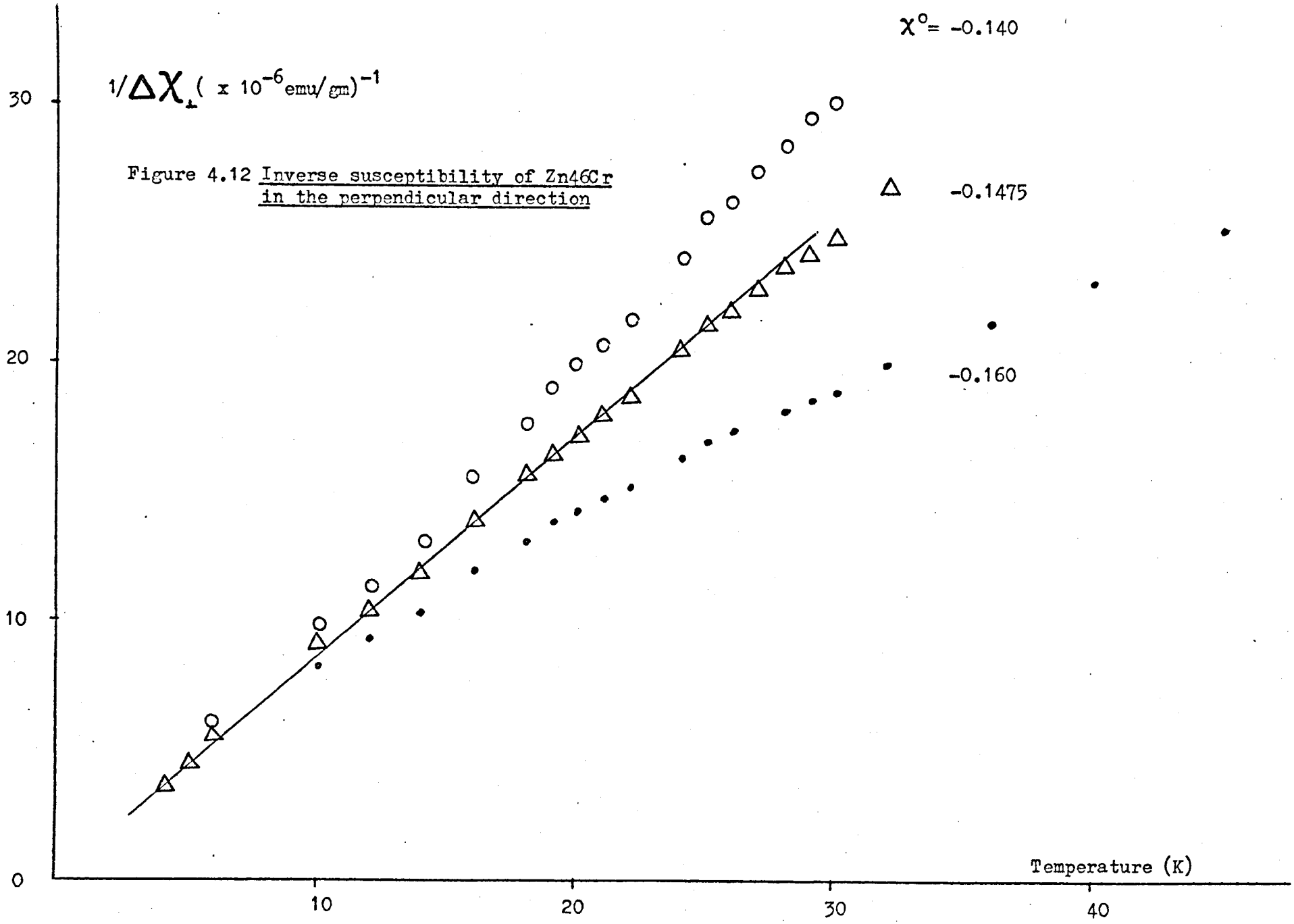

Figure 4.12 Inverse susceptibility of Zn46Cr in the perpendicular direction

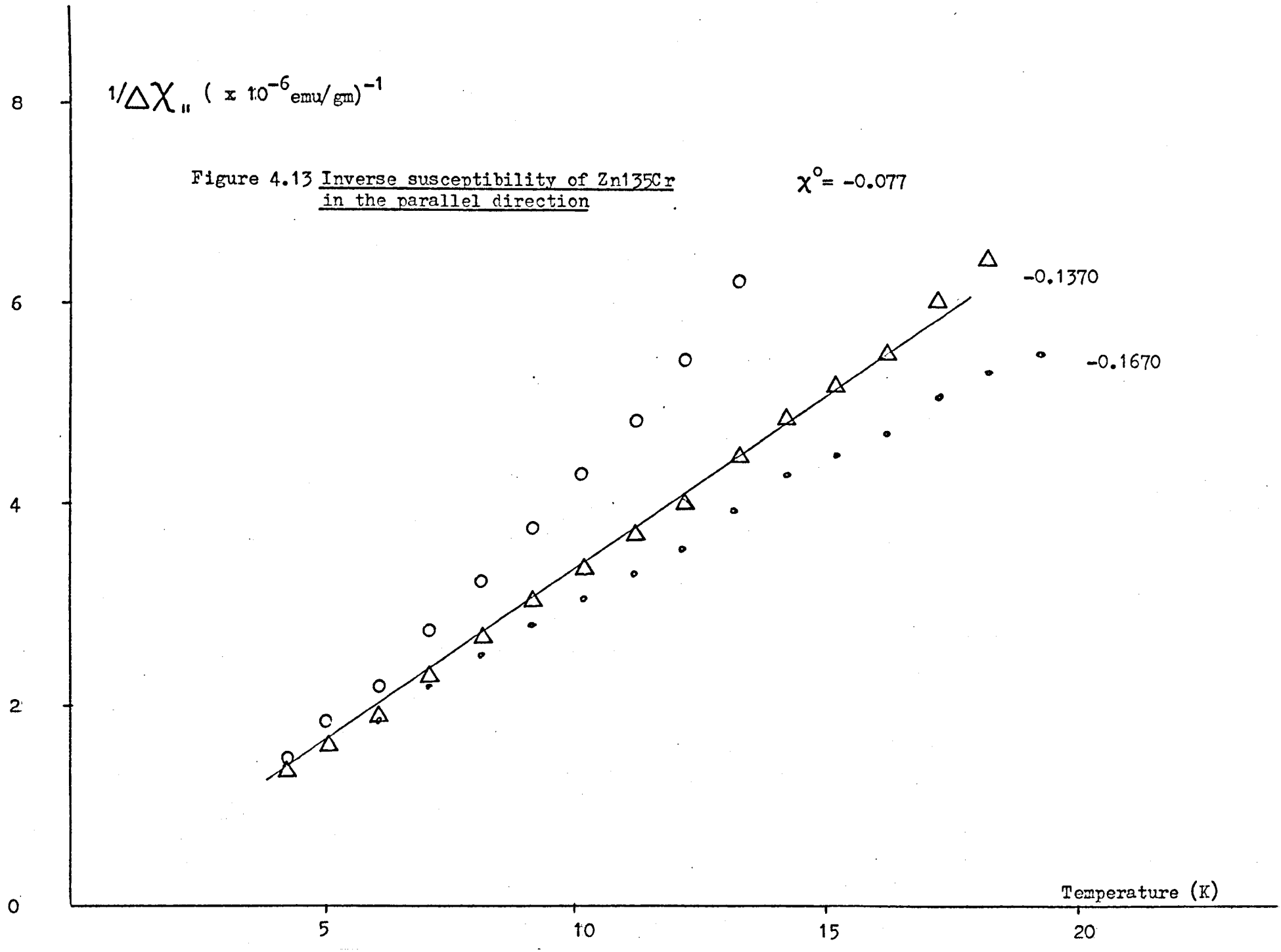

Figure 4.13 Inverse susceptibility of Zn135Cr in the parallel direction

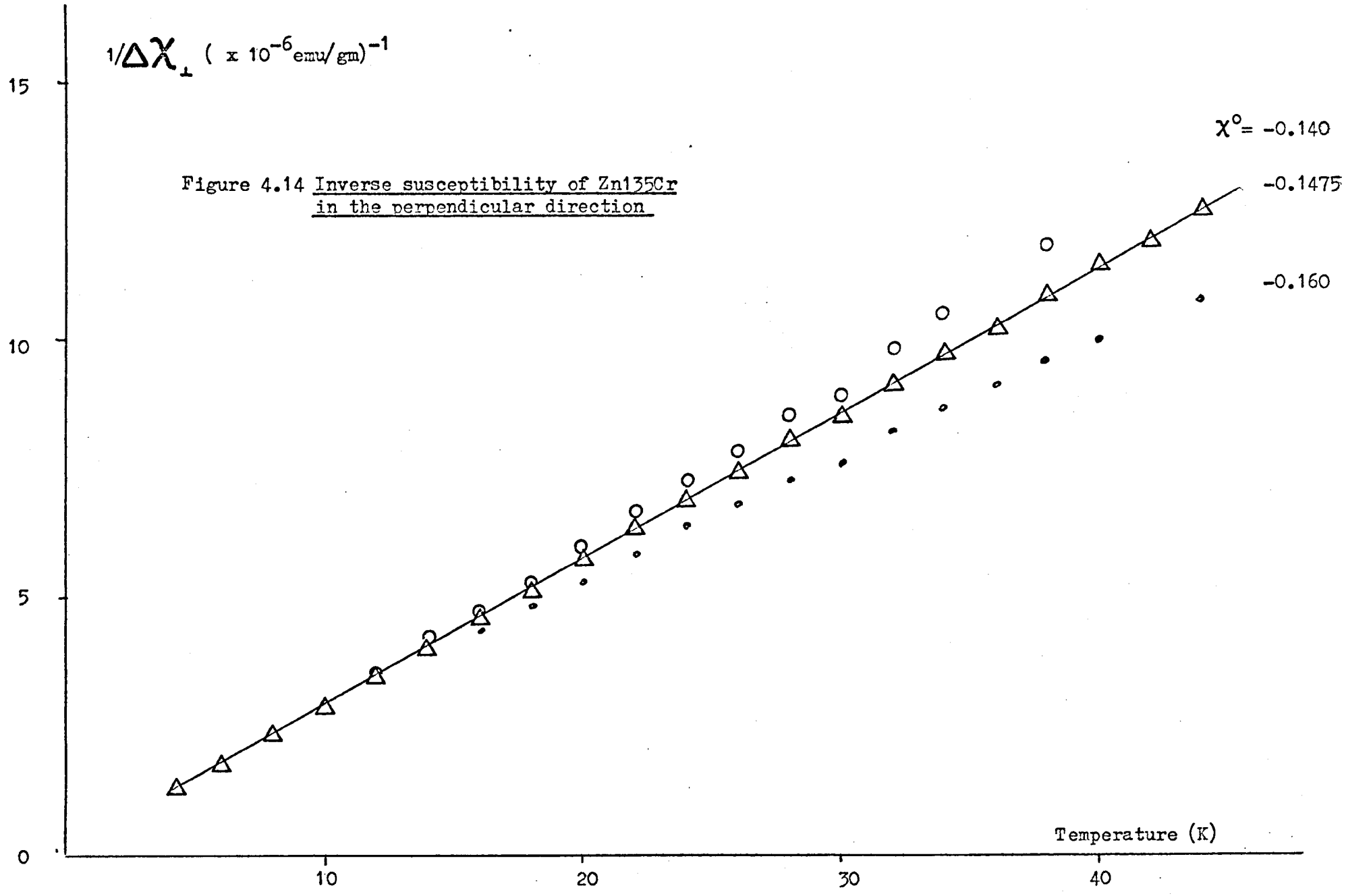

Figure 4.14 Inverse susceptibility of Zn135Cr in the perpendicular direction

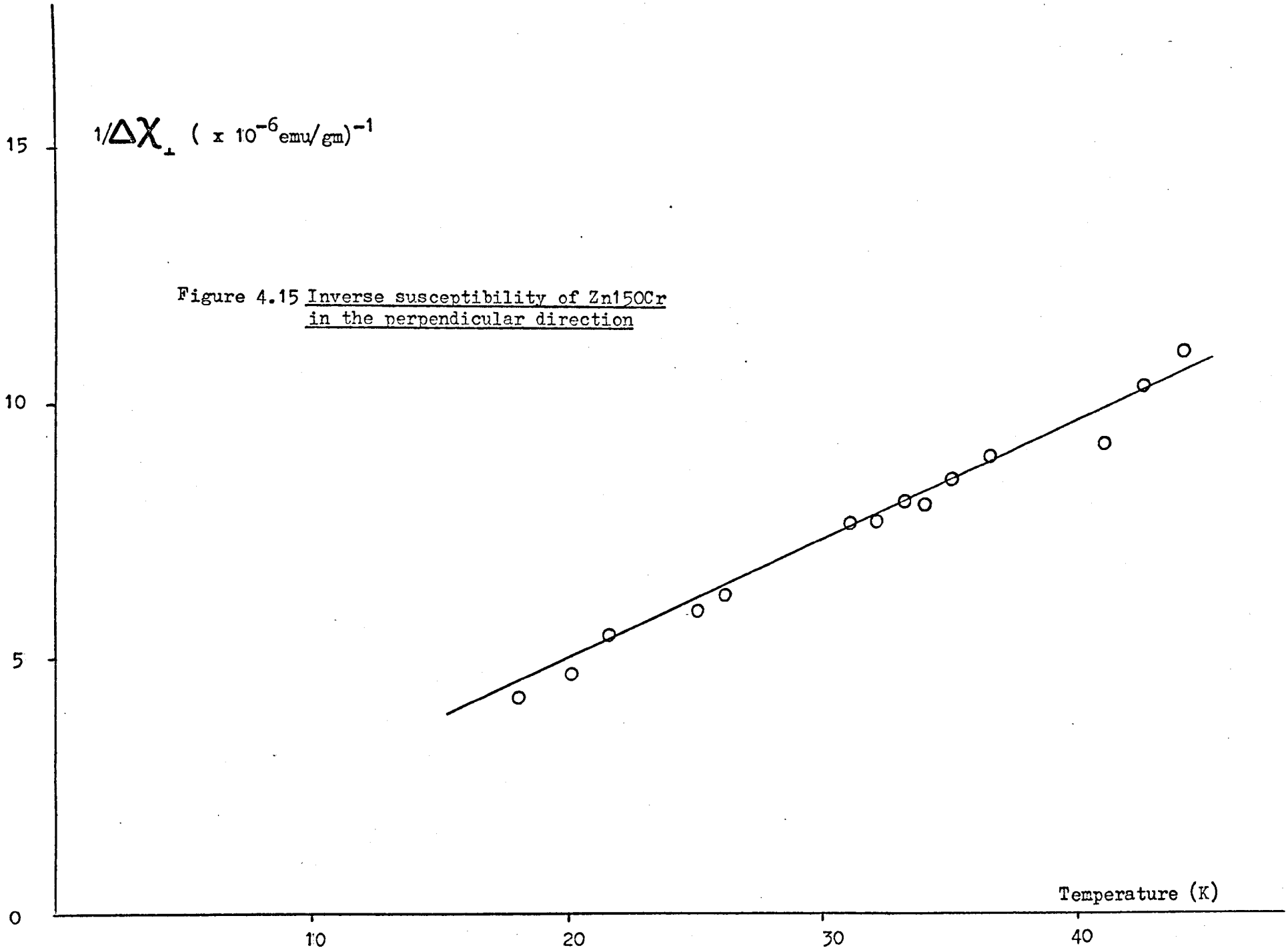

Figure 4.15 Inverse susceptibility of Zn150Cr in the perpendicular direction

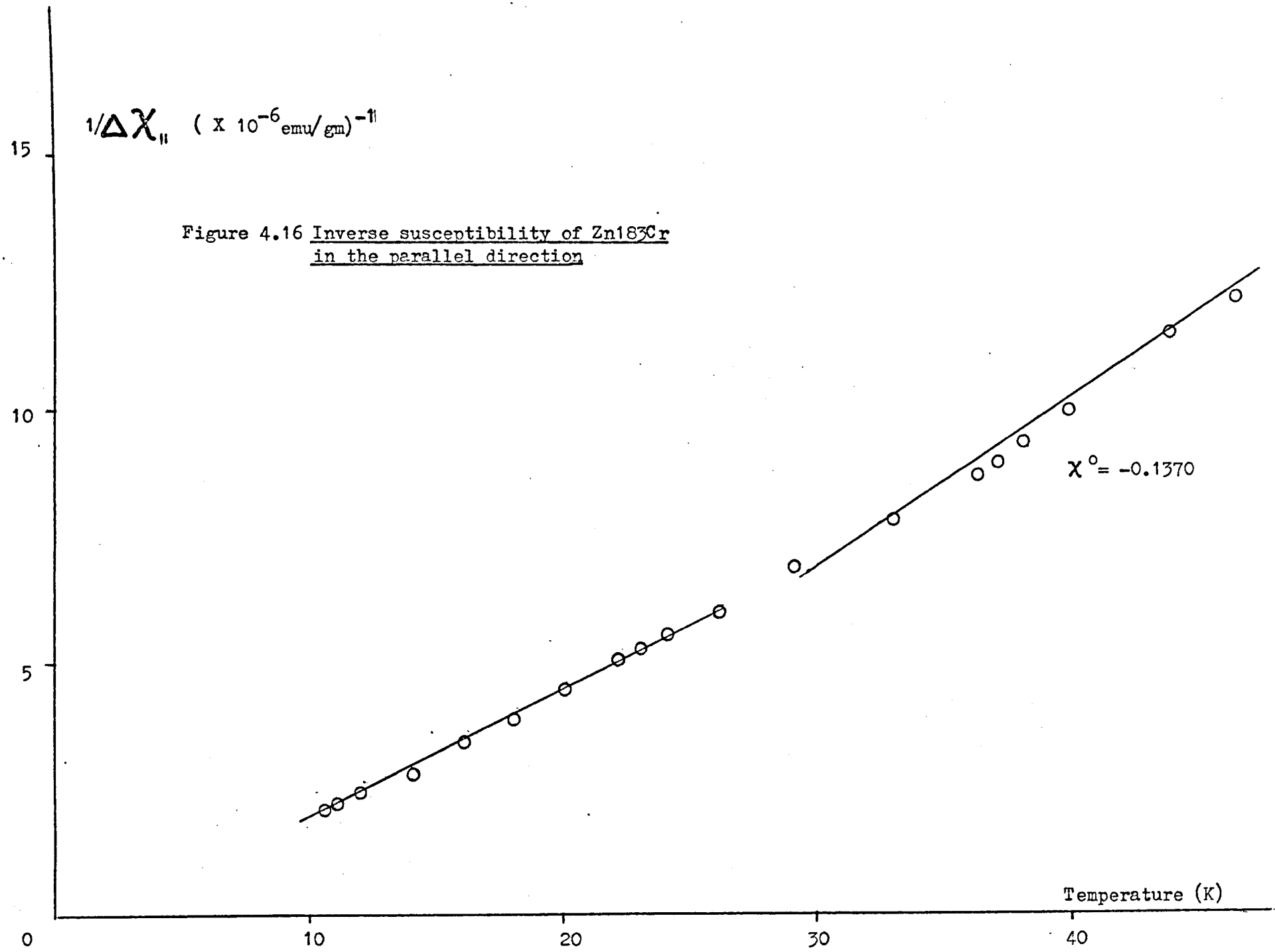

Figure 4.16 Inverse susceptibility of Zn183Cr in the parallel direction

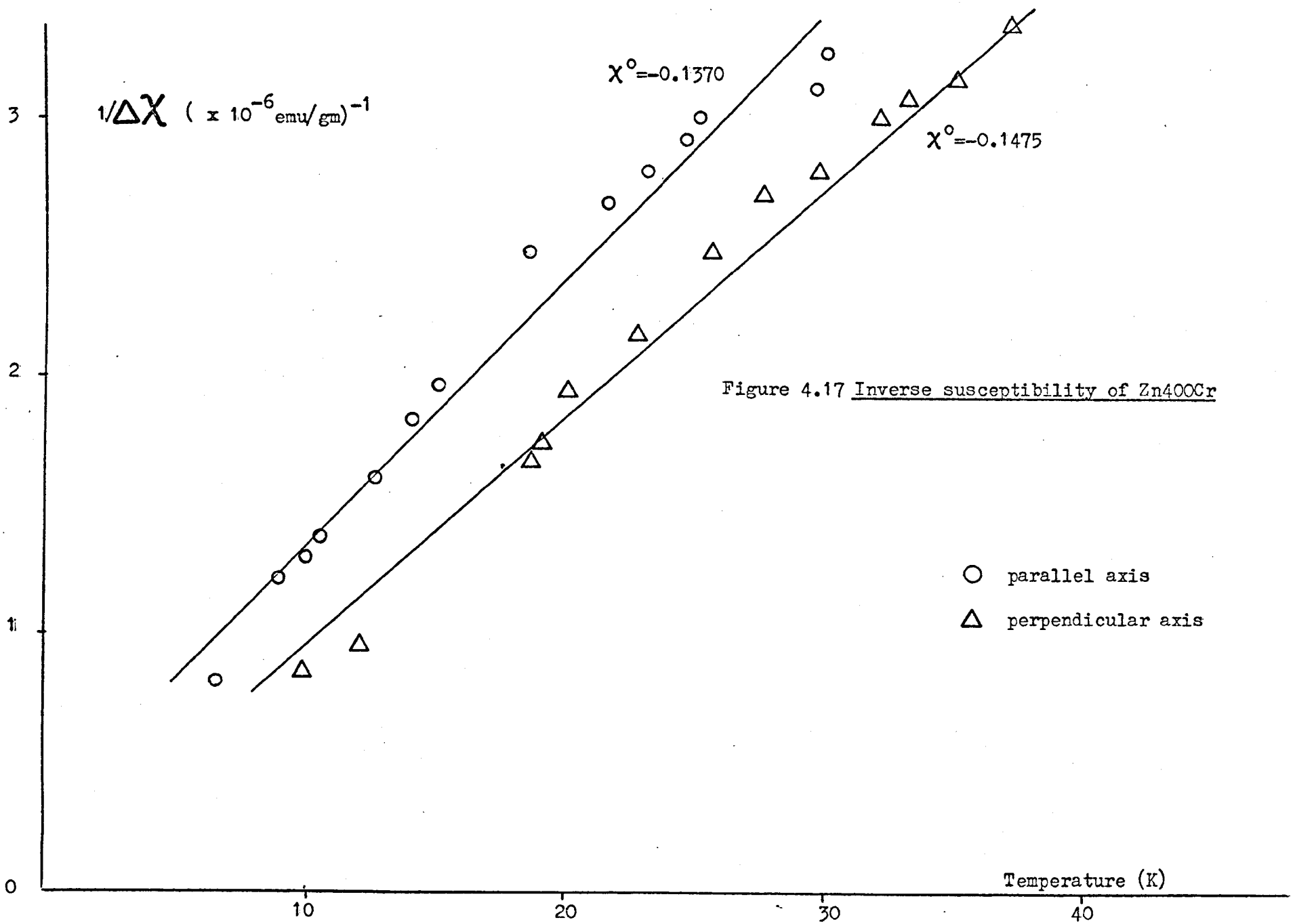

Figure 4.17 Inverse susceptibility of Zn400Cr

$$\Delta\chi_{\perp}(46) = \frac{0.662}{2.890} = 0.229 \pm 0.010$$

but $0.229 = \chi_{\perp}(46) - (-0.161)$ from equation 4.7

$\therefore \quad \chi_{\perp}(46) = 0.068 \pm 0.010$

This procedure was repeated at each temperature measurement and the results are plotted in figure 4.18. Intuitively one may expect that $\chi_{\perp}(46)$ when free of DHVA effects lies approximately at the mean of the field-dependent results, and the figure 4.18 reinforces this belief. A plot of $1/\Delta\chi_{\perp}(46)$ against T (Figure 4.19) shows that the results may be fitted to a Curie-Weiss law. Figure 4.12 shows the less ambiguous results of $1/\Delta\chi_{\perp}(46)$ against T, and figures 4.13 to 4.17 show similar plots for other crystals (Zn 135, 150, 183, 400 Cr).

To give one confidence that the above analysis has not given meaningful results merely by accident, further correlation of the data with results on pure zinc have been carried out as follows.

Berlincourt et al., (1954) have presented some results on a single crystal of zinc in the form of $\delta\chi_o$ versus H cos ϕ at a range of temperature from 4.2 to 295K. Only the results at T = 4.2K and 28.3K are of interest here (figures 4.20 and 4.21).

A torsion balance (Schoenberg, 1957) was used, so the parameters are :

$$\delta\chi_o = \chi_{\perp}^o - \chi_{\parallel}^o \qquad 4.11$$

$$H\cos\phi = H_{\perp} \qquad 4.12$$

where

$\chi_{\perp}^o$, $\chi_{\parallel}^o$ have their usual meaning,

$H_{\perp}$ is the applied magnetic field parallel to the c axis of zinc,

ϕ is the angle between H and the c axis.

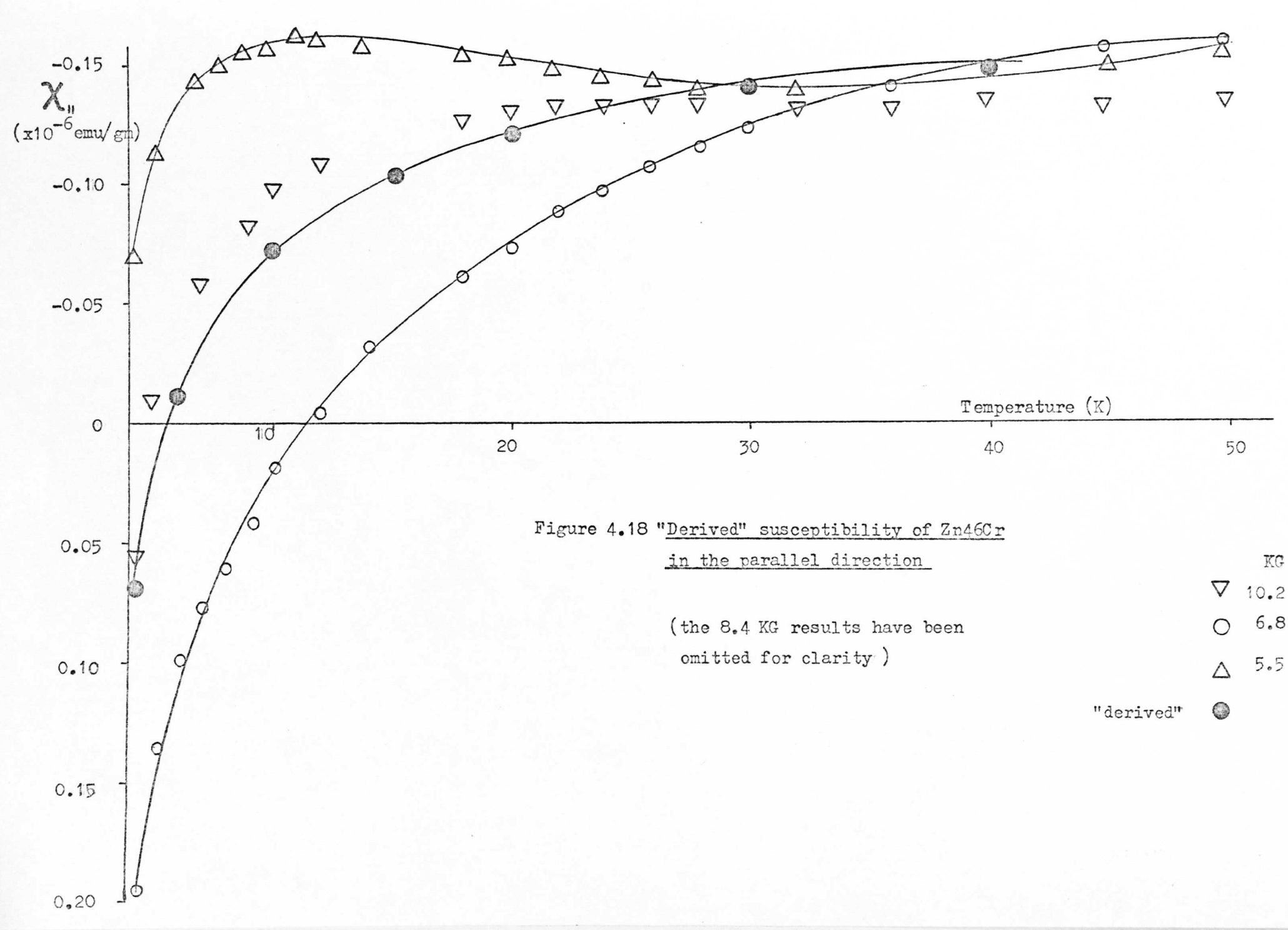

Figure 4.18 "Derived" susceptibility of Zn46Cr in the parallel direction

(the 8.4 KG results have been omitted for clarity)

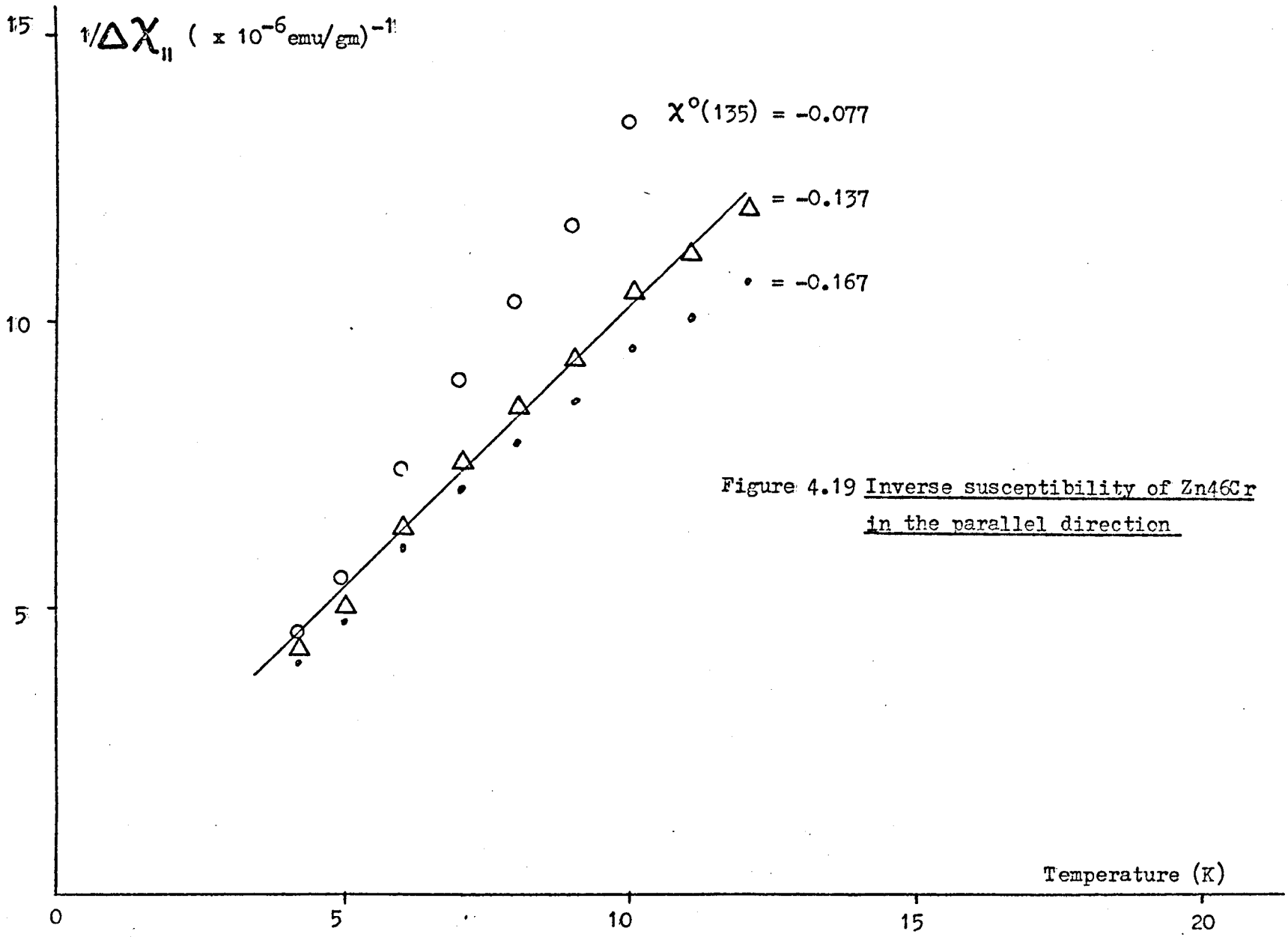

Figure 4.19 Inverse susceptibility of Zn46Cr in the parallel direction

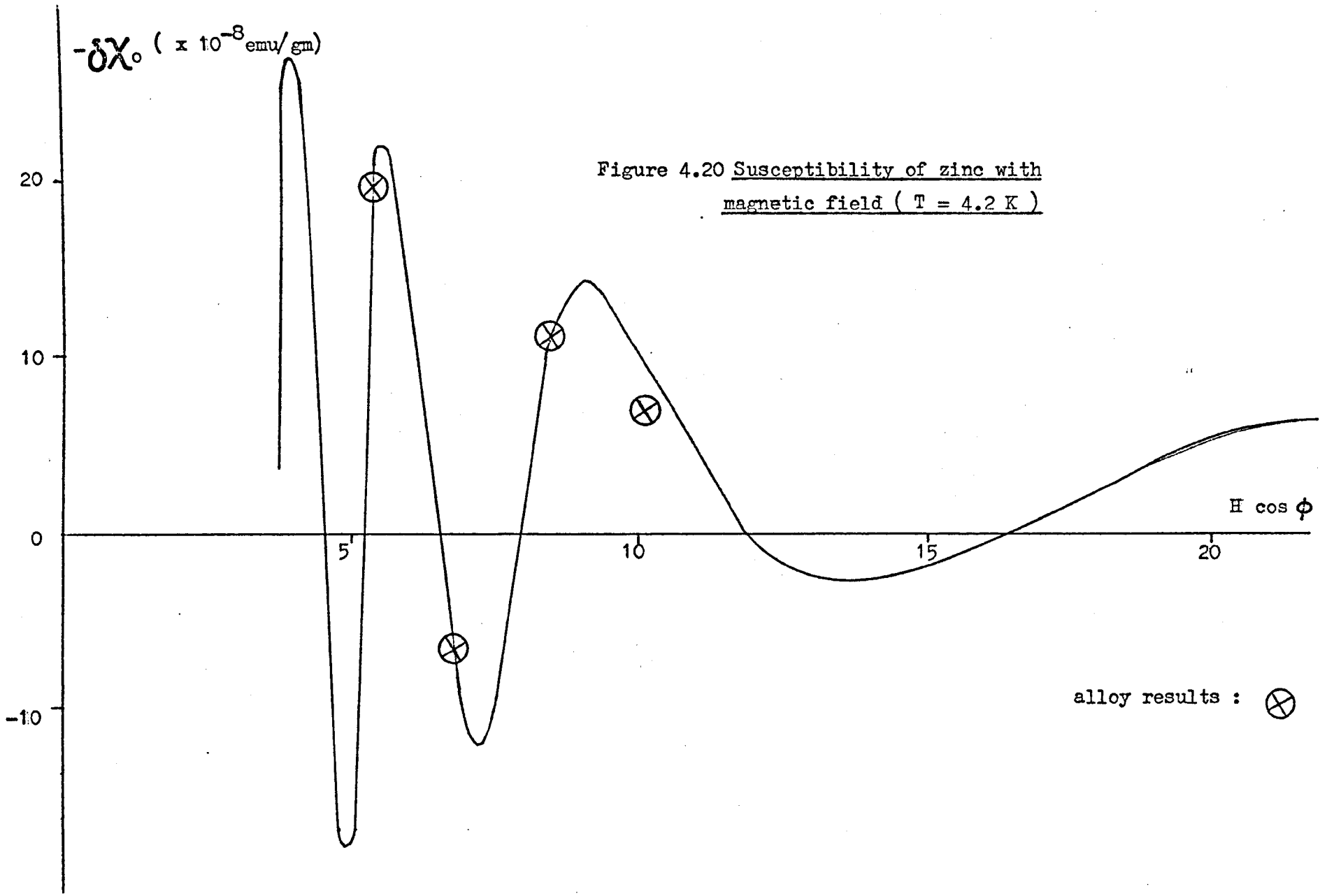

Figure 4.20 Susceptibility of zinc with magnetic field (T = 4.2 K)

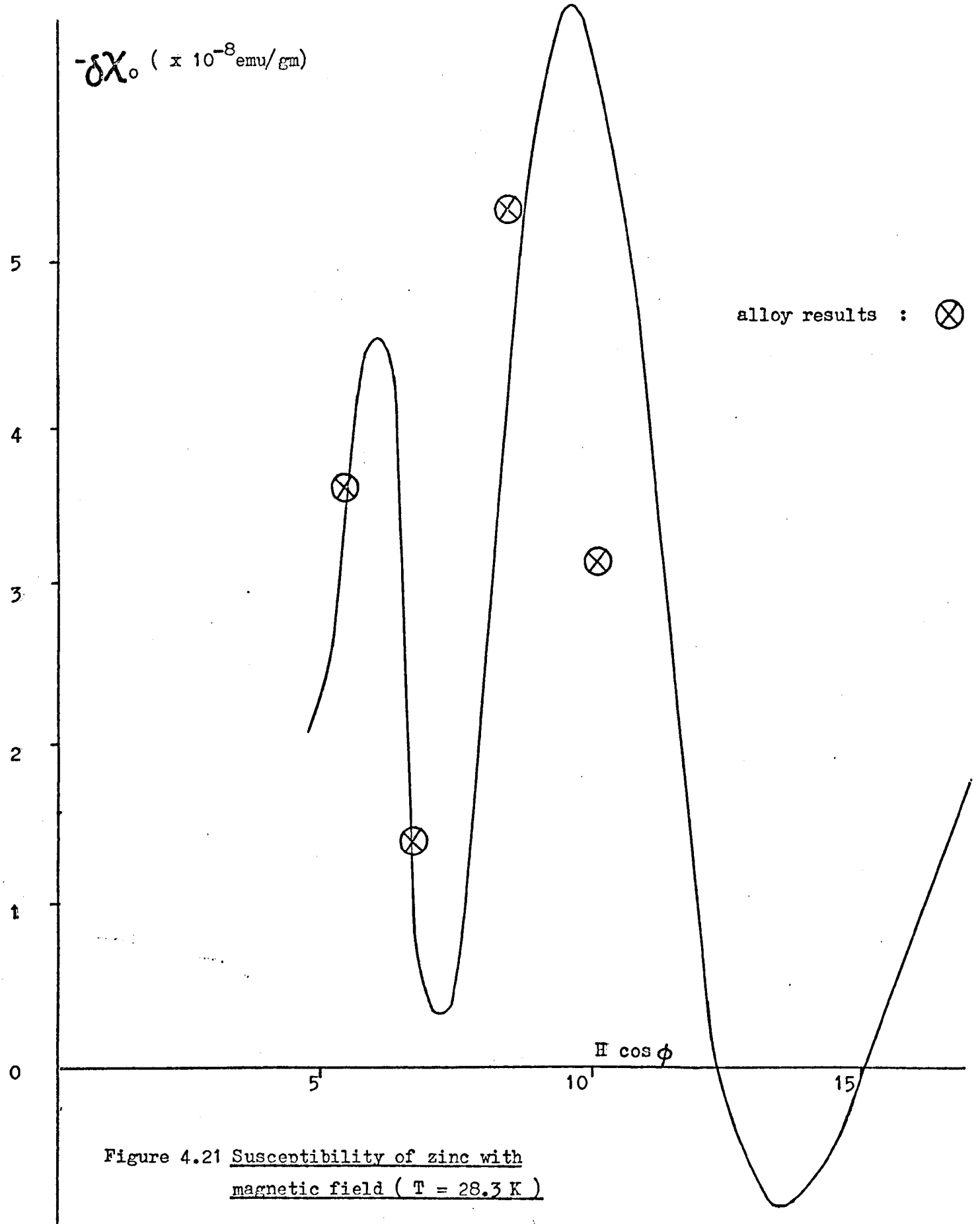

Figure 4.21 Susceptibility of zinc with magnetic field (T = 28.3 K)

(note change of scale from figure 4.20)

Equation 4.1 can be adapted for an anisotropic crystal thus :

$$\chi_{\parallel}(\underline{Zn}Cr) = \chi^{o}_{\parallel}(Zn) + \chi_{\parallel}(mag) \qquad 4.13$$

where

$\chi_m \longrightarrow \chi_{\parallel}(\underline{Zn}Cr)$

$\chi_h \longrightarrow \chi^{o}_{\parallel}(Zn)$

$\chi_{mag} \longrightarrow \chi_{\parallel}(mag)$

The susceptibility of $\underline{Zn}46Cr$ and $\underline{Zn}135Cr$ were measured as a function of temperature and four fields, viz: 5.5, 6.8, 8.4, 10.2 KG so values of $\delta\chi_o$ were read off figures 4.20 and 4.21. From figure 4.10 it can be seen that $\chi^{o}_{\perp}$ is -0.155 ± 0.005 but the 'best' low temperature value of $\chi^{o}_{\perp}$ for all the crystals measured at low temperatures was found to be -0.1475 after fitting to a Curie-Weiss law, so this value will be assumed. Equation 4.11 allows a value of $\chi^{o}_{\parallel}$ to be obtained by substituting $\delta\chi_o$ (from figures 4.20 and 4.21) and $\chi^{o}_{\perp}$, so the value for $\chi_{\parallel}(mag)$ can be determined from equation 4.13 after inserting the experimental values of $\chi_{\parallel}(\underline{Zn}Cr)$ at each field and temperature. This procedure is summarised in table 4.2.

The above procedure assumes that the phase and period of the DHVA osciallations does not change on going from Zn to $\underline{Zn}46Cr$. The very small concentration of chromium makes this unlikely (Myers, 1973). In much more concentrated alloys, the effect of alloying on the Fermi surface of zinc has been shown to be extremely small (Higgins et al., 1966) so Holt et al. (1969) have assumed the effective electron mass (and thus periodicity) for various portions of the Fermi surface (e.g. needles, lens section) remain concentration-independent over a larger range than is considered here. Increasing the temperature from 4.2 to 28.3K is likely to have an observable effect however, as shown by figures 4 and 5 in Berlincourt et al.'s paper. As a check $\chi_{\parallel}(\underline{Zn}46Cr)$ and $\chi_{\parallel}(\underline{Zn}46Cr)$ were combined similarly to 4.11 and

$\delta\chi$(Zn46Cr) is plotted on figures 4.20 and 4.21 using the symbol ⊗. A good fit is obtained for T = 4.2K except for the highest field. The fit is less good when T = 28.3K, only the points for the first two fields values falling on the line. It is probable that the particular momentum orbit on the Fermi surface of zinc that is involved is temperature dependent , especially above T ≃ 20K where both the periodicity and phase start slowly increasing (Berlincourt, 1954), giving rise to the Dingle temperature (section 4.1.7). The thermal expansion of zinc may well change the dimensions of the Brillouin zone sufficiently to alter the number of holes in the overlap region between the zone and the Fermi surface (Schoenberg, 1957).

Table 4.2. Evaluation of $\chi_{\parallel}$(mag) for Zn46Cr

H (KG)	T (K)	$\chi_{\parallel}$(ZnCr) (measured)	$\delta\chi_o$	$\chi_{\parallel}^{o}$(Zn)	$\chi_{\parallel}$(mag)	
5.5	4.2	-0.071	-0.2198	-0.3673	0.2963	0.285 ±0.014
6.8	"	0.192	-0.0496	-0.9790	0.2899	
8.4	"	0.008	-0.1056	-0.2531	0.2611	
10.2	"	0.053	-0.0918	-0.2393	0.2923	
5.5	28.3	-0.142	-0.0359	-0.1834	0.0414	
6.8	"	-0.120	-0.0083	-0.1558	0.0358	
8.4	"	-0.158	-0.0383	-0.1858	0.0278	
10.2	"	-0.136	-0.0600	-0.2075	0.0715	

The relative constancy of the 4.2K value of $\chi_{\parallel}$(mag) gives an indication that the DHVA oscillations have been successfully 'removed' to give a field indpendent term such as one would expect for chromium in zinc where only paramagnetic effects were important.

The error in the mean of χ_{II}(mag) was derived in the usual manner, with all values except the third falling within one standard deviation. It fell within two, and may be explained by noting that χ_{II}(ZnCr) and hence the measured force was very small here (the suspension wire had little effect). The Harwell microbalance, on which the above measurements were taken, was optimised for larger forces so non-linearity for very small forces could produce this effect. Despite the fourth measurement not falling as well as the others on the zinc curve in figure 4.20, its value is close to the mean.

Having derived a fairly accurate value for χ_{II}(mag) at T = 4.2K, it can now be shown how putting chromium in zinc changes χ^{o}_{II}.

From Berlincourt, $\delta\chi_{o} = -0.06$ (for $H \rightarrow 0$) (see section 4.1.4)

$$-0.06 = \chi^{o}_{II}(Zn) - \chi^{o}_{\perp}(Zn)$$

Using $\chi^{o}_{\perp}(Zn) = -0.1475$, then $\chi^{o}_{II}(Zn)$ is -0.208 ± 0.005. This value is reasonable because it predicts $\chi^{o} = 0.168 \pm 0.005$ from equation 4.6 and Bell finds (figure 4.8) that χ^{o} for pure zinc is -0.172 ± 0.003. When $c \simeq 50$mppm he finds $\chi^{o} = -0.153 \pm 0.005$.

As $\chi^{o}_{II} = 3\chi^{o} - 2\chi^{o}_{\perp}$ from 4.6 then substituting gives:

$$\chi^{o}_{II}(ZnCr) = -0.164 \pm 0.005$$

$$\therefore \chi^{o}_{II}(\underline{Zn}Cr) - \chi^{o}_{II}(Zn) = (-0.164) - (-0.208) = 0.044 \pm 0.008$$

So when $\sim$ 50mppm of chromium is put into zinc, the host susceptibility changes paramagnetically by 0.044 ± 0.008. This value can be equated with the non-magnetic term in equation 4.3 i.e. the change in χ_{e} is 0.044 ± 0.008 as χ_{DHVA} has been removed.

4.1.4. Determination of $\delta\chi_o$

Berlincourt et al. have defined their value of $\delta\chi_o$ to be the mean of the oscillations as the applied magnetic field H tends to zero. They give $\delta\chi_o = -0.03$, which predicts a change of $+0.025 \pm 0.005$ in $\chi^o_{\parallel}(Zn)$. We have chosen the value -0.06 because the oscillations are much reduced at high fields when T = 4.2K and it is easier to decide on the mean for $\delta\chi_o$.

It may be possible to decide which one is relevant by considering the following :

Pure Zinc:-

$$\left.\begin{aligned} \chi^o(Zn) &= -0.172 \\ \chi^o_{\perp}(Zn) &= -0.155 \\ \therefore\ \chi^o_{\parallel}(Zn) &= -0.206 \pm 0.005 \end{aligned}\right\} \text{ from figures 4.8 \& 4.9}$$

Zn46Cr:-

$$\chi^o(\underline{Zn}Cr) = -0.153 \quad \text{from figure 4.8}$$
$$\chi^o_{\perp}(\underline{Zn}Cr) = -0.1475 \text{ (computed)}$$
$$\therefore\ \chi^o_{\parallel}(\underline{Zn}Cr) = -0.164 \pm 0.005$$

So $\chi^o_{\parallel}(\underline{Zn}Cr) - \chi^o_{\parallel}(Zn) = 0.042 \pm 0.005$. This agrees with the previous result if $\delta\chi_o \underset{H\to\infty}{} = -0.06$ is chosen.

Alternatively one could show the consistency of this value by noting that as :

$$\chi_{\parallel}(mag) = \chi_{\parallel}(\underline{Zn}Cr) - \chi^o_{\parallel}(Zn) \text{ from equation 4.13}$$

one must modify the value of $\chi^o_{\parallel}(Zn)$ by 0.042 ± 0.005 so it becomes now $\chi^o_{\parallel}(\underline{Zn}Cr)$. This changes the value of $\chi_{\parallel}(mag)$ from 0.285 ± 0.026 to 0.243 ± 0.026, so comparing this with $\Delta\chi_{\parallel}$ in equation 4.7 where $\Delta\chi_{\parallel}(46) = 0.229 \pm 0.01$ when T = 4.2K shows that within experimental error the DHVA oscillations have been successfully and consistently 'removed'.

4.1.5. Slope and Intercept

A least squares computer programme gave the spin value n in Bohr magnetons and the intercept θ (K) for each attempt to fit to a Curie-Weiss law and the results for the best fit to a straight line are given below in table 4.3.

Table 4.3 Low temperature spin and θ values for ZnCr

c (mppm)	n (μ_B)		θ (K)	
	$\perp$ axis	$\parallel$ axis	$\perp$ axis	$\parallel$ axis
46	3.64 ±0.05	3.37 ±0.05	-0.51 ±0.09	-0.40 ±0.11
135	3.71 ±0.05	3.21 ±0.08	-0.55 ±0.12	-0.21 ±0.12
150	3.89 ±0.10	-	-0.81 ±0.30	-
183	-	3.38 ±0.07	-	+0.80 ±0.60
400	3.83 ±0.16	3.46 ±0.14	-1.4 ±1.1	-0.9 ±1.0

4.1.6. Anisotropy

Having determined unequivocally the reciprocal net susceptibility of several dilute ZnCr crystals as a function of temperature in a Curie-Weiss form (figures 4.12 to 4.17, 4.19), their ratios along the perpendicular and parallel directions can now be calculated. This is shown in figures 4.22 to 4.24. All crystals show $\Delta\chi_\perp > \Delta\chi_\parallel$ in the temperature range indicated, and the Zn46Cr and Zn135Cr

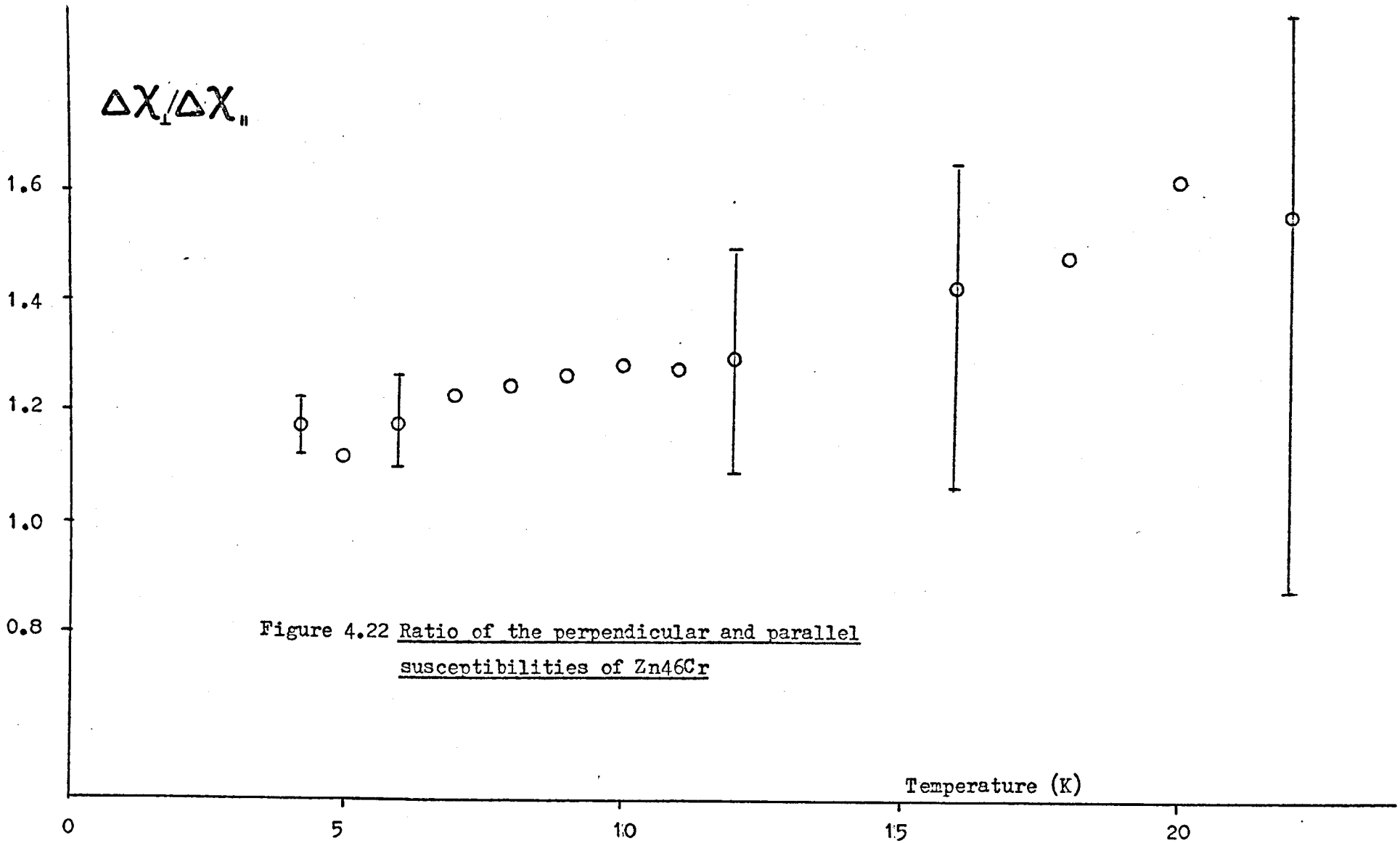

Figure 4.22 Ratio of the perpendicular and parallel susceptibilities of Zn46Cr

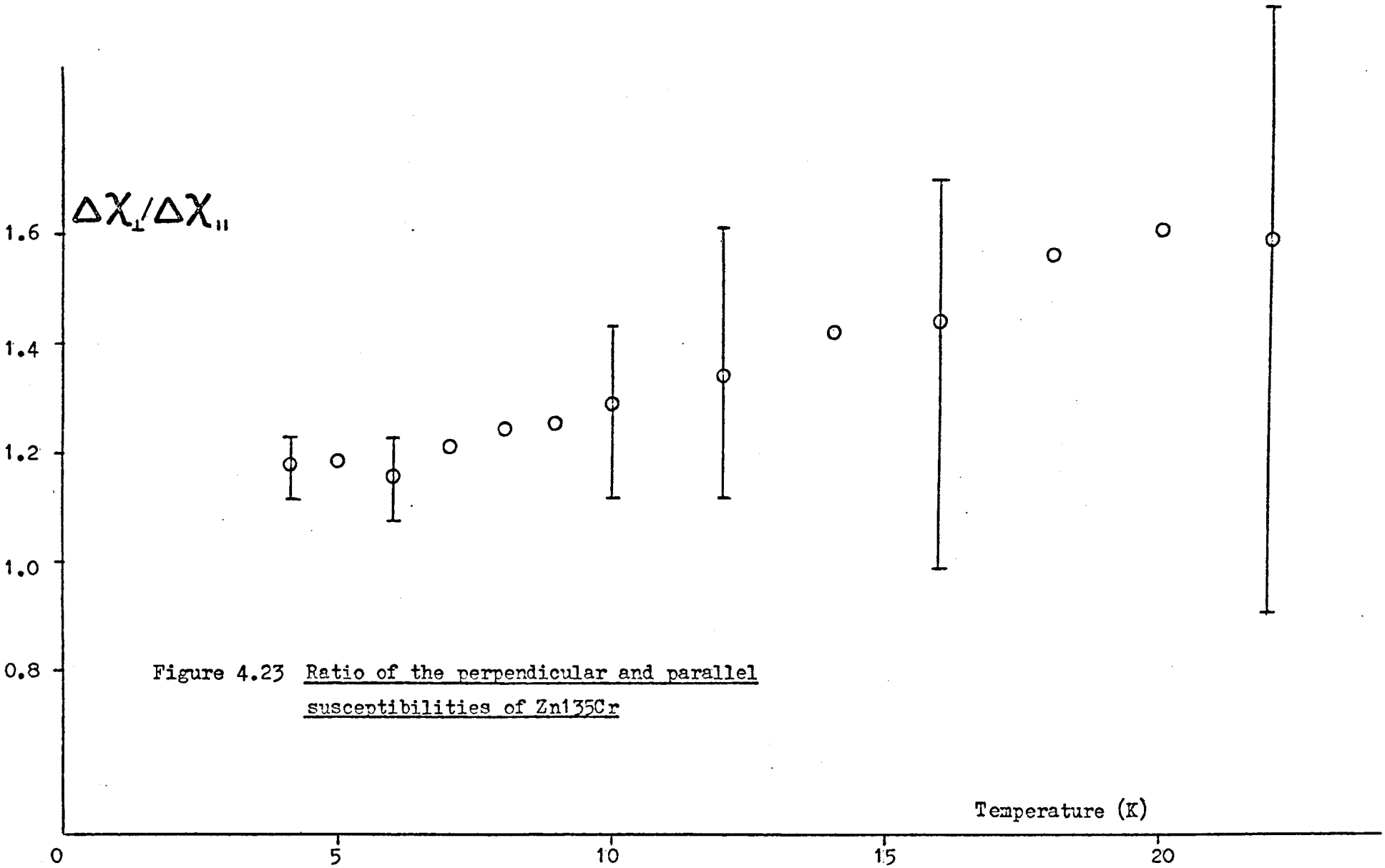

Figure 4.23 Ratio of the perpendicular and parallel susceptibilities of Zn135Cr

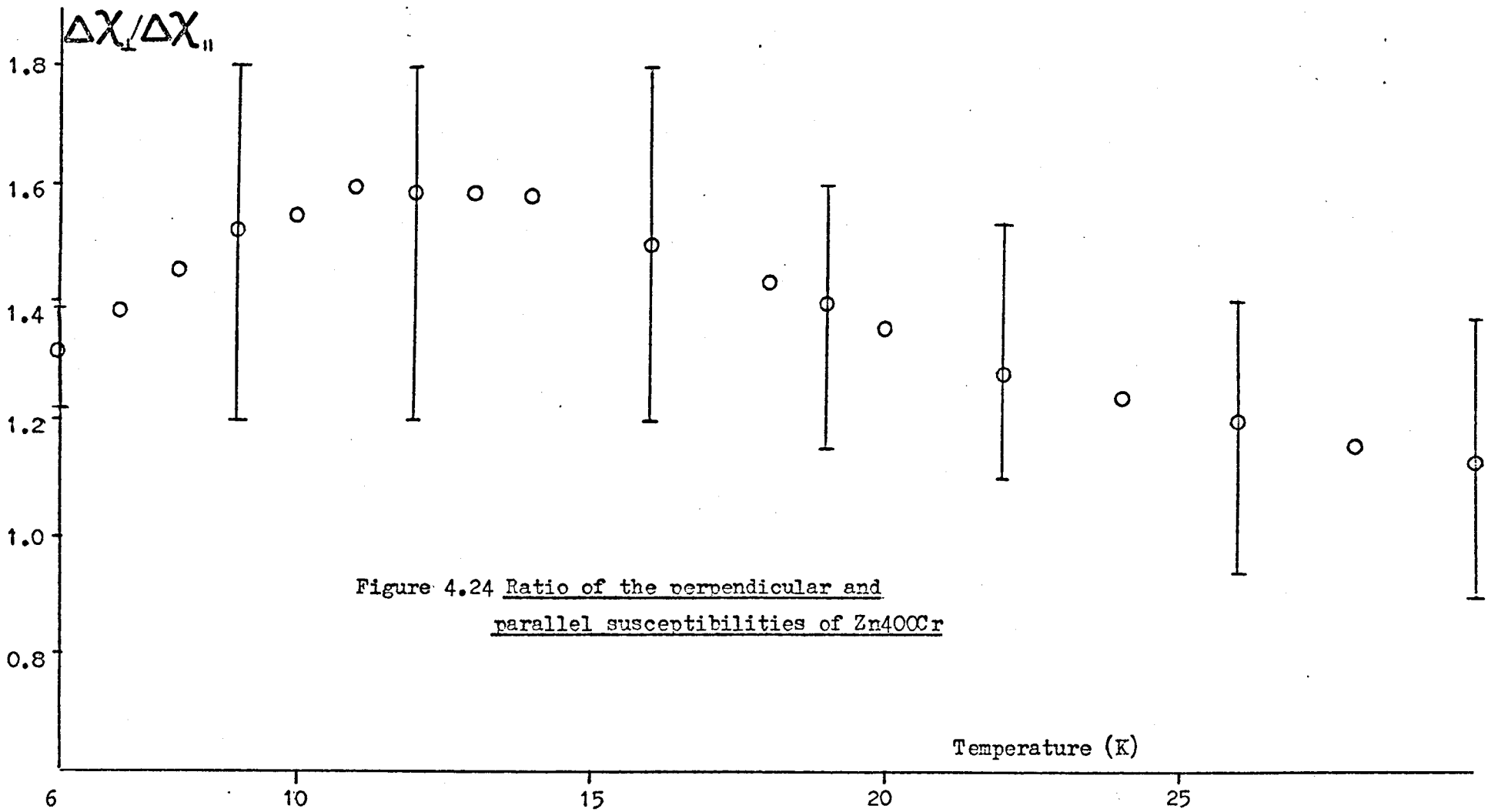

Figure 4.24 Ratio of the perpendicular and parallel susceptibilities of Zn400Cr

samples have a slight linear positive slope though this could possibly be a factor built in by the previous analysis. The error bars show further investigation here of this trend is not worthwhile. A similar initial positive slope is apparent in the Zn400Cr crystal, though this curves back within 12K to the original value and asymptotically straightens out. The errors for this sample do not increase with temperature up to ~30K due to greater amount of chromium giving a large gross susceptibility (and therefore less error in determining $\Delta\chi$). A weighted average of these results will give a more accurate overall value to the anisotropy of ZnCr. The results of this method are shown in figure 4.25 which shows that the anisotropy parameter $\Delta\chi_\perp/\Delta\chi_\parallel$ is always greater than 1 at least up to $T \simeq 30K$ and has a value of 1.22 ± 0.05 at 6 K when the host susceptibility is allowed for in the manner given above.

Recent measurements of single crystals of ZnMn have been made by Li et al. (1973) who have analysed their results in a different manner to that adopted for the ZnCr results presented here. Because the host susceptibility is expected to behave similarly in both ZnMn and ZnCr, a comparison of both sets of results will be made. In essence Li et al. measured two parameters/crystal : $\chi_\perp$ and $-\delta\chi$ (equation 4.11) and then assumed the host susceptibilities for both axes were independent of concentration (up to 475 mppm). They claim that $\Delta\chi_\parallel > \Delta\chi_\perp$ in the range ~2K to ~25K, and a modified spin-only Hamiltonian adequately described $\delta\chi$ and $\Delta\chi_\perp$ up to ~25K and ~80K respectively (figures 4.26 and 4.27). The relevant equations are (Bleaney, 1950):

$$\Delta\chi_\perp = \left(ig_\perp^2/T\right)\left(1 - j/2T \right) \qquad 4.14$$

$$\Delta\chi_\parallel = \left(ig_\parallel^2/T\right)\left(1 + j/T \right) \qquad 4.15$$

$$-\delta\chi = \left(ig_{av}^2/T\right)\left(\left(g_\perp^2 - g_\parallel^2\right)/g_{av}^2 - j(2g_\parallel^2+g_\perp^2)/2g_{av}^2T\right) \qquad 4.16$$

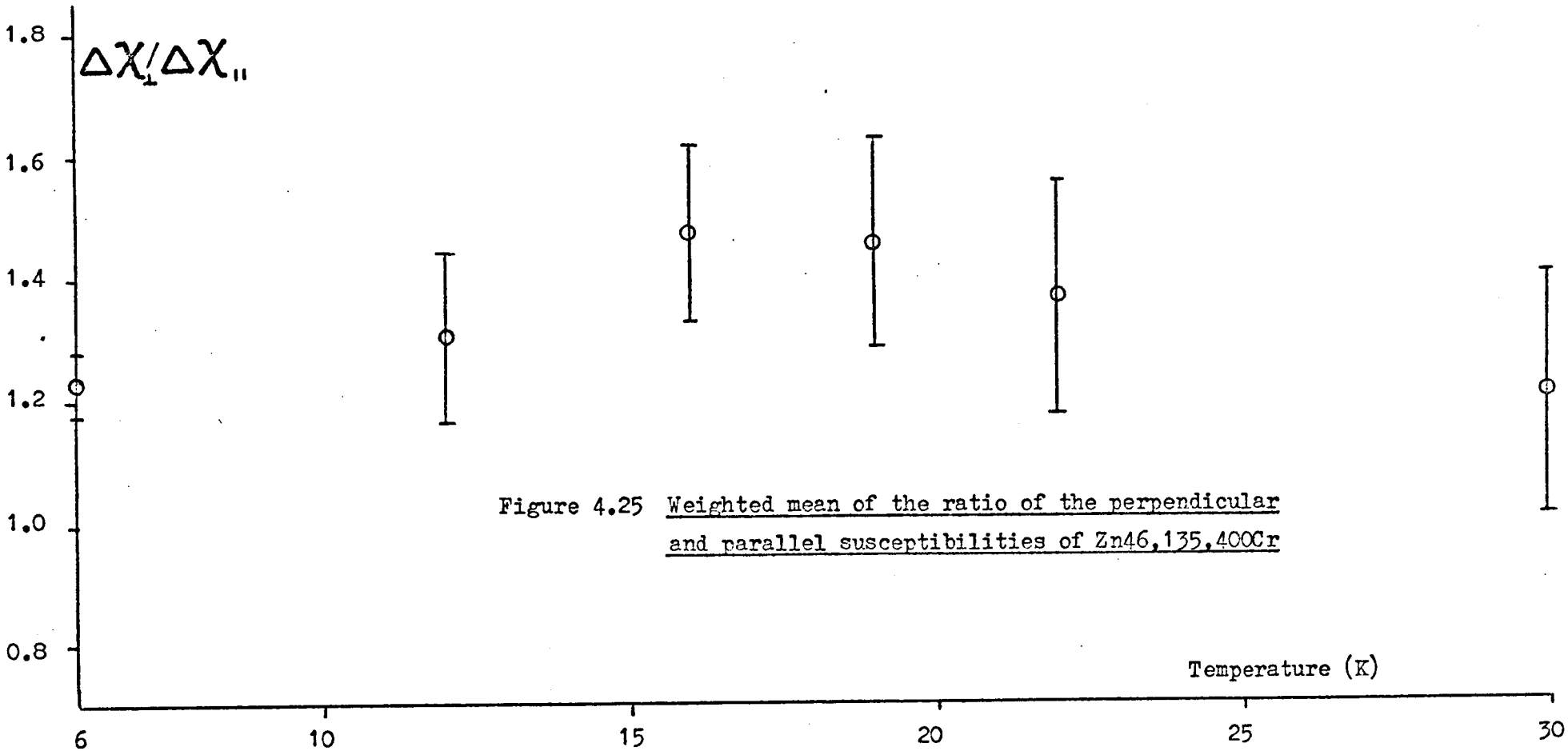

Figure 4.25 Weighted mean of the ratio of the perpendicular and parallel susceptibilities of Zn46,135,400Cr

where $i = Na\beta^2 S(S+1)c/3kA$

$j = B(2S-1)(2S+3)/15k$

$3g_{av} = 2g_\perp + g_\parallel$

$g_\perp, g_\parallel$ = g-values perpendicular and parallel to the c-axis

S = spin value (assumed 2)

B = crystal field parameter

Thus $T\delta\chi/c$ is plotted against $1/T$ in figure 4.26 assuming a g-factor anisotropy $(g_\perp - g_\parallel)/g_{av}$ of 0.5% and $A/k = 0.078 \pm 0.008$K. The host contribution to $\delta\chi$ is assumed to be due to pure zinc alone. Equation 4.14 does not fit the ZnMn results for $\Delta\chi_\perp$ so the reciprocal of the discrepancy between theory and experiment was plotted against lnT and found to be linear up to 8OK. This was done because Scalapino (1966) and others have indicated that equations 4.14 and 4.15 neglect the conduction electron contribution to the susceptibility, this contribution being expected to vary as lnT in a Kondo system. To include this effect, equations 4.14 to 4.16 are modified thus :

$$\Delta\chi_\perp = (ig_\perp^2/T)(1 - j/2T - \ln^{-1}(T/T_K)) \qquad 4.17$$

$$\Delta\chi_\parallel = (ig_\parallel^2/T)(1 + j/T - \ln^{-1}(T/T_K)) \qquad 4.18$$

$$-\delta\chi = (ig_{av}^2/T)(((g_\perp^2 - g_\parallel^2)/g_{av}^2)(1-\ln^{-1}(T/T_K)) - j(2g_\parallel^2 + g_\perp^2)/2g_{av}^2 T \qquad 4.19$$

The results for two crystals (65 mppm and 475 mppm) were fitted to equation 4.17 using the same g-factor anisotropy and A/k as before, with T_K having a value of 0.25 ± 0.04 K (Figure 4.27). It should be noted that equation 4.17 has the same appearance with these parameters as a Curie-Weiss law and that no results for $\Delta\chi_\parallel$ have been presented.

To compare ZnMn with the present ZnCr results, the same fundamental assumption that the host contribution is given solely by the pure metal will be made. This assumption is implied for $\Delta\chi_\parallel$ because Li et al. show that both $\delta\chi = \delta\chi(\text{ZnMn}) - \delta\chi(\text{Zn})$ and $\Delta\chi_\perp = \chi_\perp(\text{ZnMn}) - \chi_\perp(\text{Zn})$ hold

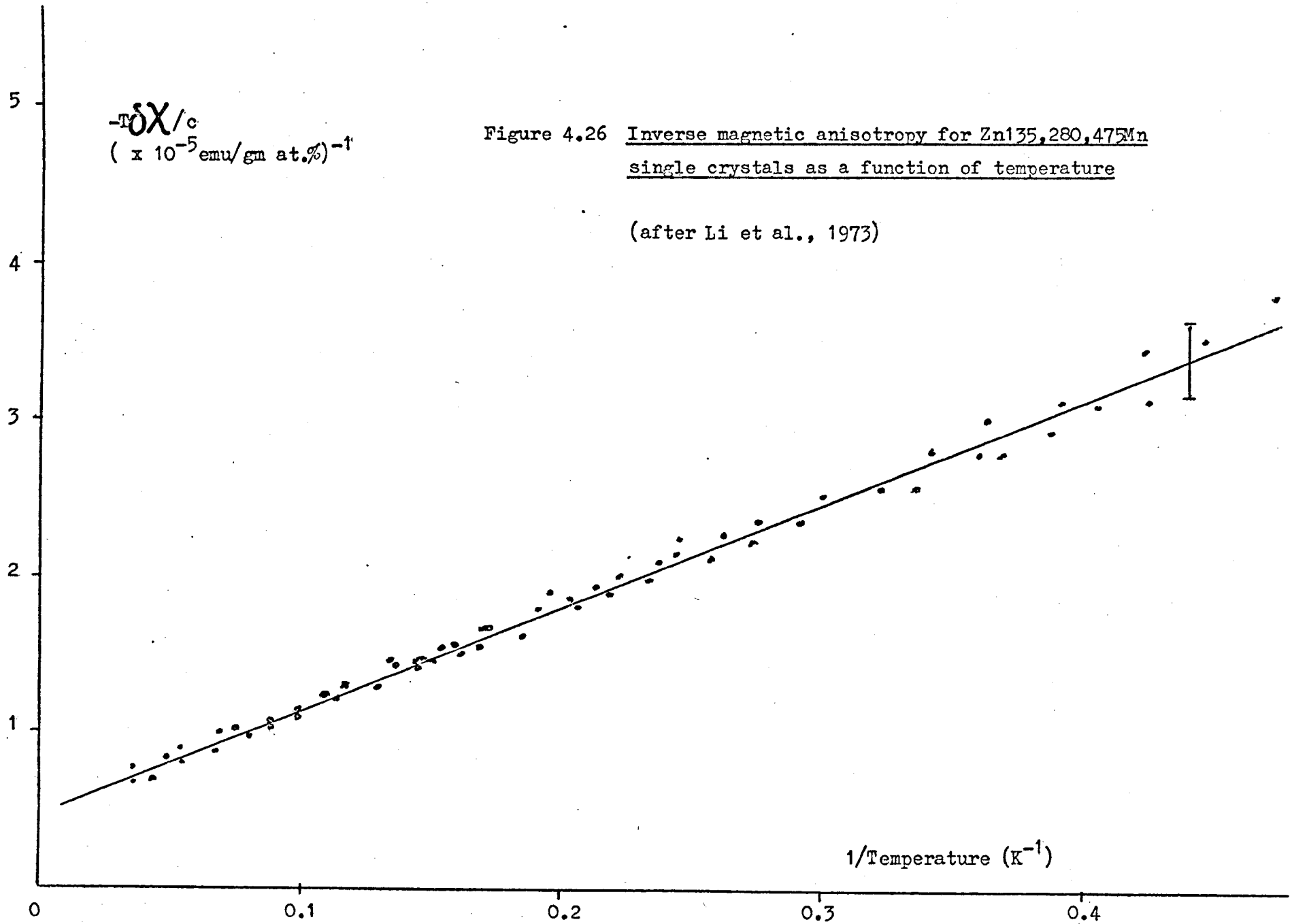

Figure 4.26 Inverse magnetic anisotropy for Zn135,280,475Mn single crystals as a function of temperature

(after Li et al., 1973)

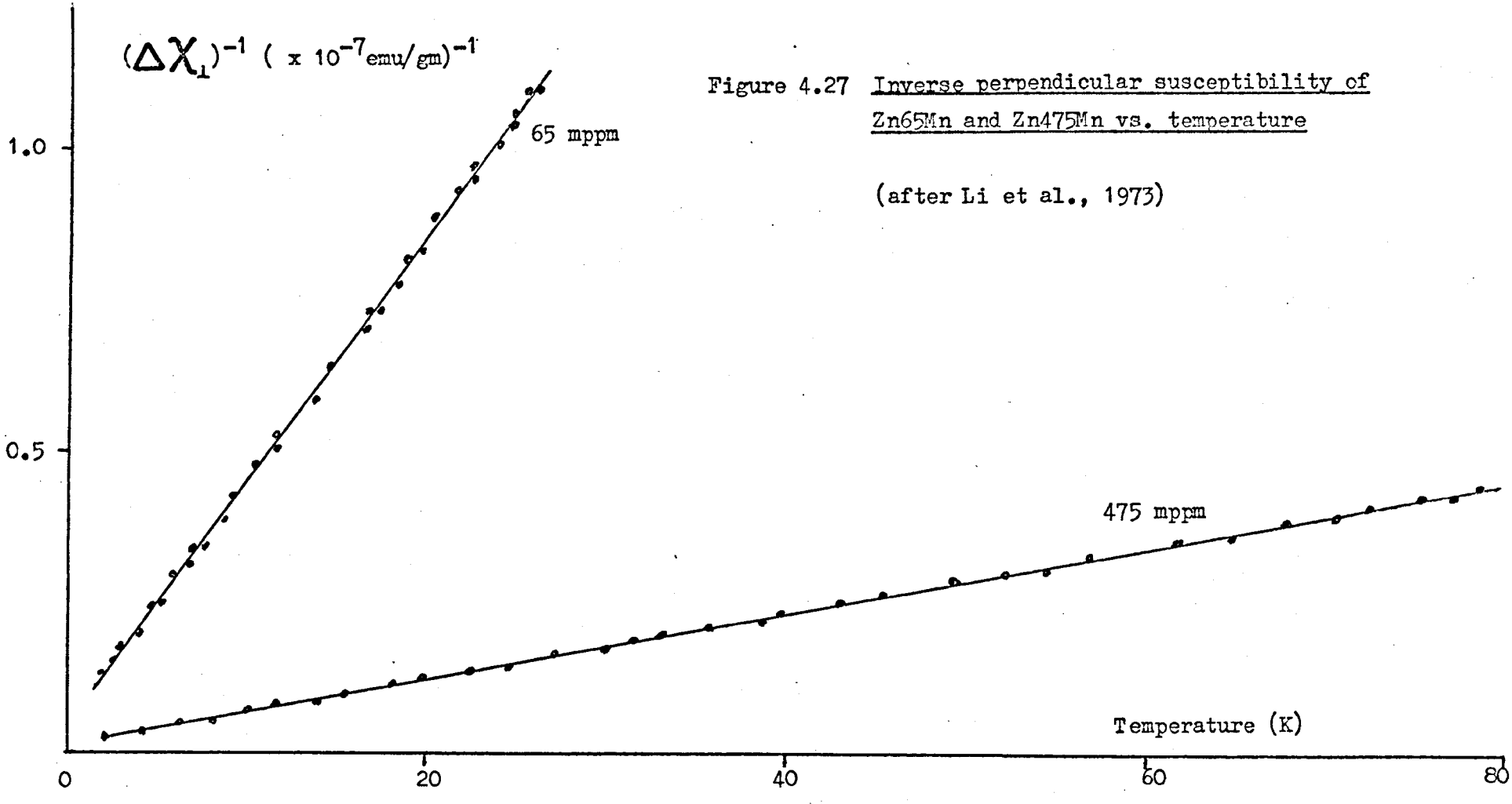

Figure 4.27 Inverse perpendicular susceptibility of Zn65Mn and Zn475Mn vs. temperature

(after Li et al., 1973)

for all concentrations measured, therefore as $-\delta\chi = \Delta\chi_{\parallel} - \Delta\chi_{\perp}$, it is expected that $\chi^{o}_{\parallel}$(host) will also be concentration-independent. This results in $\chi^{o}_{\perp} = -0.155$ from figure 4.9 and using the fact that $3\chi_{o} = \chi^{o}_{\parallel} + 2\chi^{o}_{\perp}$ (from equation 4.6) gives $\chi^{o}_{\parallel} = -0.206$ when $\chi_{o} = -0.172$ for polycrystalline zinc (present work and Bell, 1972) is inserted. The values of $\Delta\chi_{\perp}$ and $\Delta\chi_{\parallel}$ were therefore derived using equation 4.7 for the crystals Zn46, 135, 400Cr and an average of the ratio $\Delta\chi_{\perp}/\Delta\chi_{\parallel}$ is given in figure 4.28. Figure 4.29 shows the anistropy for Zn46Cr and Zn135Cr separately because it is then evident that the Zn400 Cr results are mainly responsible for making $\Delta\chi_{\perp}/\Delta\chi_{\parallel} > 1$ up to ~18K. Without these results the cross-over point becomes ~5K. Thus except at 4.2 K (where $\Delta\chi_{\perp}/\Delta\chi_{\parallel} \simeq 1.02$) this method gives $\Delta\chi_{\perp}/\Delta\chi_{\parallel}$ to be less than 1 even for the lowest concentration crystals, in complete disagreement to the low temperature results ($T \lesssim 50$ K) found previously.

4.1.7. Dingle Temperature

Information on the Dingle temperature can be gained (Schoenberg, 1957) by noting the amplitude dependence on temperature in figures 4.20 and 4.21. Dingle pointed out that the energy levels involved with the DHVA effect are "collision broadened" due to the inclusion of impurities. Consider the following equation :

$$F = (T \times \text{constant})\ (\text{fn}(H))\ \exp\left(\frac{-2\pi^2 kT}{\gamma H}\right)\ (\text{fn}(H,m)) \qquad 4.20$$

where: F = free energy
m = effective mass of electron
fn = 'function of'
γ = effective double Bohr magneton

Collision broadening has the effect of adding a parameter x (i.e. the Dingle temperature) to the temperature term in the exponential, viz:

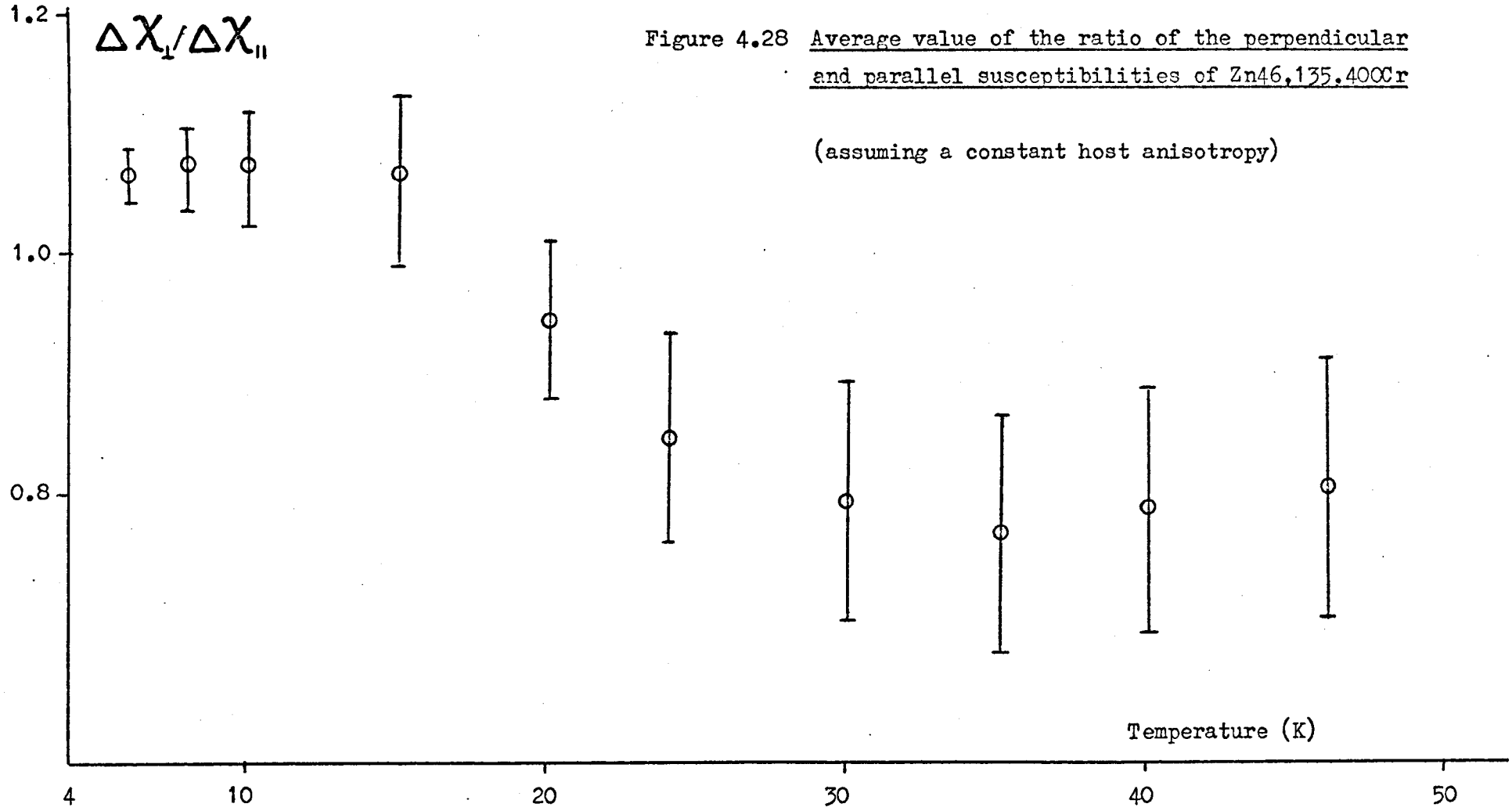

Figure 4.28 Average value of the ratio of the perpendicular and parallel susceptibilities of Zn46,135.400Cr

(assuming a constant host anisotropy)

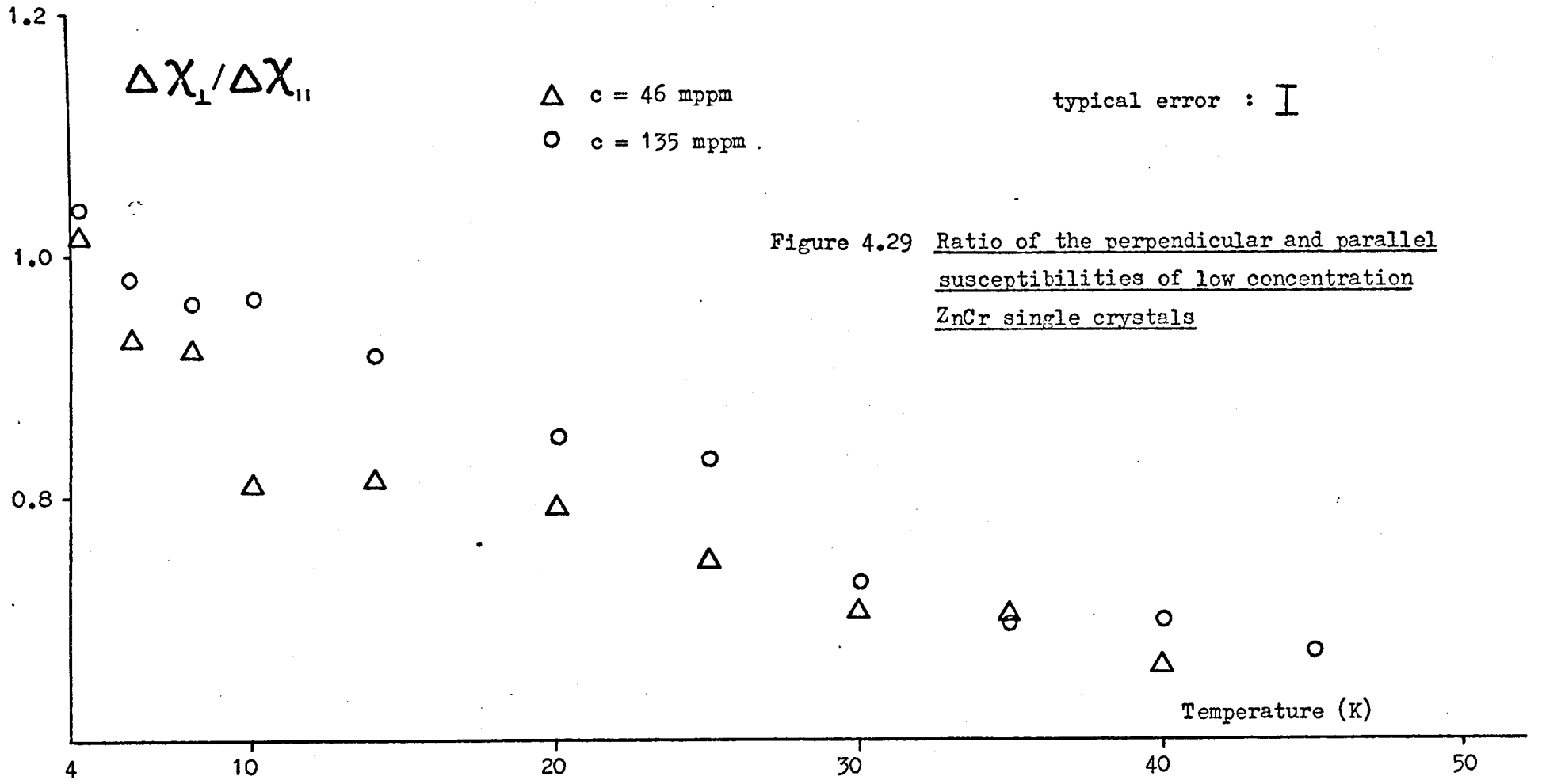

Figure 4.29 Ratio of the perpendicular and parallel susceptibilities of low concentration ZnCr single crystals

$$\frac{\gamma H}{2\pi^2 kT} \rightarrow \frac{\gamma H}{2\pi^2 k(T+x)} \qquad \text{(Dingle, 1952)} \qquad 4.21$$

where $x = \frac{h}{2\pi^2 k\tau}$ 4.22

and h = Planck's constant

τ = collision time

When $T = 4.2K$, $\delta\chi_{4.2} = 0.262$

$T = 28.3K$, $\delta\chi_{28.3} = 0.022$

Only the lowest two field values (H1 and H2 say) of $\delta\chi$ have been used here as it is apparent that these accurately follow the curve for pure zinc for which equation 4.20 holds when H is small (Schoenberg, 1957).

From 4.20 one can show that :

$$\frac{(\delta\chi(H1) - \delta\chi(H2))|_{4.2}}{(\delta\chi(H1) - \delta\chi(H2))|_{28.3}} = \frac{4.2(\exp(x + 28.3))}{28.3(\exp(x + 4.2))}$$

Solving gives: $x = 2.9 \pm 0.3$ K

$\tau = 8.3 \pm 0.8 \times 10^{-13}$ secs. from 4.22

4.1.8. Discussion

Zinc crystals with small amounts of 3d impurities in them must necessarily be investigated at low temperatures to produce measurable results. The DHVA effect is manifest only in the parallel direction in zinc and is damped by increasing both the temperature and the impurity concentration. This latter effect has been used to deduce the paramagnetic effect of chromium alone in the most dilute crystal (46mppm) by comparing the ratio of the susceptibilities of both axes to that in a more concentrated crystal (135mppm) where the field effects in $\chi_{\parallel}$ are much smaller. Increasing the concentration most probably causes a production of a small amount of intermetallic compound which would explain the

'kink' occurring at $T \simeq 24$-$32K$ in the low temperature susceptibility graphs. Further discussion of this aspect is postponed to section 4.3.2 after a chemical analysis has been presented.

A Curie-Weiss law is followd up to the highest temperature investigated here ($T \simeq 48K$) for both axes in the low concentration crystals, though for all crystals this holds up to $T \simeq 28K$, below the possible ordering temperature of the compound. Deviations from this law at low temperatures are not apparent.

An alternative means for 'removing' the DHVA effect was to correlate the data with results on pure zinc to give a field-independent contribution of the chromium in zinc at two temperatures. This has been shown to be feasible at low temperatures where the phase and periodicity do not change very much, either through increasing the temperatures from 4.2 to ~20K or increasing the concentration of chromium to $\lesssim$135mppm. The consistency between the two methods gives reasonable hope that interpretations following the removal of field effects are meaningful.

Because the Fermi surface may be distorted by putting impurities into zinc, different ways of determining the change in host susceptibility have been presented, all of which are mutually consistent except for the method adopted by Li et. al (1973).

Bell found that for polycrystalline ZnCr the spin value was 3.6 μ_B per chromium atom and the intercept θ was -0.65K in good agreement with the present results. His value of 3.6 μ_B may be deduced from $n = 1/3(n_{\parallel} + 2n_{\perp})$ though his value is 27% higher (excluding errors) than the θ calculated in a similar manner to n. The values for the Zn46Cr crystal are most likely to be correct because there is no sign of any intermetallic compound both by inspection of the

susceptibility results and the chemical analysis. It is worth pointing out here that in all cases $n_\perp > n_\parallel$, assuming χ_o is concentration-dependent, a somewhat surprising result in view of the result one would expect from simple crystal field theory (Chapter 5).

As the purpose of the foregoing analysis is to determine the anisotropy of ZnCr, the parallel axis of the most dilute crystal has been made field free and the parameter $\Delta\chi_\perp/\Delta\chi_\parallel$ plotted against T and compared with more concentrated crystals. Utilising Bell's results for polycrystalline ZnCr (figure 4.8) it is found that in all crystals $\Delta\chi_\perp > \Delta\chi_\parallel$ and a method of analysis giving the results with a minimum of error shows that $\Delta\chi_\perp/\Delta\chi_\parallel \simeq 1.23 \pm 0.05$ when $T \lesssim 12K$ though this value increases to 1.47 ± 0.15 when $T = 16K$ and then reduces to the initial value though with an increased error when $T \simeq 30K$. The peak at $T = 16K$ derives from the most concentrated crystal measured in this section (Zn400Cr) and could therefore be caused by an intermetallic compound though the maximum occurs at $\sim 10K$ below the possible ordering temperature. Alternatively levels higher than the ground state of a configuration caused by the crystaline electric field may be starting to become populated. The two less concentrated crystals show a tendency to increasing $\Delta\chi_\perp/\Delta\chi_\parallel$ with temperature though the errors become much larger than would warrant a belief in this trend. Despite the probable inclusion of some intermetallic compound in the more concentrated crystals, the results consistently show that $\Delta\chi_\perp/\Delta\chi_\parallel = 1.23 \pm 0.05$ when $T \lesssim 12K$ and it is likely that this value persists to higher temperatures, at least to $T \simeq 20K$.

The susceptibility measurements of several crystals of ZnMn (Li et al., 1973) would normally be expected to provide a fruitful comparison with similar work on ZnCr, but several assumptions made by these authors in the presentation of their results reduce the usefulness of such a study. This

will be shown by itemising and then discussing these assumptions.

(i) Zinc has a steady magnetic anisotropy.
The change in anisotropy of zinc is caused by a change in the crystallographic (c/a) ratio, which is taken to be negligible by Li et al. using the results of Lawson and Gordon (1973). In fact the oscillatory function of (c/a) is not shown to be damped to zero below the value (c/a) = 1.8340, which is the upper bound on the region of interest here (as Zn475Mn has (c/a) = 1.8284). Nevertheless over the limited temperature range (~2 K to ~25 K) the fact that $-\delta\chi/c$ is the same for Zn135,280,475Mn within the experimental error of ~10% (figure 1(a) of Li et al., 1973) shows that the phase and amplitude of the DHVA oscillations is not greatly changed from one ZnMn crystal to another.

(ii) The host susceptibility has a concentration-independent value for each axis.
This assumption for ZnMn is shown to be true for $\Delta\chi_\perp$ results (figure 4.27) and is implied for $\Delta\chi_\parallel$ from figure 4.26. The present work on ZnCr is in agreement with $\chi_\perp^o$ being constant (below ~ 77 K) where a fit to a Curie-Weiss law shows $\chi_\perp^o$ is -0.1475 for all crystals measured at low temperatures ($46 \leq c \leq 400$ mppm) but not for $\chi_\parallel^o$ also being constant. Bell (1972) has shown for polycrystalline zinc that χ_o varies with c (figure 4.11), thus enabling the concentration dependence which is contained in $\chi_\parallel^o$ to be derived. It is therefore not surprising that $\Delta\chi_\perp$ can be fitted to equation 4.17 for the various ZnMn crystals but no similar results for $\Delta\chi_\parallel$ are presented. By analogy with the ZnCr results, $\Delta\chi_\perp$ would be expected to fit any law that had an appearance similar to a Curie-Weiss law when a concentration-indpendent $\chi_\perp^o$ is assumed but would not fit the $\Delta\chi_\parallel$ results with the same assumption for $\chi_\parallel^o$. Despite this, the ramifications of allowing both axes of the host to have a constant value for ZnCr are shown in figures 4.28 and

4.29. It can be seen that the average value of $\Delta\chi_\perp/\Delta\chi_\parallel$ is greater than 1 up to $T \simeq 18$ K, but is less than 1 for $T > 18$ K, having a minimum value of 0.77 ± 0.10 at T = 35 K. The form of figure 4.28 is a consequence of the much increased paramagnetism of ZnCr over the diamagnetism of Zn at low temperatures, thereby making the choice of host susceptibility relatively unimportant here, though this does not hold as the temperature is increased, leading to the opposite resultfrom figure 4.25 where $\Delta\chi_\perp/\Delta\chi_\parallel$ is always greater than 1. In fact, if the most concentrated crystal Zn400Cr is not included in the average of $\Delta\chi_\perp/\Delta\chi_\parallel$, the cross-over point to less than unity would occur at $T \simeq 5$ K as shown in figure 4.29. The basic reason for the difference between figures 4.25 and 4.28 is that assuming $\chi_o = -0.172$ for all concentrations causes a gross change in $\chi_\parallel^o = -0.206$ from a typical value of ~ -0.1 when c > ~50 mppm (e.g. $\chi_\parallel^o = -0.107$ ± 0.030 when c = 135 mppm).

(iii) A contribution due to the Kondo effect is necessary to explain the results of ZnMn.

Figure 4.27 shows that a fit to equation 4.17 can be obtained if T_K is ~ 0.25 ± 0.04 K. The modification of equation 4.17 from equation 4.14 became necessary when it was apparent from the ZnMn results that the additon of crystal field effects in the absence of the conduction-electron contribution to the susceptibility could not explain the behaviour of $\Delta\chi_\perp$ with temperature. Consequently it can be shown for the ZnCr results that if $T.\Delta\chi_\perp$ is plotted against 1/T, the discrepancy between this and equation 4.14 does indeed vary as lnT, and a plot of $(\Delta\chi_\perp)^{-1}$ against T is linear, showing a fit may be made to an equation such as 4.17. Figures 4.12 to 4.17 already show $(\Delta\chi)^{-1}$ vs T is linear for both axes, allowing a fit to a Curie-Weiss law to be made. It was not therefore considered necessary to present similar graphs for ZnCr analysed in the manner of Li et al. for ZnMn because a Curie-Weiss law appears to provide a more comprehensive explanation of the susceptibility behaviour once the concentration-dependence

of the host and the DHVA effect have been considered in a systematic manner.

Turning now to the Dingle temperature deduced from the amplitude dependence of $\delta\chi$ with temperature, Holt et al. (1969) have shown that x for Zn92Mn and Zn18Mn are ~3.7 K and ~2 K respectively. Comparing these with x = 2.9 ± 0.3 K Zn46Cr shows that chromium has a similar effect on the Fermi surface of zinc (in this case on the needles) to that of manganese.

4.2 High Temperature

4.2.1 Introduction

When the temperature is approximately 150K or more the DHVA effects in the parallel axis of zinc and the alloys considered here have completely disappeared (figure 4.10). The field dependence of the host susceptibility is of no importance at these relatively high temperatures so the question of what to subtract from χ(ZnCr) is whether to use the value for pure zinc or a non-magnetic zinc alloy such as ZnCu, ZnFe (figure 4.10) or ZnCd (figure 4.11). Plotting the inverse susceptibility against temperature will then show if a Curie-Weiss law is followed. Greater concentrations of chromium must be dissolved in zinc crystals to give measurable paramagnetic changes from the diamagnetism of the host at high temperatures. For this experimental reason, the possibility of intermetallic compounds forming must be borne in mind.

4.2.4 Results

Figures 4.30 to 4.37 show the susceptibility and inverse incremental susceptibility as a function of temperature for both crystallographic axes. There is an increase in paramagnetism from ~370K to the highest temperature measured, ~ 470K. As Boato et al. (1966) have shown via resistivity measurements and Brown (1962) by X-ray measurements, ZnCr is not a very thermodynamically stable

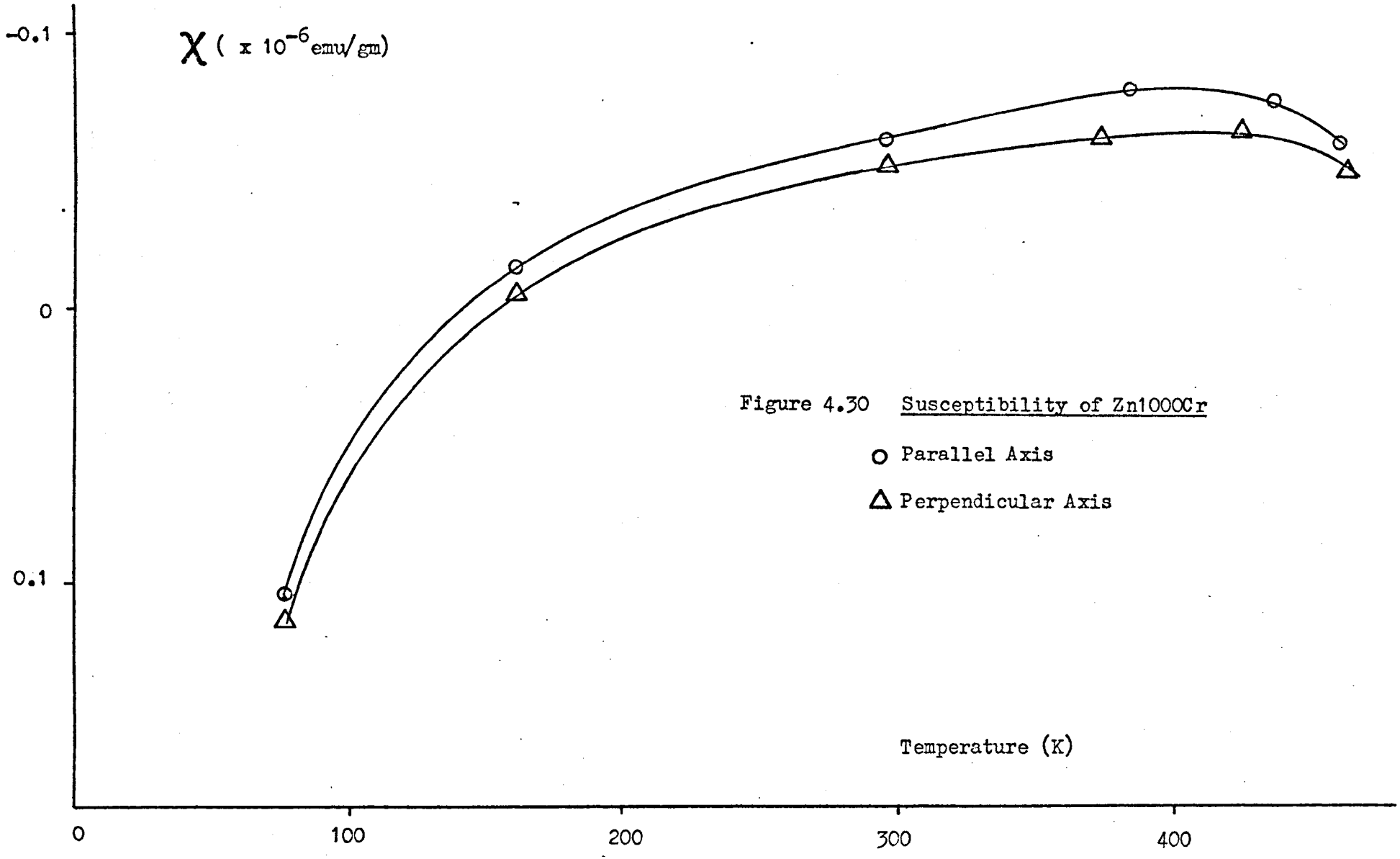

Figure 4.30 Susceptibility of Zn1000Cr

○ Parallel Axis

△ Perpendicular Axis

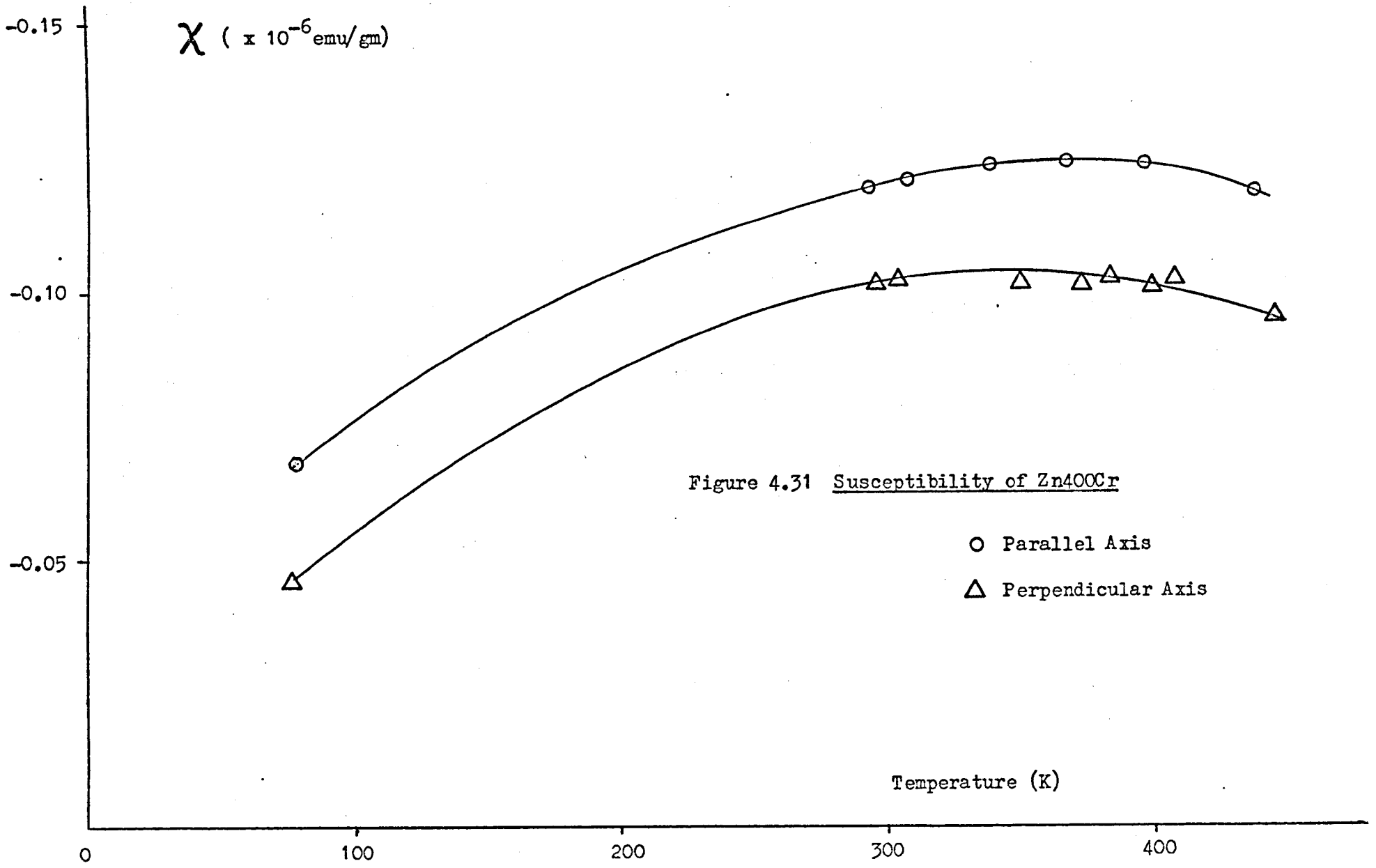

Figure 4.31 Susceptibility of Zn400Cr

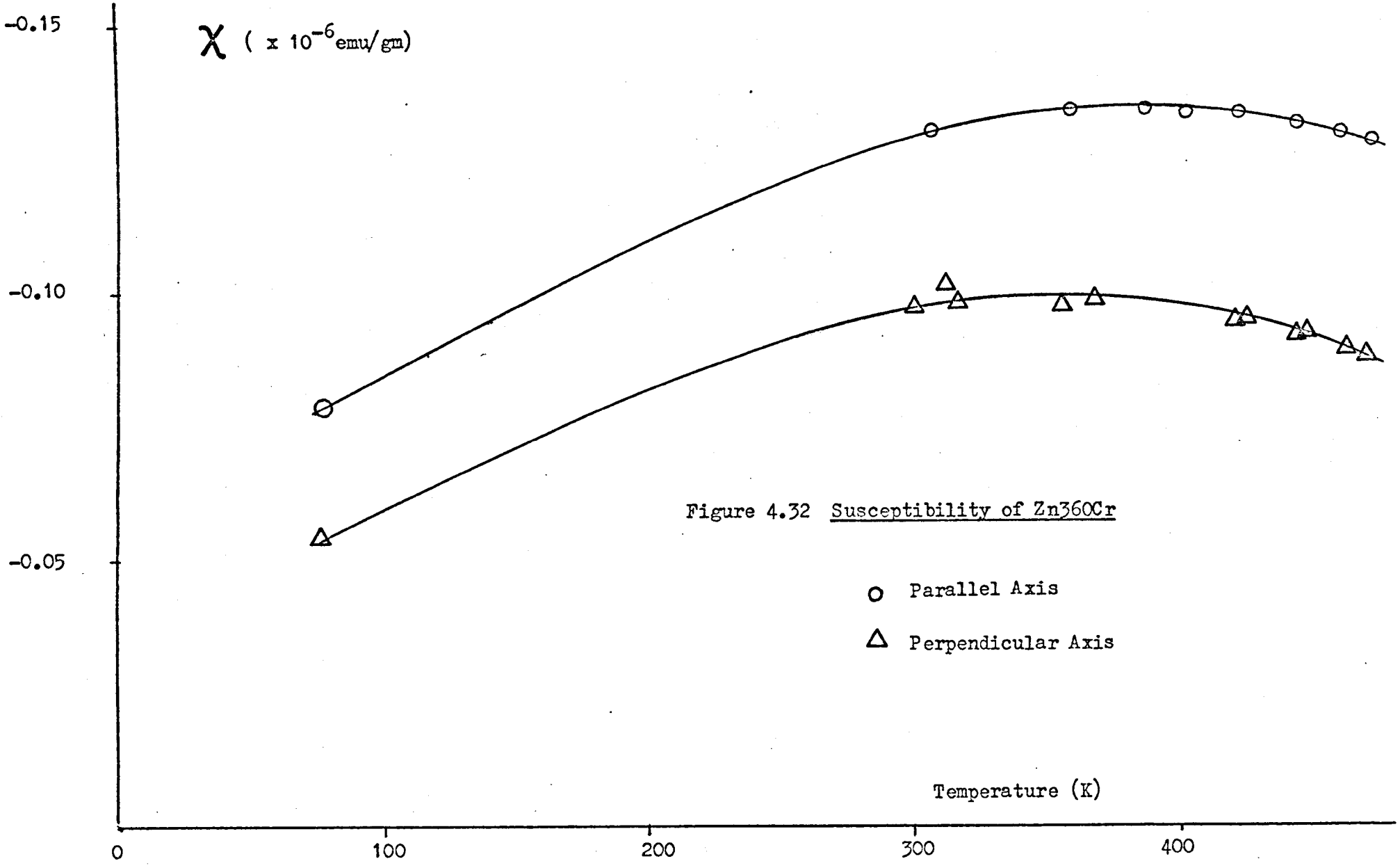

Figure 4.32 Susceptibility of Zn360Cr

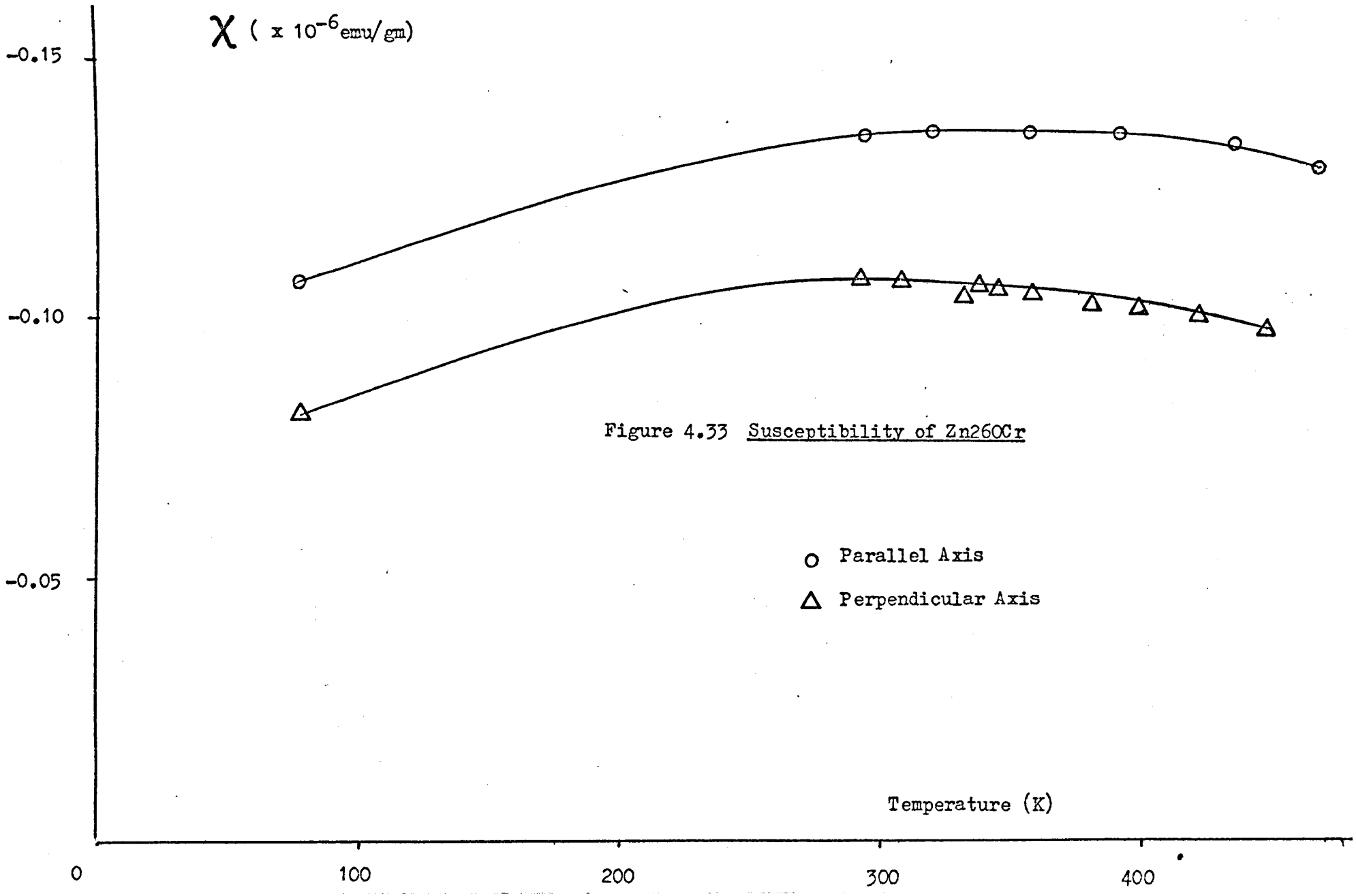

Figure 4.33 Susceptibility of Zn260Cr

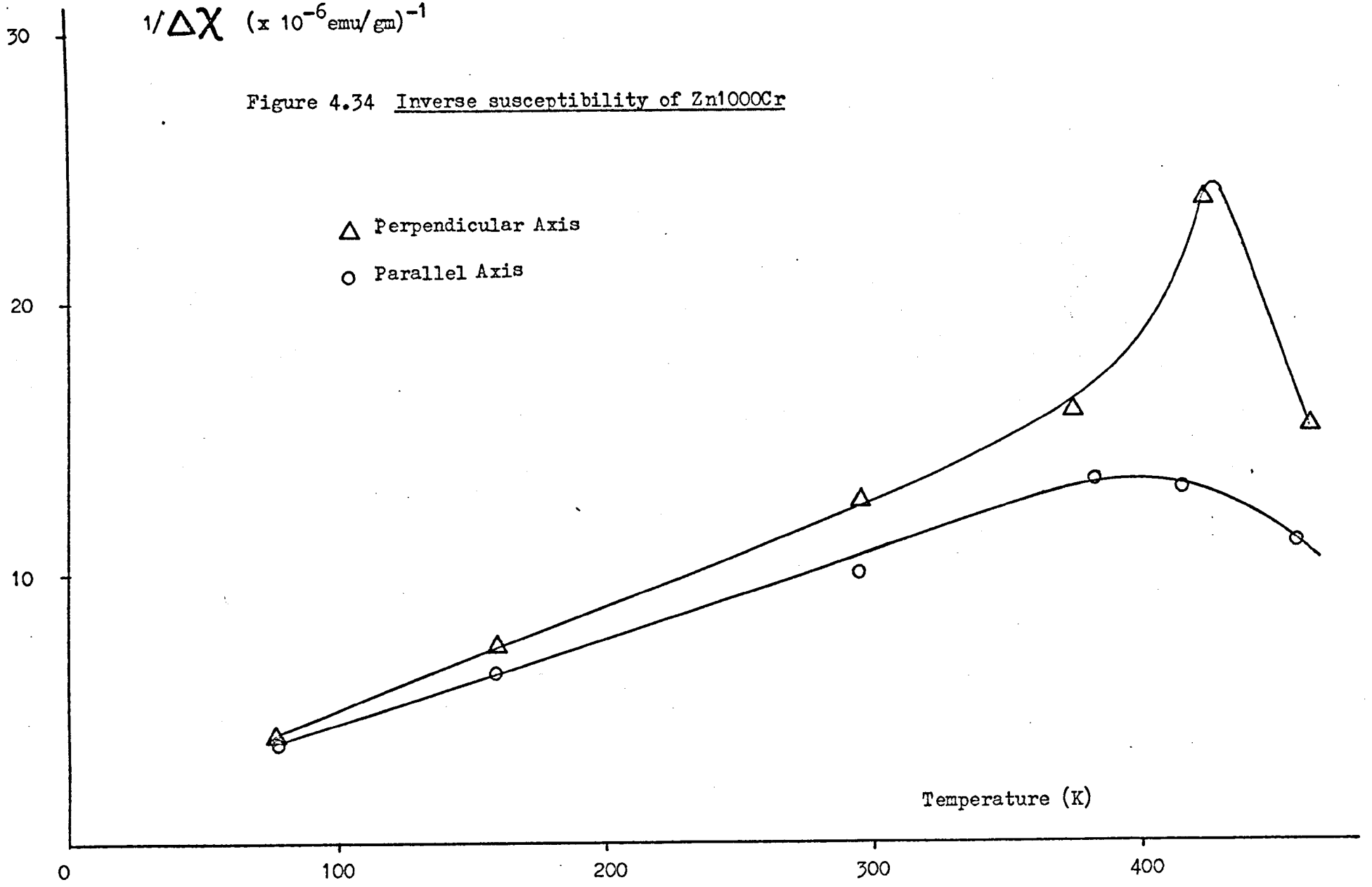

Figure 4.34 Inverse susceptibility of Zn1000Cr

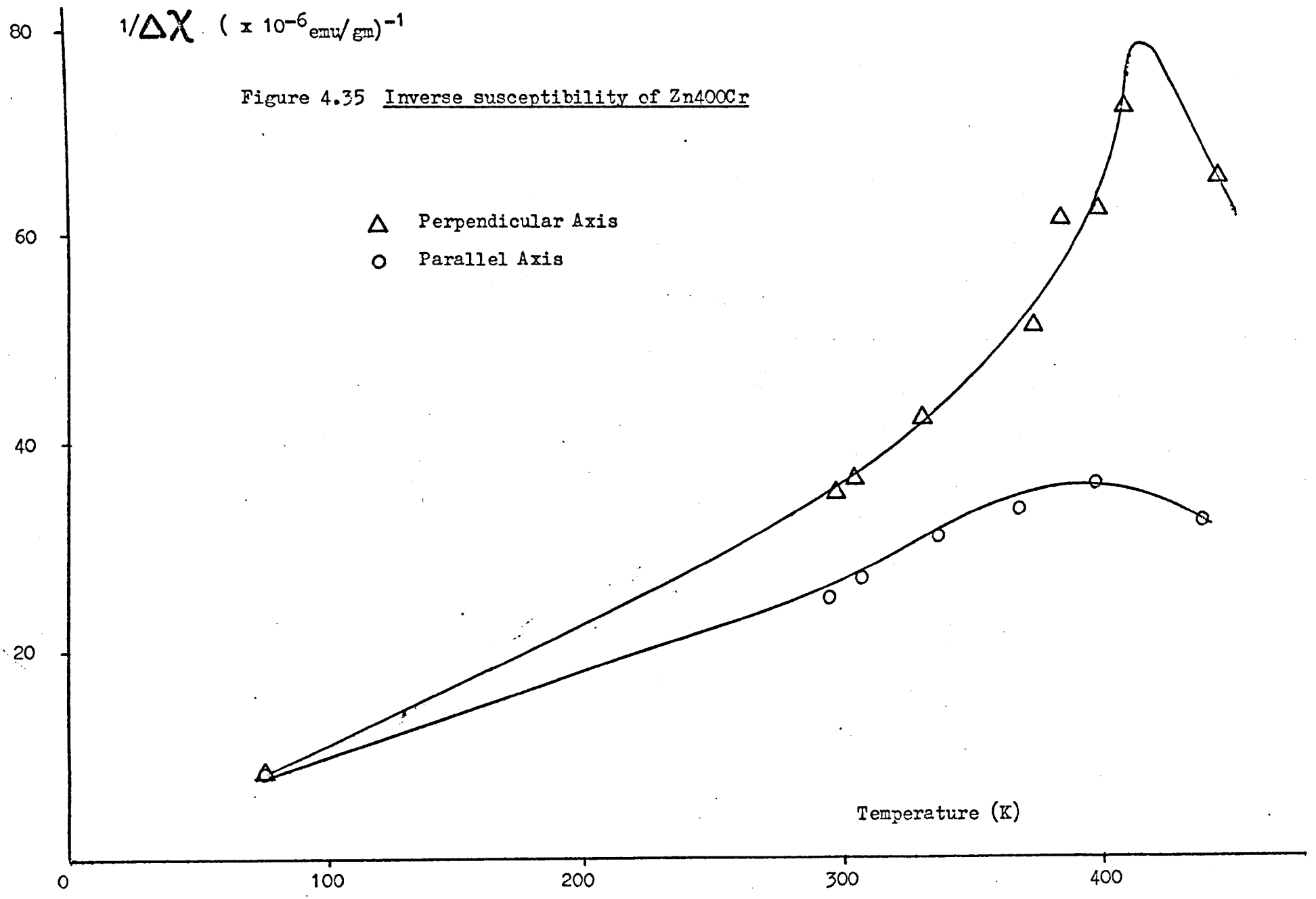

Figure 4.35 Inverse susceptibility of Zn400Cr

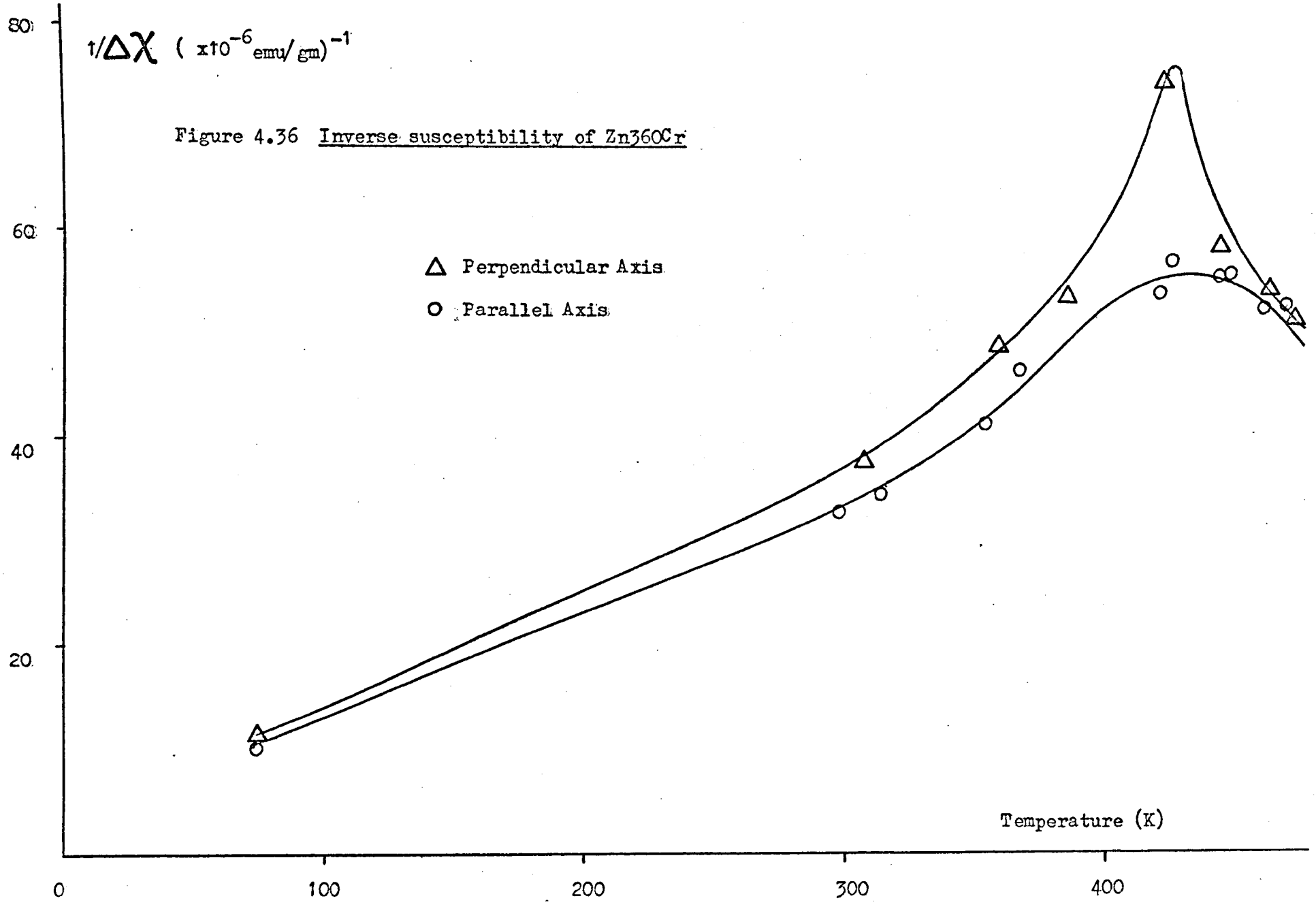

Figure 4.36 Inverse susceptibility of Zn3OCr

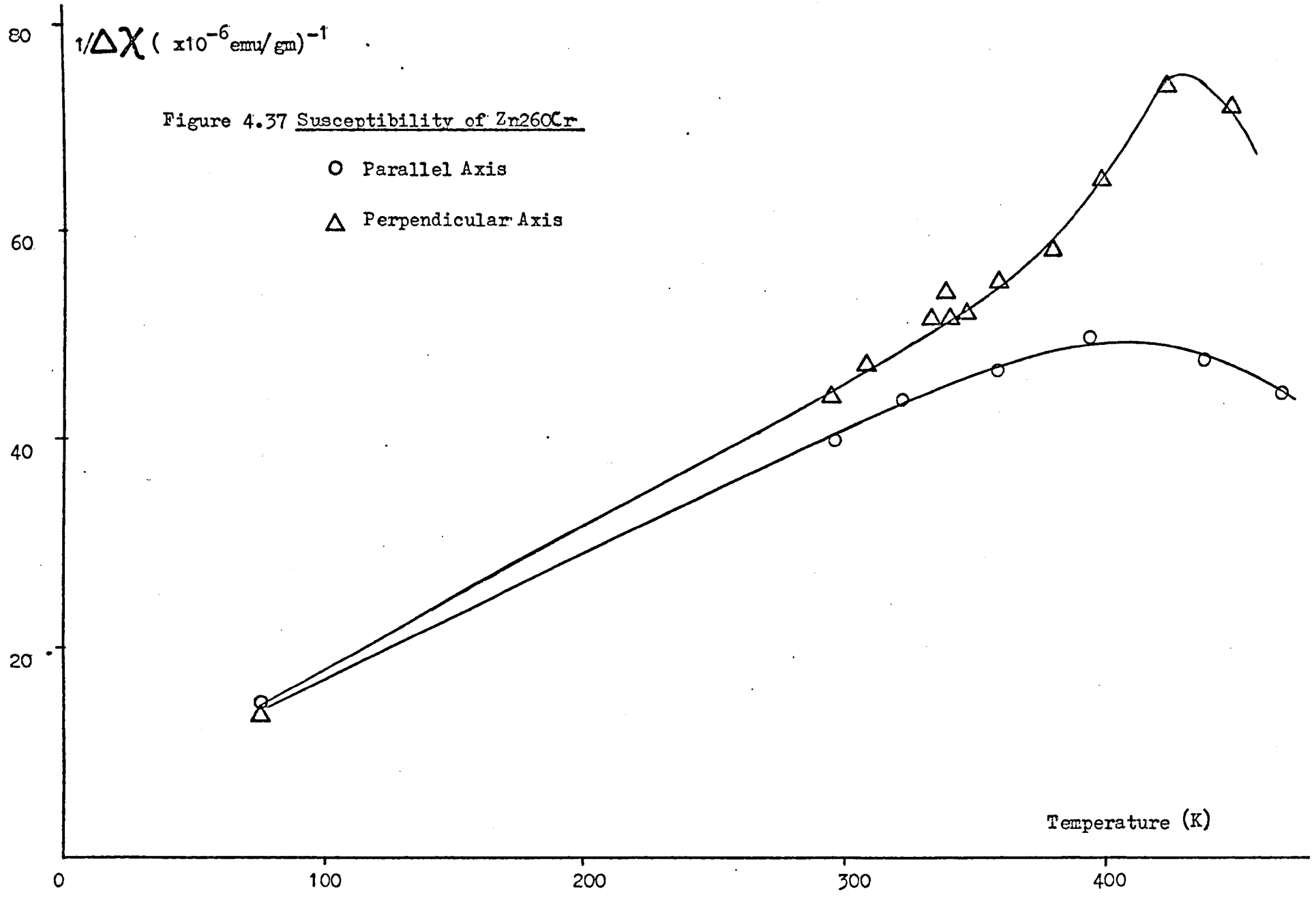

Figure 4.37 Susceptibility of Zn_2OCr

stable systems, so results were not taken with temperatures greater than ~ 0.7 of the melting point of zinc. The inverse susceptibility was calculated using figures 4.9 and 4.10 by assuming the values of the host susceptibility at each temperature was in proportion to the concentration of chromium.

The chromium concentration was found always to be less than the concentration to be expected from the weights of the components of the crystal. It is probable that partial zone refining took place when the crystal was prepared as described in section 3.4. As each crystal was cut from the centre of the boule, large concentration gradients were avoided. To check, subsequent experiments on crystals as long as the uniformity of D (section 3.1.1) allowed showed the susceptibility change due to the gradient was smaller than experimental error.

4.2.3. Discussion

The inverse susceptibility of the high temperature ZnCr alloys shows that both axes follow a Curie-Weiss law from T = 77K to ~ 320K within experimental error. This error is quite large especially in the smaller concentration as the paramagnetic effect of chromium goes as the inverse of temperature, thus making $\Delta\chi$ very small. Plotting $1/\Delta\chi$ in figures 4.34 to 4.37 perhaps exaggerates the chromium susceptibility here, though it does give an indication in which temperature range a Curie-Weiss law holds and also markedly shows up the peaks occurring at T ≃ 420K. Further discussion as to the nature of these peaks will be postponed to section 4.3.2. after chemical analysis and some aspects of intermetallic compounds have been presented.

The incremental susceptibilities show that $\Delta\chi_{\parallel} > \Delta\chi_{\perp}$ for all temperatures greater than 77K in contrast to the low temperature results. The anisotropy at T = 300K given by $\Delta\chi_{\parallel}/\Delta\chi_{\perp}$ is 1.20 ± 0.05 taking an average of all the crystals, and an average effective spin in the temperature range 77K to ~350K is $4.0 \pm 0.5\ \mu_B$ in the parallel

direction and 3.6 $\pm$ 0.5 μ_B in the perpendicular direction, again taking an average of all the crystals. The θ values are generally negative though the errors are so large in this case that it is not worth quoting a definite value. Peters et al. (1972) have presented results of chromium in liquid zinc at 1373 K and analysis of their data gives an effective spin value of 4.4 $\pm$ 0.3 μ_B . This compares well with the present results as the Fermi sphere is isotropic in the liquid state and one would expect the spin value to be closer to the free ion value of 4.9 μ_B .

4.3 Chemical Analysis

4.3.1. Results

The galvanometer reading for the various zinc and chromium crystals gave a nominal concentration from figure 3.14 and the true concentration was calculated from :

$$\frac{\left(\frac{Xc}{A(Zn)}\right)}{\left(\frac{X}{A(Zn)} + \frac{V}{A(L)}\right)} = G \qquad 4.17$$

where X = weight of ZnCr (gm)
c = concentration of Cr in Zn (mppm)
A(Zn) = atomic weight of Zn
G = galvanometer reading
V = weight of liquid (gm)
A(L) = atomic weight of dilute acid

The atomic weight of zinc is negligibly different from that of Zn(c)Cr where the concentration<0.1 atomic %. The volume of liquid does not have to be modified by the inclusion of the metal as the co-ordination sphere of water is large enough ($\sim 7\text{Å}$) to accommodate zinc and chromium atoms without any volume change, whilst assuming, quite reasonably in this case, that a true solution has been made. The density of 9 parts water to 1 part concentrated hydrochloric acid is 1.00004 so the 2 ml. volume of solution that was normally made up was

closely 2 gm. Dilute hydrochloric acid has an atomic weight of 19.8 as the above ratio of water to acid was kept constant for all samples.

All crystals considered in this thesis have been labelled by the concentration of impurity calculated by the chemical method above or inferred from this result.

Dealing with the low temperature results first, inspection of figures 4.1 to 4.7 shows that there is a noticeable change in slope at approximately 28 to 38K in the crystals where the impurity concentration is greater than ~150mppm. Bell has shown that a Curie-Weiss law is followed by ZnCr with a θ of -0.65K and an effective spin value n of 3.6 μ_B (section 4.1.3.) Equation 4.7 gives a value for the incremental susceptibilities which can be combined with equation 4.5 and then substituted into equation 4.8 thereby allowing the concentration c to be derived from the measured susceptibility, assuming $n = 3.6\ \mu_B$. This is done at convenient temperatures and compared with the analytically derived concentration.

Table 4.5 summarises this :

Table 4.5 Low temperature concentration comparison for ZnCr

T (K)	$\Delta\chi$ ($\times 10^{-6}$ emu/gm	c (mppm) from measured χ	c (mppm) analysed
4.2	0.249 ± 0.005	48.8 ± 2.7	46 ± 3
4.2	0.751	146.9	135
26	0.184	193	183
10	1.061	427.8	400

Figures 4.30 to 4.37 show the high temperature results where the most notable characteristics are that a Curie-Weiss law

probably holds from T ≃ 77K to ~340K and a peak at T ≃ 420K appears in both axes. A slightly different approach to the low temperature results above is followed as only one crystal was chemically analysed in this section so it is used to calculate the concentration of the high temperature crystals via comparison of their susceptibilities. This crystal is the Zn 400 Cr and is common to both low and high temperature experiments. Knowledge of the inferred concentration is used to calculate the isotropic susceptibility at various temperatures assuming the relevant parameters in equation 4.8 still hold. Table 4.6 shows this.

4.3.2. Discussion

The low temperature data (figures 4.5 to 4.7) show a discontinuity in the region of ~30K which does not appear indicative of an energy level becoming thermally accessible because a simple change in slope occurring at one fixed concentration-independent temperature would be expected. The point of inflexion moves higher in temperature with concentration so an intermetallic compound or compounds become a probable cause. Microprobe, X-ray and chemical analysis techniques would not be expected to show up the different phases in the sample due to the very small total amount of chromium present and lack of large samples. Optical microscopy offers the best chance of detecting small regions of intermetallic compound so a representative range of samples were cleaved under liquid nitrogen and observed using a Zeiss Ultra-Phot microscope type 63063. Under magnification of 2500x no phase change was seen, even in the most concentrated crystals, so any aggregates of compound were smaller than ~ $4 \times 10^{-10} m^2$ in surface area.

Table 4.6 High temperature susceptibility comparison for ZnCr.

T (K)	c (mppm) inferred	$\Delta\chi$ ($\times 10^{-6}$ emu/gm) measured	$\Delta\chi$ ($\times 10^{-6}$ emu/gm) from a Curie-Weiss law
77	1000 ± 20	0.272 ± 0.005	0.332 ± 0.007
"	400 *	0.109	0.129
"	360	0.099	0.116
"	260	0.072	0.084
200	1000	0.121	0.124
"	400 *	0.057	0.050
"	360	0.057	0.045
"	260	0.038	0.032
400	1000	0.054	0.062
"	400 *	0.020	0.025
"	360	0.019	0.022
"	260	0.015	0.016
440	1000	0.058	0.056
"	400 *	0.020	0.022
"	360	0.017	0.020
"	260	0.014	0.015

* This crystal concentration was used as a reference in calibrating the others.

By analogy with $Zn_{13}Mn$ which has been studied along with $Zn_{13}Fe$ and $Zn_{13}Co$ by Caplin et al. (1973) one may expect $Zn_{13}Cr$ to form. This is probably not the case because Brown (1962) reported that this does not appear to exist in a thermodynamically stable form - multiphase compounds are invariably produced when one attempts to fabricate it in a similar fashion to the Mn, Fe and Co compounds.

$Zn_{13}Mn$ has an ordering temperature of 23K when analysed by the standard method of plotting H/M (field/magnetisation) against M^2 (Arrot, 1957) at several closely spaced temperatures. It is likely that an intermetallic multi-phase compound of ZnCr would order at similar temperatures to $Zn_{13}Mn$, especially as changing the concentration of the Cr would alter the preponderance of one phase relative to another.

Figure 4.38 shows the approximate susceptibility with temperature for $Zn_{13}Mn$ from which it is apparent that the susceptibility for $T \lesssim 10K$ is of the order of 10^3 times more paramagnetic than dilute alloys of ZnCr. Assuming that a compound of ZnCr would behave similarly, an abrupt change in the susceptibility would occur at the ordering temperature. Below this, the effect due solely to the intermetallic compound would become constant as chromium spins all became aligned and the paramagnetic effect of the chromium in the 'dilute' environment would dominate, a Curie-Weiss law holding at low enough temperatures. Figure 4.16 illustrates this argument where a linear initial slope holds up to $T \simeq 24K$ is plotting the inverse susceptibility against the temperature for ZnCr, and a different slope continues from $T \simeq 32K$ to the highest measured temperature here of 46K. A Curie-Weiss law would be expected to hold above the ordering temperature for a dilute alloy containing the intermetallic compound because, again by an anlogy with figure 4.38, the susceptibility quickly falls due to increasing magnetic disorder caused by rising thermal energy.

If this is the case, one would expect that the measured susceptibility at low temperatures would give an enhanced value to the concentration of transition metal derived from a simple Curie-Weiss theory above the value gained from a chemical analysis. Table 4.5 shows this is so, where the analysed concentration figures are consistently lower (~5%) than the derived figures, though the most dilute crystal agrees within experimental error. This is not surprising as the unambiguous $\chi_\perp$ axis in figure 4.2 for Zn46Cr shows

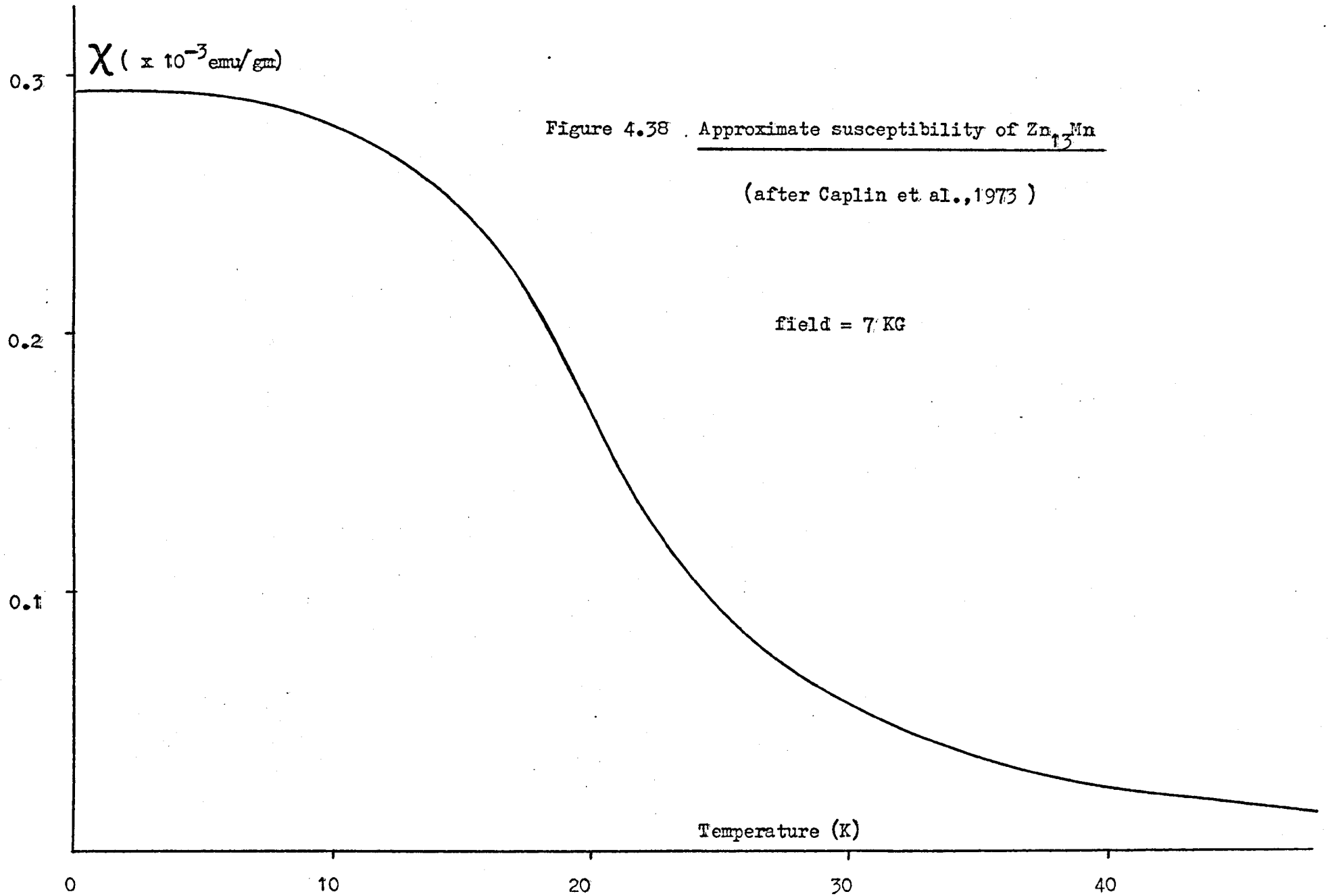

Figure 4.38 . Approximate susceptibility of $Zn_{13}Mn$

(after Caplin et al., 1973)

field = 7 KG

no tendency to order at T≃30K. Elaborate heat treatments were necessary to produce compounds of $Zn_{13}Mn$, $Zn_{13}Fe$ and $Zn_{13}Co$ so only very small amounts of any compound of ZnCr would be likely to form in the crystals studied here.

The high temperature data in figure 4.30 to 4.33 shows a distinct curvature in both axes in the range 350 - 450K. After subtraction of the relevant host susceptibility, figures 4.31 to 4.34 show the peak in the inverse susceptibility quite prominently at T ≃ 420K. The concentration in these alloys is greater than the low temperature crystals thereby increasing the probability of inclusions of intermetallic compounds. It is surprising that a linear Curie-Weiss law is so markedly deviated from at these high temperatures because, assuming from the evidence of the low temperature crystals that some form of intermetallic compound is present, T≃ 420K is an unusually high ordering temperature. Most of these type of compounds order at liquid nitrogen temperatures or below. Table 4.6 presents a similar analysis to table 4.5 though as only one crystal in the high temperature group was chemically analysed and the concentration of the others calibrated from this at 77K (well away from the possible higher ordering temperature of 420K) the comparison is between the measured and derived incremental susceptibilities at different temperatures. When T = 77K, $\Delta\chi$ (measured) is ~18% less than $\Delta\chi$ (derived) showing there is less chromium available for simple, paramagnetic Curie-Weiss effects to hold. Possibly this chromium is in a form of intermetallic compound. At higher temperatures the discrepancy between the two $\Delta\chi$'s becomes less until T ≃ 440K where the tendency is for the effect similar to that at 77K to take hold again. If, as seems feasible from figures 4.31 to 4.34 that the experimental values of the inverse susceptibility continue to decrease as the temperature is raised above 440K, then $\Delta\chi$ (measured) will again be less than $\Delta\chi$ (derived) indicating a reduction in order, and therefore of susceptibility contributed by an included compound.

Alternatively, because the temperature of these latter experiments is much greater than 15K, where Bell showed ZnCr and ZnMn polycrystals to follow a Curie-Weiss law, it need not follow a priori that the law holds for anisotropic single crystals in this temperature region. Although results indicate that between 77K and ~350K $1/\Delta\chi_a$ when plotted against T is linear, lack of data points preclude the view that the Curie-Weiss law definitely describes the experimental situation in this temperature range. Because it is unlikely that an intermetallic compound has been formed with the very high ordering temperature of 420K, the effect may be due to crystal fields (Chapter 5).

As the low temperature data show $\Delta\chi_\perp / \Delta\chi_\parallel > 1$ and $\Delta\chi_\perp/\Delta\chi_\parallel < 1$ for high temperature when analysed assuming a Curie-Weiss law holds, it is interesting to show this ratio for the whole measured temperature range. Figure 4.39 shows this in log/log form taking an average of all the crystals investigated. When $T \simeq 50K$, single crystals of ZnCr appear to become magnetically isotropic. This is a further indication that a change of population of energy levels is taking place, indicative of crystal fields. The anisotropy becomes quite marked at ~400K, more so than at ~20K thus supporting the view that thermal repopulation invalidates the application of a Curie-Weiss law at the highest temperature measured.

Figure 4.39 Ratio of average perpendicular and parallel susceptibilities of ZnCr

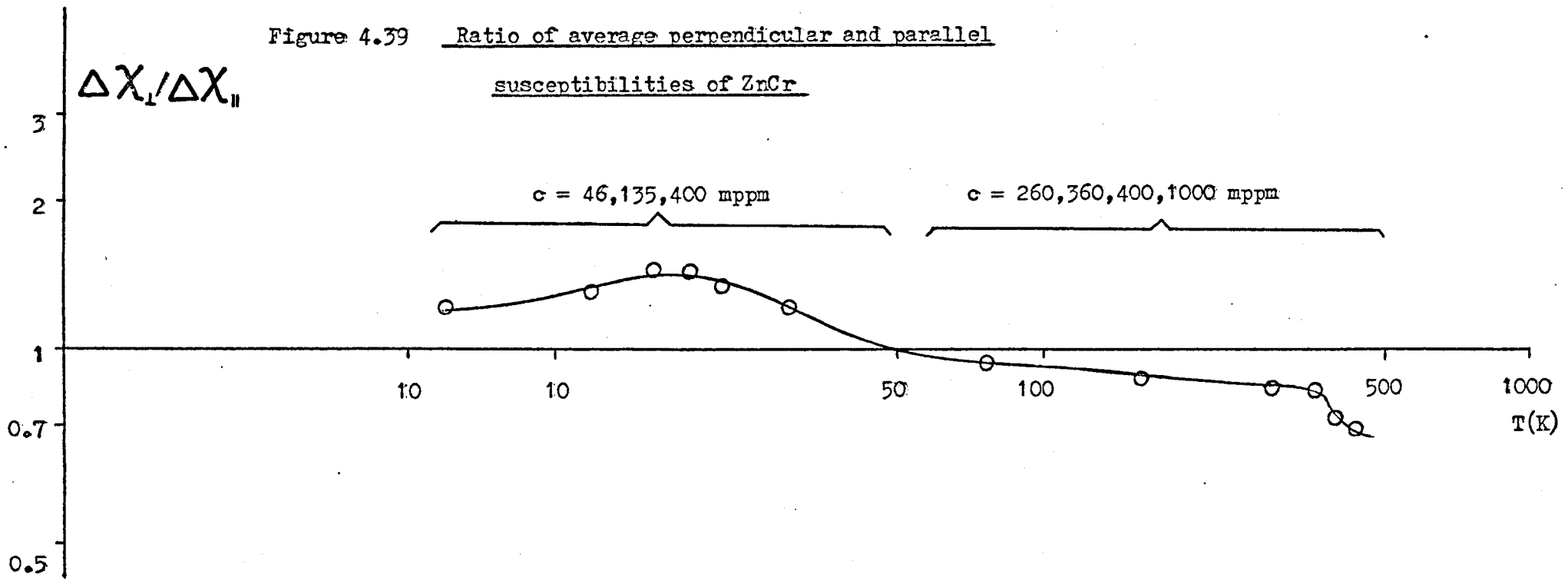

REFERENCES

Arrot, A.,	Phys. Rev.,	108,	1394,	1957
Bell, D.A.,	Ph.D. Thesis, Imperial College,			1972
Berlincourt, T.G., Steele, M.C.,	Phys.Rev.,	95	1421,	1954
Bleaney, B.,	Phys. Rev.	78,	214,	1950
Boato,G.,Bugo,M.,Rizzuto,C.,	Nuovo Cimento,	45,	226,	1966
Brown, P.J.,	Acta. Crystallogr.,	15,	608,	1962
Caplin,A.D.,Dunlop,J.B.,	J.Phys.F:Metal Phys.	3,	1621,	1973
Dingle, R.B.,	Proc. Roy. Soc.A.,	211,	517,	1952
Dupree R., Geldert D.J.,	Sol. Stat. Comm.,	9,	145,	1971
Higgins,R.J.,Marcus,J.A.,	Phys. Rev.,	141,	553,	1966
Holt,G., Myers,A.,	Phys.Kondens.Materie	9,	23,	1969
Lawson,J.R., Gordon,W.L.,	Phys.Lett.,	43,	135,	1973
Li, P.L., et. al,	Phys. Rev.Lett.,	31,	29,	1973
Myers, A.,	University of Leeds, Private Commun.,			1973
Peters,J.J., Flynn C.P.,	Phys. Rev.B.,	6,	3343,	1972
Scalapino, D.J.,	Phys. Rev. Lett.,	16,	937,	1966
Schoenberg, D.,	Prog. Low Temperature Phys. ed. C.J. Gorter. North Holland Publishing Co.,	2,	245,	1957

Chapter 5

CRYSTAL FIELDS

5.1. Introduction

In this section much of the following is of a general nature and for a more detailed explanation of fundamental crystal field theory the following authors may prove useful :

Abragam and Bleaney, 1970
Hutchings, 1964
Krupicka et. al., 1968
Martin, 1967
Orton, 1968
Park, 1964
Stevens, 1952
White, 1970

Under conditions of thermal equilibrium, the populations of energy levels (E) of paramagnetic ions in a crystal lattice are determined by the Boltzmann distribution function. This allows a simplification of the otherwise enormous task of computing all these levels because in a normal susceptibility or resistivity experiment only the levels within a few hundred cm^{-1} above the ground state will be populated. One usually calculates the ground state energy for a free ion, then includes crystal field effects. As the energy levels are field-dependent, it is possible to expand E in the following manner:-

$$E_n = E^o{}_n + E^1_n H + E^2_n (H)^2 + \text{-----} \qquad 5.1$$

where H = magnetic field
n = atomic stationary state order number

The magnetisation (M) is given by :-

$$M_n = \partial E_n / \partial H = E^1_n + 2E^2_n H + \text{-----} \qquad 5.2$$

so because the susceptibility (χ) is given by the ratio of M to H, it is possible to determine the temperature dependence of χ by including the effect of the Boltzmann distribution

viz :-

$$\chi = N \frac{\sum_n ((E_n^1)^2/kT - 2E_n^2)\exp(-E_n^o/kT)}{\sum_n \exp(-E_n^o/kT)} \qquad 5.3$$

Where N = number of atoms/unit volume

Because equation 5.3 describes paramagnetic ions in an insulator in which the magnetic moment is not saturated, M is proportional to H and there are no H terms in χ. Thus information may be gained on the energy level population by measuring the temperature dependence of χ.

In most cases, the ground state may be found from Hund's rules except when the orbital and spin momenta (L and S) are not good quantum numbers. Perturbation treatment requires successive consideration of smaller effects, so in deriving energy levels it is necessary to determine the order of the interactions. They are, for elements of the first transition group,

Coulomb interaction : $10^4 - 10^5 cm^{-1}$

Spin-orbit coupling : $10^2 - 10^3 cm^{-1}$

Magnetic field : $1 cm^{-1}$

If a paramagnetic ion is placed in a lattice site, the crystalline field approximation states that the interaction of the ion with its neighbours is entirely due to the electric field of neighbouring ions acting on the unpaired electron(s) of the paramagnetic ion. Thus the orbit of an unpaired electron will be changed. For a typical nearest neighbour distance (2Å), the electric field energy produced by an electron at a singly charged ion is $\sim 10^4 cm^{-1}$. Obviously this value may be modified by screening effects as would be expected to occur for the rare earth ions and with less modification for the 3d ions. To take this into account, three general crystal field strengths are defined: weak, intermediate and strong. The first usually applies to the

rare earth and actinide groups, the second to the iron group and the last to the platinum and palladium groups. The nature of the energy calculation thus depends on which experimental situation is relevant. As only the 3d transition group are investigated here discussion will be limited to these. Knowledge of the d-wave orbitals is necessary to determine the splittings of the d levels in a crystalline environment, and some of these are shown schematically in figure 5.1.

Figure 5.1 Angular probability distribution for the 3d orbitals in an axial environment

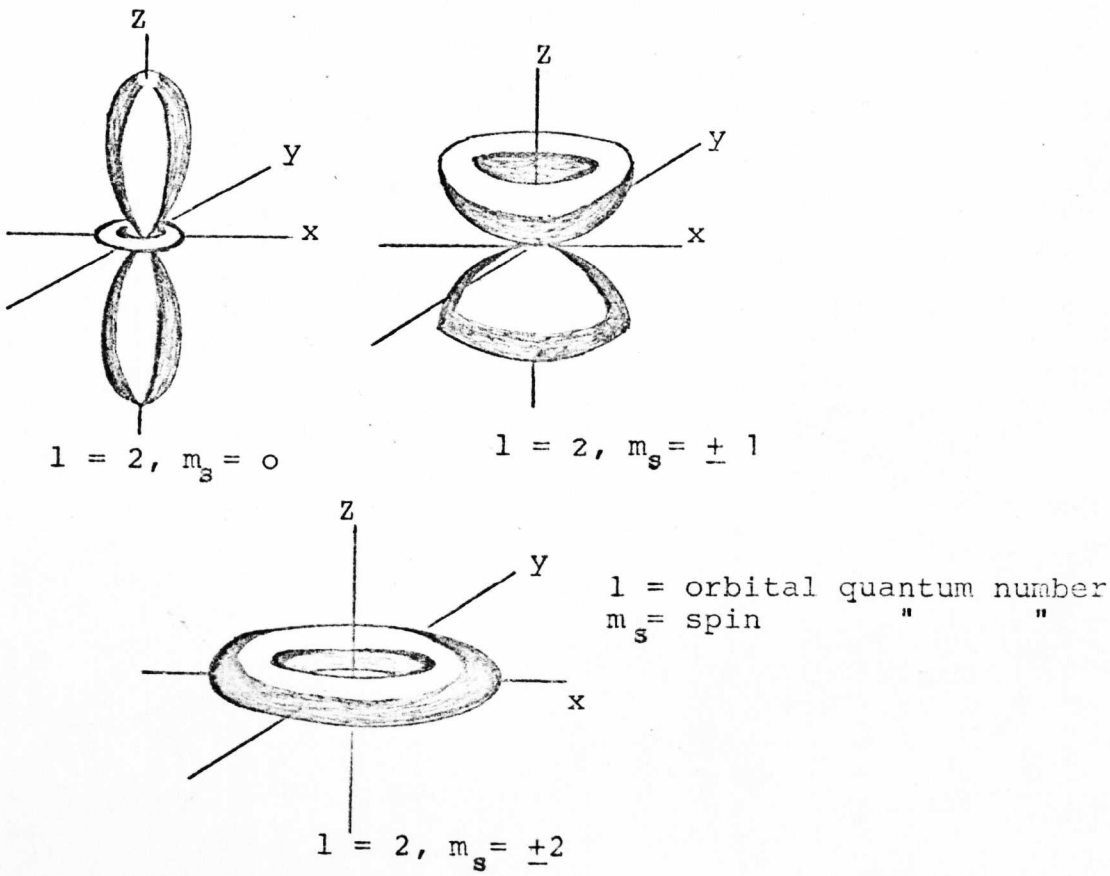

To give a quantitative answer to the energy level distribution one must determine the crystal potential V at any particular point and calculate its interaction with (to first order) an unpaired electron of the ion in question. This can be done most simply in terms of spherical harmonics where the

restrictions of the symmetry of the crystal can be easily introduced. In general a central field approximation is assumed and the atomic orbitals are written :

$$\Psi_{nlm}(r, \theta, \phi) = R_{nl}(r) \quad H'_{lm}(\theta) \; I'_{m}(\phi) \qquad 5.4$$

where n = principal quantum number
l = angular momentum quantum number
m = magnetic quantum number
r = ion-neighbour distance
θ , ϕ = coordinate angles

and $$H'_{lm}(\theta) = ((2l + 1)(l - |m|)!/2(l+|m|)!)^{\frac{1}{2}} P_l^m(\cos\theta) \qquad 5.5$$

$$I'_m(\phi) = (1/(2\pi)^{\frac{1}{2}}) \exp(i m \phi) \qquad 5.6$$

The radial function $R_{nl}(r)$ may be modified by a particular lattice such that usually it cannot be calculated, so it is left as a function to be determined. The values in the free ion case have been calculated by Freeman and Watson (1962). It is usual to write the product of equations 5.5 and 5.6 as the spherical harmonic:

$$(-1)^{((m + |m|)/2)} H'_{lm}(\theta) I'_m(\phi) = Y_l^m(\theta, \phi) \qquad 5.7$$

and the corresponding Legendre polynomials as:

$$P_l^o(x) = 1/2^l l! \frac{d^l(x^2-1)^l}{dx^l} \qquad 5.8$$

and $$P_l^m(x) = (1 - x^2)^{|m|/2} \frac{d^{|m|}}{dx^{|m|}} (P_l^o(x)) \qquad 5.9$$

where $x = \cos\theta$

Combinations of the spherical harmonics are taken to give wholly real (or imaginary) functions. It is not necessary

to go beyond the fourth order for d electrons in evaluating the crystal field potential V (sixth order for f electrons) because of orthogonality conditions of the spherical harmonics Briefly, matrix elements of the form $\langle \psi_M^* | V_n^m | \psi_{M'} \rangle$ are used to calculate the 3d electron energy, where ψ_M and $\psi_{M'}$ are defined in equation 5.4. The product $\psi_M^* \psi_{M'}$ can be written in terms of spherical harmonics and if V_n^m can be expanded in spherical harmonics, the matrix element is zero unless $n \leq 4$. It is only strictly true that V_n^m is a function of spherical harmonics if there is no covalency between the magnetic ion and the neighbouring ions, i.e. if V_n^m satisfies Laplace's equation.

Once the potential V has been derived, the next step is to calculate the electron energies. A relatively simple method of doing this is to use operator equivalents, due to Stevens (1952). Individual electrons are coupled together to give a total angular momentum value L. The (2L+1) orbital degeneracy is raised by the crystal field and then the matrix elements for states M_L, where M_L = L, L-1, - - -, -L is the orbital magnetic quantum number, are calculated using a coordinate transformation in the crystal field expansion $V = \sum A_n^m V_n^m$ viz:

Cartesian coordinates		Equivalent operators	
x	⟶	Lx	
y	⟶	Ly	etc.
xy	⟶	½(LxLy + LyLx)	etc.
r^2	⟶	L(L + 1)	etc.

For each electronic configuration, the crystal field operators give matrix elements proportional to the original potential function, two constants α' and β' corresponding to the second and fourth order terms being required. For instance, it is often necessary to evaluate terms like

$\sum(3z^2 - r^2)$. This is equivalent to $\alpha'\langle r^2\rangle$ $(3Lz^2 - L(L+1))$, where $\alpha'\langle r^2\rangle$ is an average value to be included in experimentally-determined parameters relating to $R_{nl}(r)$ in equation 5.4. The coefficients A_n^m in the potential expansion may be estimated initially from a point charge model where the field due to each of the neighbours of an ion in a crystal lattice are considered to arise from a point charge at each lattice site. As this last assumption is obviously not true, the correction needed is taken into one of the experimentally determined parameters.

Once the basic framework has been established, it will be applied to the relevant experimental situation considered here, via ZnCr. As zinc is anisotropic and leads to an anisotropic incremental susceptibility for the alloy, the theory must take this into account and predict reasonable anisotropy parameters. Equation 5.3 cannot provide an accurate description of ZnCr because for instance the chromium impurity is not in an insulating host, so it is found an easier task to determine the g values/set of energy levels. The g values for the cryostallographic orientations of zinc are proportional to the relevant χ values, thus allowing the anisotropy to be calculated from the g-value ratio.

5.2. Analysis

To determine the potential field at a particular site in a crystal due to the ions at each lattice site, one may write:

$$V = \sum_{i,n} \frac{q|e|}{|r_i - R_n|} \qquad 5.10$$

where e = electronic charge

q = valency

r_i = position of i'th electron of an ion

R_n = position of n'th ion in lattice

(note: all position parameters are vector quantities)

A basic assumption in this section is that we are dealing with a magnetic insulator, i.e. there are no inter-impurity interactions via the conduction electrons. This may not be true for ZnCr but continuing with this simplified theory will show the limitations inherent in making the assumption. Rewriting equation 5.10 in terms of spherical harmonics:

$$V = \sum_{i,n} q|e| \sum_{l,m} \frac{4\pi}{(2l+1)} \frac{r_<^l}{r_>^{l+1}} Y_l^m(\theta_{R_n}, \phi_{R_n}) Y_l^{m*}(\theta_i, \phi_i) \qquad 5.11$$

where θ_{R_n}, ϕ_{R_n} describes the orientation of R_n

$r_<^l$ denotes $|R|$ if $R < |r_i|$, and $|r_i|$ if $R > |r_i|$

$r_>^{l+1}$ denotes $|R|$ if $R > |r_i|$, and $|r_i|$ if $R < |r_i|$

Y is defined as in equation 5.7

Expanding in terms of m and l for the 3d transition case:

$$V = \sum_i A_2^o r_i^2 Y_2^o(\theta_i, \phi_i) + \sum_i A_4^o r_i^4 Y_4^o(\theta_i, \phi_i) \qquad 5.12$$

where the A terms are the coefficients of the crystal field expansion. Further terms in A are unimportant for zinc which has an hexagonal close-packed structure (D_{6h}).

Now,

$$\sum_i Y_2^o r_i^2 \propto \sum_i r_i^2(3\cos^2\theta - 1) \qquad 5.13$$

and $$\sum_i r_i^2(3\cos^2\theta - 1) = \alpha \langle r^2 \rangle V(L_2^o)$$

where $V(L_2^o) = 3L_z^2 - L(L+1)$

writing in equivalent operator form.

Similarly,

$$\sum_i Y_4^o r_i^4 \propto \sum_i r_i^4(35\cos^4\theta - 30\cos^2\theta + 3) \qquad 5.14$$

$$\propto \beta \langle r^4 \rangle . V(L_4^o)$$

where $V(L_4^o) = 35L_z^4 - 30L(L+1)L_z^2 + 25L_z^2 - 6L(L+1) + 3L^2(L+1)$

For the 3d transition case where L = 2, $V(L_4^o)$ reduces to:

$$V(L_4^o) = 35L_z^4 - 155L_z^2 + 72$$

(Abragam and Bleaney, 1970)

Summing equations 5.13 and 5.14 results in an operator $\mathcal{H}_o$:

$$\mathcal{H}_o = a(3L_z^2 - L(L+1)) + b(35L_z^4 - 155L_z^2 + 72) \qquad 5.15$$

where $a = \alpha A_2^o \langle r^2 \rangle$

and $b = \beta A_4^o \langle r^4 \rangle$

Taking the axis of quantisation along the z axis allows the diagonal matrix elements to be calculated when $\mathcal{H}_o$ operates on the M_L state viz:

$$\begin{aligned}
M_L &= 2, & \langle 2 | \mathcal{H}_o | 2 \rangle &= 6a + 12b \\
M_L &= 1, & \langle 1 | \mathcal{H}_o | 1 \rangle &= -3a - 48b \\
M_L &= 0, & \langle 0 | \mathcal{H}_o | 0 \rangle &= -6a + 72b \\
M_L &= -1, & \langle -1 | \mathcal{H}_o | -1 \rangle &= -3a - 48b \\
M_L &= -2, & \langle -2 | \mathcal{H}_o | -2 \rangle &= 6a + 12b
\end{aligned} \qquad 5.16$$

The eigenstates of equation 5.15 may be plotted in the manner of Lea et al. (1962) where these correspond to the allowed values of L_z, i.e. $|0\rangle$, $|\pm 1\rangle$ and $|\pm 2\rangle$. Firstly we define W and x such that

$$Wx = F_2 a \qquad 5.17$$

$$W(1-|x|) = F_4 b \qquad 5.18$$

where $-1 \leq x \leq 1$

and $F_2(=3)$, $F_4(=12)$ are the multiplicative constants used in determining the matrix elements used in determining equation 5.16. This modifies equation 5.15 to:

$$\mathcal{H}_o/W = xV(L_2^o)/F_2 + (1-|x|)\, V(L_4^o)/F_4 \qquad 5.19$$

Figure 5.2 represents the energy (in units of W) as a function of x and determines the ground state value of L_z for a particular x. The point charge model allows an estimation of x to be made for hexagonal close-packed metal (Kasuya, 1963) in the following manner :-

$$a = 2\alpha e^2 Z' V_2^o \langle r^2 \rangle . a_h^{-3} \qquad 5.20$$

$$b = 8\beta e^2 Z' V_4^o \langle r^4 \rangle . a_h^{-5} \qquad 5.21$$

where $V_2^o = -1.035\ (1.636 - c_h/a_h)$

$V_4^o = -(0.1127 - 0.752(1.633 - c_h/a_h))$

Z' = valence of effective point charge

c_h = nearest neighbour distance in the plane $\perp$ to the c-axis

a_h = " " " " " " // "

a and b are expected to vary only weakly with impurity atomic number (Hirst, 1970) and so should hold for all of the 3d metals in the zinc host.

Figure 5.2 Orbital energy levels of an hexagonal close-packed metal for L = 2

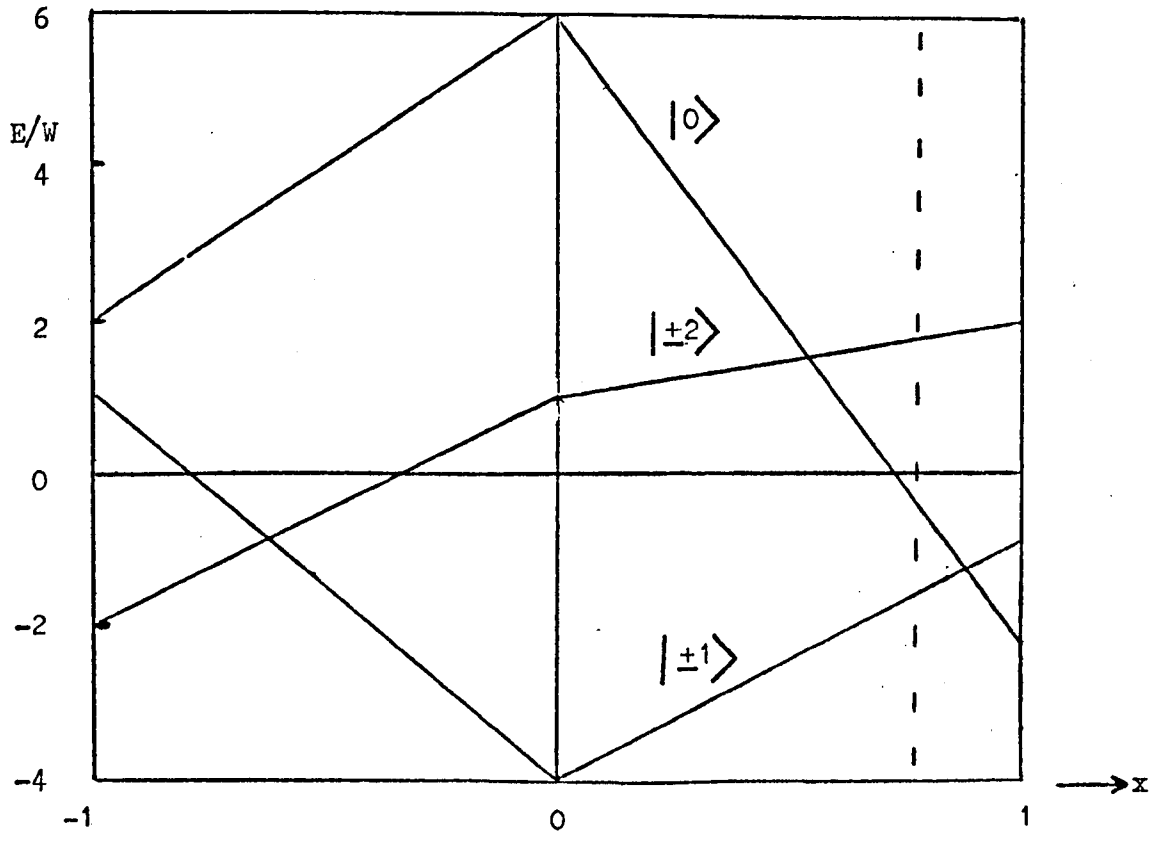

To roughly estimate x the value of c_h/a_h is taken to be 1.8284 following Li et al. (1972) who take this value to hold for single crystals of ZnMn up to a concentration of 475 mppm. Z' is assumed to be 3 and a_h to be $\sim 0.266 \times 10^{-7}$ cm. (Kittel, 1973). Substitution of the remaining constants from standard tables such as given by Stevens, 1952, Elliott and Stevens, 1953, Abragam and Bleaney, 1970, result in:-

$$x/(1 - |x|) \simeq 3.84$$

$$\therefore \quad x \simeq 0.79$$

This is shown by a dotted line on figure 5.2 and thus one would expect the $|\pm 1\rangle$ state to be lowest from this estimation. The preceding analysis neglects spin-orbit coupling λ L.S where λ is the coupling parameter and S is the total spin. Including this will give off-diagonal terms in the energy matrix, as the operator λ L.S now operates on both the orbital part (M_L) and spin part (M_s) of the electronic wavefunction. Firstly it is necessary to define λL.S so that the results will be wholly real as the potential V is real :-

$$\lambda L.S = \lambda(LzSz + LxSx + SySx)$$

or $$\lambda L.S = \lambda\, Lz.Sz + \tfrac{1}{2}\lambda(L_+S_- + L_-S_+) \qquad 5.22$$

where
$$L_+|M_L\rangle = (L(L+1) - M_L(M_L+1))^{\frac{1}{2}} |M_L+1\rangle$$
$$L_-|M_L\rangle = (L(L+1) - M_L(M_L-1))^{\frac{1}{2}} |M_L-1\rangle$$
$$S_+|M_S\rangle = (S(S+1) - M_S(M_S+1))^{\frac{1}{2}} |M_S+1\rangle$$
$$S_-|M_S\rangle = (S(S+1) - M_S(M_S-1))^{\frac{1}{2}} |M_S-1\rangle$$

Now, operating on the state $|M_L,M_S\rangle$ by λ L.S when L=2, S=2 for d electrons leads to:-

$$\lambda L.S|2,2\rangle = 4\lambda|2,2\rangle$$

and
$$\lambda L.S|2,1\rangle = 2\lambda|2,1\rangle + (\lambda/2)(0 + 4|1,2\rangle)$$
$$\lambda L.S|2,0\rangle = 0 + (\lambda/2)(0 + 2\sqrt{6}|1,1\rangle)$$
$$\lambda L.S|2,-1\rangle = -2\lambda|2,-1\rangle + (\lambda/2)(0 + 2\sqrt{6}|1,0\rangle)$$
$$\lambda L.S|2,-2\rangle = -4\lambda|2,-2\rangle + (\lambda/2)(0 + 4|1,-1\rangle)$$

Similar derivations are worked out for $|M_S,M_L\rangle = |1,2\rangle$,

---,$|-2, -2\rangle$ and given in Appendix 1. The results are presented in matrix form below (table 5.1).

The off-diagonal elements have the effect of mixing in other states to the diagonal eigenstates, and the results of this are given in Appendix 2 where the first term is the admixed state and the A,B and C coefficients are the energy states derived before spin-orbit coupling has been taken into account. The simple diagonal matrix representing this unadmixed state is given below (table 5.2).

A possible way of proceeding is to program a computer to derive the results as given above but with the advantage of being able to easily vary parameters such as A_2^o, A_4^o etc. at will, and then compare the predictions with experiment. The result of such a procedure is given in figure 5.3 which shows how spin-orbit coupling for chromium in zinc can affect the orbital energy levels when $\lambda = 60 cm.^{-1}$ and $a = 135\ cm.^{-1}$, $b = 8.75\ cm.^{-1}$ (calculated from equations 5.20 and 5.21). In most situations one would keep varying parameters until a fit between the model and experiment was achieved, but in this case it is not possible, as will be shown below.

Table 5.1 Matrix representation of λ L.S $|M_L, M_S\rangle$ (the matrix elements are zero everywhere except where indicated)

$\langle M_L, M_S \mid M_L, M_S \rangle$		$M_L = 2\lambda$					1λ					0					-1λ					-2λ				
		$M_S = \lambda$ x--																								
		2	1	0	−1	−2	2	1	0	−1	−2	2	1	0	−1	−2	2	1	0	−1	−2	2	1	0	−1	−2
	λ x 2	4																								
	1		2				2																			
2λ	0			0				$\sqrt{6}$																		
	−1				−2				$\sqrt{6}$																	
	−2					−4				2																
	λ x 2	2					2				0															
	1		$\sqrt{6}$					1				$\sqrt{6}$														
1λ	0			$\sqrt{6}$					0				3													
	−1				2					−1				3												
	−2						0				−2				$\sqrt{6}$											
	λ x 2						$\sqrt{6}$					0				0										
	1							3					0				$\sqrt{6}$									
0	0								3					0				3								
	−1									$\sqrt{6}$					0				3							
	−2											0				0				$\sqrt{6}$						
	λ x 2											$\sqrt{6}$					−2				0					
	1												3					−1				2				
-1λ	0													3					0				$\sqrt{6}$			
	−1														$\sqrt{6}$					1				$\sqrt{6}$		
	−2																0				2					2
	λ x 2																2					−4				
	1																	$\sqrt{6}$					−2			
-2λ	0																		$\sqrt{6}$					0		
	−1																			2					2	
	−2																									4

Figure 5.3 Schematic representation of the effect of spin/orbit coupling on the orbital energy levels

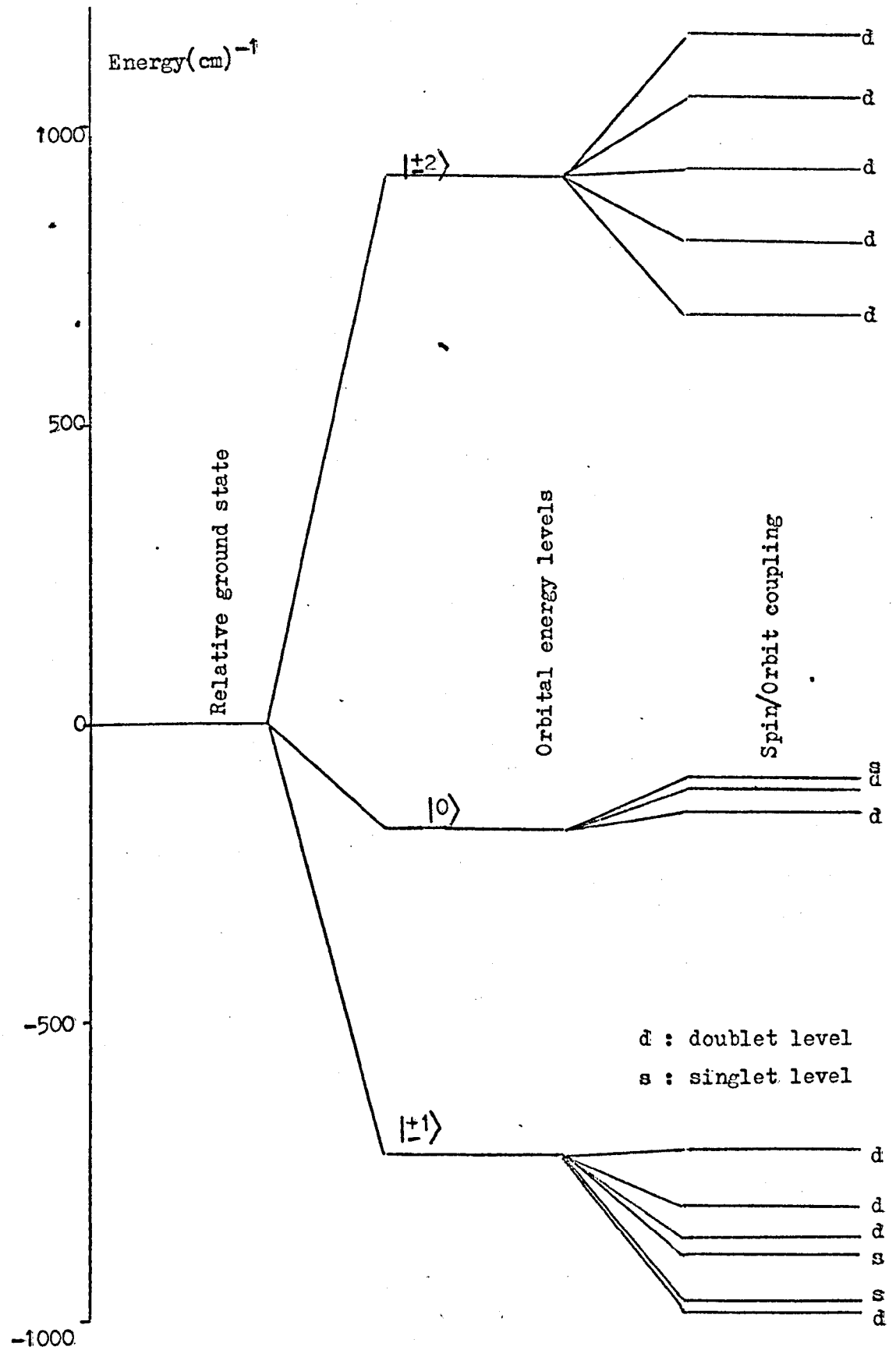

Table 5.2 Matrix representation of $\mathcal{H}_o$

$\langle M_L \mid M_L \rangle$		A	B	C	B	A
		2	1	0	-1	-2
A	2	6a + 12b	0	0	0	0
B	1	0	-3a-48b	0	0	0
C	0	0	0	-6a+72b	0	0
B	-1	0	0	0	-3a-48b	0
A	-2	0	0	0	0	6a+12b

To indicate this, an analytical method of deriving the ZnCr anisotropyis to determine the g-values by starting from the total Hamiltonian $\mathcal{H}$ which includes crystal field effects, spin-orbit coupling and the magnetic field viz:-

$$\mathcal{H} = \mathcal{H}_{CF} + \lambda L.S + (\beta H.(L+2S) \qquad 5.23$$

The g-values and hence the anisotropy will be modified according to which orbital state is lowest. It is not at all obvious on an a priori basis to say which state will be lowest (Hirst, 1970) so each state in turn will be taken as the ground state and the consequences examined to see if the simple theory presented here is an adequate explanation.

(i) $|o\rangle$ state lowest

To first order, the correction

$$V_1 = P_o(\lambda L.S + \beta H.(L+2S))P_o = 2\beta H.S \qquad 5.24$$

gives an isotropic g-value of 2 where P_o projects out an operator for the ground orbital state (Bates et al., 1968). The usefulness of the projection operators P_o here are that degenerate levels can be readily manipulated within the existing formalism to give matrix elements which have values different from zero only in the rows and

columns which correspond to the ground state. Also the P's commute with all spin operators (the unperturbed Hamiltonian does not contain spin operators) and have the same rotation invariance as $\mathcal{H}_{CF}$. It is necessary to go to second order to produce an anistropy in g.

The second order correction may be written:

$$V_2 = -\sum_{n\neq 0} \frac{P_0(\lambda \mathbf{L}.\mathbf{S} + \beta \mathbf{H}.(\mathbf{L} + 2\mathbf{S}))P_n(\lambda \mathbf{L}.\mathbf{S} + \beta \mathbf{H}.(\mathbf{L} + 2\mathbf{S}))P_0}{E_n - E_0} \qquad 5.25$$

where n corresponds to an excited energy level E_n,

E_0 is the ground state energy.

P_n can only be $|\pm 1\rangle$ and as $|\pm 1\rangle$ and $|0\rangle$ are orthogonal,

$$P_0\,(\beta \mathbf{H}.2\mathbf{S})P_n = 0$$

$$\therefore \quad V_2 = -\sum_{n\neq 0}\left(\frac{1}{E_n - E_0}\right)P_0((\lambda/2)(L_+S_- + L_-S_+) + (\lambda/2)(H_+L_- + H_-L_+))$$

$$\times P_n((\lambda/2)(L_+S_- + L_-S_+) + (\lambda/2)(H_+L_- + H_-L_+)) \qquad 5.26$$

Separating terms out in L_+ and L_-,

$$V_2 = \frac{-1}{E_n - E_0}\sum_{n\neq 0} P_0\left(\left(\frac{\lambda}{2}S_- + \frac{\beta}{2}H_-\right)L_+ + \left(\frac{\lambda}{2}S_+ + \frac{\beta}{2}H_+\right)L_-\right)$$

$$\times P_n\left(\left(\frac{\lambda}{2}S_- + \frac{\beta}{2}H_-\right)L_+ + \left(\frac{\lambda}{2}S_+ + \frac{\beta}{2}H_+\right)L_-\right)P_0 \qquad 5.27$$

Substituting the allowed values for P_n,

$$V_2 = \frac{-1}{E_1 - E_0}\, P_0\left(\left(\frac{\lambda}{2}S_+ + \frac{\beta}{2}H_+\right)L_-\right) P_{+1}\left(\left(\frac{\lambda}{2}S_- + \frac{\beta}{2}H_-\right)L_+\right)P_0$$

$$+ \frac{-1}{E_1 - E_0}\, P_0\left(\left(\frac{\lambda}{2}S_- + \frac{\beta}{2}H_-\right)L_+\right)P_{-1}\left(\left(\frac{\lambda}{2}S_+ + \frac{\beta}{2}H_+\right)L_-\right)P_0$$

$$= \frac{-1}{E_1 - E_0}\left(6\left(\frac{\lambda}{2}S_+ + \frac{\beta}{2}H_-\right).\left(\frac{\lambda}{2}S + \frac{\beta}{2}H_-\right) + 6\left(\frac{\lambda}{2}S_- + \frac{\beta}{2}H_-\right).\left(\frac{\lambda}{2}S_+ + \frac{\beta}{2}H_+\right)\right)$$

$$= \frac{-3}{2(E_1-E_0)}(\lambda^2(S_+S_- + S_-S_+) + \beta^2(H_+H_- + H_-H_+) + 2\lambda\beta(H_-S_+ + H_+S_-)) \quad 5.28$$

Neglecting terms in β^2 gives:

$$V_2 \simeq \frac{-3\lambda^2}{(E_1-E_0)}(S(S+1) - Sz^2)\ \frac{-3\lambda\beta}{(E_1-E_0)}(H_-S_+ + H_+S_-) \quad 5.29$$

where $(S_+S_- + S_-S_+) = 2(S(S+1)-Sz^2)$

The term in S(S+1) shifts the levels as a whole by a constant amount, so will be neglected. This leads to an effective spin Hamiltonian $\mathcal{H}_{eff}$ (i.e. an Hamiltonian which represents the deviation of the g-factor from the spin-only value due to spin-orbit interaction, and the zero-field splitting from the lifting of the spin degeneracy caused by both the spin-orbit coupling and the non-cubic components of the crystalline electric field. The effective Hamiltonian represents this scheme as if the effects arose merely from the components of the ionic spin interactions):

$$\mathcal{H}_{eff} \simeq 2\beta H.S + \frac{3\lambda^2 Sz^2}{(E_1-E_0)} - \frac{3\lambda\beta}{(E_1-E_0)} \cdot (H_-S_+ + H_+S_-) \quad 5.30$$

In zero field the field-indpendent term produces an energy level scheme with $|0\rangle$ below $|\pm1\rangle$ which is below $|\pm2\rangle$. The field terms shift the singlet up or down and split the doublets to some extent, and lead to effective g-values as follows:

Rewriting the last term in equation 5.30 as

$\frac{-3\lambda\beta}{(E_1-E_0)} \cdot 2(H_xS_x + H_yS_y)$ and substituting the Cartesian parameters for H and S in the first term gives:

$$\mathcal{H}_{eff} = \beta(g_xH_xS_x + g_yH_yS_y + g_zH_zS_z) \quad 5.31$$

where: $g_z = 2$ 5.32

and $g_x = g_y = 2(1-(3\lambda)/(E_1-E_0))$ 5.33

Now, for all $E_1-E_0 > 0$, the ratio of equations 5.32 and 5.33 result in $g_{\parallel}/g_{\perp} > 1$ where $g_{\parallel}$ is the value along the z direction and $g_{\perp}$ in the x, y directions. This is only observed for the high temperature results of ZnCr.

(ii) $|\pm 1\rangle$ state lowest

It is convenient to introduce a fictitious effective orbit T (=½) to describe this doublet (Bates et al., 1968). The P_0 now refer to the $|\pm 1\rangle$ states with $|M_+ = +\tfrac{1}{2}\rangle = |+1\rangle$ and $|M_- = -\tfrac{1}{2}\rangle = |-1\rangle$. To first order,

$$V_1 = P_0(\lambda L.S + \beta H.(L+2S))P_0 \quad \text{as before (equation 5.24)}$$

The only non-zero matrix elements will be the terms in $P_0 L_z P_0$, which results in :1

$$V_1 = 2\beta H.S + 2\lambda Sz.Tz + 2\beta Hz.Tz \qquad 5.34$$

Equation 5.32 shows that orbital angular momentum terms are now included, thus making it unecessary to go to second order to produce a crystal field splitting (and thus resulting in this case, in an anisotropy). The term in S_Z, T_Z gives five doublets, viz :-

$$\begin{array}{l} -2, -\tfrac{1}{2} \;;\; 2, +\tfrac{1}{2} \\ -1, -\tfrac{1}{2} \;;\; 1, +\tfrac{1}{2} \\ \;\;0, -\tfrac{1}{2} \;;\; 0, +\tfrac{1}{2} \\ \;\;1, -\tfrac{1}{2} \;;\; -1, +\tfrac{1}{2} \\ \;\;2, -\tfrac{1}{2} \;;\; -2, +\tfrac{1}{2} \end{array} \qquad 5.35$$

For the magnetic field parallel to the c-axis, the energy levels between these doublets are derived thus :-

$$\pm 2;\ \pm \tfrac{1}{2} \quad \text{——} \quad E\ (+2;\ +\tfrac{1}{2}) = 2\beta H.(2+\tfrac{1}{2}) = 5\beta H = E_+$$

$$\text{and} \quad E\ (-2;\ -\tfrac{1}{2}) = 2\beta H.(-2-\tfrac{1}{2}) = -5\beta H = E_-$$

$$\therefore \quad \Delta E = E_+ - E_- = 10\beta H$$

$$\text{As} \quad \Delta E = g_{\parallel}\beta H,\ g = 10$$

similarly,

$$\pm 1;\ \pm\tfrac{1}{2} \longrightarrow g_{\parallel} = 6$$

$$\pm 0;\ \pm\tfrac{1}{2} \longrightarrow g_{\parallel} = 2$$

$$\pm 1;\ \mp\tfrac{1}{2} \longrightarrow g_{\parallel} = 2$$

$$\pm 2;\ \mp\tfrac{1}{2} \longrightarrow g_{\parallel} = 6$$

Because the two states in the doublet are not connected by $(H_+S_- + H_-S_+)$ in equation 5.34, there is no term in x and y, therefore giving $g_\perp = 0$. Thus infinite anisotropy is predicted here.

(iii) $|\pm 2\rangle$ state lowest

Preceeding similarly to (ii), where the P_0 operators refer to the ± 2 orbital the first order effects are :

$$V_1 = P_0(\lambda L.S + \beta H.(L+2S))P_0$$

and again the only non-zero matrix elements are in P_0LzP_0, thus

$$V_1 = 2\beta H.S + 4\lambda Sz.Tz + 4\beta HzTz \qquad 5.36$$

The five doublets now become:

$$\begin{array}{l} -2, +1\ ;\ 2, -1 \\ -1, +1\ ;\ 1, -1 \\ \ 0, +1\ ;\ 0, -1 \\ \ 1, +1\ ;\ -1, -1 \\ -2, +1\ ;\ -2, -1 \end{array} \qquad 5.37$$

which leads to $g_{\parallel} = 12$ for the $\pm 2;\ \pm 1$ states

$g_{\parallel} = 8$ for the $\pm 1;\ \pm 1$ "

$g_{\parallel} = 4$ for the $0;\ \pm 1$ "

$g_{\parallel} = 0$ for the $\pm 1;\ \mp 1$ "

$g_{\parallel} = 4$ for the $\pm 2;\ \mp 1$ "

and $g_\perp = 0$ as before.

Again infinite anisotropy is predicted.

Cases (ii) and (iii) are not taken to second order because this would only reduce the infinite anisotropy and not give $g_\perp > g_\parallel$ as is found for ZnCr (Chapter 4).

Conduction electrons play an important role at low temperatures (of the order of T_K) where a spin condensation about the impurity ion appears to build up. Scalapino (1966) amongst others has calculated the susceptibility using a perturbation approach to include this effect. His expression, correct to all orders, may be written:

$$\Delta\chi = R(1 - 1/\ln(T/T_K)) \qquad 5.38$$

where $R = g^2 \mu_B^2 S(S+1)/3kT$

To see if it is possible for equation 5.38 to follow the experimental results the substitution $T_K = 0.11K$ is made. This is derived from the approximation $\theta/4.5 = T_K$ (Heeger, 1969) which should be valid in the range $7 < T/T_K < 100$ to better than ½% accuracy. This value of T_K refers to the value of $\theta_\perp$ (~0.5 K) from table 4.3 and a similar substitution of $\theta_\parallel$ (~0.4 K) predicts an anisotropy of ~0.98 for $\Delta\chi_\perp/\Delta\chi_\parallel$ at 4.2 K. At T = 50K, $\Delta\chi_\perp/\Delta\chi_\parallel \simeq 0.99$, with a virtually isotropic result at T = 500 K. Thus at low temperatures only ~2% anisotropy is predicted from the experimentally verifiable 25% change in θ and even then it is found $\Delta\chi_\perp < \Delta\chi_\parallel$, in disagreement with the experimental results.

5.3. Discussion

Simple crystal field theory predicts that the orbital singlet state $|\pm 1\rangle$ is the ground state energy level of ZnCr before spin-orbit coupling is included. Considering the assumptions made in this rather unrealistic picture, this result must be regarded only as an estimate of the actual lowest orbital level, so the calculations are not presented in detail or made to

conform with standard crystal field theory terminology in all cases. Extending the theory to include spin orbit coupling allows the anisotropy of ZnCr to be decided for each of the three possible states being lowest viz:

(i) $|0\rangle$ lowest

To second order $g_{\parallel}/g_{\perp} \geq 1$ and as $(g_{\parallel}/g_{\perp})^2 \propto \Delta\chi_{\parallel}/\Delta\chi_{\perp}$ $\Delta\chi_{\parallel} \geq \Delta\chi_{\perp}$ is predicted.

(ii) $|\pm 1\rangle$, $|\pm 2\rangle$ lowest

In both these cases $g_{\parallel}/g_{\perp} \rightarrow \infty$ so $(\Delta\chi_{\parallel}/\Delta\chi_{\perp}) \rightarrow \infty$.

The results presented on ZnCr in Chapter 4 show that $g_{\parallel}/g_{\perp} < 1$ up to ~50 K and > 1 for 50 K $< T <$ ~480K. Therefore if the $|0\rangle$ state is lowest, only the high temperature results are predicted, though the detailed form of the anisotropy cannot be followed. In general it would appear that simple crystal field theory cannot explain the ZnCr results.

Allowing T_K to change in equation 5.38 is equivalent to an anisotropic exchange, i.e. $kT_K = D\exp(-1/J|d_s)$ where D = host conduction bandwidth (9.39 eV for Zn). The approximations used are valid only for low temperatures yet the resultant anisotropy is the opposite to that found experimentally. At high temperatures ($T > 50$ K) where it is found that $\Delta\chi_{\parallel} > \Delta\chi_{\perp}$, equation 5.38 produces a closely isotropic result. It is evident that only artificial manipulation of Jd_s will enable the experimental results to be followed though this would have a much larger effect on than has been seen, e.g. a change of 10% in Jd_s at 4.2K will produce typically a 50% change in θ. Clearly equation 5.38 is inadequate to explain the ZnCr results.

References

Abragam,A., Bleaney,B., Eletron Paramagnetic Resonance of Transition Ions (Clarandon Press, Oxford). 1970

Bates,C.A., Dixon,J.M., Fletcher,J.R., Stevens,K.W.H., J. Phys. C. 1, 863, 1968

Elliott,R.J., Stevens,K.W.H., Proc. Roy. Soc. A218, 553, 1953

Freeman,A.J., Watson,R.E., Phys. Rev. 127, 2058, 1962

Heeger, A.J., Sol. Stat. Phys. 23, 283, 1969
(ed.Seitz,Turnbull,Ehrenreich. Academic Press.

Hirst, L.L., Zeit. Physik. 241, 9, 1971

Hutchings, M.T., Sol. Stat. Phys. 16, 227, 1965

Kasuya, T., Magnetism II B
(ed. Rado and Suhl) 1963

Kittel, C., Introduction to Solid State Physics, 4th edition (Wiley) 1973

Krupicka,A., Sternberk,J., Elements of Theoretical Magnetism (Illife) 1968

Lea,K.R., Leask,M.J.M.,Wolf,W.P., J. Phys. Chem. Colids 23, 1381 1962

Li, P.L., et. al, Phys. Rev. Lett. 31, 29 1973

Martin, D., Magnetism in Solids
(Illife) 1967

Orton, J.W., Electron Paramagnetic Resonance
(Illife) 1968

Park, D., Introduction to Quantum Mechanics (McGraw-Hill) 1964

Press,M.J., Hedgcock,F.T., Phys. Rev. Lett. 23, 167, 1969

Scalapino, D.J., Phys. Rev. Lett. 16, 937, 1966

Stevens, K.W.H., Proc.Phys.Soc. (London) A65, 209,1952

White, R.M., Quantum Theory of Magnetism
(McGraw-Hill) 1970

CHAPTER 6

GALLIUM ALLOY RESULTS

6.1. Susceptibility

6.1.1. Introduction

It is well known that the 3d transition metals alloyed with aluminium as a host do not possess localised magnetic moments (Flynn et al., 1967) and one would therefore expect the same for gallium as it has a virtually identical density of states and electron densities as aluminium. However, Wachtel and Nier (1965) showed that manganese in gallium did produce a moment, though they used rather high impurity concentrations (~6 at.%). Thus the susceptibility of more dilute alloys of GaMn was measured to resolve this point. Ford (1972) measured GaMn and GaCr and his work was repeated and confirmed for the Ga-3d metal alloys.

It was hoped to gain some insight into how seemingly similar hosts could give different results on alloying with the same impurities, and to obtain a value for the exchange interaction J and Coulomb interaction U.

6.1.2. Results

Figure 6.1 shows the paramagnetic susceptibility of pure gallium which was accurately measured and extended above Ford's results (1972) to a temperature of 1258K, linear behaviour being observed within the experimental error throughout the temperature range. All the metals used were 99.999% pure from Johnson Matthey or Koch-Light, except for titanium and vanadium, which were both 99.9% pure. Figure 6.2 shows the effect on the susceptibility (at 1173K) of dissolving small amounts of the 3d transition metals in gallium. As can be seen, figure 6.2 is linear for all the alloys showing that all of the impurity metal was in solution. Difficulties arose in the systems GaTi, GaV and GaCo where prolonged heat treatment was found to be necessary to dissolve even small amounts of impurity in

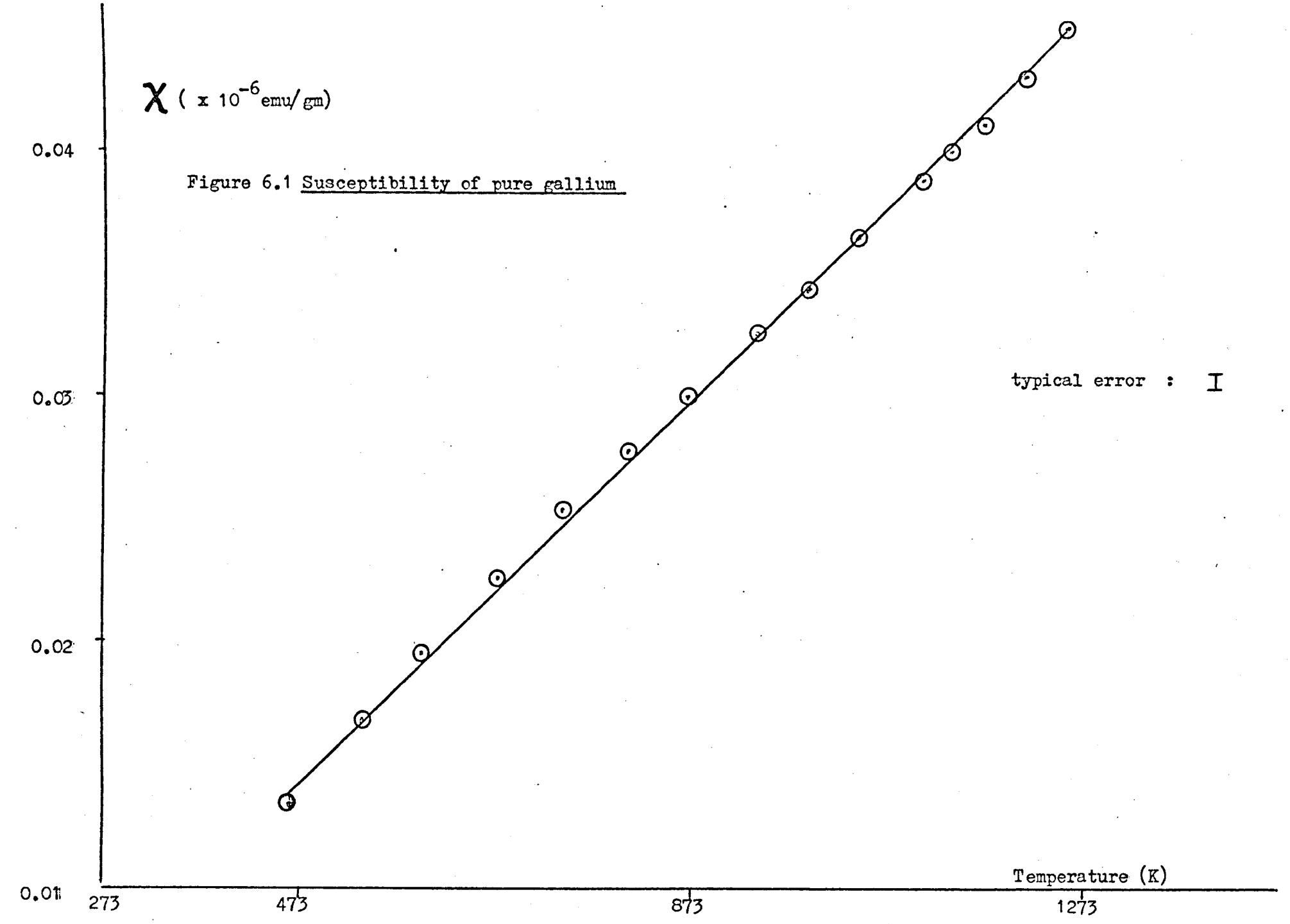

Figure 6.1 Susceptibility of pure gallium

Figure 6.2 Incremental susceptibility of 3d transition metals alloyed in liquid gallium

(1173K)

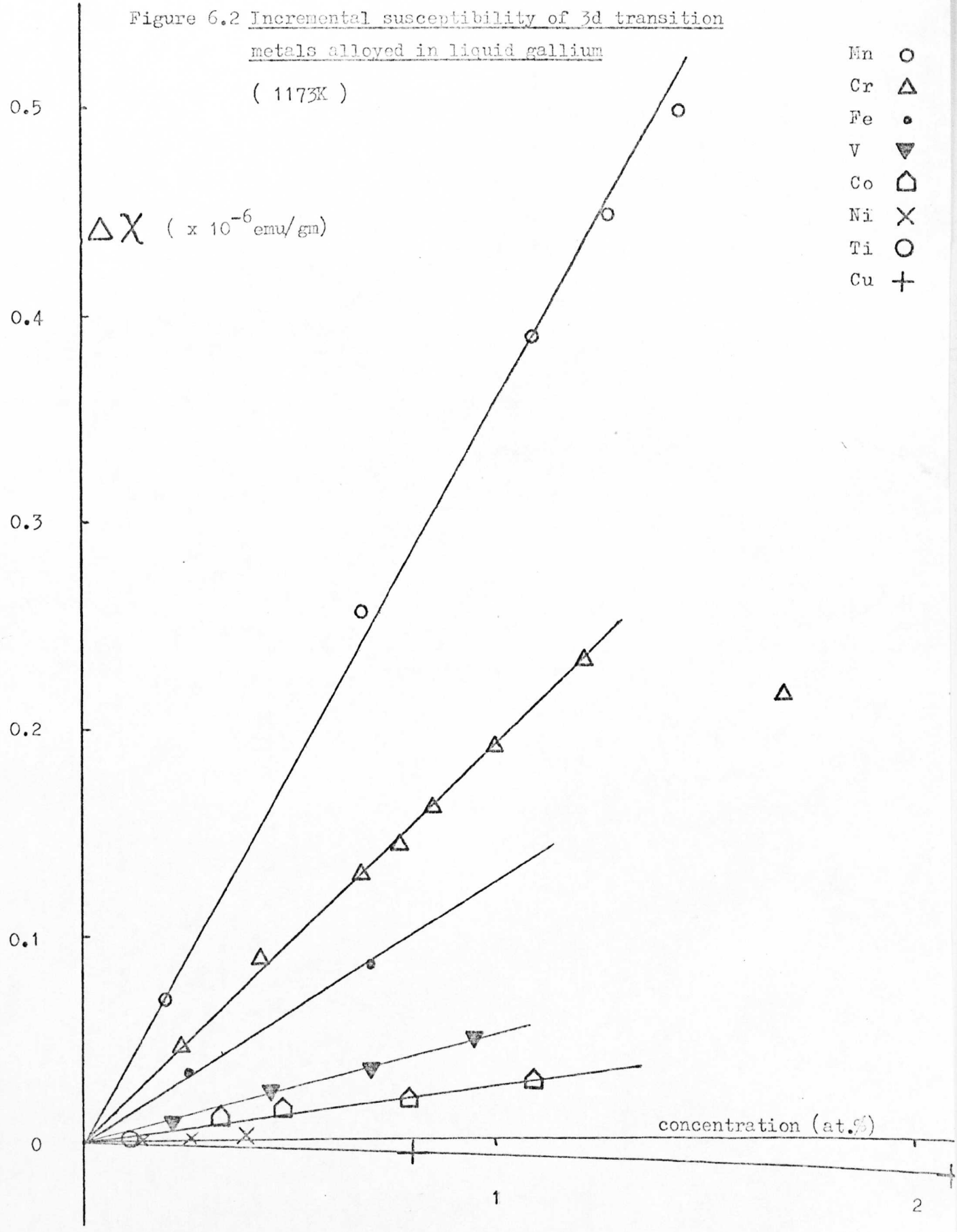

the host. (Only one sample containing 0.11% of titanium was successfully prepared; the precise value for titanium is not important, however, in the succeeding analysis). Errors in the net susceptibility normalised to one atomic per cent varied between ½% (manganese) and approximately 15% for the metals with the smallest susceptibilities (cobalt, nickel and copper). In all alloys other than GaMn and GaCr the susceptibility was found to be virtually independent of temperature; in GaMn and GaCr, however, the susceptibility increased as the temperature decreased (the change being nearly an order of magnitude greater than for the other alloys), which is usually taken to indicate a local moment. The reciprocal net susceptibility $\Delta\chi^{-1}$ was therefore plotted against temperature and this is shown in figures 6.3 and 6.4 for some of the alloys. Such a plot is linear showing that the susceptibility could be fitted to a Curie-Weiss law :-

$$\Delta\chi = \frac{Np^2_{eff}c}{3k\ (T+\theta)} \qquad 6.1$$

where $\Delta\chi$ = incremental susceptibility
N = number of impurity spins/gm.
p_{eff} = effective spin (μ_B)

consistent with local moment behaviour for both these systems. For GaMn a least squares fit to the results gave p_{eff} = $5.9\pm0.2\ \mu_B$ and $\theta = -590\pm20$K. The value of obtained for GaCr was somewhat uncertain (θ was in the range of -1000K to -4000K) and was larger than the measurement temperature so that equation 6.1 could not be simply used to deduce p_{eff}. A plot of θ against c showed that within experimental error a linear relationship approximately held, a positive slope of -2600K/at % being obtained, though the uncertainties of the results for this borderline alloy (see table 6.2) do not make it worthwhile to pursue the ramifications of a concentration-dependent model for GaCr, especially as one cannot analyse it in terms of a simple Curie-Weiss like law, although a restricted analysis using a different method (Schotte and Schotte, 1971) is possible (section 6.1.4). Measurements on some of

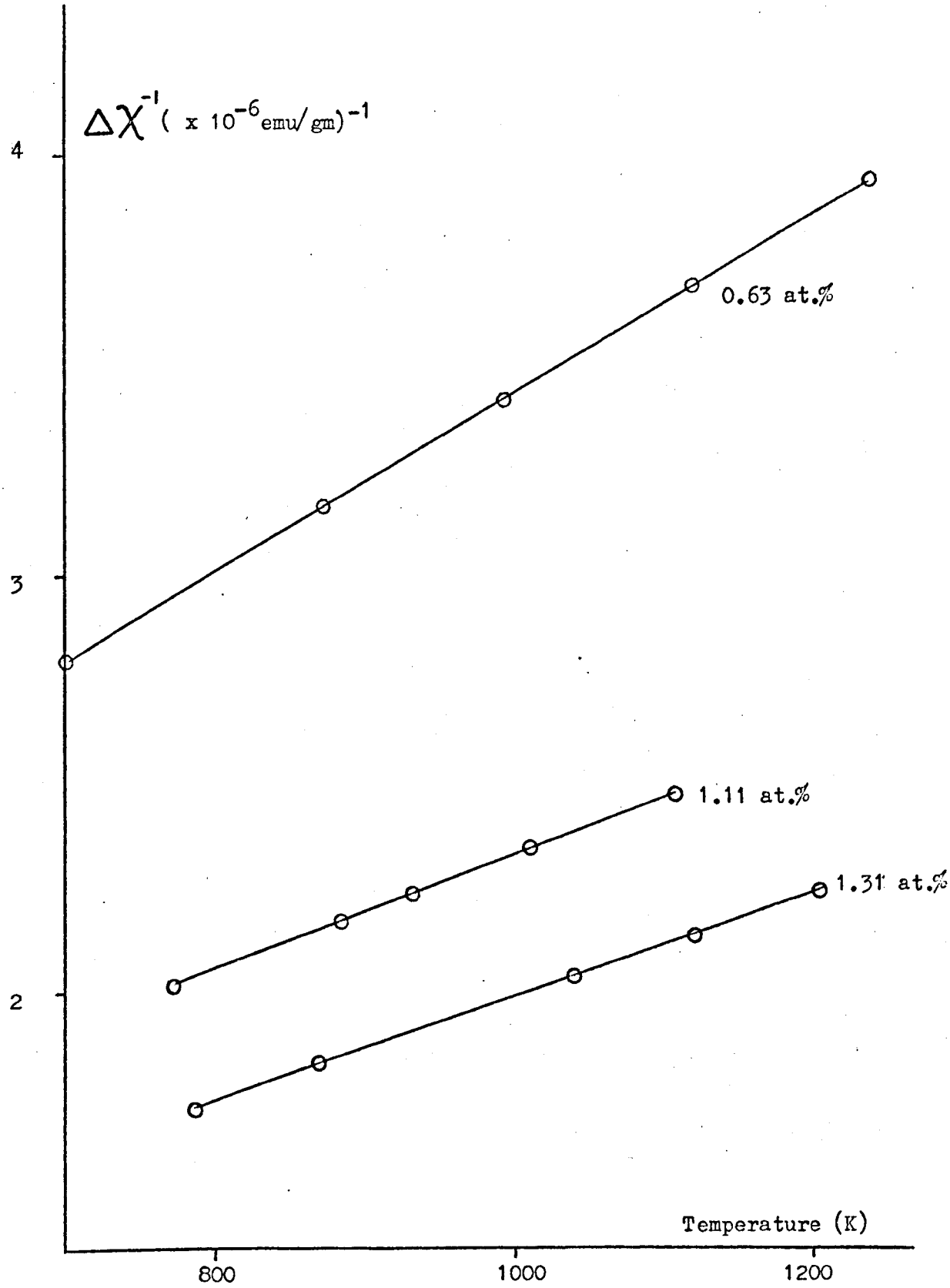

Figure 6.3 Reciprocal net susceptibility of some liquid GaMn alloys

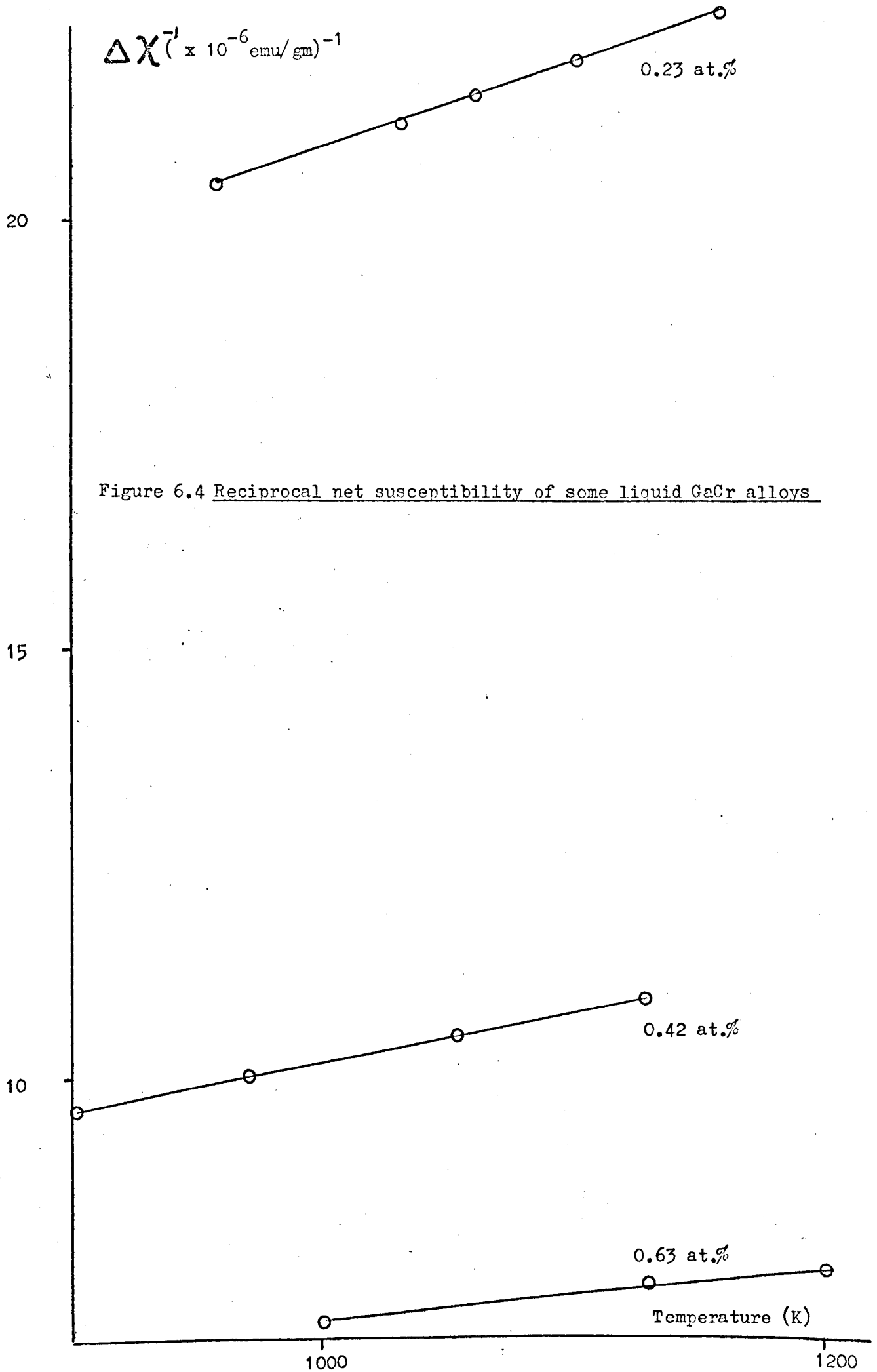

Figure 6.4 Reciprocal net susceptibility of some liquid GaCr alloys

the 3d impurities in gallium obtained in a similar manner have been reported by Peters et al., (1972). The results are in excellent agreement, except for manganese (see table 6.1 below).

TABLE 6.1 Comparison of additional susceptibilities of 3d metals in gallium from Peters et al (1972) with present work.

$\Delta\chi \times 10^{-6}$ emu/gm for 1 at.% impurity at 1373K		
	PETERS ET AL.	PRESENT WORK (extrapolated to 1373K)
Ti	---- ±0.01	0.02 ±0.01
V	0.07	0.06
Cr	0.19	0.19
Mn	0.28	0.38
Fe	0.13	0.14
Co	0.04	0.03
Ni	----	0.01(4)
Cu	----	-0.02

6.1.3. Analysis

Figure 6.5 shows the susceptibility per gram of the 3d transition metal impurities in gallium at 1173K and also the susceptibilities measured by Flynn et al. (1967) for aluminium alloys at a similar temperature. It is clear that all the impurities in gallium are considerably more magnetic than in aluminium, even though gallium and aluminium have

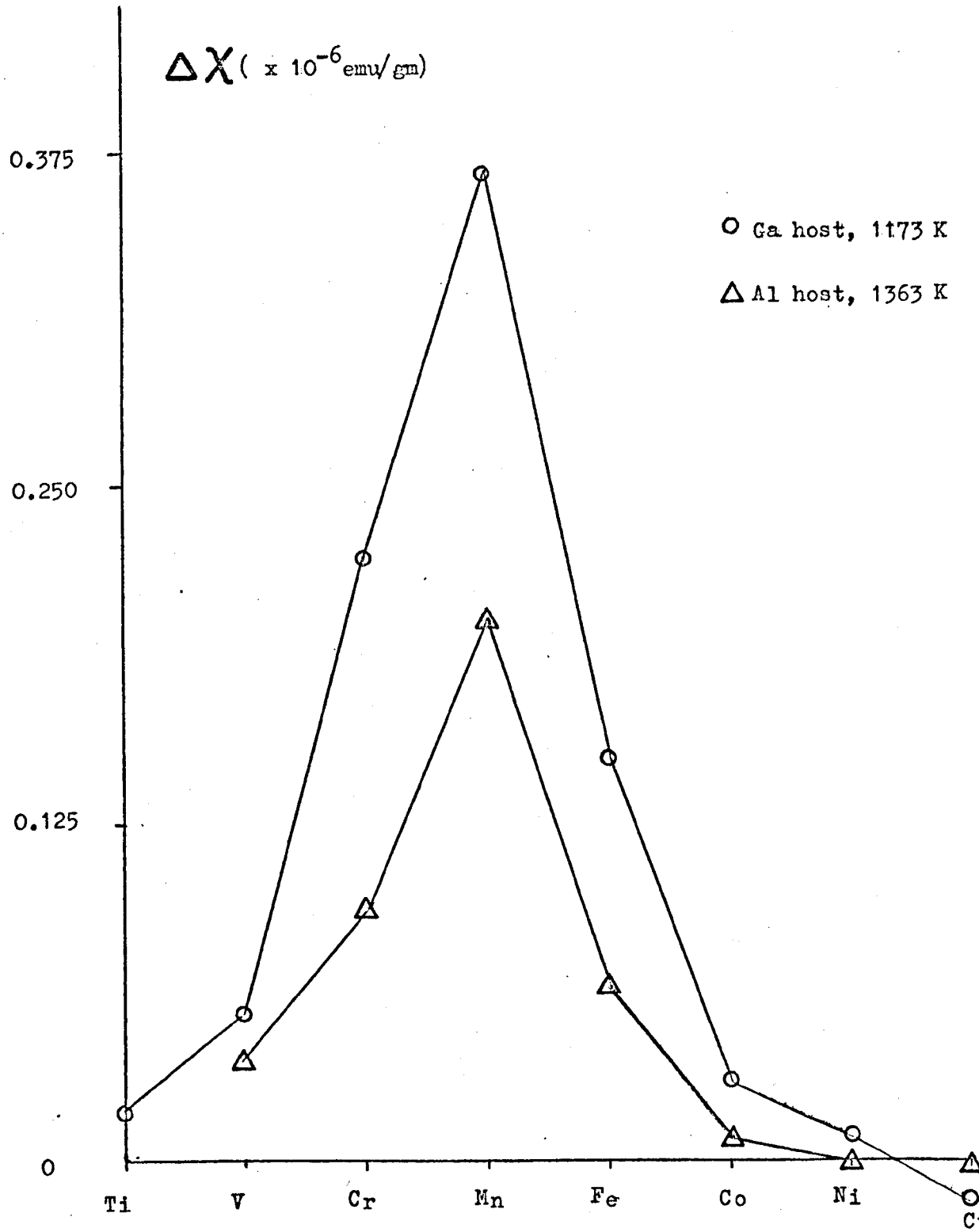

Figure 6.5 Incrmental susceptibility of 3d transition metals in liquid gallium and aluminium

the same electron density and almost certainly the same density of states in the liquid. The 3d metals in aluminium are not magnetic in a Curie-Weiss sense, and in this regime the susceptibility for both spin (χ_d) and orbital (χ_{orb}) contributions are given by (Dworin and Narath, 1970) :-

$$\chi_d = \frac{2d_d\mu_B^2}{1 - \frac{1}{5}(U+5J)\, d_d} \qquad 6.2$$

$$\chi_{orb} = \frac{4d_d\mu_B^2}{1 - \frac{1}{5}(U-J)\, d_d} \qquad 6.3$$

where ^{d}d is the impurity density of states per spin at the Fermi surface. (Dworin and Narath used a slightly modified version of Anderson's Hamiltonian to obtain full rotational invariance, consequently their interaction parameters, U and J, are slightly different from his. Putting $U = \bar{U} - \frac{1}{6}\bar{J}$ and $J = \frac{5}{6}\bar{J}$ gives the conventional $(\bar{U} + 4\bar{J})$ in the spin enhancement factor). In this model the difference in behaviour in the two hosts must arise from the different admixture interactions (V) leading to a different impurity density of states, viz :-

$\Delta = \pi d_d |V_{sd}|^2_{av}$ where the average is over the conduction electron states at the Fermi surface and Δ is the virtual d level width (Daybell & Steyert, 1968).

We are unable to determine the values of the parameters in equations 6.2 and 6.3 from total susceptibility measurements on the two systems since we have essentially two equations with four unknowns. However, the Knight shift of the impurity nucleus is related to the susceptibility by the hyperfine field H_{hfs}, by :-

$$K_{(i)} = \frac{H^{(i)}_{hfs}\, \chi_{(i)}}{B} \qquad 6.4$$

where (i) refers to spin or orbit contributions. Dworin et al., (1970) have shown that in an alloy the spin and orbital hyperfine mechanisms separately obey Korringa-like relations so that if both the Knight shift and relaxation time of the impurity are known then it is possible to determine the spin and orbital contribution to the Knight shift. (The direct s contact shift is less than about 0.1% an order of magnitude less than the experimentally observed shift, and can usually be ignored.) The orbital hyperfine field does not seem to depend strongly upon the nuclear surroundings (Yafet et al., 1964) so that a good estimate of the susceptibility can be made from the Knight shift. The Knight shift and relaxation time of ^{55}Mn in aluminium has been measured by Narath et al. (1969) and by Alloul et.al. (1971). Taking the weighted average of their Knight shifts (-2.03%) and relaxation times (19.7ms K), and assuming the s contribution to the shift is +0.07% from the measurement s of ^{63}Cu in aluminium of Blodgett et al. (1969), we find K_{orb} = +1.13% and K_d=-3.23%. These values are different from those deduced by Narath et al. (1969) and that of Narath (1972) who made a numerical error. From equation 6.4, taking H_{hfs}^{orb} as 390 kG (Freeman et al., 1965) the orbital susceptibility of manganese in aluminium is (2.3 $\pm$ 0.1) x 10^{-6} emu/gm. A combination of equations 6.2 and 6.3 results in :

$$\bar{J} = 2\mu_B^2\left(\frac{2}{\chi_{orb}} - \frac{1}{\chi_d}\right) \qquad 6.5$$

so that J can be determined from a knowledge of χ_{orb} and the total susceptibility. For manganese in aluminium we find J = 0.61 $\pm$ 0.05 eV (for an H_{hfs}^{orb} of 390 kG). ($\bar{J}$ = 0.74 $\pm$ 0.06 eV). These values assume that equation 6.5 still holds for an impurity as near to being magnetic as manganese in aluminium. A physically reasonable choice of U + 5J consistent with the above value of J ranges from about 4 eV (U = 1.0 eV) to perhaps 10 eV (U = 7.0 eV). Equations 6.2 and 6.3 are not necessarily valid for manganese in gallium because this system is magnetic so that even if the Knight shift and relaxation

times were known, we would be unable to unequivocably determine U and J.

The total susceptibility of the aluminium alloys was put equal to equation 6.2 plus 6.3 assuming a particular value of U such that U + 5J = 5 eV and also that U and J are independent of the impurity. Thus a value of d_d for 3d impurities in aluminium was found. The suceptibility of iron in gallium was used to calculate d_d for this system (as it has the largest susceptibility without being magnetic) using the same U and J. It is expected that the values for U and J for a given impurity will not be altered on changing the host from aluminium to gallium because of the similarity of electron density in the two hosts. The difference between the two systems are expected to be solely due to a change in V and hence d_d. Therefore all the d_d's for the Al-3d metals were multiplied by the ratio of iron in gallium to d_d for iron in aluminium and the resulting susceptibilities calculated. The results are, in fact, practically independent of the initial choice of U, changing by less than 5% if U changes by a factor of 7, and are shown on table 6.2 together with the experimental susceptibilities. It can be seen that the agreement is excellent since the analysis predicts that both manganese and chromium will be magnetic in gallium as observed and gives good quantitative agreement with the measured susceptibility of vanadium in gallium. No values for the experimental susceptibilities for GaMn and GaCr can be predicted as the analysis is not valid for these systems.

d_d for a particular choice of U (1.9 eV) is given in table 6.2 since it allows the relative values to be easily compared. For this choice of U the magnetic/nonmagnetic boundary occurs when d_d equals units. While manganese in aluminium is close to the HF boundary with a spin enhancement factor of about 16, chromium in gallium appears to be even closer with a density of states which is 2% to 3% greater than the magnetic limit for any reasonable value of U. (Further evidence for this analysis is that it correctly predicts when manganese in Ga-Al alloys changes from being magnetic, i.e. Curie-Weiss susceptibility,

TABLE 6.2

The theoretical susceptibilities for impurities in gallium compared with the experimental values. The density of states shown is for a particular U + 5J of 5 eV chosen since a d_d of unity marks the H-F boundary. The theoretically deduced susceptibilities including the predictions of magnetic behaviour for GaCr and GaMn are practically independent of the choice of U + 5J. The densities of states shown in brackets for GaTi, GaCo and GaNi are those deduced from the experimental susceptibilities. These are felt to be more likely than the ones deduced from the somewhat uncertain susceptibility values of aluminium alloys in these cases.

	Al.			Ga.			
	$\Delta\chi$ expt (F) ($\times 10^{-4}$ emu/gm)	d_d (eV^{-1})	T_{sf} (K)	$\Delta\chi$ exp ($\times 10^{-4}$ emu/gm)	d_d (eV^{-1})	$\Delta\chi$ th ($\times 10^{-4}$ emu/gm)	T_{sf} (K)
Ti	-	--	--	1.9 ± 0.3	(0.48)	-	---
V	3.6	0.69	8300	5.5 ± 0.3	0.81	5.6	4500
Cr	8.9	0.88	2500	mag	1.03	mag	--
Mn	16.0	0.94	1200	mag	1.11	mag	170***
Fe	5.4	0.79	4800	13.9 ± 0.4	0.93	13.9*	1450
Co	1.2	0.35	--	3.4 ± 0.4	0.41 (0.68)	1.5**	8800
Ni	0.7	0.21	--	1.4 ± 0.2	0.24 (0.39	0.8**	--

* fitted from d_d(GaFe)/d_d(AlFe)

** derived from the very uncertain $\Delta\chi$expt for these impurities in aluminium

*** θ = -590 K

(F) from Flynn et al. (1967)

to nonmagnetic, i.e. temperature independent susceptibility (Dupree and Nellist to be submitted for publication). The density of states of the 3d impurities forms a smooth curve, with a peak between chromium and manganese, if plotted through the series. The experimentally deduced values of d_d for cobalt, nickel and titanium in gallium (shown in brackets in table 6.2) lie on this curve.

6.1.4. Discussion

Although no satisfactory solution of the transition from magnetic to nonmagnetic behaviour exists at present, the concept of localised spin fluctuations has been introduced to explain the properties of nearly magnetic alloys. In this model the magnetic properties are due to spin fluctuations with a characteristic lifetime $\tau_{sf} = h/kT_{sf}$ where T_{sf} is known as the spin fluctuation temperature. In the unrenormalized version of the theory (Rivier et al., 1968) τ_{sf} becomes infinite ($T_{sf} \longrightarrow 0$) at the HF magnetic boundary. In all the renormalized versions however (e.g. Zuckermann, 1970) τ_{sf} remains finite and it has been conjectured that in the magnetic region T_{sf} may be equal to T_K, the Kondo temperature. The zero temperature susceptibility is related to the spin fluctuation temperature by (Caroli et al. 1969) :-

$$T_{sf} = \frac{10\ \mu_B^2}{\pi k\ \chi_d} \qquad 6.6$$

and the values of T_{sf} deduced in this way are shown in Table 6.2. The values shown here for liquid aluminium as host are somewhat larger (by about a factor of 2) than the values deduced from other properties in the solid. Part of this difference could well be due to a change in the density of states of aluminium on melting since even a small change would affect Δ and hence d_d. A high Curie-Weiss θ ($\sim$ 300K) has been obtained for AuV alloys by Kume (1967) and by Van Dam et al. (1972) over the temperature range 20-300K and this is similar to the T_K deduced from other properties for this alloy. The latter authors also found that the characteristic spin fluctuation temperature deduced from equation 6.6 for this system was 280K so that for AuV alloys the two characteristic temperatures appear very similar. This is not the case for GaMn alloys since θ is 590K and T_{sf} must be less than 240K (from our lowest high temperature susceptibility) and greater than 170K (obtained by extrapolating the susceptibility to 0 K). The Curie-

Weiss θ for GaMn is comparable with the T_{sf} reported for solid AlMn for which the temperature dependence of the susceptibility is very small.

There is no doubt that the localised spin fluctuation models are a necessary part of the theoretical explanation of the formation of local moments which are close to the instability limit. They have various shortcomings, the major ones being that they only descibe the non-magnetic Hartree-Fock regime and are suitable for small fluctuations only (Peters et al., 1972). It is not possible to explain, for example, the "classic" Kondo system of CuFe (Tholence et al., 1970) on this model when account is taken of the neutron-scattering experiments by Stassis et al. (1968) because they have shown that the form factor of iron in copper is temperature - independent down to 4K and that the bulk susceptibility is due entirely to the magnetisation of the atomic-like local moments - a result difficult to reconcile with fluctuations of spin density. Thus the CuFe system shows that the iron local moment is firmly magnetic (at least to 4K) and must be described in a Friedel-Anderson sense.

Despite the closeness of GaMn to the H-F boundary manganese still has the full moment for spin $S = \frac{5}{2}$ and this strongly implies that $U/\Delta > 1$ (see for example, Heeger, 1969). The value of U must therefore be consistent with this and with the value of J obtained earlier. A lower estimate of the virtual state width can be obtained assuming that the virtual level is close to the Fermi level from the smallest consistent value of $U + 5J$. The smallest value of U for which $U > \Delta$ and $U > J$ is about 1.5 eV, that is, $U + 5J > 4.5$ eV and so Δ for GaMn is greater than 1.4 eV. The lower density of state for these impurities in aluminium gives a Δ for this system of greater than 1.6 eV.

From the preceding analysis GaCr is expected to be closest of all the systems to the HF boundary and one might expect a still higher characteristic temperature for this system. The measurements do in fact give rather large values for θ but because of the small ($\lesssim$ 2%) change in susceptibility over the temperature range measured and also because one is subtracting the host susceptibility which is also weakly temperature dependent, the value of θ is very uncertain. Values for θ of - (1000-4000)K have been obtained with the lowest concentration alloys consistently giving the smallest θ indicating a possible concentration dependence. Such concentration effects are well known in solid dilute alloy systems (see e.g. Van Dam et al., 1972). Tamaki (1), (1968) has observed similar effects for chromium in liquid antimony and presents results that indicate P_{eff} is independent of c below ~2 at %, whilst θ varies approximately linearly up to the highest concentration measured : ~8 at. %. Since the measurement temperature in the GaCr system is below the Curie-Weiss θ , the value of p_{eff} deduced using equation 6.1 is not meaningful. However, a recent calculation of the magnetic behaviour of dilute alloys (Schotte and Schotte, 1971) shows that the susceptibility will be accurately Curie-Weiss like both above and below θ , providing the temperature range is not too large (less than a factor of 2). Analysis of their equation shows that the true p_{eff} can be deduced provided the ratio of θ to the mean measured temperature is known. The uncertainty in the magnetic moment calculated using the Schottes' result is much less than the uncertainty in θ and P_{eff} for GaCr is found to be (4.2 $\pm$ 0.3) μ_B, slightly less than the free spin moment.

6.1.5. Conclusion

The density of states of the 3d impurities in aluminium was found from the experimental susceptibility results after

substitution of reasonable values for the parameters U + 5J. In a similar manner the value of d_d for GaFe was found and a comparison with that of AlFe made. This was done because a) the analysis was valid for both alloys, and b) they have the largest susceptibility excluding those containing manganese and chromium (which are magnetic in gallium). Because of the assumption that U and J are independent of impurity and are expected to be the same in both hosts, the value of d_d for impurities in gallium was derived from multiplying d_d for the equivalent impurity in aluminium by the ratio of d_d for GaFe to d_d for AlFe. Thus the correct prediction of magnetic behaviour for GaCr and GaMn was obtained where d_d was 1.03 and 1.11 eV^{-1} respectively, and excellent agreement was obtained for the derived susceptibility of GaV. For cobalt and nickel where the agreement is poor it is likely that the experimental values of the suceptibility for these elements in aluminium are in error since the relative density of states is much less for cobalt than would be expected from the trend of d_d through the transition series. The assumptions of U and J remaining constant for differing impurities in such similar hosts as gallium and aluminium is borne out by the success of the analysis and the fact that by taking an experimentally-derived value for J leaves the results unchanged by $< 5\%$ even when U is changed by a factor of 7. The change in going from aluminium to gallium is signified by the change in d_d in taking AlCr and AlMn from below the non-magnetic/magnetic limit to above it (where $d_d > 1$) for GaCr and GaMn. This may be due to the quadratic dependence of d_d on V, i.e. $d_d \propto \Delta . |V|^{-2}$.

The results indicate that GaMn is strongly magnetic with a P_{eff} of $(5.9 \pm 0.2)\ \mu_B$ and a large θ. It is not surprising therefore that the spin fluctuation temperature T_{sf} ($170K < T_{sf} < 280K$) for GaMn is quite different from the value for θ. J is found to be (0.61 ± 0.05) eV for AlMn with $\Delta > 1.6$ eV, and $\Delta > 1.4$ eV for GaMn.

6.2 Resistivity

6.2.1. Introduction

As it has been shown from the susceptibility results (section 6.1.2.) that manganese in gallium has a localised magnetic moment and chromium in gallium is magnetic though close to the magnetic/nonmagnetic borderline, resistivity experiments were performed (section 3.3.4.) to complement this study. Also results are presented on the alloys GaFe and GaCu, the former to show the effect on the resistivity of going across the centre (at manganese) of the 3d impurities and the latter to obtain additional information on s and p-wave scattering in determining the incremental resistivity ($\Delta\rho$) due to d-wave scattering alone.

In general, theories predict (Nagaoka, 1967, Suhl et al., 1967, Hamann, 1967, for example) that an increase in temperature leads to a decrease in $\Delta\rho/c$ from some initial value to a final temperature-independent value for local moment systems, though a large temperature range is necessary. It was hoped that GaMn, as the most magnetic of the gallium-3d series alloys, would show this behaviour via resistivity measurements.

6.2.2. Results

Figures 6.5 to 6.8 show the temperature and concentration range for impurities of chromium, manganese, iron and copper in liquid gallium. The curvature in some of the results in figures 6.5 and 6.6 are included to show how the resistivity of the alloy departs from linearity as some of the impurity comes out of solution with decreasing temperature. Most measurements in fact were taken from high temperature to low to make this effect noticeable and to be reasonably confident of the value of the concentration. The incremental resistivity for all alloys was found to vary linearly with concentration in the range investigated (figure 6.9), subject to the above considerations, giving rise to a plot of $\Delta\rho/c$ vs. impurity at a temperature of 973 K shown in

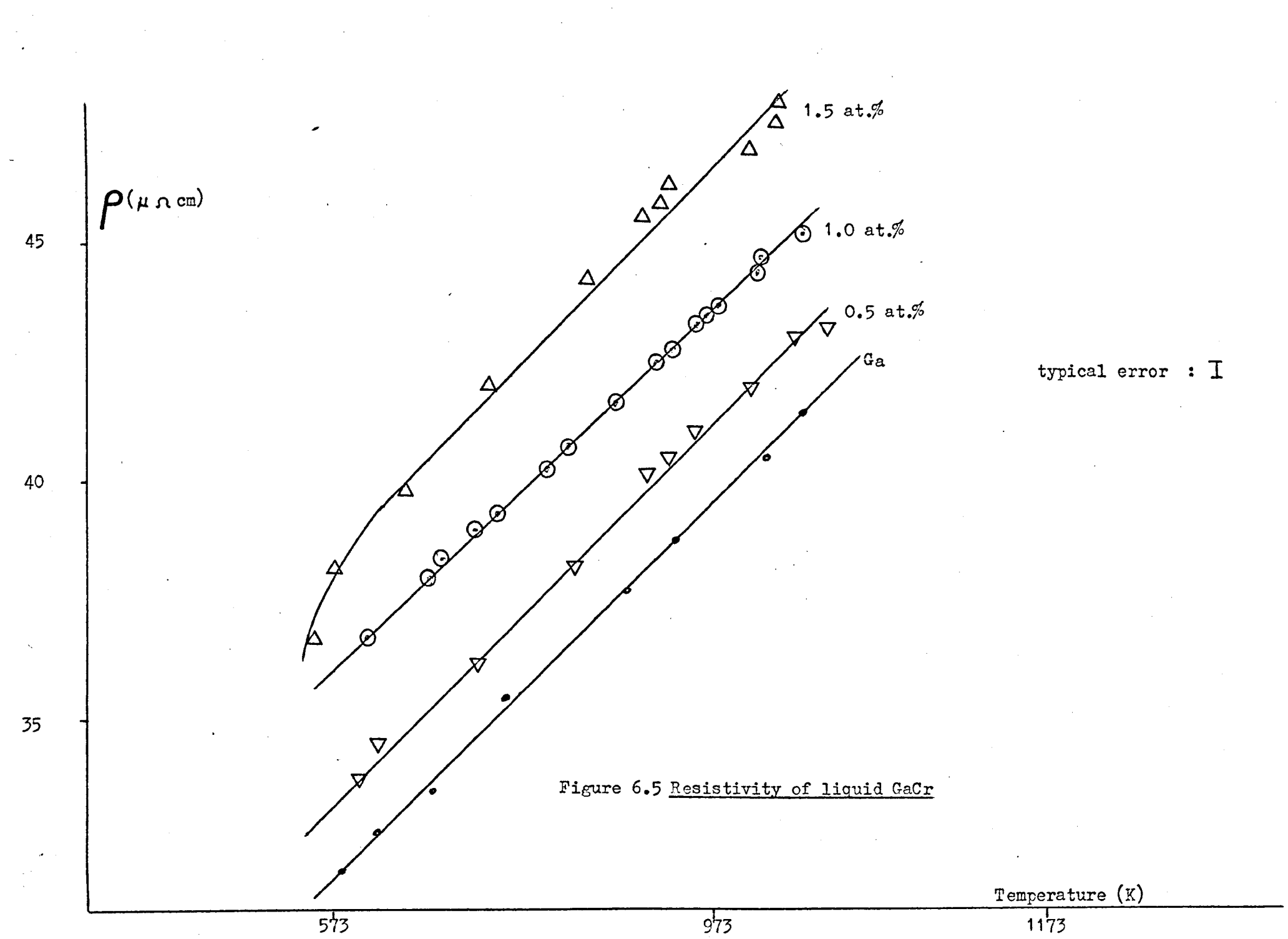

Figure 6.5 Resistivity of liquid GaCr

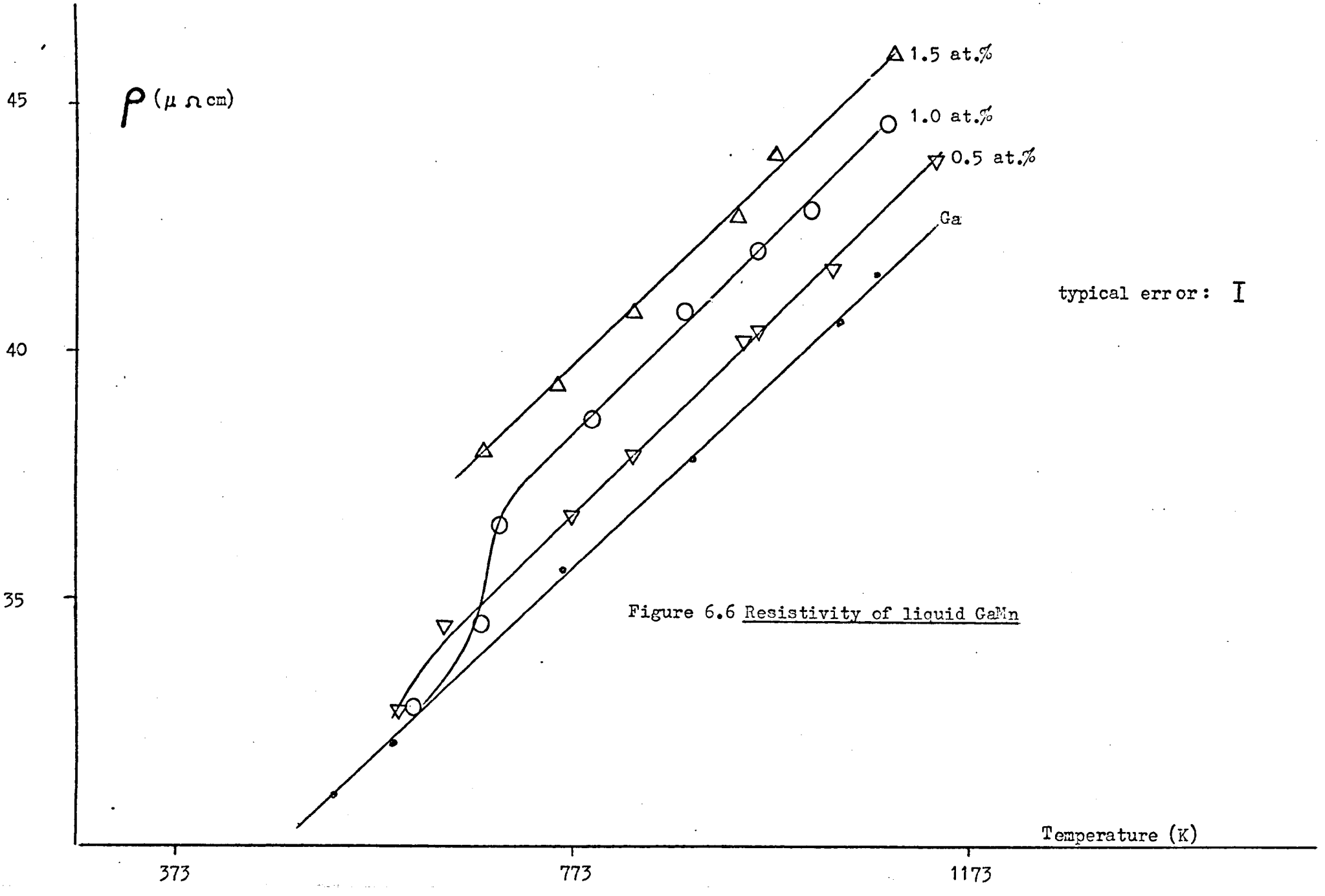

Figure 6.6 Resistivity of liquid GaMn

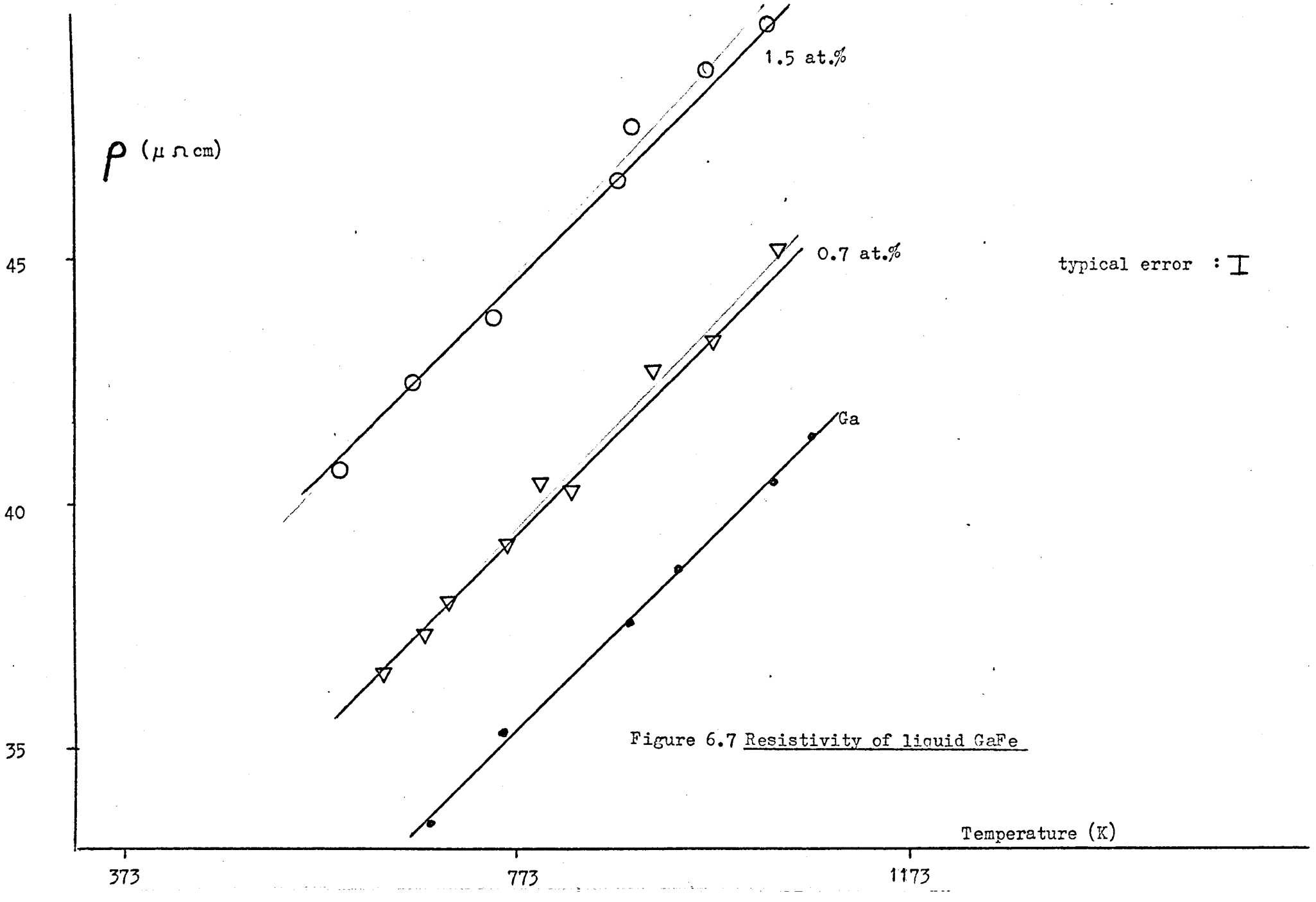

Figure 6.7 Resistivity of liquid GaFe

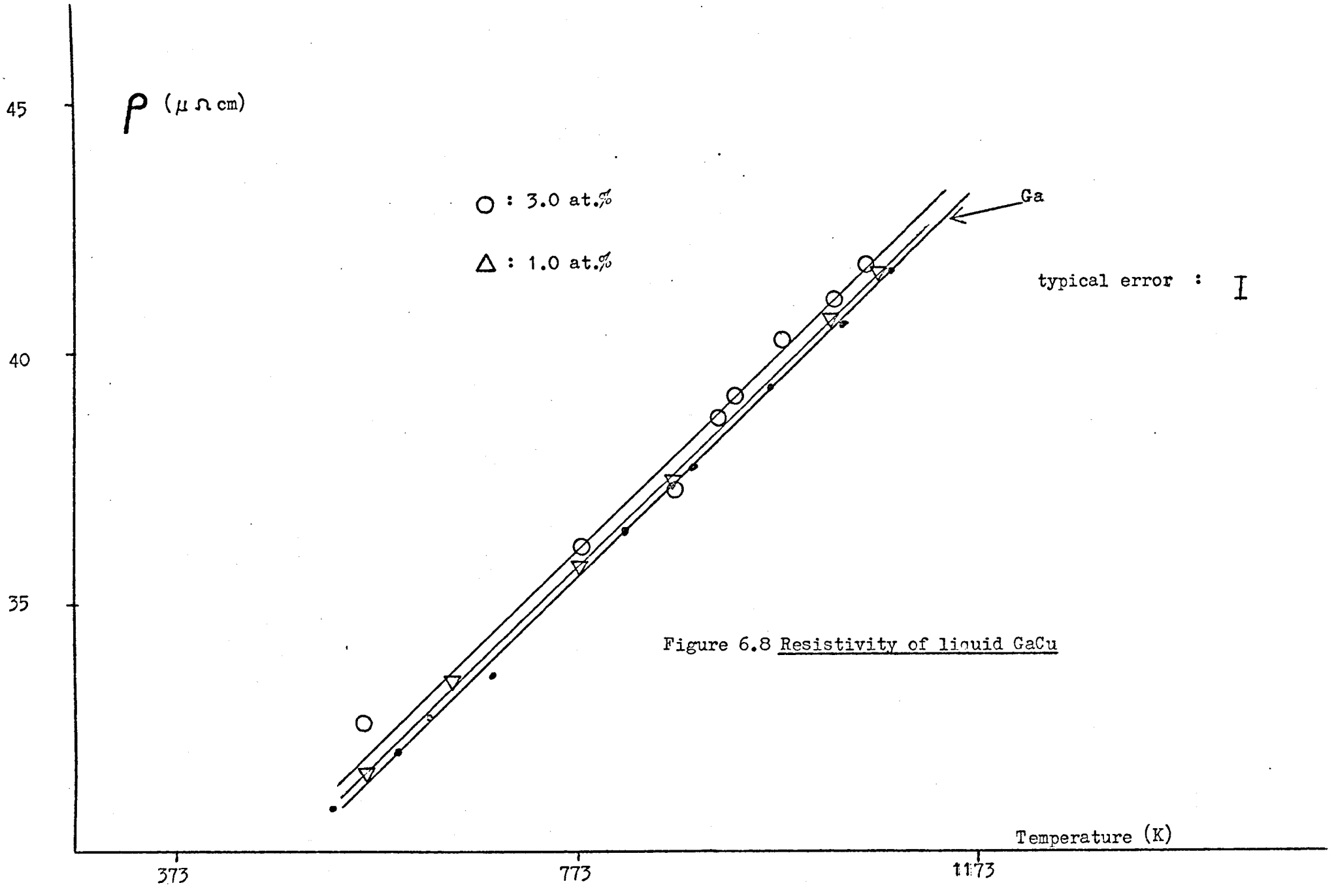

Figure 6.8 Resistivity of liquid GaCu

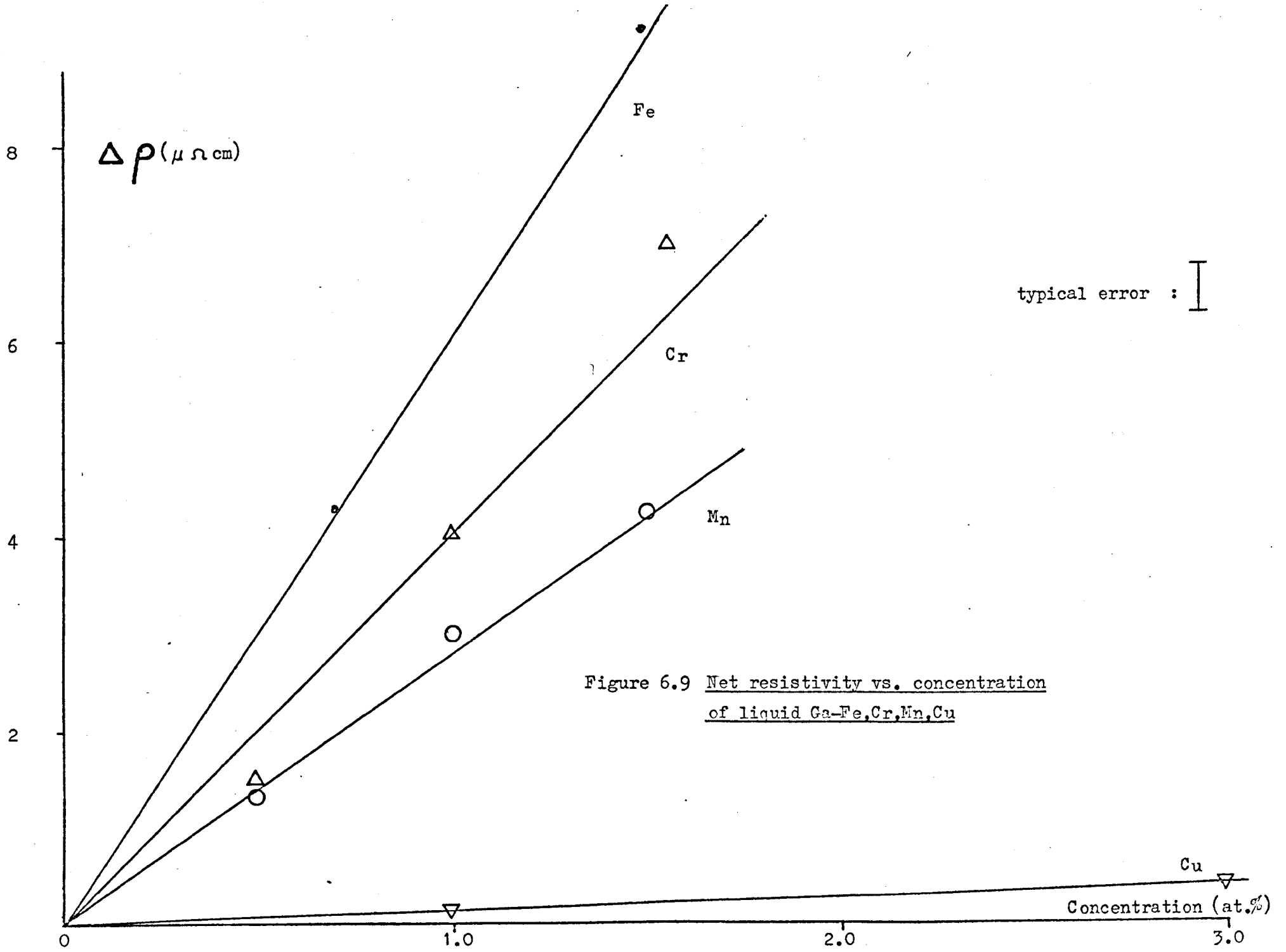

Figure 6.9 Net resistivity vs. concentration of liquid Ga-Fe,Cr,Mn,Cu

figure 6.10. For comparison, the same parameters are given for the following host metals in figure 6.11 :-

Au (1)	measured by	Guntherodt and Kunzi,	1973	(T= 1373 K)
Au (2)	"	" Loram	, 1968	(T= 300 K)
Ge	"	" Guntherodt and Kunzi,	1973	(T= 1273, 1373 K)
Sn	"	" Tamaki (1)	, 1968	(T= 1073 K)
Sb	"	" Ohno et al.	, 1973	(T= 1173 K)

They were chosen because they are all high temperature liquid state results except for Au(2), which was included to show the minimum at manganese.

6.2.3. Analysis

Inspection of figures 6.10 and 6.11 immediately show the similarities between gallium as a host compared with gold and antimony. These systems show a minimum in $\Delta\rho/c$ at the centre of the 3d transition series with a maximum at iron on one side of manganese and a less obvious maximum for gold at titanium or vanadium on the other. These results enable an estimated trend of the 3d series in gallium to be drawn (dashed line in figure 6.10), especially after taking into account the very small incremental resistivity at copper. The two peaks indicate a spin-splitting of the "virtual levels" formed by the d-levels embedded in the conduction band of the host giving rise to a magnetic system. The first possible peak at vanadium (c.f. Al 3d metals, Boato et al., 1966) is associated with the up-spin level passing through the Fermi level and the second at iron with the down-spin through the Fermi level. Superficially this indicates a magnetic system as the formation of a spin-split state presupposes the existence of a net magnetic moment.

Following Friedel (1963) that a 3d transition metal dissolved in a metallic host gives rise to the phenomenon of a 'virtual bound state' which is localised around the impurity, the best

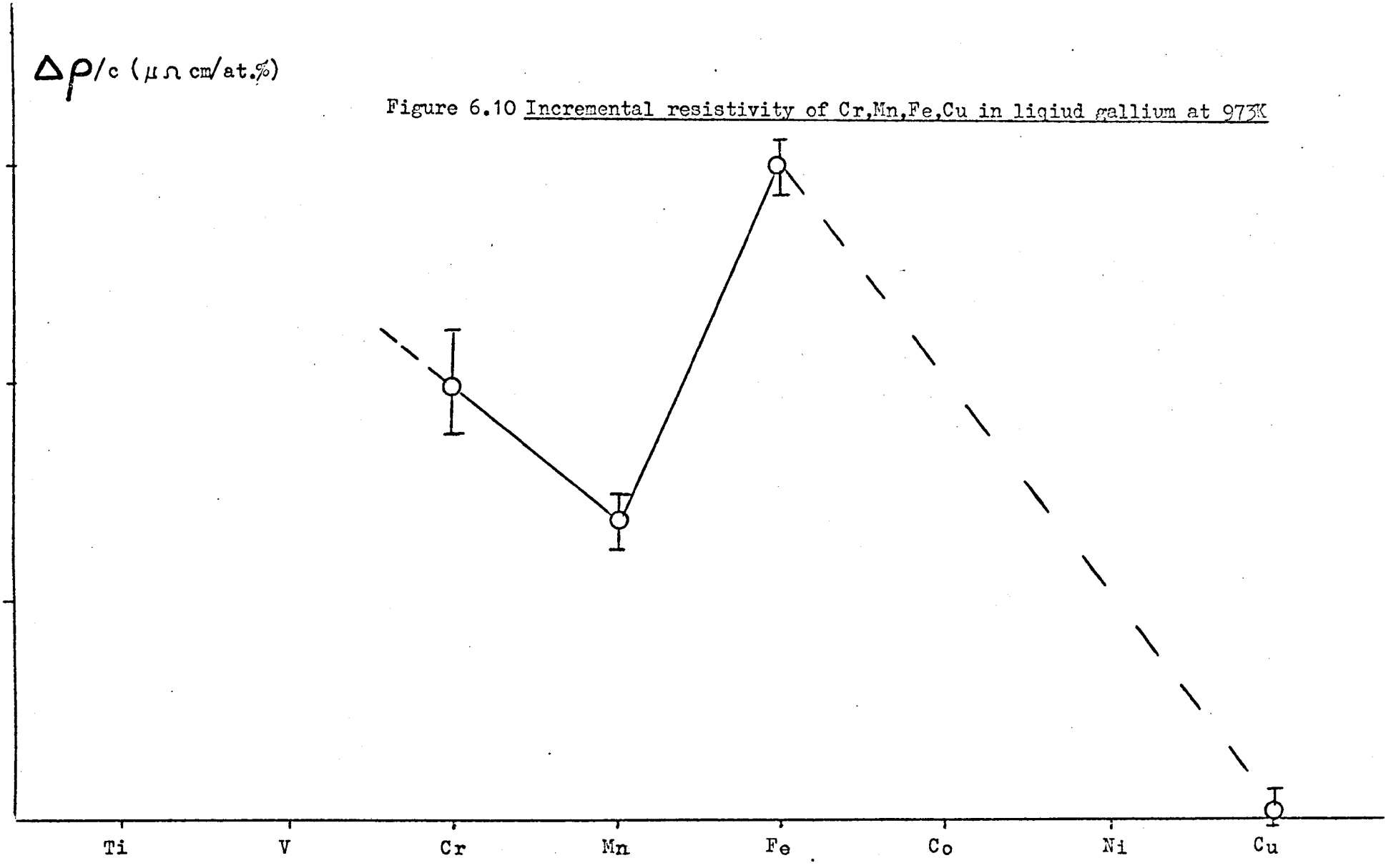

Figure 6.10 Incremental resistivity of Cr,Mn,Fe,Cu in liqiud gallium at 973K

Text cut off in original

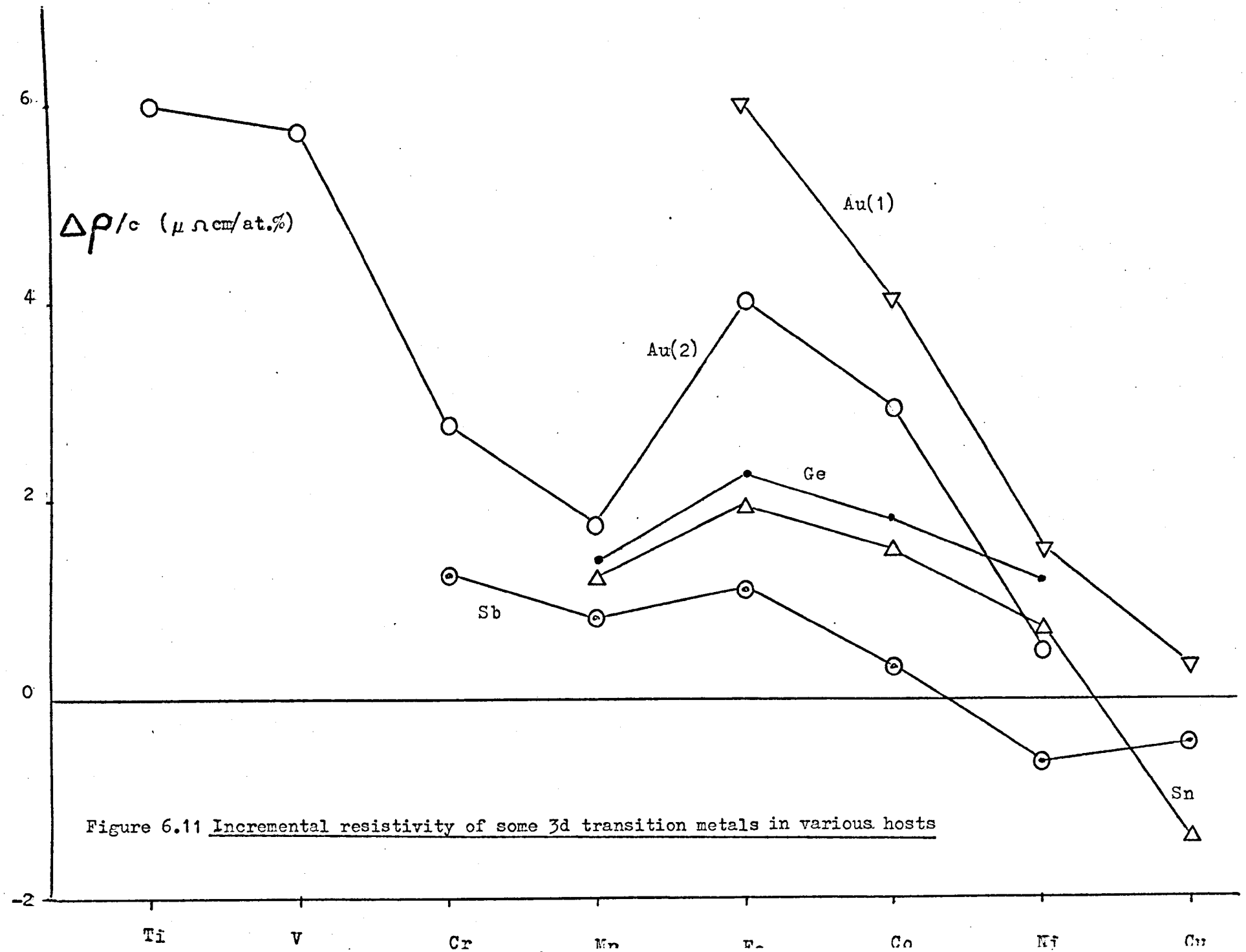

Figure 6.11 Incremental resistivity of some 3d transition metals in various hosts

way to treat the scattering problem is by the method of partial wave analysis (Boato et al., 1966; Tamaki (1), 1968). Accordingly this will be carried out for the non-magnetic alloy GaFe and extended to GaMn and GaCr.

6.2.3. (i) Partial Wave Analysis of the Resistivity Results

The two basic equations for a non-magnetic 3d impurity in a host are :-

$$\frac{\Delta\rho}{c} = \frac{h.10^{-9}}{50\, Z_h e^2 k_F} \sum_{l \geq 1} l\sin^2(\eta_l - \eta_{l-1}) \qquad 6.7$$

$$Z = \frac{2}{\pi} \sum_{l \geq 0} (2l+1)\,\eta_l \qquad 6.8$$

where the parameters are defined as in Chapter 2.

Equation 6.7 is an adaptation of a quasi-free electron approach and 6.8 is the Friedel sum rule. Substituting $Z_h = 3$ and $k_F = 1.67 \times 10^8 cm^{-1}$ for gallium results in :

$$\Delta\rho/c = 1.028.(\sin^2(\eta_1 - \eta_0) + 2\sin^2(\eta_2 - \eta_1) + 3\sin^2(\eta_2)) \quad \mu\Omega cm/at.\% \qquad 6.9$$

Gallium has an electronic structure of $(\epsilon)\ 3d^{10}4s^24p^1$ where $\epsilon = 1s^22s^22p^63s^23p^6$ and comparing this with the electronic structure of copper : $((\epsilon)3d^{10}4s^1)$ leads to a valence difference of 2. It is very unlikely that there is any d-wave scattering from copper in gallium so assuming only η_0 and η_1 are important in the GaCu system allows the s and p phase shifts to be calculated in the following manner. The incremental resistivity of GaCu at 1173 K was found to be $0.13 \pm 0.20\,\mu\Omega cm/at.\%$ and the substitution of this with $Z = 2$ and $\eta_2 = 0$ in equations 6.8 and 6.9 results in $\eta_0 = \pi - 3\eta_1$ and $\eta_1 = 0.03\pi$. This would give $\eta_0 \simeq 0.92\pi$, but due to the $\sin^2$ terms in equation 6.9 η_0 may be equated to 0.08π thus giving $\Delta\rho/c = 1.028.(\sin^2(4\eta_1) + 2\sin^2(\eta_1)) \simeq 0.13\ \mu\Omega cm/at.\%$. Because of

the large error (compared with the experimental result) it can only be said that η_o and η_1 are smaller and $\lesssim 0.08\pi$. In a similar manner the result for GaFe may be analysed but it becomes immediately apparent that only by disregarding the reasonable assumption that η_o and η_1 both remain small can equation 6.9 reproduce the result that $\Delta\rho/c = 6.00 \pm 0.25$ $\mu\Omega$cm/at.%. Thus it is found that if $\eta_2 = 0.6\pi$ is taken, (as iron is expected to have six d electrons) then values of 0.1π and 0.7π for η_1 and η_o respectively give $\Delta\rho/c = 5.78$ $\mu\Omega$cm/at.% when substituted in equation 6.9. The marked deviation of η_o from the value found for GaCu show that it is unlikely that equation 6.9 explains the experimental results of GaFe.

To explain the resistivities of GaMn and GaCr equation 6.9 must be modified. These two systems have been shown to be magnetic (section 6.1) although GaCr is a borderline case, so following Tamaki (2), (1968), Z becomes :

$$Z = Z_d = Z_{d\uparrow} + Z_{d\downarrow} \qquad 6.10$$

$$\text{thus} \quad \Delta\rho/c = 1.028(5/2)(\sin^2(\eta_{2\uparrow}) + \sin^2(\eta_{2\downarrow})) \qquad 6.11$$

This assumes that now η_2 is the dominant scattering mechanism though to include the small effects of η_o and η_1, $\Delta\rho/c$ will be made up of $\Delta\rho/c$ from the alloy in question minus $\Delta\rho/c$ from GaCu.

Taking the system GaMn first, where $\Delta\rho/c = 2.80 \pm 0.25$ $\mu\Omega$cm/at.% at 1173K, equation 6.11 gives :

$$2.80 - 0.13 = 1.028(5/2)(\sin^2(\eta_{2\uparrow}) + \sin^2(\eta_{2\downarrow}))$$

With $Z_d = 5$, the above equation can be fitted with $Z_{d\uparrow} = 3.75$, $Z_{d\downarrow} = 1.25$ (or vice versa). These values allow a comparison with the susceptibility results using equation 6.12 below.

$$S = 5/\pi\ (\eta_2\uparrow - \eta_2\downarrow) \qquad 6.12$$

As $\eta_2\uparrow,\downarrow = (\pi/5)Z_d\uparrow,\downarrow$, substitution in equation 6.12 gives $S = 2.5$. The magnetic moment (P_{eff}) for this sytstem was found to be 5.9 from susceptibility measurements and substituting S in $P_{eff} = (g^2S(S+1))^{\frac{1}{2}}$, assuming $g = 2$ gives $P_{eff} \simeq 5.9$.

Similarly for GaCr the value 4.00 - 0.13 = 3.87 $\mu\Omega$cm/at.% can be fitted to equation 6.11 within the larger error for this system (figure 6.9) with $Z_d\uparrow = 2.9$, $Z_d\downarrow = 1.1$. This results in the values of 3.45 $\mu\Omega$cm/at.% and $P_{eff} = 4.5$.

6.2.3. (ii) Variation of $\Delta\rho/c$ with temperature

Daybell and Steyert (1968) have shown that one may expect a decrease in $\Delta\rho/c$ with an increase in T for systems that show Kondo-type behaviour, the whole effect taking place over a range of ~1½ decades in lnT about T_c. It follows that for this effect to be seen in the alloys measured (figures 6.5 to 6.8) a decrease in slope in ρ vs. T for an increase in c should be apparent but inspection of these figures reveals that the alloys have ρ vs. T plots parallel to the host for all measured c values. For GaMn being clearly magnetic with a Curie-Weiss θ of about 590 K (section 6.1) a change in slope from 700 K to 1150 K should be noticeable if T_{sf} and θ are similar as found in several systems (e.g. AuV, CuFe). Because within experimental error the effect is not seen, it would appear either that the characteristic temperature as defined by resistivity experiments is different to that as defined via susceptibility, or that the experiment was performed in a limited temperature interval of $\Delta\rho/c$. vs. T curve whereby any change of slope is masked by the error. An estimation of the change with temperature that may be expected can be obtained by reference to figure 2.4 in which Rivier and Zlatic (1972) plot normalised resistivity ρ against reduced temperature x^{-1} (equation 2.24). Various temperature

regimes from T^2 (l.s.f.) behaviour to lnT (Kondo) behaviour are obtained. Thus for GaMn where T_{sf} approximately equals 200 K, substituting $Ud_d \simeq 1$ gives $x^{-1} \simeq 27$ when T = 873 K. Therefore no change in the behaviour of ρ may be expected for an increase in T as the curve in figure 2.4 has a greatly reduced slope at this x^{-1}. The temperature where one may expect a visible change ($x^{-1} \simeq 4$) is ~ 100 K where, for solubility reasons, the experiment cannot be performed. For GaCr where the substitutions T = 873 K, $Ud_d \simeq$ 1000 K are made, it is found that $x^{-1} \simeq 5.5$ assuming that θ and T_{sf} are similar. Increasing the temperature to 1073 K gives $x^{-1} \simeq 6.7$ so figure 2.4 indicates that about a 17% change in slope should be seen but which was not apparent in the resistivity results (figure 6.5) - T_{sf} is ~ (1/3)θ for GaMn so it would appear reasonable that $T_{sf} \neq \theta$ for the GaCr system. The characteristic temperature as defined by susceptibility measurements for this system shows that θ may be in the temperature interval 1000 K to 4000 K, so substituting this latter value for T_{sf} shows that x^{-1} is in the range of ~1.4 to ~1.7 for the interval 873 K to 1073 K. Thus no change in slope is expected as the curve in figure 2.4 is linear in this region. For GaFe now, substituting the values T = 873 K to 1073 K, $Ud_d \simeq 0.93$ and $T_{sf} \simeq 1500$ K gives $x^{-1} \simeq 3.4$ to 4.2, so approximately a 13% change in slope should be seen.

6.2.4. Discussion

The incremental resistivity of GaCu (0.13 ± 0.20$\mu\Omega$cm/at.%); can be adequately described using the standard theory (Friedel, 1956) but cannot reasonably account for the result of GaFe where $\Delta\rho/c$ = 6.00 ± 0.25$\mu\Omega$cm/at.%. To test the validity of the unlikely results that $\eta_o = 0.7\pi$ and $\eta_1 = 0.1\pi$ it would be convenient to know $\Delta\rho/c$ for GaCo or GaV, though the experiments to determine these would be difficult

to perform. Due to the solubility problems of these systems the operating temperatures would need to be much higher than the temperatures at which the present experiments were carried out. Loram et al. (1972) have devised an alternative procedure which can predict incremental resistivities of a particular alloy if its susceptibility behaviour is known, so an attempt to explain GaFe using this was made. Because it also gave unreasonable results, no effort to explain the procedure here is needed. Some doubts as to the validity of the GaFe results must be entertained in the in the light of this failure, although figure 6.7 indicates a linear scaling of ρ vs. c between ~ 600 K and 1100 K which, with the small error, would lead one to assume the experiment has been performed satisfactorily. A consistent error due to some metallurgical effect with the tungsten probes may have caused the high resistivity.

The GaMn and GaCr results can be explained using a modification of equation 6.9 so it becomes valid for magnetic systems. Tamaki (2), (1968), has explained SnMn in this manner and found that it is only necessary to assume integer values for $Z_d\uparrow$, $Z_d\downarrow$ to fit to his result. Assuming $Z_d = 5$ for GaMn, the values $Z_d\uparrow = 3.75$ and $Z_d\downarrow = 1.25$ correctly predict the resistivity result of 2.67 $\mu\Omega$ cm/at.% (after subtraction of the GaCu resistivity) and give excellent agreement with the magnetic moment of $5.9\mu_B$ from susceptibility measurements. Good agreement with the system GaCr can be achieved using $Z_d\uparrow = 2.9$ and $Z_d\downarrow = 1.1$, leading to $\Delta\rho/c = 3.45\mu\Omega$cm/at.% and $P_{eff} = 4.5\mu_B$. The metallurgical problems in determining $\Delta\rho/c$ for GaCr gave rise to a larger error ($\pm$ 0.050$\mu\Omega$cm/at.%) than the other systems though the magnetic moment is still ~ 8% below the value of $4.9\mu_B$ which may have been expected with S = 2. The value of P_{eff} using the calculation due to the Schottes, (1971) is $(4.2 \pm 0.3)\mu_B$, within the experimental error.

Because the experiment was performed with no applied magnetic field the results for $Z_{d\uparrow,\downarrow}$ do not define the occupation number of up and down-spin electrons uniquely so the number of spins assigned to each spin value may be reversed (within an alloy system) with equal validity.

It appears that if one compares the "universal" curve for resistivity of River and Zlatic with the experimental results for GaMn and GaCr (figure 6.5 and 6.6), the absence of a decrease of slope with increase in c at a particular T for GaMn is predicted primarily because the measuring temperature range is much higher than the characteristic temperature ($T >> 200K$), and the opposite for GaCr ($T << \sim 4000$ K). GaFe is expected to show the effect despite experimental error of the slope (~8%). Because this is not seen, it must be assumed that the characteristic temperature is different from the T_{sf} of ~1500 K as given by susceptibility measurements.

References

Alloul,H., Bernier,P.,Lanois,H., Pouget,J.P.,	J.Phys. Soc. Japan	30,	101,	1972
Anderson, P.W.,	Phys. Rev.	124,	41,	1961
Babic, E., et al.,	Sol. Stat. Comm.	10,	691,	1972
Blodgett,J.A., Flynn,C.P.,	Phil. Mag.	20,	917,	1969
Boato,G., Bugo,M., Rizzuto,C.,	Il Nuovo Cimento	45,	226,	1966
Caroli, B.,	Phys. Kondeus. Materil.	1,	346,	1963
Caroli,B., Lederer,P., Saint-James,D.,	Phys. Rev. Lett.	23,	700,	1969
Daybell,M.D., Sleyert,W.A.,	Phys. Rev. Lett.	18,	398,	1967
Daybell,M.D., Sleyert,W.A.,	Phys. Rev. Lett.	20,	195,	1968
Dworin,L., Narath,A.,	Phys. Rev. Lett.	25,	70,	1970
Flynn,C.P., Rigney,D.A., Gardner,J.A.,	Phil. Mag.	15,	1255,	1967
Freeman,A.J., Watson,R.E.,	Magnetism (ed. Rado,Suhl) Acad.Press, N.Y.	2A,	168	
Ford, C.J.,	Ph.D thesis, University of Warwick			1972
Friedel, J.,	Can. J. Phys.	34,	1190,	1956
Gunderodt,H.J., Kunzi,H.U.,	Phys. Kondeus. Materil.	16,	117,	1973
Hamann, D.R.,	Phys. Rev.	158,	570,	1967
Heeger, A.J.,	Sol. Stat. Phys. (ed. Seitz,Turnbull and Ehrentiech)	23,	283.	1969
Kondo, J.,	Prog. Theoret. Phys. (Kyoto)	32,	37,	1964
Kume, K.,	Phys. Lett.	24A,	743,	1967
Loram, J.,	Morgins Conf.		June,	1968
Loram, I.W., Grassie,A.D.C.,	Phys. Rev. B.	5,	3659,	1972
Nagaoka, Y.,	Progr.Theoret.Phys.(Kyoto)	37,	13,	1967
Narath,A., Weaver,H.T.,	Phys. Rev. Lett.	23,	233,	1969
Narath, A.,	CRC Crit.Rev.Sol.Stat.Sci.	3,11,		1972

Ohno,S., Okazaki,H.,Tamaki,S.,	J.Phys.Soc.,Japan	35,	1060, 1973
Peters,J.J., Flynn,C.P.,	Phys. Rev. B.	6,	3343, 1972
Rivier,N., Zuckermann,M.J.,	Phys. Rev. Lett.	21,	904, 1968
Schotte,K.D., Schotte,U.,	Phys. Rev. B.	4,	2228, 1971
Stassis,C., Shull,C.G.,	Phys. Rev. B.	5,	1040, 1970
Stoner, E.C.,	Rept. Prog. Phys.	11,	41, 1961
Suhl, H., Wong, D.,	Physics	3,	17, 1967
Tamaki, S., (1)	J. Phys. Soc. Japan	25,	379, 1968
Tamaki, S., (2)	J. Phys. Soc. Japan	25,	1596, 1968
Tholence,J.L., Tournier,R.,	Phys. Rev. Lett.	25,	867, 1960
Van Dam,J.E., Gubbens,P.C.M., van den Berg,G.J.,	Physica	61,	389, 1972
Wachtel,E., Nier,K.J.,	Z. Metallk.	56,	779, 1965
Yafet,Y., Jaccarino,V.,	Phys. Rev.	133A,	1630, 1964
Zuckermann, M.J.,	J. Phys. C.	3,	2130, 1970

CHAPTER 7

CONCLUSION

7.1. ZnCr Susceptibility

A straightforward analysis of the suceptibility of dilute single crystal alloys with zinc as host is hampered by the De Haas-Van Alphen oscillations in the parallel axis masking the smaller impurity effects at low temperatures ($T<77$ K). A method of overcoming this is presented in Chapter 4 for ZnCr and it is shown that a Curie-Weiss law can be fitted over limited temperature regions to the results for both crystallographic axes. If is found that $\Delta\chi_\perp > \Delta\chi_{\parallel}$ for $T \lesssim 50$K and $\Delta\chi_\perp < \Delta\chi_{\parallel}$ for $T \gtrsim 50$ K after fitting to a C-W law, though analysis in the manner of Li et al., (1973) applied to the two lowest concentration crystals (Zn46Cr, Zn135Cr) gives $\Delta\chi_\perp < \Delta\chi_{\parallel}$ for $T \gtrsim 5$ K. The anisotropy therefore changes character according to which formulae the results are fitted, so one may quite reasonably take the view that the susceptibility of ZnCr is fairly isotropic (in the low temperature region at least). Alternatively it may be argued that application of the analysis of Li et al. ignores the concentration-dependence of the host (Bell, 1972), thus making analysis in the present work preferable i.e. the anisotropy of ZnCr is given by the curve in figure 4.39.

A single C-W law for each axis is not applicable throughout the whole measured temperature range (4.2 K to $\sim$ 450 K), this is evident because the anisotropy is not linear with temperature so simple crystal field theory has been presented to try to explain this behaviour. The point charge model predicts a very large anisotropy due to a doublet energy level being lowest. Even disregarding this and assuming a singlet state is lowest (which allows a smaller anistropy to be derived) leads to incorrect low temperature results. Further,the detailed temperature behaviour is not explained so it must be concluded that simple crystal field theory is an inadequate explanation for the ZnCr system. Anisotropic

exchange also predicts incorrect susceptibility behaviour so a need exists for a more sophisticated theory including crystal field effects.

7.2 Gallium Alloy Results

A comparison between the susceptibilities of the hosts aluminium and gallium (in the liquid state) with 3d transition metal impurities allows the successful prediction of magnetic moment formation to be made for the gallium systems. It is found that GaMn is magnetic in a C-W sense with GaCr just on the magnetic/nonmagnetic borderline. The resistivity results for the Ga3d metal impurities confirm GaMn as magnetic and partial wave analysis gives good agreement for the measured incremental resistivities (except GaFe where metallurgical difficulties may be present). Partial wave analysis also gives good agreement for the spin values of GaMn and GaCr when compared with the same values derived via the susceptibility results. In magnetic systems the Kondo effect may be evident in a change of slope in the $\Delta\rho$ vs. T curves for each concentration alloy. Over the measured temperature range this effect was not seen, probably because the characteristic temperature was too far away from the measuring temperature. Analysis of the results via the universal resistivity curve of Rivier and Zlatic (1972) lends support to this view when characteristic temperatures consistent with both resistivity and suceptibility are derived.

7.3. Suggestions for further work

Taking the ZnCr results first, it is apparent that there are no crystal field models at present which can explain the behaviour of these single crystals over an extended temperature range (4.2 to $\sim$ 450 K). A need therefore exists for theory

to fill this gap. Because there is evidence that only the most dilute alloys of ZnCr presented here appear free from included intermetallic compounds ($c \lesssim 135$ mppm), further low temperature susceptibility work should preferably be on very dilute alloys (e.g. 1 to 20 mppm) though this condition requires that the experiments be carried out at $T \leq 4.2$ K. Interest arises here because the Kondo temperature for ZnCr of ~ 0.5 K (Rizzuto, 1974) could be spanned and the expected behaviour contrasted with the actual behaviour. Development of the Hirst (1970) ionic model may be at a sufficiently advanced state to apply to this system, especially as it appears at present that this model may give the most comprehensive explanation of the local moment problem. Resistivity results would be a valuable aid to characterising the ZnCr system, and this should be relatively easy to carry out as large dilute single crystals of ZnCr are readily made. An obvious extension to the present work would be to duplicate these experiments on zinc using the other 3d metals as impurities. It would be very interesting to also investigate the hexagonal close-packed systems magnesium and cadmium with 3d metal impurities. Magnesium is a nearly perfect hexagonal close-packed metal though many of its properties are isotropic. It is probable that similar amounts of impurity which can be dissolved in zinc can also be dissolved in magnesium, though with cadmium as a host the situation is about an order of magnitude down on this. Experimental difficulties are increased with magnesium due its reactiveness, though with suitable precautions these may be overcome.

The resistivity results for the Ga-3d metal alloys are incomplete as only GaCr, GaMn, GaFe and GaCu were measured. The remainder of the 3d series were found difficult to prepare even in the small quantities used for susceptibility measurements, but extension of the present work to higher temperatures ($\gtrsim$ 1100 K) should help alleviate this problem. A different cell material (e.g. alumina)may be necessary to successfully measure the resistivity of an alloy such as GaTi

which proved particularly difficult to prepare even at ~1300 K. If such a cell was made the measuring temperature range could be effectively doubled, thus allowing not only the intransigent alloys to be measured but a more exhaustive search for evidence of the Kondo effect to be carried out.

References

Bell, D.A.,	Ph.D.Thesis, Imperial College		1972
Hirst, L.L.,	Phys. Kondens. Materie,	11,	255,1970
Li, P.L., et al.,	Phys. Rev. Lett.,	31,	29,1973
Rivier, N., Zlatic, V.,	J. Phys. F: Metal Phys.,	2,	87,1972
Rizzuto, C.,	Rep. Prog. Phys. (G.B.),	37,	147,1974

Appendix I

$$
\begin{aligned}
\lambda L.S|2,2\rangle &= 4\lambda|2,2\rangle \\
\lambda L.S|2,1\rangle &= 2\lambda|2,1\rangle + \lambda/2(0 + 4|1,2\rangle) \\
\lambda L.S|2,0\rangle &= 0 + \lambda/2(0 + 2\sqrt{6}|1,1\rangle) \\
\lambda L.S|2,-1\rangle &= -2\lambda|2,-1\rangle + \lambda/2(0 + 2\sqrt{6}\,1,0\rangle) \\
\lambda L.S|2,-2\rangle &= -4\lambda|2,-2\rangle + \lambda/2(0 + 4|1,-1\rangle)
\end{aligned}
$$

$$
\begin{aligned}
\lambda L.S|1,2\rangle &= 2\lambda|1,2\rangle + \lambda/2(4|2,1\rangle + 0) \\
\lambda L.S|1,1\rangle &= 1\lambda|1,1\rangle + \lambda/2(2\sqrt{6}|2,0\rangle + 2\sqrt{6}|0,2\rangle) \\
\lambda L.S|1,0\rangle &= 0 + \lambda/2(2\sqrt{6}|2,-1\rangle + 6|0,1\rangle) \\
\lambda L.S|1,-1\rangle &= -1\lambda|1,-1\rangle + \lambda/2(4|2,-2\rangle + 6|0,0\rangle) \\
\lambda L.S|1,-2\rangle &= -2\lambda|1,-2\rangle + \lambda/2(0 + 2\sqrt{6}|0,-1\rangle)
\end{aligned}
$$

$$
\begin{aligned}
\lambda L.S|0,2\rangle &= 0 + \lambda/2(2\sqrt{6}|1,1\rangle + 0) \\
\lambda L.S|0,1\rangle &= 0 + \lambda/2(6|1,0\rangle + 2\sqrt{6}|-1,2\rangle) \\
\lambda L.S|0,0\rangle &= 0 + \lambda/2(6|1,-1\rangle + 6|-1,1\rangle) \\
\lambda L.S|0,-1\rangle &= 0 + \lambda/2(2\sqrt{6}|1,-2\rangle + 6|-1,0\rangle) \\
\lambda L.S|0,-2\rangle &= 0 + \lambda/2(0 + 2\sqrt{6}|-1,-1\rangle)
\end{aligned}
$$

$$
\begin{aligned}
\lambda L.S|-1,2\rangle &= -2\lambda|-1,2\rangle + \lambda/2(2\sqrt{6}|0,1\rangle + 0) \\
\lambda L.S|-1,1\rangle &= -1\lambda|-1,1\rangle + \lambda/2(6|0,0\rangle + 4|-2,2\rangle) \\
\lambda L.S|-1,0\rangle &= 0 + \lambda/2(6|0,-1\rangle + 2\sqrt{6}|-2,1\rangle) \\
\lambda L.S|-1,-1\rangle &= 1\lambda|-1,-1\rangle + \lambda/2(2\sqrt{6}|0,-2\rangle + 2\sqrt{6}|-2,0\rangle) \\
\lambda L.S|-1,-2\rangle &= 2\lambda|-1,-2\rangle + \lambda/2(0 + 4|-2,-1\rangle)
\end{aligned}
$$

$$
\begin{aligned}
\lambda L.S|-2,2\rangle &= -4\lambda|-2,2\rangle + \lambda/2(4|-1,1\rangle + 0) \\
\lambda L.S|-2,1\rangle &= -2\lambda|-2,1\rangle + \lambda/2(2\sqrt{6}\,-1,0\rangle + 0) \\
\lambda L.S|-2,0\rangle &= 0 + \lambda/2(2\sqrt{6}\,-1,-1\rangle + 0) \\
\lambda L.S|-2,-1\rangle &= 2\lambda|-2,-1\rangle + \lambda/2(4|-1,-2\rangle + 0) \\
\lambda L.S|-2,-2\rangle &= 4\lambda|-2,-2\rangle + \lambda/2(0 + 0)
\end{aligned}
$$

Appendix II

$$|\widetilde{2,2}\rangle = |2,2\rangle + 0$$

$$|\widetilde{2,1}\rangle = |2,1\rangle + 2|2,2\rangle \text{ /A-B}$$

$$|\widetilde{2,0}\rangle = |2,0\rangle + \sqrt{6}|1,1\rangle \text{ /A-B}$$

$$|\widetilde{2,-1}\rangle = |2,-1\rangle + \sqrt{6}|1,0\rangle \text{ /A-B}$$

$$|\widetilde{2,-2}\rangle = |2,-2\rangle + 2|1,-1\rangle \text{ /A-B}$$

$$|\widetilde{1,2}\rangle = |1,2\rangle + 2|2,1\rangle \text{ /B-A}$$

$$|\widetilde{1,1}\rangle = |1,1\rangle + \sqrt{6}|2,0\rangle \text{ /B-A} + \sqrt{6}|0,2\rangle \text{ / B-C}$$

$$|\widetilde{1,0}\rangle = |1,0\rangle + \sqrt{6}|2,-1\rangle \text{ /B-A} + 3|0,1\rangle \text{ / B-C}$$

$$|\widetilde{1,-1}\rangle = |1,-1\rangle + 2|2,-2\rangle \text{ /B-A} + 3|0,0\rangle \text{ / B-C}$$

$$|\widetilde{1,-2}\rangle = |1,-2\rangle + 0 + \sqrt{6}|0,-1\rangle \text{ / B-C}$$

$$|\widetilde{0,2}\rangle = |0,2\rangle + \sqrt{6}|1,1\rangle \text{ /C-B}$$

$$|\widetilde{0,1}\rangle = |0,1\rangle + 3|1,0\rangle \text{ /C-B} + \sqrt{6}|-1,2\rangle \text{/ C-B}$$

$$|\widetilde{0,0}\rangle = |0,0\rangle + 3|1,-1\rangle \text{ /C-B} + 3|-1,1\rangle \text{/ C-B}$$

$$|\widetilde{0,-1}\rangle = |0,-1\rangle + \sqrt{6}|1,-2\rangle \text{ /C-B} + 3|-1,0\rangle \text{/ C-B}$$

$$|\widetilde{0,-2}\rangle = |0,-2\rangle + 0 + \sqrt{6}|-1,-1\rangle \text{/ C-B}$$

$$|\widetilde{-1,2}\rangle = |-1,2\rangle + \sqrt{6}|0,1\rangle \text{ /B-C}$$

$$|\widetilde{-1,1}\rangle = |-1,1\rangle + 3|0,0\rangle \text{ /B-C} + 2|-1,1\rangle \text{/ A-B}$$

$$|\widetilde{-1,0}\rangle = |-1,0\rangle + 3|0,-1\rangle \text{ /B-C} + \sqrt{6}|-1,0\rangle \text{/ A-B}$$

$$|\widetilde{-1,-1}\rangle = |-1,-1\rangle + \sqrt{6}|0,-2\rangle \text{ /B-C} + \sqrt{6}|-1,-1\rangle \text{/ A-B}$$

$$|\widetilde{-1,-2}\rangle = |-1,-2\rangle + 0 + 2|-1,-2\rangle \text{/ A-B}$$

$$|\widetilde{-2,2}\rangle = |-2,2\rangle + 2|-1,1\rangle \text{ /A-B}$$

$$|\widetilde{-2,1}\rangle = |-2,1\rangle + \sqrt{6}|-1,0\rangle \text{ /A-B}$$

$$|\widetilde{-2,0}\rangle = |-2,0\rangle + \sqrt{6}|-1,-1\rangle \text{/A-B}$$

$$|\widetilde{-2,-1}\rangle = |-2,-1\rangle + 2|-1,-2\rangle \text{/A-B}$$

$$|\widetilde{-2,-2}\rangle = |-2,-2\rangle + 0$$